THREE DIMENSIONAL PROSTATE CANCER MODEL SYSTEMS

Eman Mohamed Othman Mosaad
M.Sc. Biochemistry/Chemistry

Submitted in fulfilment of the requirements for the degree of
Doctor of Philosophy (Research)

Institute of Health and Biomedical Innovation, Translational Research Institute
School of Biomedical Sciences, Faculty of Health
Queensland University of Technology
2018

Keywords

3D culture, bone marrow niche, bone mesenchymal stem/stromal cells (BMSC), bone metastasis, bone regeneration, co-culture, drug-screening platform, *in vitro* modelling, luciferase reporter system, microtissue, micro-tumour, Microwell-mesh, prostate cancer (PCa).

Abstract

Metastatic Prostate cancer (PCa) invades the bone in approximately 85% of PCa patients, and when this occurs successful treatment becomes more elusive and mortality rates increase. After reaching the bone, it is believed that the PCa cells take up residence in the haematopoietic stem cell (HSC) niche and feed off niche signals that promote quiescence. This quiescent state and the niche microenvironment may assist PCa to evade the immune system and chemotherapy. Additionally, the bone marrow niche microenvironment may contribute to the evolution of PCa cells that are not dependent on androgen and that are refractory to androgen deprivation therapy (ADT). The characterization of these processes, and the development of therapeutics to treat bone metastatic PCa, have been delayed by the lack of effective *in vitro* model systems.

The **OVERALL AIM** of my Thesis was to develop a more effective *in vitro* 3D microtissue PCa model system that mimicked some aspects of the bone marrow niche microenvironment and PCa cell interaction in bone metastasis, thus enabling elucidation of how bone marrow niche cell composition influences growth of metastatic PCa cells and subsequent drug sensitivity.

I **HYPOTHESIZED** that it would be possible to mimic PCa cell interaction with the bone marrow niche *in vitro* through the use of a microtissue model. Specifically, I hypothesized that bone marrow niche cells and PCa cells assembled into microtissues, using a high throughput microwell system, would enable replication of the metastatic bone marrow niche. Using the microwell system, I executed the following AIMs, which each address major questions related to the establishment and evolution of PCa and drug treatment response within the bone marrow niche:

AIM 1: Characterization of bone marrow-derived stromal cells in a high throughput microwell platform (Chapter 2);

AIM 2: Characterisation of PCa cells in an improved high throughput microwell platform (the Microwell-mesh platform) that retains microtissues within discrete microwells and its utilisation as a drug-testing platform (Chapter 3);

AIM 3: Development and utilization of a high throughput cell viability assay that enables cell-specific quantification in a co-culture system (Chapter 4) and;

AIM 4: Development of co-cultures of PCa cells and bone marrow-derived stromal cells using the Microwell-mesh platform and utilising the cell-specific viability assay for drug-screening in co-cultures (Chapter 5).

To address AIM 1 (Chapter 2), an in-house fabricated microwell platform was used to efficiently manufacture thousands of multicellular bone marrow mesenchymal stromal cells (BMSC) spheroids. BMSC spheroid size relative to cell number, proliferation and differentiation capacity were characterised and contrasted against 2D controls. The capacity of bone morphogenetic protein 2 (BMP-2) to improve the osteogenic capacity of BMSC spheroids was specifically characterised. While the trilineage differentiation capacity of 3D spheroids was similar to 2D monolayer cultures, the results revealed that cells in 3D spheroids exhibited a decline in cell proliferation and concurrent reduction in cellular size. BMP-2 affected osteogenic outcomes in both 2D and 3D cultures, with the greatest calcium accumulation observed in the 2D monolayer cultures and a low quality bone-like tissue formation in 3D spheroids. The outcomes from this chapter informed the design of experiments in AIM 4 (Chapter 5).

To address AIM 2 (Chapter 3), the use of a microwell platform that utilises a nylon mesh to retain 3D micro-tumours in discrete microwells; termed the *Microwell-mesh* was described. The Microwell-mesh enables the manufacture of ~150 micro-tumours per well in a 48-well plate, and response to anti-tumour drugs can be readily quantified. The results demonstrated that 3D micro-tumours, unlike 2D monolayers, were not hypersensitive to Docetaxel or Abiraterone Acetate, providing a superior platform for the evaluation of sequential drug treatment. In summary, the Microwell-mesh provided an efficient 3D micro-tumour platform for single and sequential drug-screening.

To address AIM 3 (Chapter 4), the stability of the luciferase reporter gene expression was evaluated for prostate and breast cancer cells in co-culture system with bone marrow stromal cells. It was shown that while the luciferase expressing cell number can be assessed in mono-cultures using the cell-specific bioluminescence (CS-BLI) assay, it was challenging to apply this technique to the co-culture model. In co-cultures, the type of cell, the response element of the promoter region in the reporter system and the methodology of cell transfection/transduction were all crucial determinants on the reporter gene expression stability. C42B cell line transduced with a stable reporter system in mono- and co-cultures, namely C42B-MSCV-luc, was used in subsequent studies to enable evaluating C42B cell number in co-culture system using the CS-BLI assay (Chapter 5).

To address AIM 4 (Chapter 5), the Microwell-mesh platform was used to manufacture hundreds of 3D co-culture micro-tumours formed from PCa and bone stromal cells. The co-culture micro-tumours retained in the Microwell-mesh was used as a drug-screening platform. To specifically quantify the PCa cell number in multicellular co-cultures, the CS-BLI assay described in Chapter 4 was used. The proliferation and drug response of PCa cells in a 3D direct co-culture system was demonstrated. The impact of bone marrow stromal cells on C42B cell proliferation was significant after 24 hours of co-culture establishment contrasted to C42B mono-cultures. Our results demonstrated that 3D micro-tumours, unlike 2D mono- or co-cultures, were less sensitive to Docetaxel. By contrast, the sensitivity of PCa cells to anti-androgen treatment was not modified by the presence of stromal cells in the 3D micro-tumours. In summary, the Microwell-mesh provided a powerful 3D culture platform for assembling complex micro-tumours, and enabling efficient drug-screening.

The outcomes of this thesis were that the merits of using a high throughput microwell platform to efficiently manufacture hundreds of multicellular spheroids was evaluated. The Microwell-mesh was then evaluated as a drug-screening platform. A critical finding was the discovery of instability of the CS-BLI assay which was promoter and/or cell line dependent and which would need to be verified with each cell line before use. Finally, the first multicellular co-culture micro-tumour

system as a potential drug-screening platform for bone metastatic PCa was developed.

Table of Contents

List of Figures

List of Tables

List of Abbreviations

2D	2 dimensional
3D	3 dimensional
DAPI	4',6-diamidino-2-phenylindole stain
ANOVA	Analysis of variance
ADT	Androgen deprivation therapy
ANG-1	Angiopoietin 1
Anxa 2	Annexin II
BPH	Benign prostatic hyperplasia
BMSC	Bone marrow-derived mesenchymal stromal cells
BMPs	Bone morphogenetic proteins
CaSR	Calcium sensing receptor
CSCs	Cancer stem cells
CAFs	Cancer-associated fibroblasts
CAM	Cancer-associated macrophages
CRPC	Castrate resistant prostate cancer
CS-BLI	Cell-specific bioluminescence imaging
CSS	Charcoal stripped fetal bovine serum
CXCL12	Chemokine (C-X-C motif) ligand 12
CXCR4	Chemokine (C-X-C motif) receptor 4
CTCs	Circulating tumour cells
CMV	Cytomegalovirus
DHR123	Dihydrorhodamine 123
DTCs	Disseminated tumour cells
DMEM	Dulbecco's modified Eagle's medium
DPBS	Dulbecco's phosphate buffered saline
ET-1	Endothelin-1
EGFR	Epidermal growth factor receptor
ECM	Extracellular matrix
FBS	Fetal bovine serum
FGF	Fibroblast growth factors
GAG	Glucoseaminoglycans
GFP	Green fluorescent protein
Gαs	Guanine-nucleotide-binding protein stimulatory α subunit
HSC	Haematopoietic stem cell
HGF	Hepatocyte growth factor
HIF-1α	Hypoxia inducible factor 1α
IGFBP-3	Insulin-like growth factor-binding protein
IGF	Insulin-like growth factors
ICAM-1	Intercellular adhesion molecule
JAK2	Janus kinase 2
Luc	Luciferase
LFA-1	Lymphocyte function-associated antigen 1
LPA	Lysophosphatidic acid
MMPs	Matrix metalloproteinases
MSC	Mesenchymal stem/stromal cells
MPL	Myeloproliferative leukemia virus oncogene

OCT	Optimal Cutting Temperature
OPN	Osteopontin
PDGF	Platelet-derived growth factors
PDMS	Polydimethylsiloxane
PCa	Prostate cancer
PSA	Prostate specific antigen
Ptpm1	Protein tyrosine phosphatase
PDK2,4	Pyruvate dehydrogenase kinase 2, 4
RANKL	Receptor activator of nuclear factor Kappa-B ligand
RLU	Relative bioluminescence
SDF-1	Stromal derived factor 1
TPO	Thrompoietin
TIMPs	Tissue inhibitors of metalloproteinases
TGF-β	Transforming growth factor
TRAMP	Transgenic adenocarcinoma mouse prostate
TURP	Transurethral resection of the prostate
VCAM-1	Vascular cell adhesion molecule 1
VEGF	Vascular endothelial growth factor
VLA-4	Very late antigen-4

Statement of Original Authorship

The work contained in this thesis has not been previously submitted to meet requirements for an award at this or any other higher education institution. To the best of my knowledge and belief, the thesis contains no material previously published or written by another person except where due reference is made.

QUT Verified Signature

Signature:

Date: _____24/04/2018_____

Acknowledgements

I wish to extend my sincere gratitude to my principal supervisor Associate Professor Michael Doran for the opportunity to work in his group for the last four years, as well as for his guidance and intellectual engagement during this time. In addition, I would like to thank my associate supervisor, Prof Judith Clements for her assistance and advice throughout my PhD. I also would like to thank my external supervisor, Dr Karen Chambers, who was the first to introduce me to the prostate cancer research area, for her help, guidance and valuable suggestions.

I wish also to express my gratitude to all members of Doran Laboratory, previous and recent members, especially Dr Betul Kul, Dr Michael Osiecki, Dr Kathryn Futrega, Ms Myfanwy King, Dr Vu Thuy, Dr James Palmer, Mr Eric Franklin, Ms Ena Music, Ms Melissa Monterosso, Ms Bianca Nowlan and Ms Poanna Tran. I am very grateful for the scientific, intellectual, social and spiritual enrichment you add to my life. I gratefully acknowledge the Australian Prostate Cancer Research Centre – Queensland (APCRC-Q) meetings which were full of scientific brainstorming and useful discussion. I also acknowledge Dr Brian Gloss of the Garvan Institute of Medical Research, Dr Inge Seim of the Queensland University of technology for their intellectual input in this project. In addition, I thank the facility mangers at the Translational Research Institute, Dr Sandrine Roy (Microscopy facility) and Dr David Sester (Flow cytometry facility) for their valuable discussion and advice. I would like to thank the Ministry of Higher Education – Egypt for their support and provision of my PhD scholarship.

Finally, I would like to thank my family for their support and their guidance throughout my life especially during my PhD. I cannot express my gratitude for my late mother who always supported me and encouraged me to achieve my dream of finishing my PhD, before she passed away three years ago. I also acknowledge my father and my siblings' advice and assistance throughout the hard times of my PhD journey. Lastly, I would like to sincerely thank my soul mate, my caring partner, my husband for his encouragement and support throughout my PhD.

Chapter 1: Introduction and literature review

Prostate cancer (PCa) is the second most common cancer worldwide in men, and the most common cause of cancer death. In an advanced aggressive form of the disease, the bone marrow is the most common secondary tumour site. The first-line treatment for advanced PCa is androgen deprivation therapy (ADT). However, the PCa cells can develop a phenotype that no-longer responds to androgen deprivation, and this cancer is termed "castrate resistant prostate cancer" (CRPC) and it is virtually intractable.

Over the past decades, much of the field has focused on efforts to better understand the mechanisms involved in bone metastasis and the evolution of the CRPC phenotype. A significant barrier to progress is the lack of *in vitro* models that effectively mimic the metastatic bone microenvironment.

This chapter will outline the stages of PCa progression, the composition and biology of the bone marrow niche, metastasis to bone marrow niche and the current trends in PCa bone metastasis *in vivo* and *in vitro* models. Finally, an outline of the remaining chapters of the thesis will be described.

1.1 INCIDENCE, PREVELANCE AND MORTALITY OF PROSTATE CANCER

Among the various cancers diagnosed in males, PCa is the second most common cancer worldwide [1]. In 2012, more than one million men worldwide were diagnosed with PCa [2]. Improved PCa diagnostics has contributed to the increasing incidence rates of the disease [3]. Most of the newly diagnosed cases (70%) appear in developed regions, with the highest incident rates in Australia/New Zealand and North America [4]. There is evidence that genetic determinants play an important role in the risk of developing prostate cancer; for instance, prostate cancer incidence is higher in African black populations, relative to Asian populations [5]. It is important to appreciate that the significant increase in diagnosis has not translated into a significant decrease in PCa mortality rates; PCa remains the fifth leading cause

of death from cancer in men worldwide and an estimated 1.7 million new cases and 499,000 PCa-related deaths are predicted to occur annually by 2030 [2].

1.2 DIAGNOSIS

In the past, PCa diagnosis was the result of clinical examination following investigation into symptoms such as urinary obstruction [6]. Recently, the increase in incidence reflects the widespread use of predictive diagnosis using blood tests for prostate specific antigen (PSA) [7]. PSA is a kallikrein-related serine protease that is passively released in the bloodstream mainly by the cells of the prostate gland [8].

If PCa is suspected, PSA levels are quantified in the patient's blood serum and a digital rectal examination is performed [9]. These examinations can be confounded by the presence of benign prostatic hyperplasia (BPH), which can also result in the enlargement of the prostate [10]. The incidence of BPH also increases with age, and many of the symptoms are similar to those observed in PCa patients [11]. Thus, a first step in PCa diagnosis generally involves confirming that the patient's symptoms are not solely the manifestation of BPH.

Benign Prostatic Hyperplasia: In BPH the enlargement of the prostate is associated with an increase in PSA, and sometimes with urinary obstruction [12]. There are a number of methods used to ablate or remove prostate tissue in order to open up the flow of urine. Historically, many patients with BPH enlargement are treated with Transurethral resection of the prostate (TURP) [13]. During the TURP process PCa can sometimes be diagnosed via the histological examination of the prostate tissue collected during the operation [14], [15].

PCa diagnosis: If PSA levels and a digital rectal examination suggest that PCa may be present, the clinician will request tissue biopsies in attempt to validate a PCa rather than BPH diagnosis [16]. During the biopsy process, several (~12) biopsies are taken from different locations for histological examination [17]. Based on the morphology of the cancer cells recovered from the biopsies, a score is assigned to the cancer to reflect its perceived aggressiveness. The assigned score is called a Gleason score, in which the grading system is based on five different histological patterns

(from 1 to 5; 5 is the most aggressive pattern) of PCa. A Gleason score of a tumour can be created by adding the two most common grade patters in the tumour, therefore the least aggressive cancer has the lowest score, 2, and the score increases with the aggressiveness of the tumour, with score of 10 indicating the most aggressive form of the cancer [18], [19]. Recently, the international society of urological pathology has improved the overall Gleason grading system [20]. The new grading system was validated in a multi-institutional study on more than 20 thousand radical prostatectomy cases. This new grading system includes 5 Grade Groups; where the less aggressive cancer has Grade Group 1 = Gleason score ≤ 6, Grade group 2 = Gleason score 3 + 4 = 7, Grade group 3 = Gleason score 4 + 3 = 7, Grade group 4 = Gleason score 4 + 4 = 8 and the most aggressive cancer has Grade Group 5 = Gleason scores 9 and 10. This modified grading system was found to be more simpler and more accurate in predicting progression and was approved by the World Health organization [19]. According to the grading results, if the biopsies are positive, it is common to use ultrasound imaging to further assist in diagnosing PCa stage and containment within the prostate capsule [21]. Invasion of the seminal vesicles and enlargement of the pelvic lymph nodes can be detected by computed tomography [22]. If PCa treatment involves a radical prostatectomy, higher resolution imaging methods such as magnetic resonance imaging are often used to help identify the boundaries of the tumour growth [6], [23].

PSA blood level and biopsy-based diagnosis does not always result in a proactive treatment approach [24], and thus there is concern that in low grade PCa this increase in diagnostic resolution enables “over diagnosis” rather than enhancing our capacity to prevent disease advancement [7]. This is concerning because in some cases PCa does not advance to a stage that requires treatment or intervention. What is required is the capacity to predict if the PCa identified early in a specific individual is likely to evolve into a more aggressive form of the disease, and if aggressive preventative therapies are warranted [25], [26]. The need for such diagnosis capacity will increase with the predicted increase in PCa incidence.

1.3 DISEASE PROGRESSION AND CONVENTIONAL TREATMENTS

There are numerous treatment strategies (reviewed in [27]) which are commonly performed depending on the PCa stage/severity and age of the patient [28]. PCa progression and the commonly used treatments are represented in Figure 1.1. The available treatments include active surveillance in the cases of the least aggressive PCa, radical prostatectomy, androgen deprivation therapy, brachytherapy, chemotherapy and radiotherapy [29], [30]. In some circumstances, more than one strategy is used in combination to achieve more desirable outcomes and to reduce the risk of tumour progression or recurrence [31]. Following early diagnosis of non-symptomatic localized PCa, the treatment varies widely from active surveillance to radical prostatectomy or radiotherapy depending on the individual patient [32]. Treatment approaches are influenced by cost, age, and physician bias or opinion. Despite the growing numbers of studies discussing the reasons that motivate a patient to choose one treatment over the other [33]–[35], optimal treatment approaches remain controversial. While active surveillance is predominant in older men with less than 10 years life expectancy, radical prostatectomy survival rates often yield greater than 10 years disease-free outcomes in patients under the age of 65 [36]. These observations highlight how perceived life expectancy can impact on treatment decision-making. Additionally, perceptions regarding the impact of treatment side-effects and complications appear to be the most controversial factors influencing treatment selection [37].

Radiotherapy offers an alternative strategy to radical prostatectomy to destroy or eliminate localized tumours [38], and this technology is rapidly evolving. Currently, there are two primary approaches to radiotherapy; namely external radiation beam and radioactive seeds implantation. Three-dimensional conformal radiotherapy is performed using an external beam of radiation [39], [40]. Improvements in technologies that enable real-time tracking of the prostate's physical location and focusing of the radiation beam are increasing the precision of this therapy [41]. Increased precision should translate into improved efficacy and a reduction in treatment side effects [42]. It will take a few more years for data using these new methods to become readily available with longer follow up periods. The second radiotherapy approach involves the surgical placement of radioactive seeds into the prostate tissue; a process termed brachytherapy [43]. Both forms of

radiotherapy are sometimes used as a second-line treatment following radical prostatectomy [44].

Since Huggins *et. al.,* (1941) [45] found that removal of the testicles, which are the main source of testosterone hormone, dramatically decreased prostate cancer progression, it was reasoned that the PCa cell growth was dependent on androgen. Androgen deprivation therapy (ADT) is now achieved by preventing the luteinizing hormone secretion from the pituitary gland, rather than by physical castration [46]. ADT is not effective in some patients where the PCa cells can grow in castrate-levels of androgens, in the stage termed CRPC. CRPC may present as the progression of pre-existing tumour and/or the appearance of new metastases.

CRPC was initially termed androgen-independent disease, as it no longer responds to first line ADT. However, further studies revealed that the growth of cancer cells in CRPC patients is still dependent on androgen signalling. In relapsed patients, PSA levels continue to increase during ADT. This indicates the activation of androgen receptor (AR) transcriptional activity including the androgen response elements that regulate PSA expression. In CRPC, AR in PCa cells is found to be continuously activated via different mechanisms (reviewed in [47]). Early studies on the development of castrate-resistance showed that increased expression of AR in PCa cells leads to higher sensitivity of the AR signalling pathway in response to reduced levels of androgens [48]–[50]. Many studies revealed the role of ADT as a selective pressure for evolution of AR gene mutations and development of CRPC [51]–[54]. Furthermore, various AR gene mutations are found to be related to reducing the specificity of the interaction between AR and its ligand (androgens). These mutations enable alternative steroidal molecules, such as estrogens and progesterone, to activate AR [55], [56]. Moreover, expression of AR splice variants can provide an additional mechanistic explanation for CRPC development [57], [58]. AR variants are found to upregulate steroidogenic enzymes to increase biosynthesis of testosterone and dihydrotestosterone from adrenal androgens within the tumour microenvironment [59]–[61]. It was also found that AR variants can provide ligand-independent activation mechanism to upregulate the expression of AR-regulated genes which can explain the persistent AR transcriptional activity during ADT [62], [63].

The various mechanisms of continued AR signalling suggest that the combination of potent anti-androgens and enzymatic blockage can provide a reasonable therapeutic approach for CRPC patients. The drugs commonly used in the clinic today as high affinity anti-androgen hormonal therapy to treat relapsed CRPC patients include enzalutamide (also called MDV3100) [64], abiraterone acetate [65] and bicalutamide [66]. Enzalutamide has an anti-tumour effect, by inhibiting the nuclear translocation of the androgen receptor [67], and it has apoptotic and anti-DNA binding effects [68]. Abiraterone acetate, as an anti-androgen drug, targets prostate cancer cells by inhibiting the enzyme CYP17A1 which is an essential enzyme in synthesis of testosterone [69]. Abiraterone is increasingly favoured to treat clinically advanced castrate-resistant metastatic PCa [70]. Bicalutamide acts as a nonsteroidal AR antagonist by binding to the ligand binding domain of AR to mediate a conformational change that inhibits the normal function of AR [47]. Despite the success of these drugs in the clinic, it's important to consider cancers do become refractory to these agents and the tumour will eventually progress.

Similar cascade inhibition strategies include drug combinations [70]–[73] such as gefitinib with prednisone. Gefitinib inhibits epidermal growth factor receptor (EGFR) tyrosine kinase enzyme that is necessary for tumour cell growth [74], while prednisone is a synthetic corticosteroid drug that is effective as an immunosuppressant drug [75]. However, it is still controversial to define a specific drug combination for every stage in PCa progression.

With some differences in efficacy, ADT treats both localized and metastatic PCa, as long as the cancerous cells are androgen dependent [76]. In more advanced stages, such as metastasis or relapsed cases after ADT or radiotherapy, chemotherapy is usually the only remaining treatment option for advanced stages of the disease. Chemotherapeutic drugs have a cytotoxic effect that targets the cancerous cells. For instance, docetaxel targets fast dividing cells, by stabilizing microtubules, which then inhibits cell division prompting a programmed apoptotic response [77]. Docetaxel is a member of the Taxane drug family which includes paclitaxel and cabazitaxel [78]. Also, radium-223 acts as calcium mimic and targets the DNA of the cancerous cells in the bone metastatic PCa. Radium-223 selectively binds to the area of increased bone turnover within the osteoblastic metastases microenvironment and emits high

energy alpha particles to induce double stranded DNA breaks with minimized toxic effect on adjacent healthy tissue [79], [80].

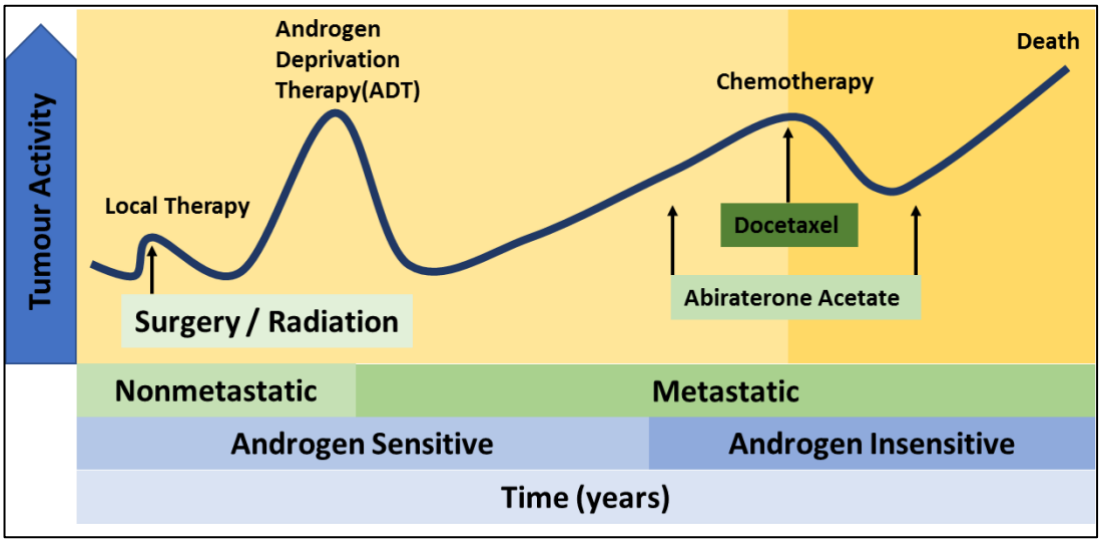

Figure 1.1. Prostate cancer (PCa) progression timeline. PCa is usually diagnosed at the localized stage where local therapy, such as partial or total prostatectomy is performed. Radiation therapy is also recommended in the case of localized tumours. If there is tumour recurrence, androgen deprivation therapy (ADT) is usually the next line of therapy. If the tumour cells become active again, possibly after 3-5 years, the tumour can advance to a more aggressive form where the PCa cells evolve into an androgen-independent phenotype. This is generally associated with the PCa cells having already metastasised to distant sites. The common targets of metastatic PCa are the lymph nodes and the bone. Active bone metastatic PCa is associated with localized pain and skeletal-related complications. At this late stage, PCa cells are mostly resistant to chemotherapeutic drugs and the survival rate is very low.

Despite the advances in early stages of PCa treatment outcomes [81], most of the therapeutic strategies are still controversial and are more complicated with aggressive forms of the disease, specifically bone metastasis [82]. Pain-relief is an essential consideration in the treatment of symptomatic bone metastatic PCa [83]. Therefore, treatment of bone metastasis in PCa patients consists of treating the cancer with docetaxel, for instance, whilst reducing bone pain with a combination of drugs, such as denosumab and bisphosphonates which have anti-osteoporotic effects [84], [85]. Bisphosphonates, such as clodronic acid, effectively control pain and

hypercalcemia by direct osteoclast activity suppression in terms of adhesion, proliferation and differentiation [86]. These drugs were found to have an anti-neoplastic effect, as they enhance tumour cell apoptosis and prevent the release of essential growth factors necessary for tumour growth [87]. Likewise, denosumab prevents osteoclast proliferation, differentiation and survival by inhibiting the receptor activator of nuclear factor Kappa-B ligand (RANKL) [88]. Immunosuppressant drugs such as prednisone which is combined with docetaxel, as a cytotoxic regimen, are sometimes used. This approach was found to deliver 3-months survival and improve the quality of life for cancer patients [89], [90].

Although there are number of drugs available with multiple modes of action, a significant challenge in the field is estimating the optimal drug selection and sequence to treat patients [91], [92]. Typically, cancers will become resistant to one drug, necessitating treatment with a new drug or combination of drugs [93]. Identifying the optimal combination or sequence of drug treatment has been challenging because of the rapid development of new drugs, the extended timeline of some treatment regimens and the variation in treatment regimens across different centres, coupled with the challenge of actually quantifying patient response [94]. Therefore, there is a critical need for a robust model of the disease to emulate the different PCa stages and to enhance and facilitate the drug discovery procedure as well as treatment protocols.

1.4 BONE METASTASIS

PCa cells can metastasise to new sites, such as the bone, lung and liver [95]. Several studies, using autopsies, indicated that PCa mostly spread via a hematogeneous pathway through periprostatic to prespinal veins [96]–[99]. The primary factor that correlates with metastasis is primary tumour volume, with a significant incidence in metastasis observed when the primary tumour exceeded 4 millilitres or 4 cubic centimetres [100]. Approximately 90% of metastatic prostate cancer patients suffer from bone metastases and when bone metastasis occurs treatment becomes more elusive and mortality rates increase [95], [101]. The hypothesis of how metastasis occurs can be summarized in the following steps.

Disassociation from the primary tumour: The cancerous cell migrates from the original tumour to circulate in the blood stream until it reaches a new favourable site where it can adhere and then proliferate [102]. In the case of PCa, Matrix metalloproteinases (MMPs) are found to be increased in tumour tissues and thought to be the main factor enabling the release of metastatic tumour cells into the circulation [103]. MMPs are expressed in normal tissues at low levels and cause degradation of the basement membrane. The activity of MMPs is regulated by tissue inhibitors of metalloproteinases (TIMPs) which reverse their action in the healthy tissue [104], [105]. Elevated serum levels of MMPs in PCa patients enhance PCa cell liberation from primary tumours into the blood stream as circulating tumour cells (CTCs) [103] [106]. CTCs have been detected in the blood stream of both primary and secondary cancer patients [107], [108]. Distant metastasis can occur when CTCs disseminate to a new site. At the new site the CTCs are referred to as disseminated tumour cells (DTCs) [109].

Like some other malignancies, PCa contains cells that have "stem-like" characteristics, including the ability to self-renew [110]. These cells are sometimes called "cancer stem cells (CSCs)". It should be noted that both the defining concepts and terminology remain quite controversial [111]. Nevertheless, the cancer stem cell theory assumes that it is these cells that can initiate secondary growth after therapy [112]. By necessity, cancer stem cells and CTC must share some common characteristics [113].

The bone marrow as a destination: The enriched mineralized extracellular matrix, and the high volumetric blood flow through the marrow, may explain a portion of the high incidence of PCa bone metastasis [114]. However, when PCa cells metastasise to the bone it is thought that they might take up residence in the haematopoietic stem cells (HSC) niche [115]. This observation suggests that PCa cell lodgement in the bone marrow may be an active process. It is reasoned that CTCs may home to the bone marrow niche in a manner analogous to how HSC home to the marrow [116].

1.4.1 Haematopoietic stem cells niche

The HSC niche is a unique microenvironment found within the bone marrow of adult humans [117]. This niche microenvironment functions to regulate HSC, and most critically it functions to preserve the HSC population over an individual's lifetime [118]. With billions of new blood cells generated daily in an adult [119], this proliferative load would normally be expected to exhaust the source population from which the blood cells are derived. However, the bone marrow niche functions to enable the production of more mature lineage committed progenitor cells (rather than HSC), onto which virtually the entire proliferative load is placed, whilst simultaneously preserving the majority of the HSC in a quiescent state [120]. Therefore, commitment to either cell fate is precisely controlled by the niche according to the body's requirement for new blood cells.

1.4.2 Niches within the niche

The HSC niche is thought to contain two different regions, namely the endosteal and the vascular regions [121]. The endosteal niche mainly refers to the region where osteoblasts, osteoclasts and osteoprogenitors interact [122]. The endosteal niche is thought to primarily maintain quiescent HSC. Whilst the more primitive HSC appear to reside near the endosteum; the adjacent vascular niche is thought to contain HSC populations that are slowly cycling to generate progenitor cells [123]. In the vascular niche, HSC interact with vascular endothelial cells and surrounding reticular cells. The function and the boundaries of the two regions are not clearly distinguished from each other. Thus, the two niches are interlaced and the niche function is maintained by balanced interactions of HSC with the cellular and physiochemical compartments of both sites [124]. In the following section, essential interactions between HSC and the niche are reviewed.

1.4.3 How haematopoietic stem cells find the niche

HSC homing to the bone marrow is primarily regulated by the chemokine (C-X-C motif) ligand 12 (CXCL12)/chemokine (C-X-C motif) receptor 4 (CXCR4) axis [125]. Whilst CXCL12 is normally expressed by many different cells, the major source of CXCL12 is osteoblasts found within the bone marrow [126], also known as

stromal derived factor 1 (SDF-1). This is quite an elegant system whereby the niche stromal cells secrete CXCL12 in a hypoxic microenvironment, and the HSC express the receptor for CXCR4 [127]. HSC home towards the CXCL12 produced by the niche, and once within the niche the continued exposure to CXCL12 promotes the adhesion of HSC to niche support cells.

Bone marrow endothelial cells express CXCL12 causing the adhesion of HSC on their surface [128]–[130]. This adherence provides a mechanism by which these cells can attach to the vessel walls and then migrate into the vascular niche [130], [131]. The interaction between CXCL12 and CXCR4 enables initial homing and attachment in the sinusoids, but other cell-cell adhesion molecules enable the final anchoring within the niche. Tie2/angiopoietin 1 (Ang-1) interaction between HSC and osteoblasts enhances adhesion [132]. Vascular cell adhesion molecule-1 is a ligand on the surface of osteoblasts, stromal reticular cells and endothelial cells and the receptor of this ligand, very late antigen-4 (VLA-4), is expressed by HSC [133]. Moreover, annexin II (Anxa 2) is an essential receptor, with the CXCL12/CXCR4 axis, for adhesion and homing of HSC, and regulation of osteoblast activity, as it works as an anchor for CXCL12 [134].

In addition to the CXCL12/CXCR4 axis, the expression of other receptors on HSC also affects homing. For example, guanine-nucleotide-binding protein stimulatory α subunit (Gαs), of which conditional deletion in mice causes the HSC to lose its ability to migrate towards the bone marrow, which reflects its importance in the homing process [135].

1.4.4 The physiochemical microenvironment in the haematopoietic stem cell niche

The physiochemical properties of the HSC niche are known to play key roles in the maintenance of HSC, and therefore may be relevant to the maintenance of PCa in a quiescent or stem-like state. Two key physical properties are the calcium and oxygen gradients in the niche [136] [137].

During bone resorption, increased concentration of Ca^{2+} by the action of osteoclast activity affects the localization of HSC to the endosteal surface via calcium sensing receptor (CaSR) which is expressed by HSC [136].

Hypoxia is thought to be an essential feature within the niche microenvironment. It is believed that there is a controlled oxygen gradient that is higher within the vascular niche and lower within the endosteal niche [138]. Hypoxia directly regulates the CXCL12/CXCR4 homing axis discussed above. Reduced oxygen tension induces CXCL12 by the stromal cells and CXCR4 expression by the HSC [139]. Additionally, the quiescent state and long-term preservation of HSC are believed to be controlled, in part, by hypoxia inducible factor 1α (HIF-1α), which is stabilized by hypoxia [140], [141].

1.4.5 The cells and signals in the haematopoietic stem cell niche

The signal interactions within the niche are complex, but through the use of gene knockout animal models, the role of various factors is increasingly being elucidated. It is now known that in the bone marrow HSC niche there are many types of cells that contribute to maintaining this unique microenvironment; these include, Nestin+ mesenchymal stem/stromal cells (MSC, also known as perivascular cells) [142], osteoblasts [143], pre–osteoblasts, endothelial cells, neural cells and adipocytes [123]. Each type of these cells has a specific role in bone maintenance and blood cell formation by providing a favourable home for HSC [116].

The cycling behaviour of HSC is precisely controlled within the niche. This key decision point is guided by niche pathways including Wnt, Notch, Hedgehog, bone morphogenetic proteins (BMPs), Tie2/Ang-1 and osteopontin (reviewed in [123]). On the other hand, thrompoietin (TPO)/ myeloproliferative leukemia virus oncogene (MPL) signalling regulates the quiescent state [144], with the aid of two other regulating signals which are Lnk, an adaptor protein that has inhibitory effects on the TPO/MPL axis [145], and Janus kinase 2 (JAK2), a protein that regulates both Lnk and MPL [146].

In regards to the two different regions of the niche, the abundance of quiescent HSC relative to the cycling cells can define the function of each region. In the endosteal niche, osteoblasts provide signals of quiescence, such as osteopontin

(OPN) [147], VLA-4/ vascular cell adhesion molecule 1 (VCAM-1), lymphocyte function-associated antigen 1 (LFA-1)/intercellular adhesion molecule (ICAM-1) [148]. Whereas in the vascular niche, endothelial cells express growth factors like insulin-like growth factor-binding protein (IGFBP-3) and E-selectin [149], which affect HSC proliferation and expansion. Based on these findings, the osteoblastic niche is responsible for keeping HSC in a quiescent state, with the endothelial (vascular) niche promoting the differentiation and proliferation of HSC [116].

Moreover, there are other cellular factors that influence HSC quiescence/proliferation regulation in the bone marrow niche. For instance, nerve cells can control the expression of CXCL12 on perivascular cells and this action is controlled by a circadian rhythm [150]. Immune cells also have a crucial role in HSC regulation, where macrophages in the bone marrow regulate the CXCL12 abundance in the niche microenvironment which in turn affects the rate of HSC mobilization to the blood [151].

1.4.6 PCa cells hijack HSC sites in the bone marrow niche

In the bone metastatic stage of PCa, it is believed that PCa targets the hematopoietic stem cell (HSC) niche in the bone marrow [115], [152]. As reviewed previously, bone marrow is a complex organ in the human body that incorporates several types of cells that reside in a stream of growth factors [153], [154]. This includes immune cells, stromal cells, endothelial and blood cells. In a healthy human, this microenvironment interacts positively to provide the home of HSC, blood-forming cells, where it can self-renew or differentiate into various blood cell types to meet the body's needs [115]. However, in such chemokine-rich microenvironment, tumour cells can feed off the niche signalling to reside in the bone marrow. Figure 1.2 schematically illustrates the sites of the bone marrow HSC niche that can be hijacked by PCa metastatic cells.

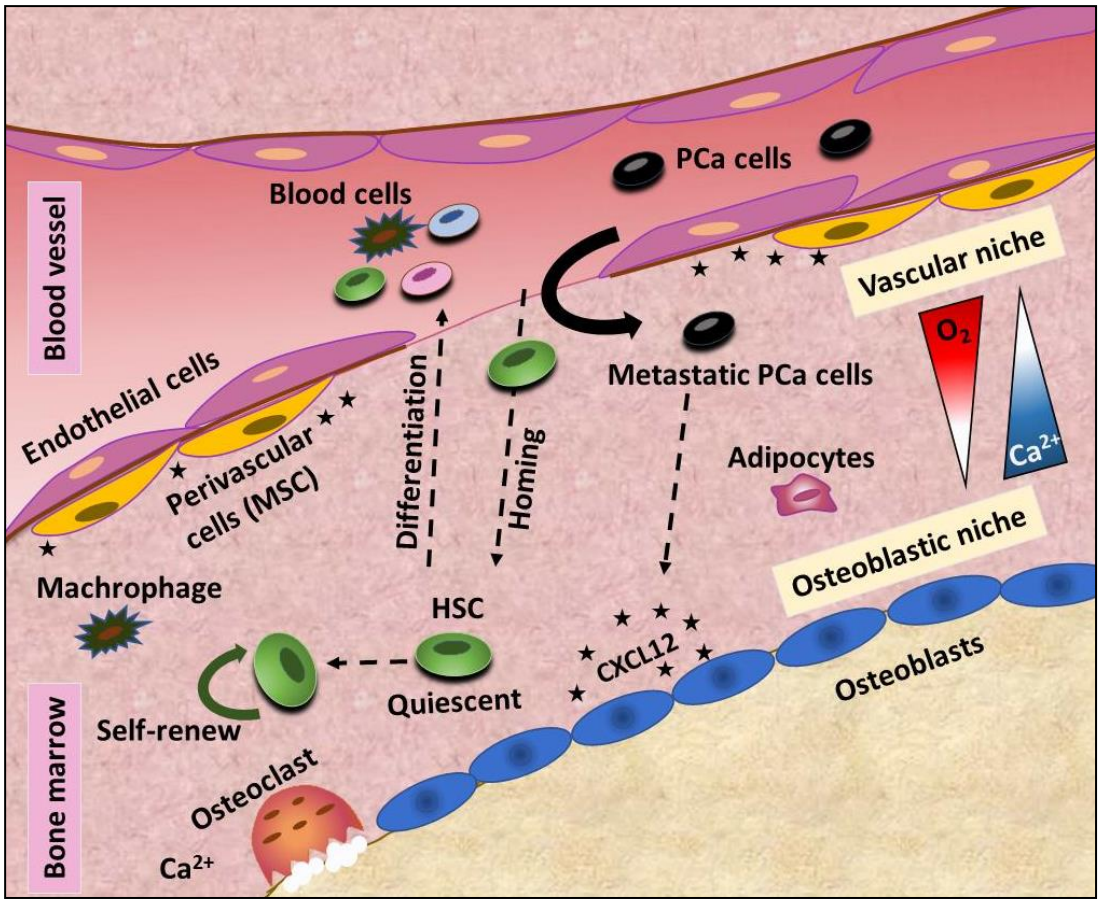

Figure 1.2. Schematic representation of bone marrow niche and prostate cancer (PCa) invasion. In the bone marrow, PCa cells hijack the haematopoietic stem cells (HSC) sites. The osteoblastic and vascular niches are the main two sites that regulate HSC fate such as homing, quiescence, self-renewal and differentiation, via interactions with cellular and molecular compartments of the niche.

PCa CTCs have the ability to migrate to the bone marrow HSC niche using similar signalling mechanisms to HSC [155]. At the signalling level, prostate tumour cells have the ability to overexpress CXCR4 that can bind with CXCL12 produced by bone marrow niche stromal cells and osteoblasts [156].

Within the niche, endothelial cells were found to facilitate the adherence of the cancerous cells [157]. Hematopoietic and endothelial cells release pro-angiogenic factors that facilitate angiogenesis [158]. Adhesion of cancer cells to osteoblasts via Anxa2 induces dormancy of cancer cells within the endosteal niche [159].

After residence in the bone marrow niche, PCa cell behaviour can be paradoxically different and perhaps unpredictable, with PCa cells triggering both

bone formation and bone resorption pathways [160]–[162]. The high concentration of local growth factors eluted during bone resorption, such as TGF β, insulin-like growth factors (IGF), fibroblast growth factors (FGF) and platelet-derived growth factors (PDGF), enhances the growth and propagation of cancerous cells [160]. PCa cells secrete BMPs, which can recruit osteoblast precursors and activate the formation of vascular endothelial growth factor (VEGF), which in turn causes osteoblast stimulation leading to bone formation [163]. Endothelin-1 (ET-1), produced by cancer cells, enhances osteoblast proliferation and amplifies the effect of BMPs, IGF-I&II, PDGF, and FGF [164]. On the other hand, inflammatory reactions instigated by tumour growth result in elevated levels of IL-6, an osteoclast activator which leads to bone resorption [165], [166]. This range of behaviours reveals how the balance of signal molecules in the niche is able to influence PCa cells and in turn how the PCa cells are able to influence the native tissue.

1.5 PROSTATE CANCER MICROENVIRONMENT

In the primary tumour site, the tumour microenvironment supports cancer cell progression, rather than prevent tumorigenesis. Similarly, in bone metastatic PCa, the tumour microenvironment was found to have a supportive role that enables the disseminated cancer cells to reside in the bone marrow, evade the immune system, stay in dormancy or actively proliferate to form a micrometastasis [167]. The supportive role may coincide with several changes to the stroma including, but not limited to, migration of immune cells, fibroblast recruitment, extracellular matrix remodelling and angiogenesis [168], [169].

Beside the aforementioned cellular factors, physiological factors also appear to play a crucial role in the tumour microenvironment. These include hypoxia, acidity, nutrients and growth factor gradients [170], [171]. In this section, the main cellular interactions in the PCa microenvironment will be reviewed.

1.5.1 Stromal cells

A stromal-epithelial interaction was early demonstrated in studies on embryonic development. In the early stages of development, epithelial differentiation

is induced by adjacent stromal cells [172]. This supportive action is mediated by extracellular matrix components and soluble paracrine signalling. After maturation, a new crosstalk balance is established, where the mature epithelial cells maintain stromal differentiation [173]. On the other hand, stromal cells in primary tumour site are crucial players in the tumour microenvironment and their role in tumour growth, invasion and migration is yet to be clearly defined. During tumorigenesis the genetic mutations acquired by the epithelial cells induce the "activation" of the surrounding stroma to express myofibroblastic markers [174]. This active stroma, also called cancer-associated fibroblasts (CAFs), has a fundamental role in cancer progression and migration [175]. Moreover, there is a growing evidence of the cancer initiation potential of CAFs. From primary tumours, patient-derived samples were utilized in a co-culture system to demonstrate the tumorigenic capacity of tumour stromal cells [176]–[178]. CAFs from high Gleason score patients, indicating high aggressiveness of PCa, induced the evolution of cancerous phenotype of normal prostate epithelial cells. It is believed that their action is mediated via ECM proteins and growth factors[179].

In bone metastatic PCa, the complex microenvironment of the bone marrow is capable of accommodating the tumour cells throughout the multi-step process of metastasis development. The initial engagement of circulating PCa cells in the bone marrow is mainly mediated by endothelial cells, MSC and osteoblasts via CXCL12/CXCR4 homing axis, as discussed previously. In addition, tumour cells express integrins, such as $\alpha_v\beta_3$ and $\alpha_v\beta_5$, which can bind to bone extracellular matrix components such as bone sialoprotein (BSP), and osteopontin (OPN) [180]. Similarly, tumour cells express cytokine receptors, such as the receptor activator of nuclear factor Kappa-B (RANK), which promote colonization in the bone marrow via binding to its ligand (RANKL) secreted by osteoblast lineage cells [181], [182]. E-cadherin expressed by tumour cells can enhance binding to osteoblasts which express N-cadherin [183]. Therefore, tumour cells colonise the endosteal surface in the bone marrow.

After colonisation, the disseminating tumour cells survive in the new microenvironment and can reside in dormancy for long periods. The osteoblast-derived long-lived quiescent bone lining cells are believed to support the long-term dormancy of PCa cells which can be for decades [184]. The binding of annexin II on

bone cells to its receptor on PCa cells can control tumour cell growth/dormancy [185].

The reactivation of dormant tumour cells to grow and form a micrometastasis is likely to be an active process by the bone marrow microenvironment compartments [157]. Osteoclasts and osteoblasts are believed to be active players in the reactivation process [182]. Tumour cells can secrete a vast number of growth factors which can activate and recruit osteoclasts to induce bone resorption. The accumulation of released growth factors in the bone resorption microenvironment can enhance tumour cell growth and further production of osteolytic and osteoblastic factors [186]. This results in establishing what is known as the vicious cycle of bone metastases which supports tumour growth in the bone [184], [187]. Additionally, other cell types in the bone marrow were found to enhance the tumour growth, such as MSC and adipocytes [188], [189], both of which appear to be potentially supportive of metastatic cell growth [190].

From the signalling pathway perspective, stromal-epithelial carcinoma interaction is mediated by several families of growth factors either in primary or metastatic sites. Tumour proliferation stimulating factors include fibroblast growth factor (FGF) family, insulin-like growth factor (IGF) family, epithelial growth factor (EGF) family and hepatocyte growth factor (HGF). In addition, these factors can play a part in tumour initiation [191]. Differently, transforming growth factor-β (TGF-β) can induce both tumour progression and tumour suppression processes. Several studies support the role of TGF-β in tumour growth inhibition [179], [192]. However, stromal-secreted TGF-β indirectly enhances cancer progression via impairing immune surveillance, activating angiogenesis and evolution of tumour metastatic phenotype [193], [194].

1.5.2 Immune cells

One of the hallmarks of cancer is the inflammatory microenvironment [195]. The specialized white blood cell, the macrophage, is one of the critical cellular compartments in the tumour microenvironment. The M2 polarized macrophages (also termed as alternatively activated macrophages) have tumour supportive activity due to their role in angiogenesis [196], [197]. The M2 macrophages are alternative

form of the “classically activated” M1 macrophages which activate immune response by producing high amounts of inflammatory cytokines and reactive oxygen species [198]. Cancer-associated macrophages (CAM) were found to enhance cancer progression by not only secreting growth factors, but also by providing the ECM degrading enzymes [195]. To recruit immune cells, tumour cells secrete specific proteins that activate macrophages [199]. The high occupancy of CAMs in the tumour microenvironment is one of the critical indicators of low prognosis and high probability of cancer metastasis [200]. In PCa, the influence of CAMs on cancer progression and growth is still controversial [201], [202]. However, there are several studies that suggest synergetic interaction between immune cells and other stromal cells in the tumour microenvironment can boost malignancy [197], [203], [204].

1.6 PROSTATE CANCER MODELLING

Despite the significant improvements in targeted therapies, PCa remains a challenging disease to treat especially in the advanced bone metastatic stages. Approximately 30% of advanced PCa patients exhibit an initial resistance to docetaxel [205], which is the most common conventional chemotherapy regimen. After the PCa cells metastasise to bone marrow, the mortality rates increase. It appears that the bone marrow niche microenvironment may promote quiescence in a subset of PCa cells [115], and this quiescent state and the immune-modulating microenvironment generated by the MSC may protect these cells from chemotherapy and the immune system [116]. This sustained “holding state” within the bone marrow niche may enable the evolution of castrate resistant prostate cancer (CRPC) which is the most advanced stage of the disease.

The scarcity of realistic preclinical models of advanced disease is the one of the obstacles in this research area. However, there are a number of *in vitro* and *in vivo* models designed to recapitulate the mechanisms involved in PCa and its bone metastasis. Some examples will be reviewed in the following sections.

1.6.1 *In vivo* animal models of PCa

In vivo animal models have been widely developed and have contributed to considerable advancements in PCa modelling (reviewed in [206] and [207]). In this section, some available mouse models and their limitations will be outlined.

At the outset, it is important to consider that there are anatomical differences between human and mouse prostates [208], which are thought to be the reason behind the lack of spontaneous PCa in mice. Therefore, PCa is initiated in mouse models through the introduction of genetic mutations or implantation of human PCa cell populations.

Genetically engineered mouse models

In 1999, the National Institutes of Health (NIH) founded the Mouse Models of Human Cancer Consortium (MMCC) in an effort to develop models of human cancer [209]. Since then, genetically engineered mouse (GEM) models of PCa have evolved two main generations. The first generation of GEM utilized probasin promoter driving viral oncogenes such as SV40 large T antigen to yield the transgenic adenocarcinoma mouse prostate (TRAMP) model [208]. The second generation incorporated the single and multiple molecular changes observed in human disease such as over expression of MYC and loss of phosphatase and tensin homolog (PTEN) [210], [211]. Most available GEM models were initially derived to physiologically mimic human PCa, however, with some limitations. For instance, development of neuroendocrine tumours is spontaneous in transgenic mouse models [212], whereas it may arise *de novo* in only 5-10% of PCa patients and is much more commonly observed following therapeutic treatment regimens [213]. The TRAMP model develops modest androgen independent tumours, which can rapidly evolve into CRPC [214], [215]. This model bypasses several stages of early disease and only recapitulates a specific advanced stage of the human disease. In addition, bone metastasis is very rare in transgenic mouse models, where the circulating tumour cells prefer to invade soft tissues such as the lungs and lymph nodes [212], [216], [217]. This limits the possibility to mimic bone metastasis, which is the common progression in human disease [95].

Human PCa cell implantation models

Implantation of immortalised PCa cell lines or serially passaged patient-derived samples into immunodeficient mice models, also known as xenograft model, is now gaining wide popularity in the field [218]. The advantage of using patient-derived xenograft model is that it promotes primary cell growth with maintaining the characteristics of the original tumour and can provide a better mimic of the drug response [218], [219]. Despite the relative high success of the known xenograft models, establishing a new successful model with a new patient-derived tumour sample is very limited [220]. This indicates that this process is not efficient and cannot be standardised between various laboratories.

In some PCa mouse models, researchers considered the influence of the microenvironment on the tumour growth where they co-transplanted human PCa cells with stromal cells. For instance, when LNCaP cells were co-transplanted with human stromal cells, LNCaP cells were tumourigenic and a more vascularized subcutaneous tumour model was established; whereas LNCaP-Matrigel tumours showed no evidence of angiogenesis [221]. Similarly, patient-derived tumour samples were able to grow and develop tumours when transplanted under the renal capsule with mouse stroma [220]. It has been reported that stromal cells play an important role in PCa mouse models due to their critical role in PCa tumour growth [179], [187], [222].

Human PCa cell implantations have been used to model bone metastasis of PCa [223]. For example, a bone metastatic model can be established by injecting PCa cell lines intravenously. Nevertheless, development of metastatic tumour in these models is cell line-dependent, where more aggressive cell lines, such as C42B and PC3 cells, show bone metastasis in high percentage of transplanted animals and less aggressive cell lines, such as LNCaP cells, show low/no bone metastasis [224], [225].

It is worth noting that intravenously injected cells were found to be trapped in the lung vasculature due to a pulmonary first-pass effect, thus limited quantities of injected cells can reach the target tissues [226], [227]. To bypass this limitation, cells can be injected directly into the bone. Most tested cell lines directly transplanted into the bone had success regardless of the cell type [225], [228], [229].

It is important to consider that migration of intravenously injected tumour cells to the bone is distinct from developing a metastatic tumour in the bone after a direct injection of PCa cells into the bone [230]. Intra-bone injection is not mimicking all stages of migration, invasion and development of a tumour in the bone. Through these steps of metastasis, a restricted selection process occurs to permit a specific cellular phenotype to survive and develop a new tumour in the distant site [231]. These aspects of this process are bypassed in the mouse models where tumour cells are directly injected in the bone. Nevertheless, these tumour models enable mimicking some aspects of the bone microenvironment.

In addition, there is evidence that human PCa cell respond differently to human versus mouse bone. Several studies where human bone had been implanted in mice demonstrated that human PCa cells preferentially home to human bone implants rather than to mouse bone [232]–[235]. This unexpected behaviour is thought to reflect species–species differences between the cytokines and homing molecules expressed by human bone marrow cells relative to murine bone marrow cells. As PCa bone metastasis appears to have a number of species-specific requirements, modelling this process in mice remains challenging.

In summary, studies using human PCa cell implantation in mice can replicate physiological conditions regarding some aspects such as molecular and cellular mechanisms of cancer development and progression. However, they cannot model all aspects of the cross-talk and interaction between human tumour cells and all other human cell components, due to the fact that the majority of the cellular and matrix microenvironment is of mouse origin [236]. This has motivated the evolution of more sophisticated humanised mouse models, such as generating humanised bone microenvironment in immunodeficient mice and establishing human haematopoietic systems in these mice [237], [238].

In addition to the technical limitations of existing *in vivo* models, mouse models tend to be expensive and time consuming. This has motivated the development of *in vitro* models that can be assembled from all human cells.

1.6.2 *In vitro* models of PCa

Due to the complexity, it has been challenging to recapitulate the PCa tumour microenvironment *in vitro* either in primary or metastatic sites. However, there are a vast number of studies that have tried to recapitulate interactions between particular cell types involved in the cancer-invaded microenvironment [239]. Bone marrow niche mimicking is particularly challenging due to its complexity. Several researchers studied the effect of bone marrow stromal cell secreted chemokines on the proliferation and migration of PCa cells using Boyden chambers as one of the widely-used tools to demonstrate indirect cellular interactions. Bone marrow stromal cells co-cultured with PCa cells express several factors that enhance tumour cell growth and invasion [240]. PCa cells were found to have boosted migration capacity in the presence of bone marrow-derived mesenchymal stromal cells' conditioned media [241]. This enhanced migration was reversed when SDF-1 antagonist was supplemented to the conditioned media, which implies the motility enhancement activity of SDF-1 on PCa cells.

For more complex models, tissue-engineering platforms were involved in the field of stromal-cancer cell interaction [242]. A recent study observed increased migration and proliferation of cancer cells directly co-cultured with osteo-differentiated bone marrow-derived MSC [243]. Moreover, an increased proliferation of cancer cells was observed in the tri-culture of cancer cells with stromal cells and endothelial cells. Bersini and colleagues [239] tri-cultured MSC-derived osteoblasts and endothelial cells with a cancer cell line to study their migration and invasion capability in a 3D vessel-like microfluidic system.

In another study, primary human bone cells were grown on scaffolds to form tissue-engineered bone constructs. Subsequently, the bone constructs were co-cultured with PCa cells grown as three dimensional spheroids in hydrogel to recapitulate PCa invaded bone microenvironment. The proliferation of cancer cells increased compared to monocultures. Similar to the primary tumour microenvironment, TGF-β was one of the most activated upstream regulators in PCa progression in this multi-cellular bone metastatic PCa model [244].

1.7 DRUG-TESTING PLATFORMS

Successful development and selection of a novel potent anti-tumour drug is a long process that includes several stages of preclinical studies and clinical trials [245]. Drug attrition rates in oncology is greater than other areas of therapeutic focus [218]. Out of many promising drug candidates in the preclinical development of anti-tumour drug, only 5% are licensed after showing sufficient efficacy in clinical trials [246], [247]. The high failure rate is partly due to limitations of preclinical tools that poorly mimic the physiological conditions and limit early stage prediction.

In this section, tissue culture techniques will be discussed as a fundamental stage in preclinical *in vitro* studies.

1.7.1 Two dimensional (2D) tissue culture

Preclinical *in vitro* PCa studies are usually performed using traditional two dimensional (2D) tissue cultures, combined with some techniques such as wound healing and Transwell migration assays [248]. Since Harrison et. al., (1907) [249] established the first cell culture of neural tissue, substantial improvements have been achieved on the cell culture techniques in the last century. However, correlation of results from 2D tissue culture studies and *in vivo* scenarios has been questioned; and subsequently a wide recognition of the limitations of 2D cultures has been confirmed [247], [250].

Multiple differences have been observed between cells grown in 2D cultures and what is observed *in vivo*, such as differences in cell polarity, cell morphology, receptor expression and cellular architecture. Typically, in 2D cultures, tissues are grown as cell monolayers on a flat surface. Therefore, cell-cell interaction and extracellular matrix contacts are limited in 2D cultures. Not only is the plastic material interaction a poor biological mimic, the interaction with the underlying surface results in artificial polarization of the cells [251]. Adhesion to the ultra-rigid 2D surface results in the cytoskeletal tension in the cell being many fold greater than under physiological conditions [252]. The high tension induces Rho/ROCK signalling and this stimulates a number of cascades including accelerated cell

proliferation [253]. This increased cell proliferation is an important consideration in cancer drug-testing as this makes the cells hypersensitive to chemotherapeutics that target proliferating cells [254]; this artefact results in misleading results being generated when using traditional 2D tissue culture. Moreover, unlike 3D cultures, 2D cultures cannot mimic acinar formation which is a key element of the invasive behaviour of cancerous epithelial cells [255].

To a certain degree, 2D tissue culture studies significantly improved our understanding of the different mechanisms that occur in PCa, but it was not enough to give rise to a powerful model of PCa or, the more complicated, bone metastatic PCa [242]. In trials to develop a physiological mimic, the functional unit of tissue must be considered rather than single cells. Therefore, alternative tissue culture techniques are being developed, specifically 3D tissue culture techniques [256].

1.7.2 Three dimensional (3D) tissue culture

In the physiological status, cells exist within a 3D environment known as the extracellular matrix (ECM) which facilitates cell-cell contact and alters nutrients and drug transport [257]. To mimic this *in vitro*, various 3D tissue culture techniques have been developed. The main goal of 3D culture techniques is the formation of cell aggregates in environments where cell–cell interactions dominate over cell–substrate interactions, through aggregation of cells maintained in close proximity to each other. Cell aggregates have many different names in the literature, such as cell spheroids, microtissues and micromass [258]–[260].

Ideally, a 3D culture system that is suitable for drug-screening should have the following criteria: simple technique with uncomplicated processing, not expensive or require specialized equipment, not labour-intensive, create homogenous cell aggregates that are easily accessible. This ideal 3D culture system should permit the ECM accumulation in 3D architecture. The 3D culture technique should enable the control of cell aggregate size to facilitate mimicking different regions of the tumour for drug penetration studies. Finally, high throughput screening should be feasible with this ideal 3D culture system. In this section, the feasibility of utilising the commonly used 3D culture techniques as a drug-testing platform will be discussed.

Hanging drop technique: this method allows the formation of cell aggregates by using a small aliquot of single cell suspension pipetted into wells, then the tray is inverted and the aliquots of cell suspension turn into hanging drops. The cell aggregates at the tip of the drop are kept in place due to the surface tension [261]. The reproducibility of this technique is relatively high and the produced cell spheroids are homogenous and easily accessible [262]. However, this method is labour intensive and its utilisation as a drug-testing platform may not be viable [263]. This method can only accommodate small volumes (up to 50 μl including the drug to be tested), as it is the surface tension that keeps the drop hanged cannot support larger volumes.

Agitation-based technique: In this technique, cells are prevented to adhere to the container walls due to continuous motion of the cell suspension by gentle stirring as in spinner flask bioreactors, or by rotation of the container as in rotational culture systems [264]. This method enables large scale production of easily accessible cell aggregates [265], [266]. However, this method has several drawbacks that make it not ideal for drug-testing, such as uncontrolled cell aggregate size, requirement of specialized equipment and the shear force exposure that can affect cell behaviour [264], [265], [267].

Matrix- and scaffold-based techniques: In the matrix-based technique, cells are embedded in/on artificial or natural matrices to enhance cell organisation in 3D structure. As a natural matrix, Matrigel is a widely used animal-originated laminin-rich extracellular matrix (ECM) in 3D tissue culture [268]. However, Matrigel has many characteristics that limit its use in high throughput drug-screening systems. Due to its biological nature, Matrigel contains undefined constituents and growth factors. Cell aggregates in Matrigel tend to be not uniform. Additionally, batch-to-batch variation of Matrigel make it difficult to compare and correlate results from different research groups [242], [269].

Advances in biomaterials and tissue engineering enabled the manufacture of scaffold-based models using chemically-defined hydrogels, such as collagen, laminin, alginate and biodegradable materials [257]. In reality, 3D porous scaffolds often only offer a curved 2D surface and therefore are not truly 3D cultures [270]. When hydrogels are used with the scaffold-based models, the cells interact with the gel rather than with each other [271]. Whilst this may mitigate against the artificial

polarity introduced by 2D surfaces, no gel matrix truly mimics natural matrices and actual cell-cell contact can again be minimal.

Microfluidic platforms: In this method, microchannels are used to deliver fluids to selected areas of patterned platform [272], [273]. Using the microfluidic patterning technique, several platforms have been developed with non-adherent substrates that permit the formation of cell aggregates [274][275]. In such platforms, the fluids transfer can be achieved by capillary forces or by pressure using specialized pumps. The access to the cell aggregates can be problematic in these platforms [273]. Although there are many tissue and tumour models have been studied using microfluidic platforms, there are major challenges in recapitulating *in vivo*-like environments with enhanced architectural and cellular complexities [276].

Forced-floating technique: Similar to the hanging drop method, aliquots of single cell suspension is dispensed in the wells of a tissue culture plate. However, the vessel surface is modified to prevent cell attachment, resulting in forced-floating cells which tend to adhere to one another forming a cell aggregate [277]. A number of synthetic materials have been developed for surface modifications to reduce cell attachment and produce a cell-repellent surfaces, such as the most widely used polyethylene glycol (PEG)-based materials and poloxamers polymers (also known as Pluronics) (reviewed in [272]). This 3D culture technique has many advantages due to the relatively simple processing, the inexpensive materials used, the high reproducibility and the compatibility with high throughput testing. However, the surface coating step before cell seeding can consume time and can be labour-intensive process particularly in large-scale experiments [256], [278].

For more advanced 3D culture platforms, the microwell platforms can be manufactured by soft lithography techniques such as Microcontact Printing. Among the various 3D tumour models reviewed recently [279], the microfabricated platform was found to provide one of the most powerful tools in cancer research. In such platforms, the cells are cultured in micro-patterned non-adherent platforms "microwells" to form cellular aggregates "microtissues" varying in size and shape according to the seeded cell number and the geometry of the platform.

Scaffold-free 3D cell aggregates have long been regarded as the gold standard for *in vitro* drug-testing [251]. Furthermore, it is now well-known that the tumour microenvironment plays a crucial role in cellular behaviour and fate [280], [281].

Therefore, developing a 3D *in vitro* model of PCa that consider the cancer microenvironment complexity is urgently needed. Such a powerful model can help studying bone metastatic PCa biology and serve as a therapeutic testing platform for more efficient evaluation of next generation therapeutics.

1.8 HYPOTHESIS AND AIMS

The **OVERALL AIM** of my Thesis was to develop a more effective *in vitro* 3D microtissue PCa model system that mimicked the bone marrow niche microenvironment and PCa metastatic microenvironment, thus enabling elucidation of how bone marrow niche cell composition influences PCa cell growth and subsequent drug sensitivity.

I **HYPOTHESIZED** that it would be possible to mimic prostate cancer cell interaction with the bone marrow niche *in vitro* through the use of a microtissue model. Specifically, I hypothesized that bone marrow niche cells and PCa cells assembled into microtissues, using a high throughput microwell system, would enable replication of the metastatic bone marrow niche. Using the microwell system, I executed the following interlinked aims:

AIM 1: Characterisation of bone marrow-derived stromal cells in a high throughput microwell platform (Chapter 2);

AIM 2: Characterisation of PCa cells in an improved high throughput microwell platform (the Microwell-mesh platform) that retains microtissues within discrete microwells and its utilisation as a drug-testing platform (Chapter 3);

AIM 3: Development and utilization of a high throughput cell viability assay that enables cell-specific quantification in a co-culture system (Chapter 4) and;

AIM 4: Development of co-cultures of PCa cells and bone marrow-derived stromal cells using the Microwell-mesh platform and utilising the cell-specific viability assay for drug-screening in co-cultures (Chapter 5).

Chapter 2: Does 3D culture support osteogenic differentiation of mesenchymal stromal cells?

2.1 ABSTRACT

Bone marrow-derived mesenchymal stromal cells (BMSC) represent a promising candidate in regenerative medicine applications due to their multipotent differentiation capacity, paracrine signalling-driven regenerative and immuno-modulatory capacities, and viability as an off-the-shelf allogeneic transplantable cell product. BMSC *in vitro* expansion cultures are typically performed using 2-dimensional (2D) monolayers. However, 3-dimensional (3D) cultures can potentially provide a superior physiological mimic, and generate 3D tissues that are more suitable for use in tissue engineering applications. The recent development and commercialization of high throughput 3D culture platforms are accelerating our capacity to characterise and optimise 3D BMSC cultures. In this study, an in-house fabricated microwell platform was used to efficiently manufacture thousands of multicellular BMSC spheroids. BMSC spheroid size relative to cell number, proliferation and differentiation capacity were characterised and contrasted against 2D controls. We specifically characterised the capacity of bone morphogenetic protein 2 (BMP-2) to improve the osteogenic capacity of BMSC spheroids. While the trilineage differentiation capacity of 3D spheroids remained similar to 2D monolayer cultures, our results reveal that cells in 3D spheroids demonstrated a reduction in cell proliferation and concurrent reduction in cellular size over time. BMP-2 enhanced osteogenic outcomes in both 2D and 3D cultures, however calcium accumulation in 2D monolayer cultures was greater than in 3D spheroid cultures. In summary, BMSC spheroids manufactured in microwells offer a powerful tool to efficiently study *in vitro* 3D cell behaviour in multiple simultaneous replicate tissues and in geometry that better replicates the *in vivo* environment.

2.2 INTRODUCTION

Mesenchymal stromal cells (MSC) are a rare cell population that are widely distributed in the connective tissue of most adult organs, where they appear to play a

critical role in tissue repair and regeneration [282]. MSC have been effectively isolated and characterised from many adult tissues, and most commonly from bone marrow aspirates [283], placenta [284] and adipose tissue [285]. The defining characteristics of MSC have been described as including plastic-adherence, expression of specific expression profile of cell surface markers and the ability to differentiate to the mesodermal lineages, including osteogeneic, chondrogenic and adipogenic [286]. The multi-potential and immune-modulatory potential of MSC suggests that these cells may be able to contribute to a very broad range of clinical applications, from direct tissue regeneration [189], to disease modelling, and cell-based therapy which exploit MSC paracrine signalling to stimulate endogenous repair processes or modulate inflammatory processes [287], [288].

Bone marrow-derived MSC (BMSC) are increasingly being studied in mesodermal tissue repair applications, such as bone and cartilage regeneration [289], [290]. Musculoskeletal defects, including damaged cartilage and bone defects, represent an enormous healthcare cost burden and are obvious first target for MSC-based therapies [291]. Repair of cartilage remains extremely challenging using any methodology, whilst the gold standard for bone defect repair or bridging remains the use of bone autografts [292]–[295]. Bone autograft material is limited in its supply, and its harvest is associated with donor site morbidity and phantom pain [296]. Considerable pre-clinical data, and some clinical data, already suggest that BMSC can be utilized in place of autografts to enable effective bone defect repair [238], [297]–[300]. Much of the field is now focused on how to guide BMSC to most effectively contribute directly or indirectly (paracrine signalling) to bone defect repair [301]–[305].

Among the various growth factors explored to boost osteogenesis, bone morphogenetic proteins (BMPs) are the most studied, and have been shown to enhance bone formation both *in vitro* and *in vivo* [306]. In 2002, BMP-2 gained humanitarian FDA approval for use in specific orthopaedic applications [307]–[310]. While powerful, clinical use of BMP-2 is associated with adverse outcomes such as increased bone resorption, cyst formation, hematoma formation or ectopic bone formation [291], [311], which has limited clinical uptake in some instances. Nevertheless, despite the FDA issuing a warning on life-threatening complications of BMP-2 in 2008 [312], the overall frequency of BMP-2 use in the clinic continues to

rise [313]–[315]. An alternative to delivering BMP-2 directly into patients, may be to use BMP-2 to guide BMSC differentiation *in vitro* and then deliver osteo lineage-committed cells into patients to regenerate localised bone defects.

BMSC are generally expanded in 2-dimensional (2D) monolayer cultures, and then osteogenic differentiation is frequently tested or characterised in 2D monolayers. This differentiated, and mineralised, cell product cannot be easily harvested and transplanted into a patient. New technologies, which enable the high-throughput manufacture of 3D tissue spheroids, offer the potential for expanded MSC to be organised into microtissue spheroids and differentiated into osteoblasts. These microtissue spheroids could be assembled into larger tissues and/or even directly injected into bone defect sites.

BMSC organised into spheroids behave differently than those organised into 2D monolayers [316]–[318]. While the differentiation of 2D BMSC monolayers in medium supplemented with BMP-2 has been thoroughly characterised, the same cannot be said for how 3D BMSC spheroids respond to BMP-2 *in vitro*. Understanding this basic BMSC-BMP-2 biology is a key first step before being able to fully exploit 3D BMSC spheroids as bone tissue models, or as injectable bone tissue repair therapeutics. Herein we used a high throughput microwell platform to manufacture hundreds of uniform BMSC spheroids, and characterise their differentiation potential with a specific focus on their response to BMP-2 medium supplementation.

2.3 MATERIALS AND METHODS

BMSC isolation

Human bone marrow aspirates were collected at the Mater Hospital (Brisbane, Australia) from fully informed and consenting healthy volunteer donors. In accordance with the Australian National Health and Medical Research Council's Statement on Ethical Conduct in Research Involving Humans, ethical approval was granted through the Mater Health Services Human Research Ethics Committee and Queensland University of Technology Ethics Committee (number: 1000000938). Aspirates were collected from the iliac crest of volunteer donors. Mononucleated cell isolation was achieved by density gradient centrifugation, using Ficoll-Paque Plus (GE Healthcare), as previously described [319]. Bone marrow aspirates were

diluted 1:2 with PBS (Thermo Fisher) containing 2 mM EDTA. Then the diluted sample was carefully overlayed on top of the Ficoll-Paque plus and centrifuged for 30 minutes at 400x*g*. The mononucleated cells collected from the interface were then washed, resuspended in low glucose Dulbecco's modified Eagle's medium (DMEM-LG) supplemented with 10% fetal bovine serum (FBS, Thermo Fisher) and 1% penicillin/streptomycin (Thermo Fisher). Cells were then cultured overnight in a humidified incubator containing 5% CO_2 with 20% O_2 atmosphere at 37°C. Tissue culture plastic-adherent cells were enriched by removing the medium containing non-adherent cells, and fresh culture medium added to each flask. Subsequent BMSC expansion was performed in 2% O_2 and 5% CO_2 atmosphere at 37°C. Cells were passaged when the monolayer reached approximately 80% confluency using 0.25% Trypsin/EDTA (Thermo Fisher). All experiments were performed using BMSC between passage 2 and 5.

Microwell plate fabrication

An in-house fabricated microwell platform was used to manufacture multicellular spheroids. The fabrication of polydimethylsiloxane (PDMS, Slygard) microwell arrays was performed as described previously [258], [290]. Briefly, liquid PDMS (1:10 curing agent to polymer ratio) was permitted to cure over a patterned polystyrene mold having the negative of the desired microwell pattern for 1 hour at 80°C. A sheet of PDMS with the microwell array pattern cast into it (each microwell had dimensions of 800*x*800 square microwells and 500 μm in depth) was produced and peeled from the moulds. PDMS discs of ~1 cm^2 were punched from the PDMS sheets using a wad punch. Individual 1 cm^2 microwell inserts were then glued into 48-well culture plates. Plates with microwell inserts were submerged in 70% ethanol for 1 hour for sterilisation, followed by rinsing 4 times with Dulbecco's phosphate buffered saline (DPBS). To prevent cell adhesion to the PDMS during culture, the PDMS microwell inserts were soaked in 0.5 mL of sterile solution of 5% Pluronic-F127 (Sigma-Aldrich) in DPBS for 5 minutes and then rinsed 3 times with DPBS before cells were seeded.

2D and 3D culture establishment

Single cell suspensions were added to plates with or without microwell inserts to form 3D cell spheroids or 2D cell monolayers, respectively. Figure 2.1 illustrates a schematic representation of 2D and 3D cultures. Each well in a 48-well plate (Nunc)

inserted with PDMS patterned-discs contained ~150 microwells. The number of cells per spheroid could be controlled by adjusting the total number of cells added in suspension over the PDMS inserts during seeding. For example, as there were ~150 microwells, a suspension of 90,000 cells generated 150 spheroids of 600 cells each (Figure 2.1c). Specific sizes were used for subsequent assays based on initial screening studies. For BMSC characterization in 3D spheroids, 300 and 600 cells/spheroid were used. For BMSC differentiation and BMP-2 treatment experimets, 1000 cells/spheroid was used.

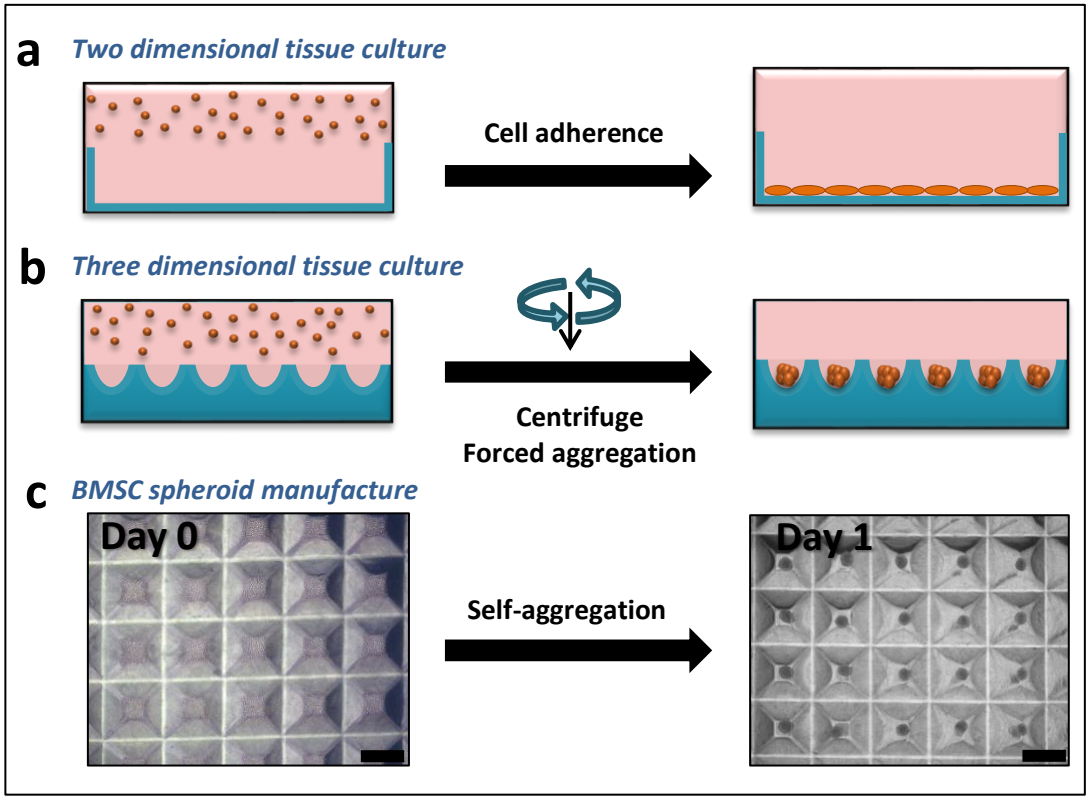

Figure 2.1. Two and three dimensional culture platform. (a, b) Illustration of 2D and 3D culture platforms. **c)** Bright field images of BMSC cultured in the 3D platform at day zero and after one day of incubation, resulting in self-aggregation of the BMSC into spheroids. Scale bar = 500 µm.

BMSC flow cytometry characterization and trilineage differentiation

The isolated cells were characterized by flow cytometry for the expression of BMSC surface antigens; CD44, CD90, CD105, CD73, CD146, CD45, CD34 and HLADR [286]. Cells were trypsinised at passage 2 and stained with fluorescent-conjugated antibodies or isotype controls as per the manufacturers' instructions

(Miltenyi Biotec). Stained cells were washed and resuspended in MACs buffer (Miltenyi Biotec) then flow cytometry was performed on a BD LSRII flow cytometer (Becton Dickinson). Data was analysed using FlowJo software (TreeStar, USA).

Mesodermal trilineage differentiation capacity was characterised by culturing the cells in osteogenic, adipogenic and chondrogenic induction medium for 14 days. The medium consisted of high glucose DMEM media (DMEM-HG; Thermo Fisher) containing 100 μM sodium pyruvate, 1X Gluta-Max (Thermo Fisher), 100 U/ml penicillin, and 100 μg/mL streptomycin (1% P/S; Thermo Fisher), in addition to the supplements to induce trilineage differentiation which are listed as following: for osteogenesis, 10% FBS, 100 nM dexamethasone (Sigma-Aldrich), 50 μM L-ascorbic acid 2-phosphate (Sigma-Aldrich) and 10 mM β-glycerol phosphate (Sigma-Aldrich); for adipogenesis, 10% FBS, 10 μg/mL insulin (Sigma-Aldrich), 1 μM dexamethasone (Sigma-Aldrich), 200 μM indomethacin (Sigma-Aldrich) and 500 μM 3-isobutyl-1-methyl xanthine (Sigma-Aldrich); and for chondrogenesis, 10 ng/mL TGF-β1 (PeproTech), 100 nM dexamethasone (Sigma-Aldrich), 200 μM L-ascorbic acid 2-phosphate (Sigma-Aldrich), 40 μg/mL L-proline (Sigma-Aldrich) and 1% ITS-X (Thermo Fisher). Culture medium was replaced with fresh media twice per week.

To study the osteogenesis in 3D cultures, a serial dilution of 200, 400, 600, 800, 1000 and 2000 cells/spheroid were cultured for 14 days in osteogenesis media and images were captured using an Olympus DP26 digital camera (Japan) and diameters of 50 spheroids were measured using Microscopy software (CKX14, CellSens Entry). Then, bone-like microtissues were collected and DNA and calcium quantitation were performed.

For BMP-2 treatment, BMSC were seeded in 2D monolayers ($60x10^3$ cells/cm^2) or 3D spheroids (1000 cells/spheroid) and cultured in DMEM-HG media containing 100 μM sodium pyruvate, 1x GlutaMax (Thermo Fisher), 10% FBS, 100 U/ml penicillin, and 100 μg/mL streptomycin (1% P/S; Thermo Fisher) for the control samples. For the test samples, the same medium containing one/all of the osteogenesis induction medium supplements (as indicated previously in this section) in the presence or absence of 10 ng/mL BMP-2 (INFUSE Bone Graft Kit, Medtronic) was used. A BMP-2 dose dependent response was initially tested (Supplementary Figure 2.1) and 10 ng/mL BMP-2 was used in further studies.

DNA and Calcium quantitation

The Quant-iT PicoGreen dsDNA assay (Thermo Fisher) was performed as per the manufacturers' instructions to fluorescently measure the double stranded DNA content of viable cells. The TE buffer (20 mM tris-HCl, 2 mM EDTA and 1% Tween 20) was used to digest the cells. The samples were incubated with the PicoGreen reagent before reading on a plate reader (BMG Omega LABTECH) with 485 nm excitation and 520 nm emission. The corresponding DNA content was estimated based on comparison with a standard curve generated using ʎ DNA.

Calcium content was measured chemically using the colorimetric method described by Van den Dolder *et al.* [320]. Cultures were incubated overnight in 10% acetic acid with shaking. Samples were allowed to react with o-cresolphthalein (Sigma-Aldrich) complex. The optical density of the final reaction product was measured using a Multiskan Go Spectrophotometer (ThermoFisher). Calcium chloride serial dilutions were used to generate a standard curve and the corresponding Ca^{2+} content was calculated using the standard curve. Values of Ca^{2+} content were normalized to the corresponding DNA content of the same sample.

BMSC spheroids over extended culture

BMSC were seeded in 3D platforms in two densities; 300 and 600 cells/spheroid and cultured for 14 days. At 1, 3, 5, 7, 9, 12 and 14 days, images were captured using an Olympus DP26 digital camera (Japan) and diameters of 50 spheroids were measured using Microscopy software (CKX14, CellSens Entry). At the same time points, spheroids were collected for DNA quantification. At days 1, 7, and 14, spheroids were collected for immunofluorescent staining.

Quantification of BMSC diameter in 3D and 2D cultures

BMSC were cultured in 2D ($60x10^3$ cells/cm^2) and in 3D (600 cells/spheroid) for 1 and 8 days. On the day of collection, cultures were dissociated using 0.25% Trypsin/EDTA (Thermo Fisher). For 2D cultures, cell monolayers were rinsed with DPBS and covered with 0.25 ml of Trypsin/EDTA. For 3D cultures, cell spheroids were collected into tubes, centrifuged to pellet the spheroids, rinsed with DPBS and incubated with 0.25 ml Trypsin/EDTA. All cultures were incubated at 37ºC for approximately 30 minutes with frequent mechanical agitation to ensure 3D spheroid dissociation. Cells were collected as a single cell suspension after being passed

through a cell strainer (35 µm). Solutions of cell suspension in MACs buffer (Miltenyi Biotec) were then analysed using a CytoFlex flow cytometer (Beckman Coulter). Fluorescent beads (Latex beads, Coulter) with defined sizes were used as controls. Data was analysed using FlowJo software (TreeStar, USA).

Histological and immunofluorescence staining

At the end of the culture period, monolayer cultures were fixed using 4% paraformaldehyde (PFA) for 15 minutes at room temperature then treated with the appropriate stain(s) (see below). Spheroids were harvested by vigorously flushing the media on the top of 3D platforms and then collecting the suspended spheroids into low-binding Eppendorf tubes. Cell spheroids were fixed with 4% PFA for 30 minutes at room temperature, followed by permeabilisation using 0.5% Triton X-100 in DPBS for 30 minutes at room tempetaure.

To generate histological sections, spheroids were collected and snap frozen in Tissue-Tek Optimal Cutting Temperature (OCT) solution (Sakura Finetek). Frozen tissue sectioning was performed using an HM525 NX Cryostat (ThermoFisher) to obtain 7 µm sections which were placed onto poly-lysine coated slides (Thermo-Scientific) and preserved frozen for later processing.

Fixed monolayers, spheroids or cryosections were stained for extracellular bone mineralization or intracellular oil droplets. Alizarin Red S stain (Sigma-Aldrich) was used at a concentration of 1% to stain calcium deposits, while 1% Oil Red O stain (Sigma-Aldrich) was used to stain droplets. OsteoImage bone mineralization assay (Lonza) was used as per the manufacturer's instructions to stain the hydroxyapatite portion of bone-like nodules deposited by the 2D or 3D cultures. Histological sections of chondrogenic differentiated BMSC were stained with Alcian blue stain (Sigma-Aldrich) to detect glycosaminoglycans (GAG). Staining of nuclei was performed using 4',6-diamidino-2-phenylindole stain (DAPI, Sigma-Aldrich) or nuclear fast red (Sigma-Aldrich). To confirm staining specificity, parental undifferentiated BMSC cultured in maintenance media were fixed and stained with OsteoImage or Oil Red O and DAPI staining and represented the negative controls.

Immunofluorescent staining was performed for the mesenchymal protein marker vimentin in BMSC monolayers and proliferating cell marker Ki67 in BMSC spheroids. To prevent non-specific binding, 5% bovine serum albumin (Sigma-

Aldrich, A7906) was used in the blocking step for 1 hour at room temperature. For BMSC monolayers, samples were incubated overnight at 4°C with an Alexa Fluor 488-tagged fluorescent antibody for vimentin (Santa Cruz Biotechnology, sc-6260 AF488; 1:200). For BMSC spheroids, samples were incubated with Ki67 (Abcam, ab92742; 1µg/mL) overnight at 4°C followed by 1 hour incubation at room temperature with secondary antibody conjugated with Alexa Fluor 594 (Thermo Fisher; 1:500). DAPI stain (Sigma-Aldrich) was then used for 30 minutes at room temperature to stain nuclei. Stained monolayers were imaged using an Olympus microscope, while cell spheroids were imaged using a Ziess confocal microscope.

Osteoblasts Live/dead staining

Using the LIVE/DEAD® Viability/Cytotoxicity Kit (Thermo Fisher), *in situ* staining of osteoblast spheroids was performed in the microwell platform as per the manufacturer's instructions. Briefly, a staining solution with a final concentration of 4 µM ethidium homodimer-1 and 2 µM calcein-AM was made in a fresh culture media. Staining solution was added to the spheroids and incubated for 30 minutes at 37°C. Image acquisition was performed using an EPI-fluorescence microscope (Nikon).

Statistical analysis

Results are displayed as the mean values of two independent donors each with 4 biologically independent replicate cultures. The error bars indicate one standard deviation. Statistical significance of data was evaluated using two-way analysis of variance (ANOVA) in Prism software version 6.0 (GraphPad). The P values obtained in each comparison are represented by asterisks in graphs, with relative values detailed in the future captions.

2.4 RESULTS

BMSC characterization by flow cytometry

BMSC surface antigens expression was characterised by flow cytometry [286]. BMSC stained >95% positive for BMSC-associated markers (CD44, CD90, CD105, CD73 and CD146), and <5% positive for haematopoietic markers (CD45, CD34 and HLADR) (Figure 2.2).

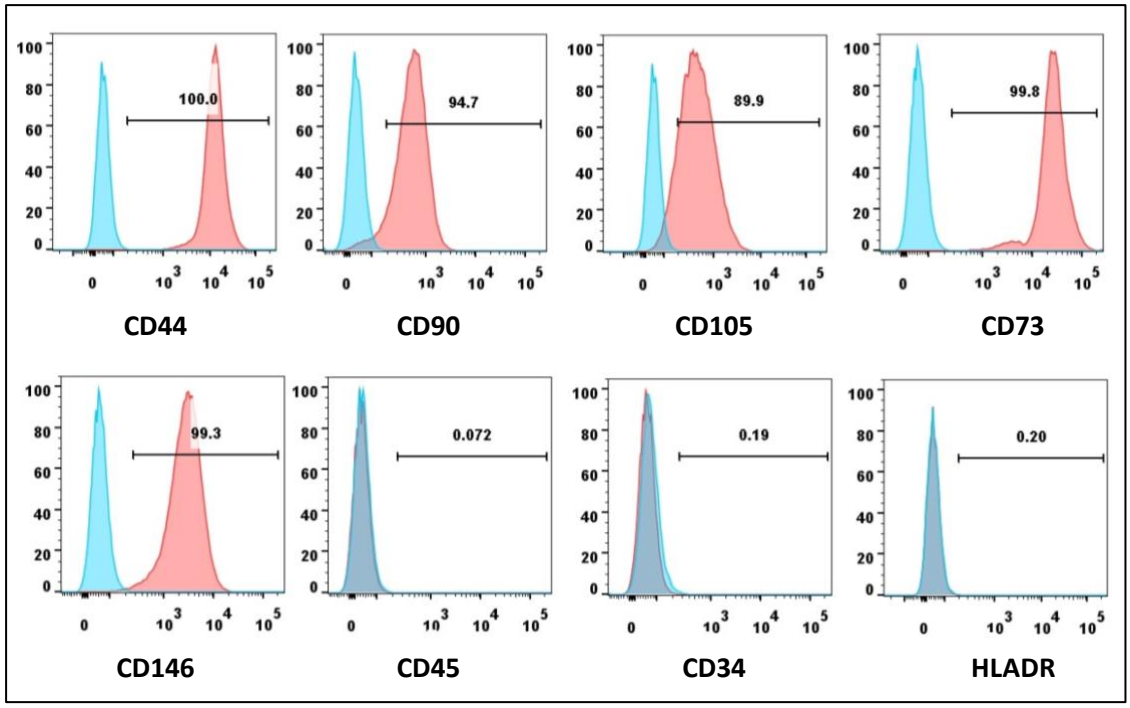

Figure 2.2. BMSC flow cytometry characterization. Cells were positive for MSC-associated markers (CD44, CD90, CD105, CD73 and CD146) and negative for haematopoietic markers (CD45, CD34 and HLADR). Positive marker expression was > 95% and negative marker expression was < 5% of the total cell population.

BMSC differentiation in 2D and 3D cultures

In 2D monolayers, BMSC were either expanded in maintenance medium or differentiated to osteoblast or adipocyte-like cells for 14 days (Figure 2.3). Expanded BMSC expressed the mesenchymal phenotype marker vimentin (green) (Figure 2.3d). Following 14 days of differentiation induction, formation of adipocytes or osteoblasts were confirmed and characterized by the accumulation of intracellular lipid droplets (Figure 2.3e) or formation of extracellular hydroxyapatite and calcium nodules (Figure 2.3f), respectively. In 3D cultures, BMSC differentiated to produce tissues of the three characteristic mesodermal lineages (Figure 2.4). Stained sections of osteogenically induced BMSC spheroids revealed hydroxyapatite deposition (Figure 2.4d), while sections of adipogenically induced BMSC spheroids stained positive for lipid vacuoles (Figure 2.4e). Sections from BMSC spheroids that had been induced with chondrogenic medium had cartilage-specific matrix (GAG) staining across the full width of the spheroids (Figure 2.4f).

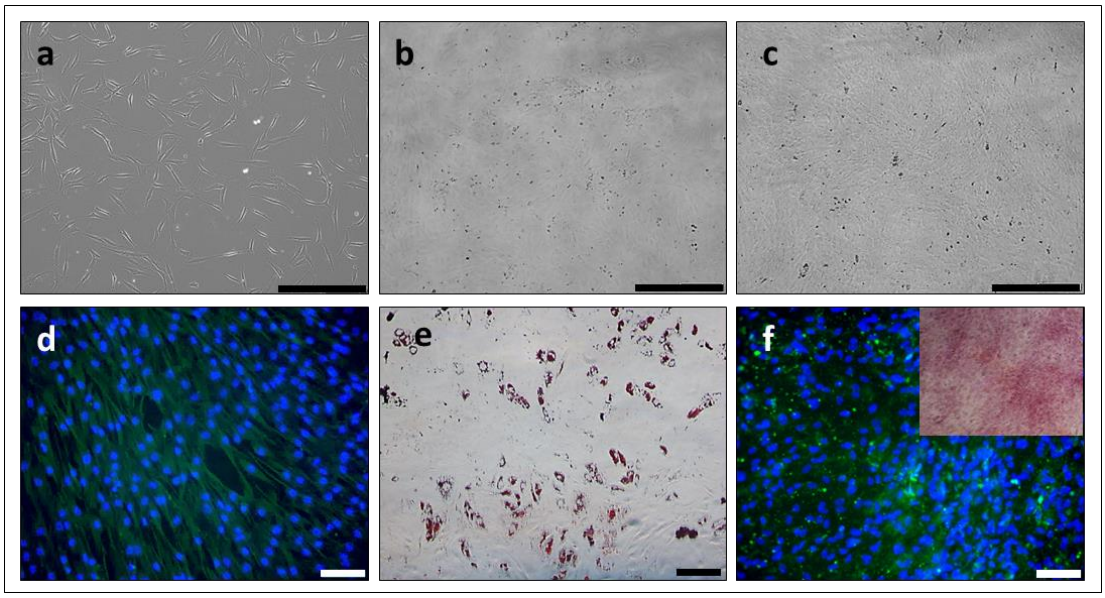

Figure 2.3. Parental and differentiated BMSC in 2D cultures. (a, b, c) Bright field images of BMSC maintained in expansion medium (parental), adipogenesis differentiation medium, and osteogenesis differentiation medium, respectively. **(d)** BMSC maintained in expansion medium stained for the mesenchymal marker, vimentin (green). **(e)** Intracellular lipid droplets stained positively with Oil Red O (red) in BMSC cultured in adipogenic medium. **(f)** Hydroxyapatite matrix stained positively with OsteoImage (green) in BMSC cultured in osteogenic medium. The inset shows that calcium nodules in these cultures stained positively with Alizarin Red S (red). Nuclei were stained with DAPI (blue); scale bars = 100 µm.

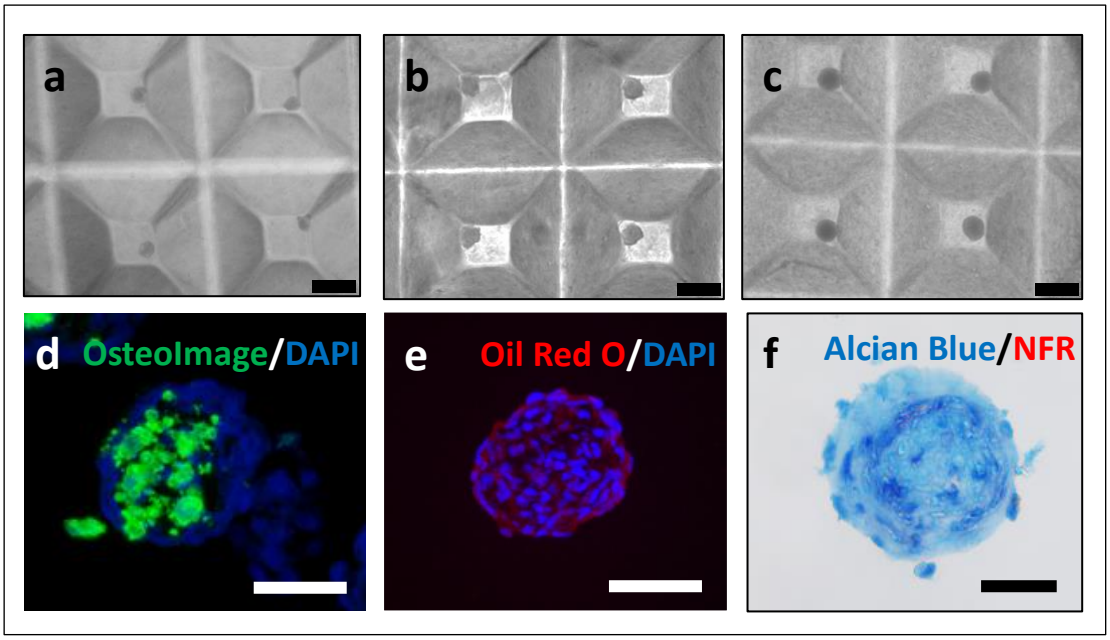

Figure 2.4. BMSC differentiation in 3D cultures. Spheroids were generated from 1000 BMSC. **(a, d)** BMSC differentiated down the osteogenic lineage, **(b, e)** BMSC differentiated down the adipogenic lineage, **(c, f)** BMSC differentiated down the chondrogenic lineage. **(a, b and c)** Bright field images of differentiated microtissues; scale bar = 200 µm. **(d, e and f)** Cryosections of BMSC spheroids differentiated to osteoblasts (stained for hydroxyapatite matrix, green), adipocytes (stained to reveal intracellular lipid droplets, red) and chondrocytes (stained to reveal GAG in matrix, blue), respectively. Nuclei were stained with DAPI in D and E and with Nuclear fast red in F. Scale bar = 50 µm.

BMSC spheroid size and cellular size analysis over extended cultures

We manufactured uniform BMSC spheroids of two sizes (300 and 600 cells/spheroid). Over 14 days of culture in maintenance medium (DMEM-LG + 10% FBS) there was a significant time-dependent reduction in spheroid diameter (Figure 2.5a, b). This was associated with a sharp decline in the cellular content of the 3D spheroids as determined by the temporal loss of DNA content in cultures (Figure 2.5c). By day 7 of culture, the 300 cells/spheroid mean diameter was equivalent to the 600-cell/spheroid mean diameter, and both cultures had equal DNA content (Figure 2.5b, c). Immunofluorescent staining of BMSC spheroids at different time points demonstrated a significant reduction in proliferating cell number with extended cultures. Noticeably, the initial cell number of BMSC spheroids appeared to have no influence on the cell proliferation behaviour in 3D geometry. Spheroids of

both sizes contained a core of non-proliferating cells, surrounded by a layer of proliferating cells on the outer surface of the spheroid (identified as Ki67 positive cells, Figure 2.5d). Moreover, the proliferating cells on the spheroid surfaces decreased over time in the cultures.

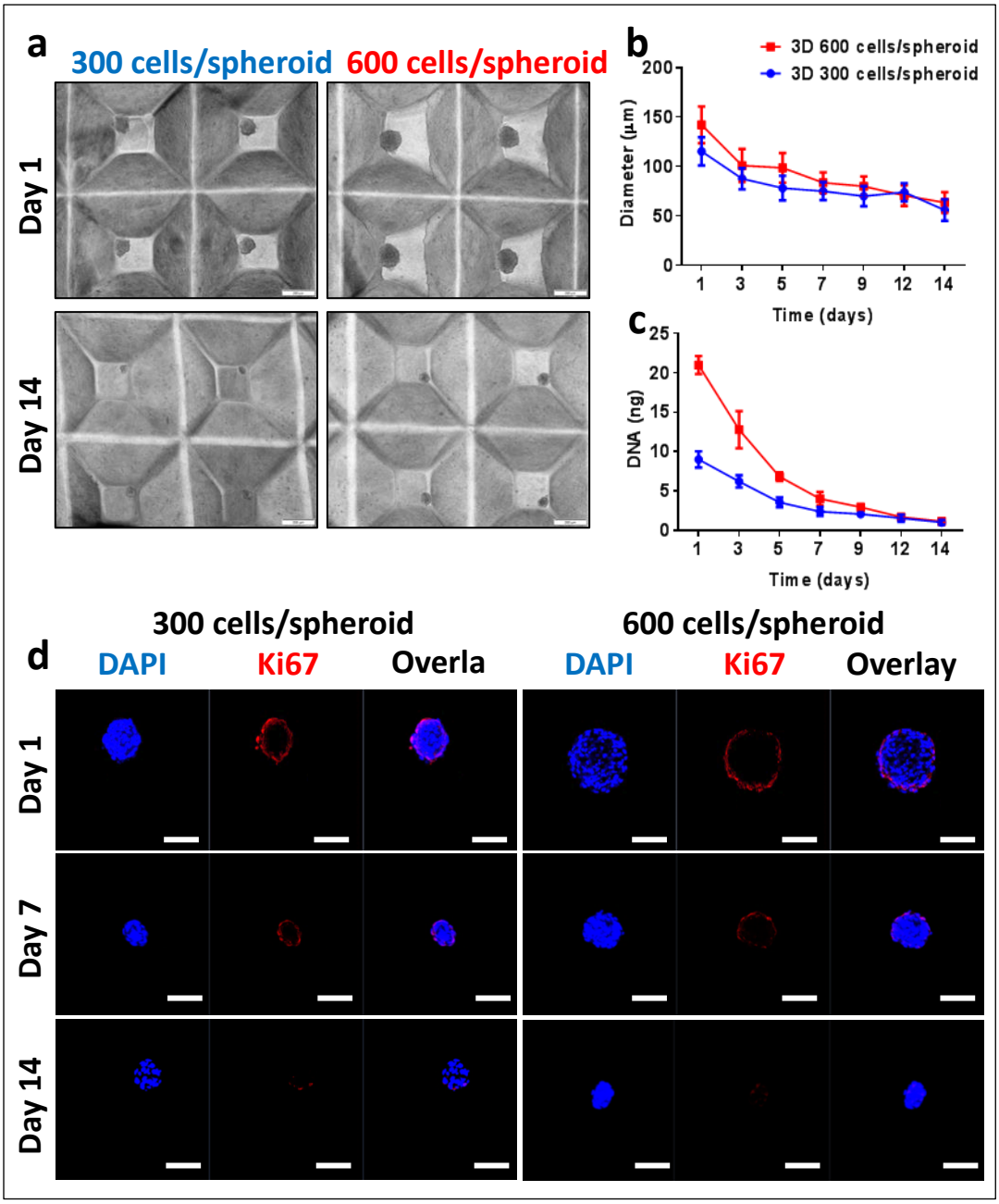

Figure 2.5. Characterisation of BMSC in 3D spheroids. BMSC were seeded in the 3D microwell platform to manufacture spheroids derived from 300 or 600 cells and cultured for 14 days. **(a)** Bright field images of spheroids were acquired at day 1 and 14. **(b)** Spheroid diameter and **(c)** DNA content were assessed every second day. **(d)** Confocal images of spheroids (300 and 600 cells/spheroid) stained with Ki67 (red) and nuclear stain (DAPI; blue) were acquired on day 1, 7 and 14 of culture. Spheroids in panel **a** were used to generate data of corresponding time points in panel **b** and **c**. Scale bar = 100 µm.

The diameter of individual cells was measured on day 1 and day 8 of culture. In both 2D and 3D cultures, a significant decrease in cell size was observed after 8 days of culture. The magnitude of the cell size decline was approximately the same in 2D and 3D cultures between day 1 and day 8 cultures. However, the total reduction in cell size was greatest in 3D cultures, with these cultures yielding the smallest cells. Following a single day of 3D culture, the average diameter of cells in 3D spheroids was less than in 2D cultures at day 1 and day 8 by approximately 20% and 10%, respectively (Figure 2.6a). Cell diameter in 3D spheroids continued to decline and had an average smaller diameter than that in 2D cultures at day 8. Bright field images of BMSC show confluent cell monolayers in 2D cultures and sharp decrease in spheroid size in 3D cultures after 8 days of culture (Figure 2.6b).

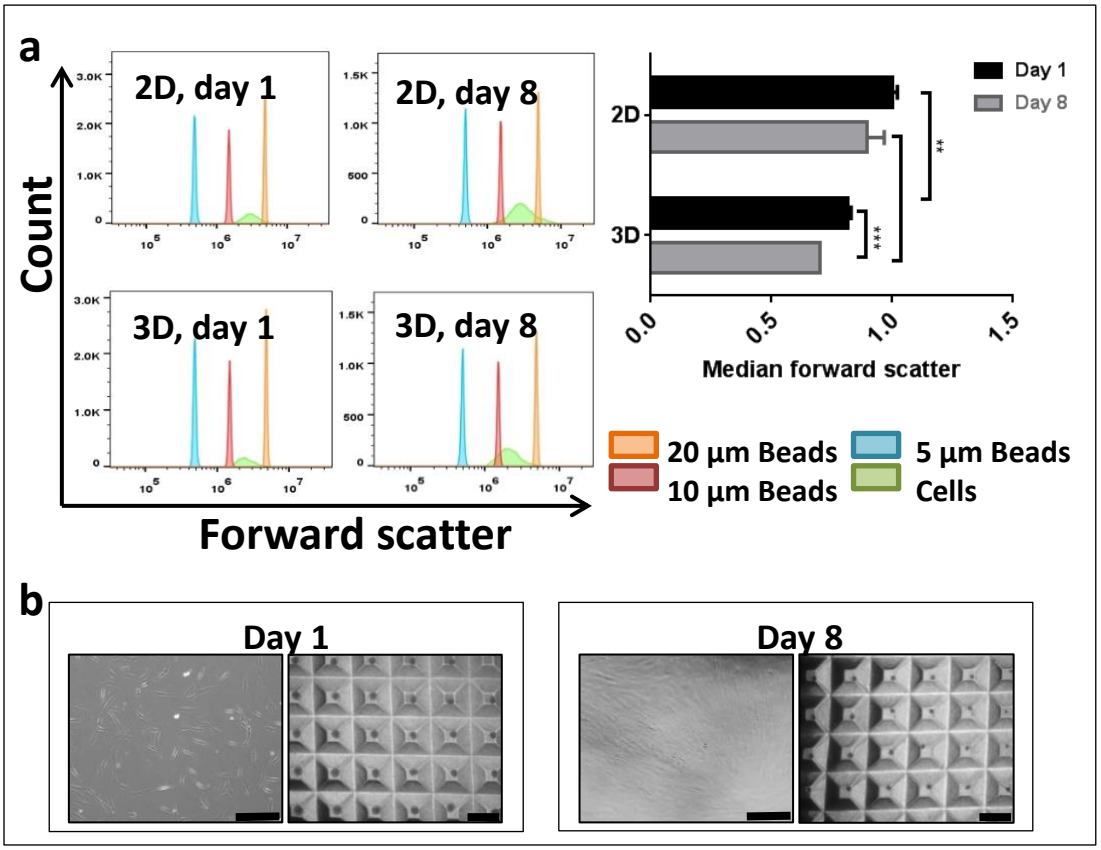

Figure 2.6. BMSC cell size in 2D and 3D cultures. (a) The size of cells cultured in 2D monolayers and 3D spheroids after 1 day or 8 days of culture was estimated using flow cytometry with reference fluorescent beads having defined diameters (20, 10 and 5 µm). The right panel represents a numerical illustration of the forward scatter median values of 4 replicates normalized to the 2D cultures at day 1. Statistical significance was calculated using two-way ANOVA (Dunnett's test). ** and *** indicate $P<0.001$ and $P<0.0001$, respectively. **(b)** Bright field images of cells in 2D monolayers (left) and 3D spheroids (right) at days 1 and 8 of cultures. Scale bar = 200 µm.

Osteoblast differentiation is associated with cell size decrease

When we tested the osteogenic-induced BMSC over 14 days of differentiation, a decrease in spheroid size was also observed. Therefore, a serial dilution of cells/spheroid was performed to characterise how spheroid size impacted osteogenesis. A greater initial cell number per spheroid resulted in larger spheroids at day-14 of culture (Figure 2.7a), but this effect was only seen up to 1000 cells/spheroid, thereafter doubling the cell number made no detectable difference on

spheroid diameter. Calcium accumulation indicated that the BMSC spheroids had undergone osteogenesis and formed bone-like tissues. DNA quantification was used as an indirect measurement of cell number. Surprisingly, the smallest spheroids produced the highest quantity of calcium per DNA; while the other 5 tested spheroid sizes demonstrated less than 50% of the Ca^{2+}/DNA content relative to the smallest spheroids (Figure 2.7b). Nevertheless, greater total calcium accumulation was associated with increasing cell number per spheroid. In every spheroid size, calcium nodules and live/dead staining revealed uniform distribution of accumulated calcium throughout the spheroid diameter and a live core at the centre of the spheroids (Supplementary Figure 2.2).

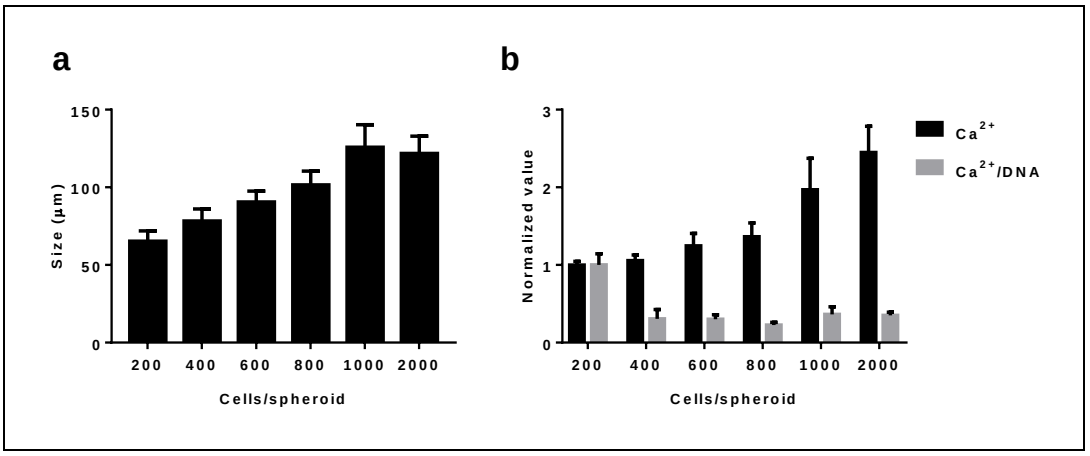

Figure 2.7. Osteogenesis in 3D cultures. (a) The diameters of osteoblast spheroids formed from 200, 400, 600, 800, 1000 and 2000 cells were measured. The size of bone-like microtissues could be controlled by varying the initial cell number per spheroid. Results represented as the mean diameter values of 50 spheroids. **(b)** Ca^{2+} and Ca^{2+}/DNA ratio was quantified in bone-like tissues and normalized to the spheroids formed from 200 cells/spheroid. Osteogenesis in 3D spheroids was associated with greater calcium accumulation with increasing cell number per spheroid. However, cells in smaller spheroids accumulated greater calcium per unit of DNA (Ca^{2+}/DNA). Similar results were obtained in replicate studies using 2 BMSC donors, each performed with 4 replicate cultures.

Effect of osteogenic media components and BMP-2 on calcium accumulation

BMP-2 is known to induce BMSC osteogenesis *in vitro*. In our 2D cultures, calcium deposition increased in a dose dependent manner when osteogenesis

induction culture medium was supplemented with BMP-2. However, there was no significant change in calcium content when BMP-2 was added to cells cultured in expansion medium (DMEM-LG + 10% FBS, Supplementary Figure 2.1). Thus, the component(s) contained within the osteogenesis induction media appeared to be necessary for BMP-2 to drive *in vitro* osteogenesis. Therefore, we tested the influence of the three individual components of the osteogenesis induction media with 10 ng/mL BMP-2 on the formation of calcium deposits.

In 2D monolayers, osteoblasts accumulated more calcium per ng DNA when cultured in complete osteogenic media with or without BMP-2 supplementation compared to cultures in maintenance medium alone (Figure 2.8). In the presence of BMP-2 in the osteogenic media, calcium accumulation was 20 fold greater than the osteogenic media alone. A significant increase in calcium per DNA was also observed in 2D monolayers cultured in maintenance media supplemented with BMP-2 and β-glycerolphosphate.

In 3D spheroids, osteogenic media alone induced a non-significant increase in the calcium accumulation per ng DNA (Figure 2.8). However, the BMP-2 supplementation caused a significant increase of calcium per ng DNA (>2 fold change). Similar to 2D cultures, BMP-2 alone or with one component of the osteogenic media has no ability to contribute to the calcium accumulation in 3D spheroids, except in case of β-glycerolphosphate where it induced >3 fold increase in calcium per ng DNA in 3D spheroids. In contrast to 2D cultures, cell spheroids cultured in osteogenic media failed to retain calcium matrix.

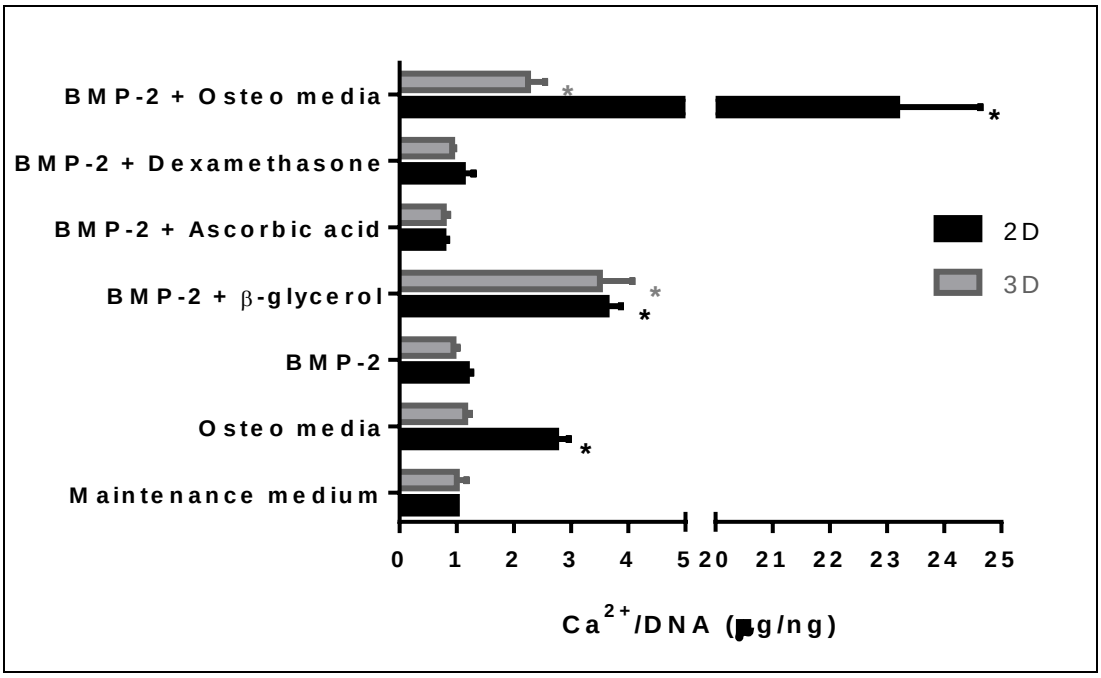

Figure 2.8. Effect of osteogenic media components and BMP-2 on calcium accumulation in 2D monolayers and 3D spheroids. Calcium content relative to total DNA content was assessed in 2D monolayer and 3D spheroids of BMSC cultured in DMEM-HG media (Maintenance medium), DMEM-HG media plus all osteogenesis induction media supplements (Osteo media), 10 ng/mL BMP-2 (BMP-2) alone, 10 ng/mL BMP-2 plus all osteogenesis induction media supplements (BMP-2 + Osteo media) or plus the individual osteogenesis induction media supplements (β-glycerol phosphate, β-glycerol; L-ascorbic acid 2-phosphate, Ascorbic acid and dexamethasone, Dexamethasone). Similar results were obtained in replicate studies using 2 donors each containing 4 replicate cultures. Statistical significance was calculated using two-way ANOVA (Tukey's test). * indicates $P<0.0001$ compared to the corresponding control in maintenance medium.

Bone-specific matrix formation versus fat-specific oil droplet accumulation

To investigate osteogenic matrix in the tested conditions, 2D monolayers and 3D spheroid sections were stained for hydroxyapatite (Figure 2.9 and 2.10). In 2D cultures, hydroxyapatite formation was observed in the presence of osteogenic induction medium both in the presence or absence of BMP-2, with a greater staining intensity in the presence of BMP-2 (Figure 2.9). However, the addition of BMP-2 to maintenance medium (DMEM-HG + 10% FBS) alone or in the presence of a single

component of osteogenesis media showed no evidence of hydroxyapatite formation in 2D cultures. In all culture conditions where BMP-2 was included, there was a positive staining with Oil Red O indicating the presence of oil droplets. The exception was cultures supplemented with β-glycerolphosphate only, with cultures demonstrating no direct evidence of differentiation to osteogenic or adipogenic lineages (Figure 2.9).

In 3D spheroid sections, hydroxyapatite matrix was detected in spheroids cultured in complete osteogenic media. However, the formation of bone-specific matrix was generally undetectable in the other culture conditions tested. But in the presence of BMP-2 in the osteogenic media, a very weak staining of hydroxyapatite was observed and it is distributed throughout the spheroid diameter (Figure 2.10). In contrast, fat droplet staining was observed in spheroids cultured in medium supplemented with BMP-2 regardless of the presence or absence of osteogenic induction media components.

In terms of spheroid morphology, it was observed that, in the absence of BMP-2 (maintenance and osteogenic media), 3D cultures showed compacted smaller spheroids, whereas spheroids cultured in BMP-2 supplemented media were more dispersed and larger in size.

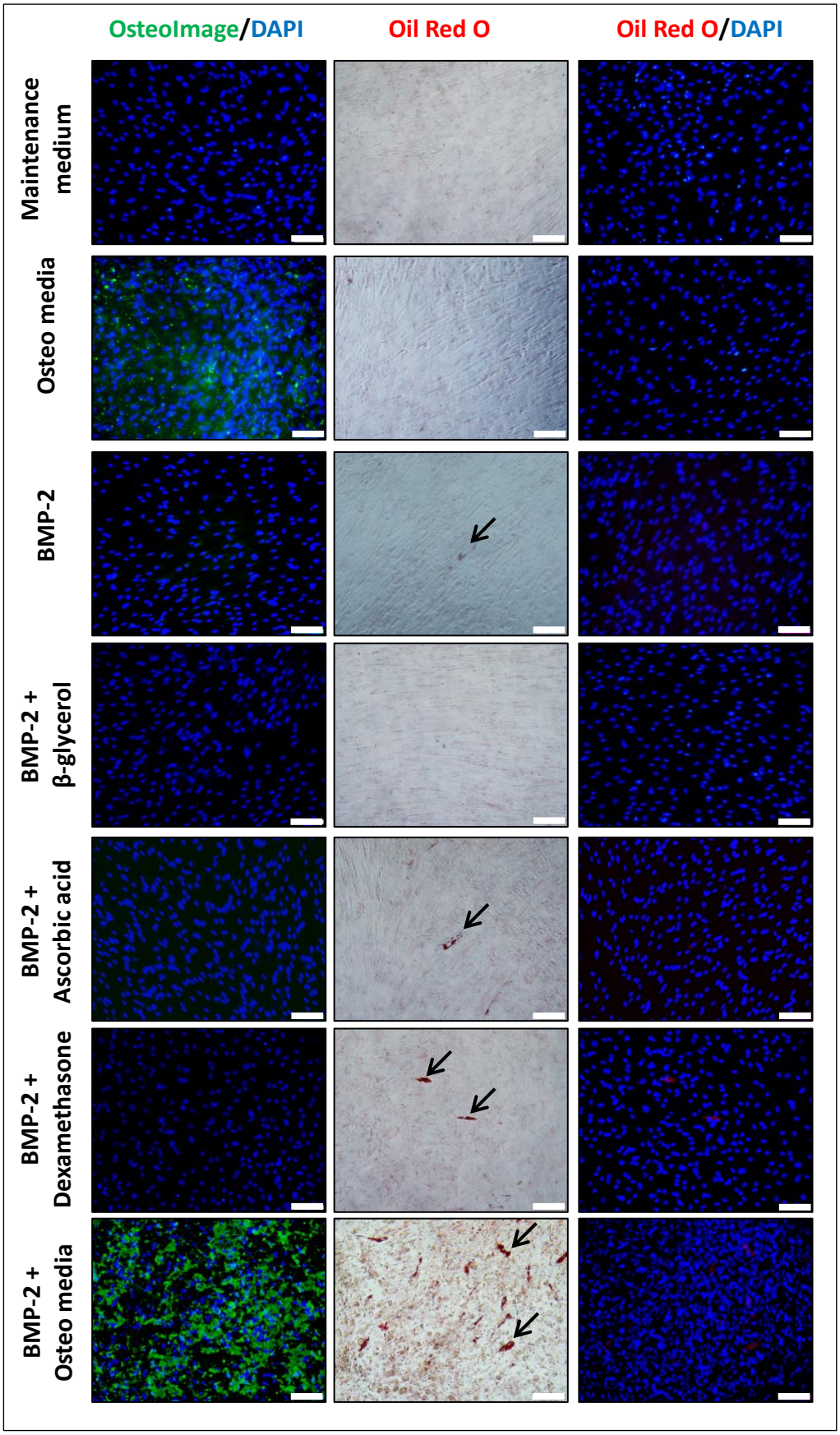
OsteoImage/DAPI
Oil Red O
Oil Red O/DAPI
Maintenance medium
Osteo media
BMP-2
BMP-2 + β-glycerol
BMP-2 + Ascorbic acid
BMP-2 + Dexamethasone
BMP-2 + Osteo media

Figure 2.9. Hydroxyapatite and oil droplet staining of osteo-differentiated BMSC monolayers. 2D monolayer of BMSC cultured in DMEM-HG media (maintenance medium), DMEM-HG media plus all osteogenesis induction media supplements (Osteo media), 10 ng/mL BMP-2 (BMP-2) alone, 10 ng/mL BMP-2 plus all osteogenesis induction media supplements (BMP2+Osteo media) or plus the individual osteogenesis induction media supplements (β-glycerol phosphate, β-glycerol; L-ascorbic acid 2-phosphate, Ascorbic acid and dexamethasone, Dexamethasone). Fluorescent hydroxyapatite stained with OsteoImage (green), fat droplets with Oil Red O (red) and nuclear stain with DAPI (blue). BMSC cultured in maintenance medium functioned as negative staining controls. Arrows point to cells that have stained positive for fat droplets. Scale bar = 100 µm.

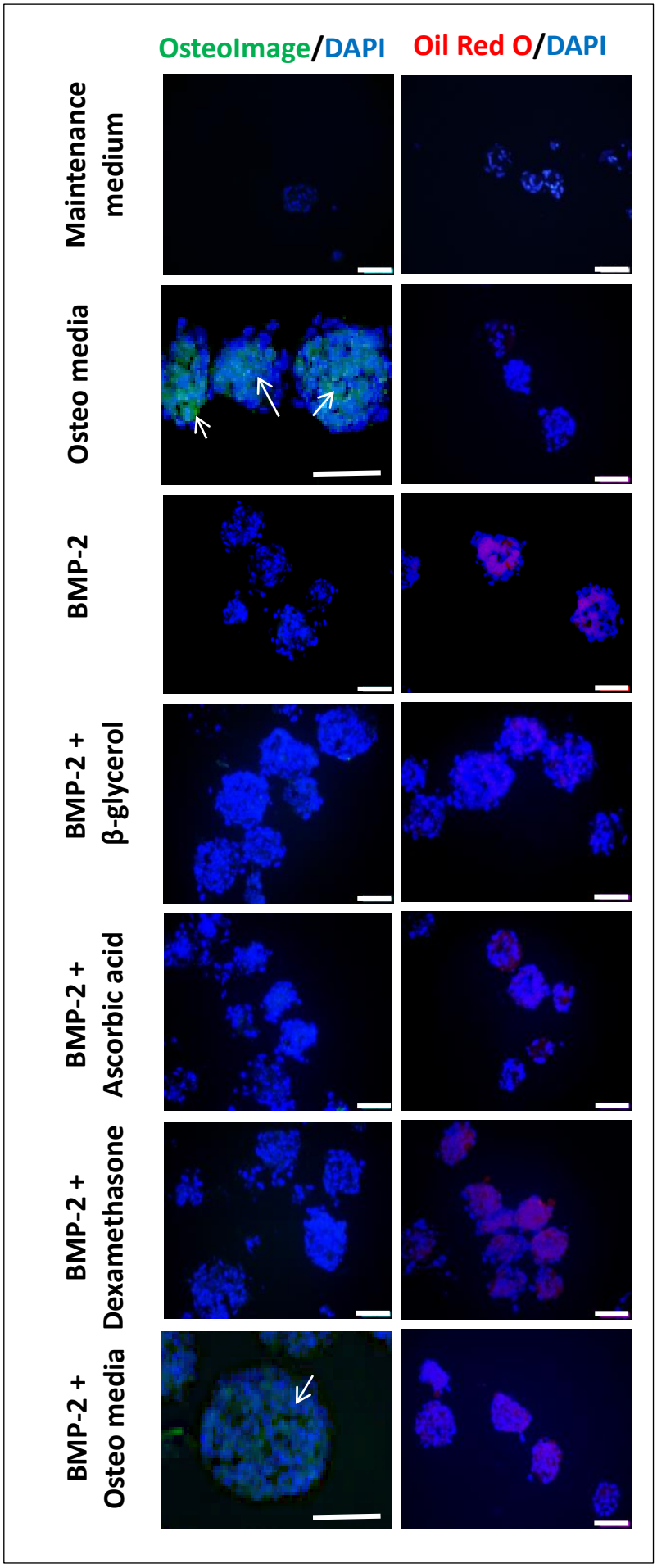
OsteoImage/DAPI
Oil Red O/DAPI
Maintenance medium
Osteo media
BMP-2
BMP-2 + β-glycerol
BMP-2 + Ascorbic acid
BMP-2 + Dexamethasone
BMP-2 + Osteo media

Figure 2.10. Hydroxyapatite and oil droplet staining of osteo-differentiated BMSC 3D spheroids. 3D spheroids of BMSC cultured in DMEM-HG media (maintenance medium), DMEM-HG media plus all osteogenesis induction media supplements (Osteo media), 10 ng/mL BMP-2 (BMP-2) alone, 10 ng/mL BMP-2 plus all osteogenesis induction media supplements (BMP2+Osteo media) or plus the individual osteogenesis induction media supplements (β-glycerol phosphate, β-glycerol; L-ascorbic acid 2-phosphate, Ascorbic acid and dexamethasone, Dexamethasone). Fluorescent hydroxyapatite stained with OsteoImage (green), fat droplets with Oil Red O (red) and nuclear stain with DAPI (blue). BMSC cultured in maintenance medium functioned as negative staining controls. Arrows point to cells that have stained positive for hydroxyapatite. Scale bar = 50 μm.

2.5 DISCUSSION

Bone marrow-derived MSC have significant potential in regenerative medicine. Many clinical applications have been pursued on the basis of the multipotential differentiation capacity of BMSC [298], [321]–[323]. In the present study, BMSC demonstrated the characteristic features of MSC, including plastic-adherence, expression of MSC surface markers and trilineage differentiation capacity in both 2D and 3D cultures. Trilineage differentiation was validated by staining the accumulated matrix formed by the cells (Figure 2.3 and Figure 2.4). Our data demonstrate that BMSC, assembled into spheroids using a microwell platform, can form 3D bone-like, fat-like and cartilage-like tissues.

A number of groups are investigating and optimising BMSC differentiation in 2D and 3D cultures, and it is common to find that BMSC behaviour differs depending on geometry. The high tensile stress in 2D cultures modifies cell morphology leads to different transcriptional profiles and signal transduction pathways that are not necessarily similar to what these cells would experience in the body, and not similar to what has been previously observed in 3D cultures [251], [324]. The reduced cytoskeletal stress in 3D culture has been shown to preserve MSC multipotency in *in vitro* cultures [325]. This is consistent with studies demonstrating that Nanog gene expression, which has a critical role in cell pluripotency maintenance and fate determination [326], is upregulated in 3D cultures [327]. Additionally, there is evidence that MSC differentiation capacity can be

greater in 3D cultures, relative to 2D cultures [328]. The benefits of 3D culture are very well established in BMSC chondrogenesis assays [278], [290]. Independent of superior or inferior differentiation outcomes, it is rational to assume that 3D cultures of BMSC can potentially provide a superior physiological mimic, and that studies performed in 3D are more likely to parallel *in vivo* processes.

Microtissues assembled in microwell are gaining popularity in tissue culture and tissue engineering applications. A strength of the microtissue/microwell approach is that hundreds of uniform microtissues of defined sizes can be rapidly and consistently manufactured [278], [290], [329]. This uniformity allows for the rapid and rigorous evaluation of how specific culture conditions influence cell behaviour in hundreds of replicate tissues. While considerable work has been completed in the BMSC microtissue space, no group has carefully characterised the impact of BMP-2 on BMSC differentiation in 3D microtissues. This is an important area of research, as both BMSC and BMP-2 are likely tools to be used in bone defect repair.

In our study, we found that there was a significant decline in BMSC spheroid size, and a decrease in the number of proliferating cells over a 14-day culture period (Figure 2.5). This observation was consistent with a previous study that reported a decrease in BMSC spheroid size over time [328]. These authors interpreted the observation of reduced spheroid size as being caused by cell compaction due to oxygen and nutrient diffusion gradients. However, we report that the decrease in spheroid sizes was associated with a considerable decrease in the size of individual cells. The size of individual cells in 3D spheroids is considerably smaller than the cells used to assemble the spheroids, and smaller than the cells in control 2D monolayers (Figure 2.6). The size of cells in confluent 2D monolayers also decreased with time. This reduction in size correlates with a reduction in proliferation as the contact inhibited cells delay proliferation in the increasingly confluent cultures [330], [331]. In 3D cultures, the reduction in cell size was significant after only 24 hours of culture. At the time points tested, the magnitude of change in cell size in 2D versus 3D cultures was similar. Overall, it is important to note that the cell size reduction was greatest in 3D cultures, and that the reduction in cell size relative to the cells used to form the spheroids was marked.

Cells normally increase in volume or mass before entering a proliferative cycle [332]. We reason that cells are not increasing or maintaining volume in 3D culture,

because most cell are exiting proliferative cycles. Low rates of cellular proliferation have been reported for many cell types cultured in 3D spheroids [258], [333], [334], and we anticipate that the cells in these spheroids are also smaller. One other previous study reported that maintaining MSC in 3D cultures relaxes the cytoskeleton tension, decreases integrin-mediated adhesion to the matrix and increases cadherin-mediated cell-cell interaction, leading to a decrease in cell size compared to 2D cultures [327], which is consistent with our findings. In addition to the influence that cell proliferation has on cell behaviour, the reduced cell size in 3D cultures may significantly influence cellular response to various internal stimuli by modifying the nuclear to cytoplasmic ratio and by reducing diffusion lengths.

Scaffold-free microtissues for bone regeneration have several advantages over monolayer cultures. Besides the better *in vivo*-like conditions, microtissues are less prone to wash out than single cells after injection in the defect area [335], [336]. Microtissues increase the osteogenic potential of the progenitor cells [328], [337]. Microtissues can increase the cell load of a scaffold more than the single cells, which increase the number of inoculated cells in a bone defect [338]. In this study and previous studies from our group [289], [290], [329], we have provided a powerful technology to manufacture size-controlled bone-like and cartilage-like microtissues in a high throughput system. In the microwell platform, hundreds of uniform bone-like microtissues can be produced for direct injection in a bone defect or to load a scaffold with the microtissues. The cells growing in 3D cultures can accumulate calcium deposits and form hydroxyapatite as shown by quantitative assay and histological staining.

BMP-2 is a well-known osteoinductive factor that has been extensively used in clinical applications [339], [340]. We found that delivering exogenous BMP-2, in combination with osteogenic induction media, enhanced calcium accumulation of BMSC in *in vitro* 2D and 3D cultures (Figure 2.8). However, enhanced formation of the bone-specific matrix hydroxyapatite was only observed in 2D cultures which were associated with intracellular oil droplets accumulation. According to 2D cultures staining, adipogenic differentiation occurred in cultures exposed to BMP-2 either in the presence or absence of osteogenesis induction media supplements. In 3D cultures BMP-2 addition also induced adipogenesis in all of the tested tissue culture medium conditions (Figure 2.10). The capacity of BMP-2 to promote osteogenesis

and adipogenesis simultaneously in 2D BMSC monolayer cultures has been reported by others [341], [342], but this has not been reported previously in 3D cultures. Understanding the pleiotropic effects of BMP-2 is key to maximising its clinical utility. While BMP-2 is commonly used *in vivo* to promote bone regeneration, the quality of the *de novo* bone is generally poor [311]. It may be possible to use BMP-2 to commit BMSC to an osteo-lineage *ex vivo* prior to transplantation, but the propensity for BMP-2 to drive adipogenesis would have to be overcome.

To conclude, microtissues of BMSC assembled in microwells provide a powerful tool to study and optimise 3D cell differentiation processes. BMSC cultured in 3D microtissues decrease in size. Less calcium matrix accumulated in 3D microtissues, than in 2D monolayer equivalents. However, 3D microtissues could be injected *in vivo*, offering a potential strategy to use these tissues in bone regeneration. BMP-2 increases osteogenic differentiation, but simultaneously drives adipogenic differentiation.

Acknowledgement

The authors would like to thank the National Health and Medical Research Council (NHMRC) of Australia for funding this research, the Ministry of Higher Education of Egypt for supporting E.M., the bone marrow aspirates donors, Mr Eric Franklin for assistance with BMSC isolation and Dr David Sester at the flow cytometry core facility at the Translational Research Institute (TRI) for assisting with cell size quantification.

Authorship

E.M. designed and performed research, conceived the experiments, analysed data and wrote the paper.

K.C. and J.C. designed research and wrote the paper.

K.F. designed research.

M.R.D. designed research, conceived the experiments and wrote the paper.

Funding

M.R.D. is funded by the National Health and Medical Research Council (NHMRC) of Australia CDF Fellowship and Prostate Cancer Foundation of Australia. E.M is supported by the Ministry of Higher Education of Egypt.

Conflict of interest

The authors declare that they have no conflict of interest.

2.6 SUPPLEMENTARY DATA

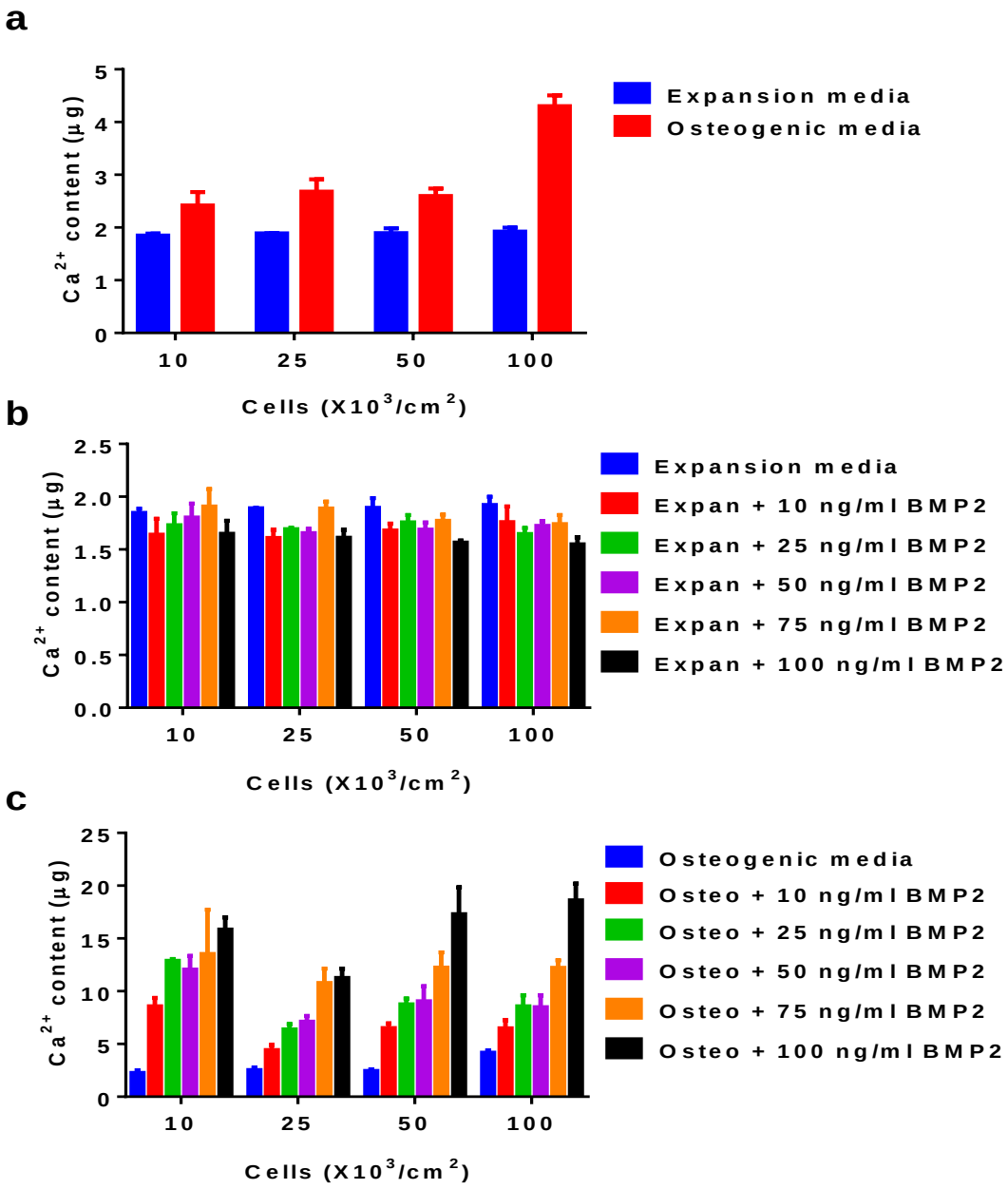

Supplementary Figure 2.1. Calcium accumulation in 2D monolayer cultures in different cell seeding densities. (a) Calcium content remains constant in the expansion media, while it gradually increases with increasing monolayer cell density when cultured in osteogenic medium. **(b)** Increasing concentrations of BMP-2 have no significant effect on the calcium quantification when cells cultured in expansion medium. **(c)** BMP-2 induces a dose-dependent increase in calcium accumulation by osteoblast monolayers. Error bars represents standard deviation (Two donors each had four replicate cultures).

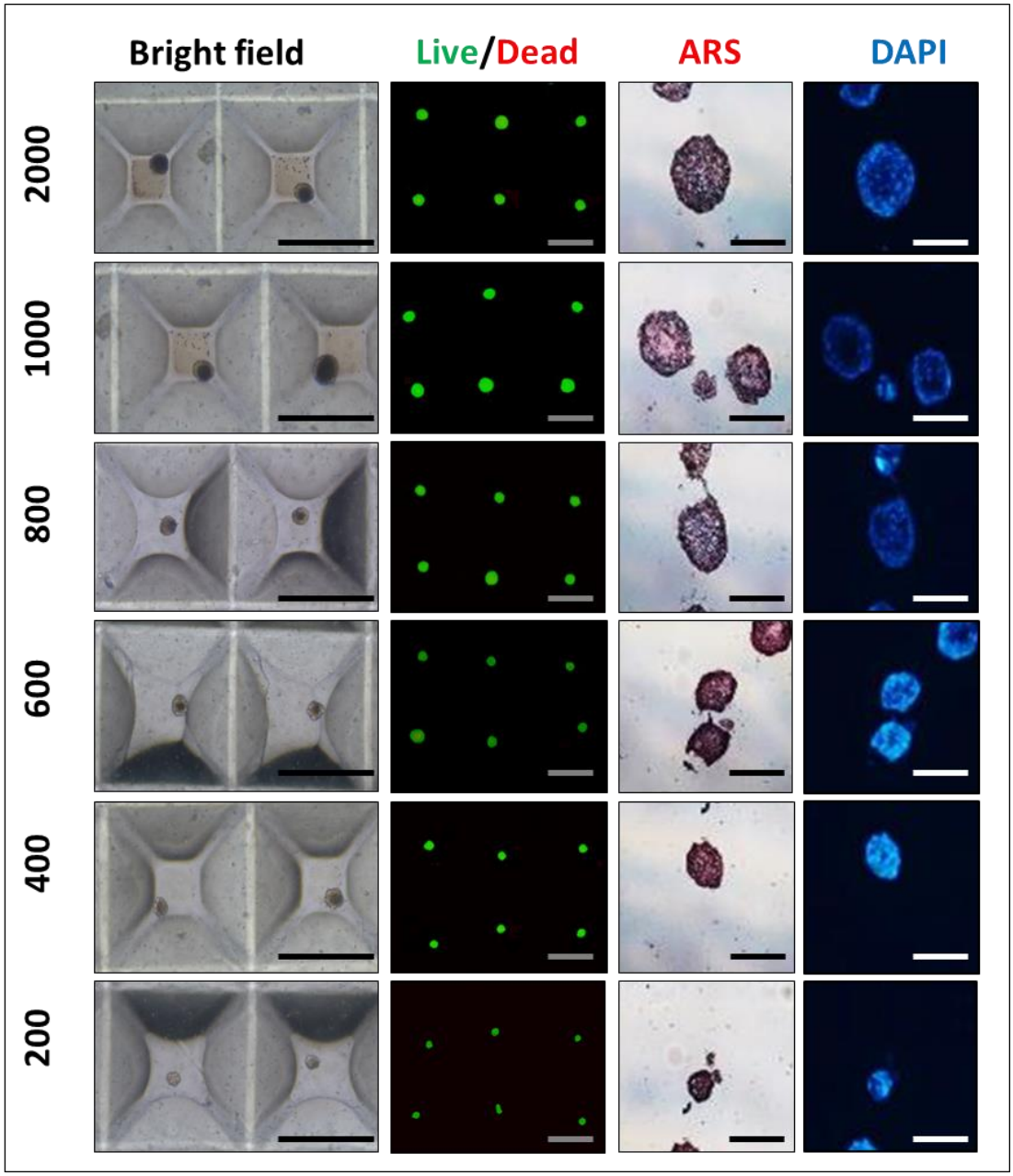

Supplementary Figure 2.2. Bone-like microtissues in 3D cultures. A range of BMSC spheroid sizes (2000-200 cells/spheroid) were cultured for 14 days in osteogenic induction medium. Bright field images of spheroids were acquired (scale bar=500µm); live (green)/dead (red) staining was performed *in situ* (scale bar=500µm); and cryosections were stained with Alizarin Red S dye (ARS; red) and nuclear stain with DAPI (blue) (scale bar=100µm).

Chapter 3: The Microwell-mesh: A high-throughput 3D prostate cancer spheroid and drug-testing platform

Chapter status: Published online in Scientific Reports (10/01/2018)

Manuscript title: The Microwell-mesh: A high-throughput 3D prostate cancer spheroid and drug-testing platform

Contributor	Statement of contribution
Eman Mosaad Signature: Date: 24/04/2018	Designed research (D) Performed research (P) Analysed data (A) Wrote Manuscript (M)
Judith Clements and Karen Chambers	Aided with A and M
Kathryn Futrega	Aided with M
Michael R. Doran	Aided with D, A and M

Principle Supervisor Confirmation

I have sighted email or other correspondence from all Co-authors confirming their certifying authorship.

Michael R. Doran

Signature: Date:

Chapter 3 preface:

As described in chapter 2, the microwell system was used to manufacture hundreds of BMSC, bone-like or fat-like microtissues in a high throughput capacity. However, the microwell platform used in chapter 2 is not suitable as a drug-screening platform where multiple culture medium exchange is required. In Chapter 3, a modified microwell platform, termed as the Microwell-mesh, was used to manufacture and retain 3D PCa micro-tumours in discrete microwells. Chapter 3 describes the utilization of the Microwell-mesh system as a drug-screening platform.

3.1 ABSTRACT

Treatment following early diagnosis of Prostate cancer (PCa) is increasingly successful, whilst the treatment of advanced and metastatic PCa remains challenging. A major limitation in the development of new therapies is the prediction of drug efficacy using *in vitro* models. Classic *in vitro* 2-dimensional (2D) cell monolayer cultures are hypersensitive to anti-cancer drugs. As a result, there has been a surge in the development of platforms that enable three dimensional (3D) cultures thought to better represent natural physiology and better predict drug efficacy. A deficiency associated with most 3D culture systems is that their complexity reduces the number of replicates and combination therapies that can be feasibly evaluated. Herein, we describe the use of a microwell platform that utilises a nylon mesh to retain 3D micro-tumours in discrete microwells; termed as the Microwell-mesh. The Microwell-mesh enables the manufacture of ~150 micro-tumours per well in a 48-well plate, and response to anti-tumour drugs can be readily quantified. Our results demonstrate that 3D micro-tumours, unlike 2D monolayers, are not hypersensitive to Docetaxel or Abiraterone Acetate, providing a superior platform for the evaluation of sequential drug treatment. In summary, the Microwell-mesh provides an efficient 3D micro-tumour platform for single and sequential drug-screening

3.2 INTRODUCTION

Common 2-dimensional (2D) monolayer cell culture generally fails to mimic the complex behaviour of native tissue. 2D culture limits cell-cell interaction, modifies gene expression and limits tissue-like matrix accumulation [324]. From a cancer cell biology perspective, one of the most perturbing factors is the high tensile stress experienced by cells cultured on rigid 2D tissue culture plastic surfaces [251], [258]. This stress triggers abnormally high cell proliferation rates, which can directly impact or confound the sensitivity of cells to anti-cancer drugs, which often specifically target proliferating cells [256].

The merits for the use of 3D spheroids to study drug response in cancer research have long been appreciated. In 2002, Jacks and Weinberg summarized the merits of 3D cultures, and closed with the statement "*Suddenly, the study of cancer cells in two dimensions seems quaint, if not archaic*" [251]. Despite disadvantages, the use of 2D culture in cancer drug-screening remains common, as standard 2D

tissue culture plates are inexpensive, high throughput fluidics systems are compatible with such plates, and a range of platforms are available to facilitate imaging or characterisation of 2D cultures maintained in standard 2D tissue culture plates. Transition to the widespread use of 3D cultures in cancer research is dependent on the development of efficient culture systems that enable similar high throughput capacities.

A number of recent innovations are enabling improvements in the efficiencies of establishing and characterising 3D cultures. Methods for establishing 3D cultures include the use of hydrogel matrices such as Matrigel, or scaffold-free systems including hanging drop culture systems, microfluidic platforms, and microwell platforms [343], [279]. The advantage of the later three, relative to hydrogel approaches, is that they enable the manufacture of 3D cell spheroids of controlled size and rely on the cells to produce their own endogenous extracellular matrix. Our group previously demonstrated the utility of microwell platforms to manufacture hundreds of 3D micro-tumours from prostate cancer (PCa) cells and subsequently characterise their response to anti-cancer drugs.

In our previous work, we utilised a microwell platform fabricated from polydimethylsiloxane (PDMS), with an array of approximately 150 microwells/cm^2. This microwell platform, like others previously published in the literature [344], [345], [328], enabled the uniform distribution of cells into microwells at the bottom of a culture well plate by brief centrifugation. Cells in discrete microwells will aggregate to form 3D micro-tumours that can then be permitted to grow in culture and/or be treated with drug(s). A major limitation of microwell platforms, such as the one used in our previous study, is that the addition of drug(s) or the exchange of medium can easily displace micro-tumours from their discrete microwells. Displaced micro-tumours can be lost through medium exchange or fall into adjacent microwells where they can amalgamate with other micro-tumours, resulting in a culture of heterogeneous micro-tumour sizes and numbers. To overcome this limitation our group developed the "Microwell-mesh" [290]. The unique feature of the Microwell-mesh is that it has a nylon mesh with a 36 μm pore size fixed over the microwells. The openings in the mesh are large enough to allow a single cell suspension to pass through and aggregate at the bottom of each microwell, while small enough to prevent aggregated micro-tumours from escaping individual

microwells. This feature enables the simultaneous and efficient manufacture of hundreds of uniform micro-tumours, in a format that facilitates the multiple medium exchanges required for complex and/or sequential drug treatment.

In our previous work we utilised the Microwell-mesh to manufacture spheroids of cartilage tissue [290]. Herein, we describe the fabrication and use of a Microwell-mesh platform with smaller microwells, tailored for the formation of micro-tumours and anticancer drug-testing. We demonstrate that the Microwell-mesh can be used to establish micro-tumours from defined numbers of PCa cells, and that micro-tumour growth and regression in response to drug treatment can be quantified using methods compatible with high throughput screening assays. Specifically, we characterise the formation and growth of micro-tumours assembled from C42B and LNCaP PCa cells, and microtissues assembled from prostate stromal myofibroblasts WPMY-1 cells. We explore the micro-tumour response to two drugs commonly used for the treatment of advanced PCa; treatments evaluated include androgen targeted therapy, Abiraterone Acetate, and single or sequential doses of the taxane chemotherapy, Docetaxel.

3.3 MATERIALS AND METHODS

Cell lines and standard cell culture

All cell lines were obtained from the American Type Tissue Collection (ATCC) and included the androgen-responsive C42B and LNCaP cells and prostate myofibroblasts WPMY-1 cells. Cell lines were authenticated at the Genomic Research Centre (GRC; Brisbane, Australia) using Short Tandem Repeat (STR) analysis. STR profiles of the cell lines were compared to the ATCC STR Database to verify cell line identity; and all cell lines showed ≥80% match to the corresponding reference STR profile. Cells were cultured in low glucose Dulbecco's modified Eagle's medium (DMEM-LG) supplemented with 10% fetal bovine serum (FBS; Thermo Fisher) and 1% penicillin/streptomycin (Thermo Fisher). For some assays, FBS was replaced with 10% charcoal stripped fetal bovine serum (CSS; Thermo Fisher) to mimic androgen deprivation conditions. Cells were grown in a cell culture incubator at 37°C and 5% CO_2. All cells were passaged when monolayers reached ~80% confluency using 0.25% Trypsin/EDTA (Thermo Fisher).

Microwell-mesh design and fabrication

The fabrication of microwell arrays of polydimethylsiloxane (PDMS) was performed as described previously [258], [290]. Briefly, a polystyrene mold was used to cast arrays of approximately 150 microwells/cm2. Each microwell was 800 x 800 μm square, by 500 μm deep. Liquid PDMS was poured onto polystyrene molds to form 2 mm thick sheets and cured at 60oC for 1 hour. Discs, 11 mm in diameter were punched out of the PDMS sheets using a wad punch (Amazon). Disc size was selected such that these discs would fit snuggly into 48-well plates (Nunc, Thermo Fisher Scientific). Nylon mesh (36 μm2 pore openings, part number: CMN-0035, Amazon) was fixed to the top of the microwells using silicone glue (Selleys, Australia). Once the glue had cured, excess mesh was trimmed from the disc inserts using scissors. Inserts were then anchored into individual wells in 48-well plates by placing a small amount of silicone glue at the bottom of the well, and the insert pressed into the well. Plates with Microwell-mesh inserts were sterilized in 70% ethanol for 1 hour, followed by several (3-4) washes with Dulbecco's phosphate buffered saline (DPBS), and stored wet in DPBS until use. To prevent cell adhesion to the PDMS surface, wells with Microwell-mesh inserts were treated with 0.25 mL of sterile 5% Pluronic-F127 (Sigma-Aldrich), which was centrifuged at 1,000 g to penetrate into each microwell, and permitted to adsorb to the PDMS surface for >10 minutes [346]. Treated surfaces were washed twice with DPBS prior to cell seeding.

Cell seeding and culture in the Microwell-mesh

In this study, we aimed to form micro-tumours (cancer cells) and microtissues (non-cancer cells) from 600 cells each. Inserts had approximately 150 microwells each, and so single cell suspensions containing 90,000 cells in 0.5 mL of medium were seeded into each microwell-mesh-containing well of 48-well plates. Plates were then centrifuged at 400 x g for 5 minutes to force cells through the mesh and aggregate the cells uniformly at the bottom of each microwell. Standard 2D culture controls were established by seeding cells at 10,000 cells/cm^2. The aggregation of cells into microwells was visually confirmed using an Olympus CKX14 microscope, and images captured using an Olympus DP26 digital camera (Japan) and Microscopy software (CKX14, CellSens Entry). Plates were then transferred to a cell culture incubator maintained at 37°C and 5% CO_2.

Cultures were maintained for up to 14 days. A half-volume (0.25 mL) culture medium exchange was performed every second day. Images were captured every two days for diameter measurement. A minimum of 50 micro-tumours formed from C42B or LNCaP cells and microtissues formed from WPMY-1 cells were measured per time point. Four replicate cultures were harvested every second day for DNA quantification or at day 1 and 7 for immunofluorescent staining.

Immunofluorescence staining and confocal imaging

Spheroids were harvested by peeling the nylon mesh from the microwells, and collecting the spheroids into Eppendorf tubes. Spheroids were fixed using 4% PFA for 30 minutes at room temperature, followed by permeabilisation using 0.5% Triton X-100 in DPBS for 30 minutes at room temperature. To prevent non-specific binding, 5% bovine serum albumin (Sigma-Aldrich, A7906) was used in the blocking step for 1 hour at room temperature. Cell aggregates were then incubated with primary antibody for Ki67 (Abcam, ab92742) at 1 µg/mL overnight at 4^{o}C. The anti-rabbit secondary antibody conjugated with Alexa Fluor 594 (Thermo Fisher; dilution 1:500) was added to the aggregates for 1 hour at room temperature, followed by the nuclear stain, 4',6-diamidino-2-phenylindole (DAPI, Sigma-Aldrich), for 30 minutes at room temperature. Stained spheroids were imaged using a Zeiss 510 Meta confocal microscope.

Drug-testing in cell cultures

Docetaxel (Sigma-Aldrich, 01885), Abiraterone Acetate (Sigma-Aldrich, SML 1527) and Enzalutamide (Haoyuan Chemexpress, HY-70002) were purchased as powders and dissolved in Dimethyl sulfoxide (DMSO; Sigma-Aldrich, 472301), then aliquoted and stored at -80^{o}C. On the day of treatment, an aliquot was thawed and diluted to the indicated concentrations using culture media. Before selecting the culture densities used in drug-testing experiments, multiple cell densities were tested, specifically 5000, 25,000 and 45,000 cells/cm^2 in 2D cultures and 150, 300 and 600 cells/micro-tumour in 3D cultures. The impact of prolonged culture period prior single Docetaxel treatment was also tested.

For drug-testing experiments, cells were seeded in 48 well plates at 10,000 cells/cm^2 in 2D cultures and 600 cells/micro-tumour in 3D cultures. All cells were cultured overnight to permit plastic adherence or self-aggregation in 2D and 3D

cultures, respectively. The treatment protocols used to evaluate the anti-tumour drugs are illustrated schematically in Figures 3.1, 3.6a and Supplementary Figure 3.1. For anti-androgen treatment (Figure 3.1a), cultures were first initiated in medium containing 10% FBS (day 0) and permitted to stabilise overnight. The next day (day 1), culture media were replaced with fresh culture medium supplemented with 10% CSS to mimic androgen deprivation conditions for 48 hours. On day 3, culture medium was replaced with fresh 10% CSS medium containing Abiraterone Acetate or Enzalutamide and cultures were incubated for a further 48 hours. Following this period (on day 5), cultures were assessed for metabolic activity, as well as ATP and DNA content. For single cytotoxic drug treatment experiments (Figure 3.1b and supplementary Figure 3.1), cultures were established overnight or for 3 days in 10% FBS and then treated with medium containing 10% FBS and Docetaxel for 72 hours.

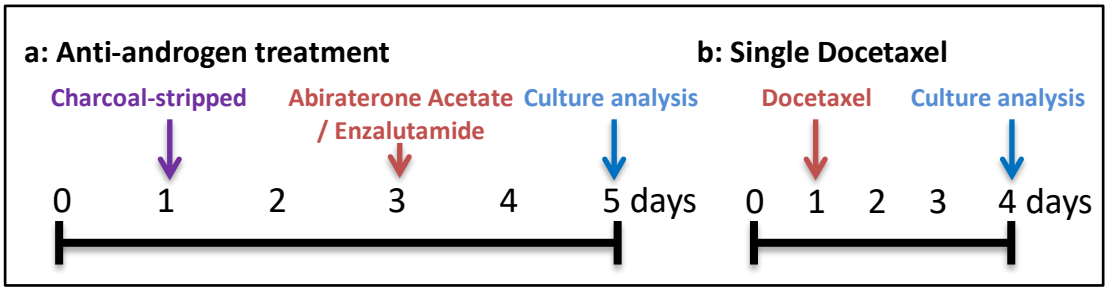

Figure 3.1. Drug treatment protocol. (a) For androgen deprivation, cell cultures where seeded in standard FBS supplemented medium on day 0 and replaced with CSS medium 24 hours later (day 1) to starve cells of androgen. On day 3, Abiraterone Acetate or Enzalutamide was added to cell cultures. Cultures were terminated on day 5 and analysed using the specified methods. **(b)** A single treatment of Docetaxel was performed after 24 hours of seeding the cells (day 1). Drug response was then assessed following three days of exposure to Docetaxel (day 4).

In experiments where cells were exposed to sequential Docetaxel treatment (Figure 3.7a), the cultures were permitted to recover from the first Docetaxel treatment for 72 hours in drug-free medium supplemented with 10% FBS. Following this recovery period, cells were exposed to a second 72-hours round of Docetaxel. The metabolic activity and DNA content of Docetaxel-treated cells were quantified

at day 4 for single dose-treated cultures and at day 4, 5, 7, 10 and 11 for sequential dose-treated cultures.

Metabolic activity measurement

AlamarBlue is a metabolic assay commonly used as an indirect method to estimate viable cell numbers. The AlamarBlue assay consists of a non-fluorescent blue dye (Resazurin), which is reduced to a fluorescent pink compound (Resorufin) by the action of mitochondrial and cytoplasmic reductases of living cells [347].

One of our objectives was to determine whether the AlamarBlue assay could be used by direct addition and incubation of the AlamarBlue reagent in the Microwell-mesh cultures and subsequently assessed by placing the entire plate in a fluorescence plate reader. To optimise the AlamarBlue assay, several concentrations of the assay reagent (3, 5 and 10% of the culture volume) were added to the culture media of increasing number of PCa cells in 2D monolayers and 3D Microwell-mesh cultures. Plates were incubated at 37^{o}C for 1 to 5 hours. Data was acquired by two different settings of the spectrophotometer plate reader, where the fluorescence measurement was collected from the top or the bottom of the plate. The fluorescence was detected using a FLUOstar Omega Microplate Reader (BMG LABTECH) with 544 nm excitation and 590 nm emission. The fluorescence values were plotted against cell numbers to determine the linearity of the assay and to identify the optimum reagent concentration and incubation time for performing the assay *in situ* (directly in the Microwell-mesh plate).

ATP measurement

The amount of ATP in the 2D or 3D Abiraterone Acetate treated cultures was measured using the CellTitre-Glo 3D Cell Viability Assay kit (Promega) according to the manufacturer's instructions. This assay relies on the addition of exogenous thermostable luciferase enzyme that generates a luminescence signal from the conversion of D-luciferin in the presence of cellular ATP. Similar to the AlamarBlue assay, quantification of ATP in cell lysates is often used as an indirect estimate of the number of viable cells. At the specified time points, half of the culture media volume was removed and replaced with the ready-to-use cell lysis reagent. To facilitate lysis, plates were placed on an orbital plate shaker for 5 minutes, and then incubated for a further 20 minutes at room temperature. Samples were collected and

bioluminescence was measured using a PHERAstar FS plate reader (BMG LABTECH). A standard curve was generated using ATP disodium salt (Sigma-Aldrich, A7699). Results are represented as values normalised to the amount of ATP produced in the control cultures (10% FBS-supplemented media conditions).

DNA quantification

DNA quantification was performed as another means to estimate cell number. The Quant-iT PicoGreen dsDNA assay (Thermo Fisher) was used as per manufacturer's instructions to fluorescently measure the double stranded DNA content contained in cell cultures. To lyse cell monolayers and spheroids, two freeze/thaw cycles were performed in TE buffer (20 mM Tris-HCl, 2 mM EDTA, pH 7.5) containing 1% Tween 20. Cell lysates were mixed with PicoGreen reagent and fluorescence read using 485 nm excitation and 520 nm emission (FLUOstar Omega Microplate Reader; BMG LABTECH). DNA content was calculated using a standard curve of ʎ DNA as a reference. Results are represented as values normalised to the amount of DNA in the control cultures (10% FBS-supplemented media conditions).

Cellular oxidative activity assessment

Dihydrorhodamine 123 (DHR123) was utilised to quantify reactive oxygen species within the LNCaP cells cultured in androgen-deprived conditions. Following drug treatment as described above (Figure 3.1a), cells were washed to eliminate remaining drug then incubated with 1 µg/mL DHR123 for 1 hour at 37°C, followed by two wash steps with DPBS. Cells were then trypsinized, resuspended in MACs buffer (Miltenyi Biotech), and analysed on a BD LSRII flow cytometer (Becton Dickinson). Data was analysed using FlowJo software (TreeStar, USA). The mean fluorescence values of four individual samples were calculated and represented in the results section following normalization against control culture (10% CSS-supplemented media conditions).

Statistical analysis:

Results represent the mean values of 3 independent experiments, each performed with 4 biological replicate cultures, unless mentioned otherwise. Error bars represent standard deviations. Statistical significance of data was evaluated using one-way or two-way analysis of variance (ANOVA), where specified, using

Prism software, Version 6.0 (GraphPad). P-values for each comparison are represented by asterisks as indicated in figure captions.

3.4 RESULTS

The Microwell-mesh retains micro-tumours in discrete microwells

A central goal of our work was to create a microwell platform and method that would ultimately lend itself to complex sequential drug-testing. We trialled using traditional open top microwell platforms but found that micro-tumours were often displaced from their discrete microwells, and randomly accumulated in adjacent wells (Figure 3.2a). Based on these results we fabricated the Microwell-mesh platform shown in Figure 3.2b and 3.2c. The Microwell-mesh platform enabled retention of multicellular micro-tumours in discrete microwells during sequential medium and drug exchange.

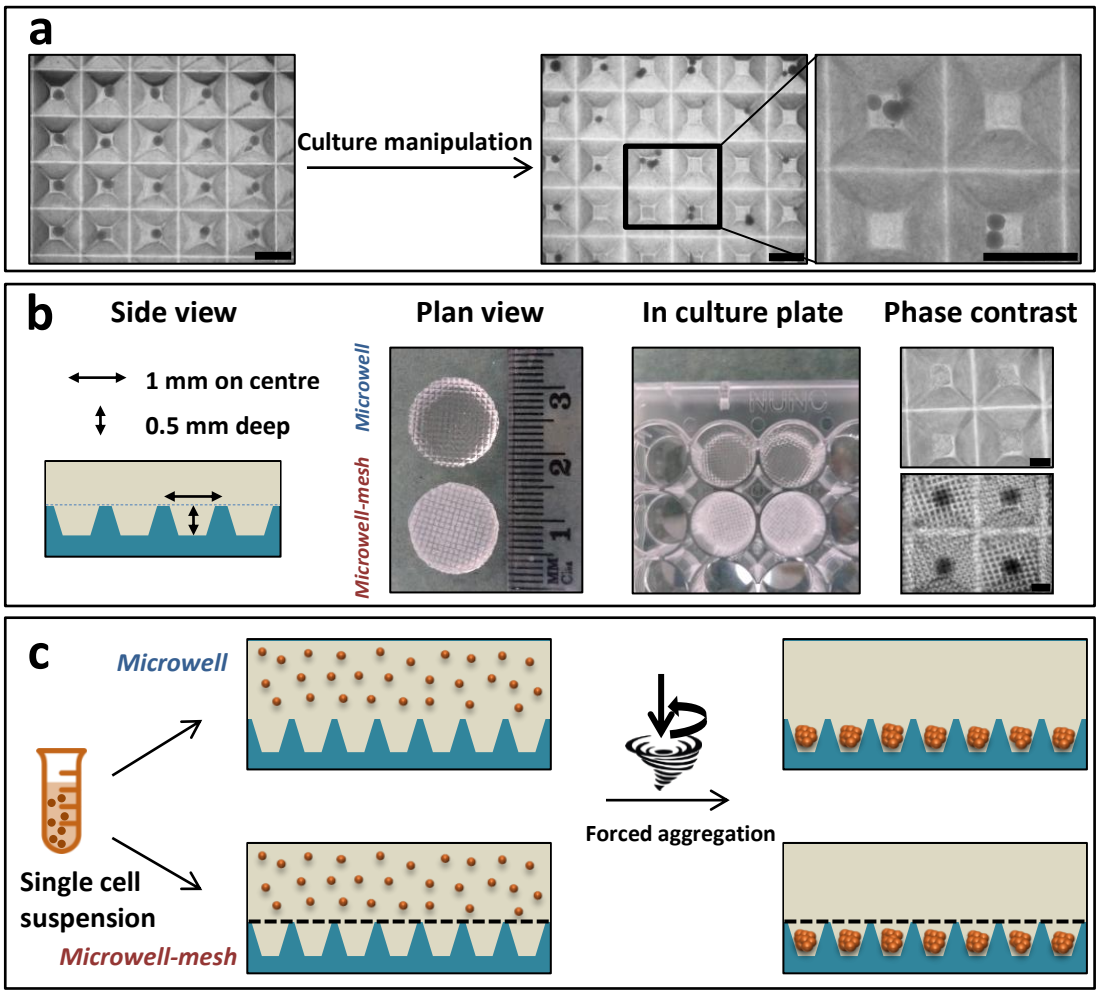

Figure 3.2. Microwell platform manufacture and establishment of 3D micro-spheroid culture. (a) The traditional open-top microwell platform results in dislodged spheroids following culture media exchange (scale bar = 500 µm). **(b)** Schematic illustration and bright field images show PDMS discs with and without the mesh which can be inserted in 48-well tissue culture plates and cells aggregated after 24 hours of seeding cell suspension (scale bar = 200 µm). **(c)** Schematic illustration of cell seeding using traditional open-top microwells (top) and Microwell-mesh being microwells modified with a 36 µm mesh-top (bottom) large enough to allow single cells to pass through, but small enough to retain spheroids within discrete microwells.

Cell numbers can be assessed in the Microwell-mesh using AlamarBlue

To ensure that the Microwell-mesh insert did not interfere with assessing the AlamarBlue assay in 3D cultures, we measured the fluorescence of the assay directly in the plate well, and following transfer of the reacted media to a new well plate

(containing no Microwell-mesh insert). To optimise the AlamarBlue assay in 3D Microwell-mesh cultures, titrations of cell numbers were prepared to generate standard curves and also compared to 2D monolayer cultures (Supplementary Figure 3.2). Measurements were taken at 1, 2, 3, 4 and 5 hours at 3%, 5% and 10% concentrations of AlamarBlue. The cumulative results indicated that the most reliable results could be obtained when measurements were performed with 3% AlamarBlue reagent and incubated for 2 and 3 hours in 2D and 3D cultures, respectively. We trialled reading the AlamarBlue fluorescence signal either by transferring portions of the medium to black 96-well plates, or reading the fluorescence signal directly from the Microwell-mesh plate either from the bottom or top of the plate (Figure 3.3 and Supplementary Figure 3.2). All modes of measurement generated similar, linear standard curves. This result indicated that neither the PDMS insert nor the clear tissue culture wells compromised the sensitivity of the AlamarBlue assay, and indicated that *in situ* measurement of AlamarBlue fluorescence was a suitable strategy to quantify relative cell numbers directly from the Microwell-mesh plates.

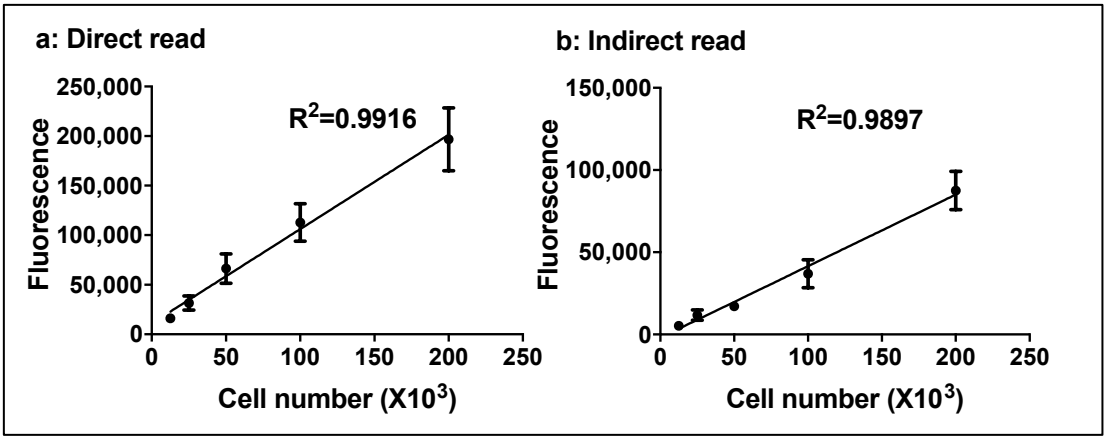

Figure 3.3. AlamarBlue assay optimization in Microwell plates. No significant change in the linearity of the AlamarBlue assay after 3 hours incubation with 3% of AlamarBlue reagent when the fluorescence was acquired *in situ* **(a)** or when the reaction product was transferred to a black 96-well plate **(b)**.

PCa 3D micro-tumour growth

We quantified the growth of C42B and LNCaP micro-tumours and WPMY-1 microtissues each initiated from 600 cells over culture periods of 14 days with a half-

volume culture medium exchange every second day. Micro-tumours generated from both PCa cell lines increased in diameter with a corresponding increase in DNA quantity over the first 5-7 days, after which proliferation rates gradually plateaued (Figure 3.4a). By contrast, microtissues formed from prostate myofibroblasts (WPMY-1) continued to proliferate over 14 days as evidenced by increasing DNA quantity and spheroid diameter (Figure 3.4a). Bright field images showed the three-dimensionality of the uniform micro-tumours/microtissues generated from the three cell lines under examination in the microwell platform. Therefore, the volume of the micro-tumours/microtissues were calculated using the diameter measurements over time following the formula $V = 4/3\ \pi\ r^3$; where V is the volume and r is the diameter of the sphere (Supplementary Figure 3.3).

Ki67 staining was used to identify proliferating cells in 3D micro-tumour cultures. Confocal images of the micro-tumours revealed that Ki67 positive cells were evenly distributed throughout the spheroids at day 1, but by day 7 most proliferating cells were localised in the outer surface of the micro-tumours (Figure 3.4b). Similar to the micro-tumours, WPMY-1 microtissues showed the same distribution of Ki67 positive cells at day 1 and day 7 of culture.

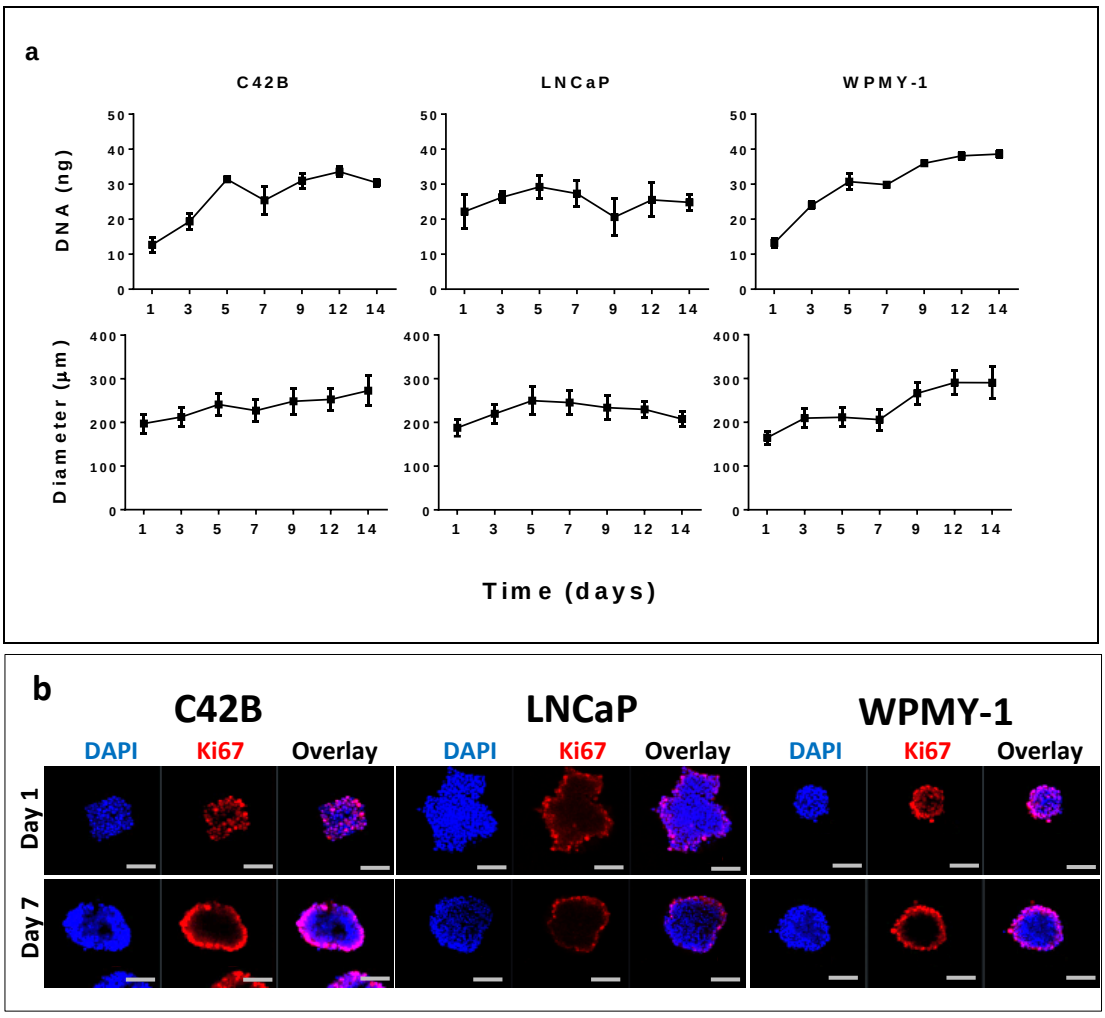

Figure 3.4. Characterisation of prostate cancer cell lines in 3D micro-tumour culture. (a) Prostate cancer (C42B and LNCaP) and prostate myofibroblasts (WPMY-1) cell lines were cultured in the 3D platform (600 cells/spheroid) and the growth of cell spheroids was assessed by DNA quantification and spheroid diameter measurement. DNA quantification data represents the mean value of four replicate cultures. A minimum of 50 spheroids were measured per time point for diameter measurement. **(b)** Confocal images of spheroids (600 cells/spheroid) stained with Ki67 (red) and nuclear stain (DAPI; blue) were acquired on day 1 and 7 of culture. Scale bar = 100 µm.

3D micro-tumours of PCa cells are less sensitive to conditions that replicate androgen deprivation

Androgens are a critical player in prostate cancer cell growth and progression to advanced stage castrate resistant PCa results in the cells becoming resistant to anti-

androgen treatment [205]. Therefore, we hypothesized that our 3D culture system would better reflect the response to androgen deprivation compared to 2D monolayer cultures. To test this hypothesis, we cultured PCa cell lines in an androgen deprived setting (CSS- supplemented culture media), and then treated the cells with Abiraterone Acetate, a first-in-class inhibitor of the CYP17A enzyme to prevent the biosynthesis of androgens intracellularly from their steroidal precursor [348] and used three different assays to assess the cellular responses in our 2D and 3D cultures.

In 2D monolayers, PCa cell lines (C42B and LNCaP) cultured in androgen-depleted media (CSS) showed a reduction in metabolic activity, as assessed by the AlamarBlue assay, and a reduction in ATP and DNA quantity, compared to androgen-replete media (FBS) (Figure 3.5a). A 48-hour treatment of 2D PCa cultures with increasing concentrations of Abiraterone Acetate (0-20 µM) resulted in an unexpected increase in metabolic activity (AlamarBlue assay) and this was dose-responsive in both cell lines ($P<0.0001$ for 10 and 20 µM). In contrast, cellular ATP concentrations were unchanged at lower Abiraterone Acetate concentrations (5 and 10 µM) in 2D PCa cell cultures and slightly reduced at the highest concentration (20 µM) in only the C42B cultures ($P<0.01$), relative to control cultures in CSS plus vehicle (0 µM). DNA concentrations were unchanged in response to Abiraterone Acetate in both PCa cell lines, compared to control. Similarly, LNCaP cells monolayer treated with Enzalutamide instead of Abiraterone Acetate demonstrated an unexpected dose-dependent increase in AlamarBlue readout. While the AlamarBlue readout increased with increasing doses of Enzalutamide, ATP concentrations were unchanged and DNA concentrations slightly decreased with higher Enzalutamide concentration (1 µM and 20 µM) (Supplementary Figure 3.4). We continued to evaluate the response of PCa cells to anti androgen in 3D micro-tumour culture, but restricted our focus to characterising cell response to Abiraterone Acetate.

In 3D micro-tumour cultures, metabolic activity and ATP quantity was not significantly different between androgen-depleted and androgen-replete cultures for both PCa cell lines (Figure 3.5a). In contrast, a significant drop in DNA quantity was observed in 3D cultures under androgen-depleted conditions. The addition of increasing concentrations of Abiraterone Acetate to 3D cultures (0-20 µM) did not result in changes in metabolic activity, ATP quantity or DNA quantity, except for in

C42B cultures, where the ATP concentration was slightly reduced at 20 μM Abiraterone Acetate ($P<0.01$). Overall, 3D PCa cultures were much less responsive to both androgen-depletion and Abiraterone Acetate treatment, compared to 2D cultures.

To determine whether the increased metabolic activity, measured by AlamarBlue assay, in Abiraterone Acetate-treated 2D cultures was due to an increase in the mitochondrial redox activity, we tested the mitochondrial redox activity of drug treated LNCaP cells (Figure 3.5b). Fluorescence intensities of vehicle or DHR123 treated cells were analysed by flow cytometry. Results showed no significance change in mitochondrial oxidation potential in Abiraterone Acetate-treated cells compared to untreated cells, while a significant increase in metabolic activity measured by AlamarBlue assay was shown in a parallel experiment. The bright field images revealed no significant change in the cellular morphology of low dose (0-10 μM) Abiraterone Acetate-treated LNCaP cells compared to the control, except in the high dose of Abiraterone Acetate (20 μM) where the cells showed more irregular morphology.

It is important to mention that we observed no change in AlamarBlue fluorescence in cell-free cultures treated with Abiraterone Acetate (Supplementary Figure 3.5) which confirms cellular participation in the reduction of the AlamarBlue and not a direct reduction by the drug.

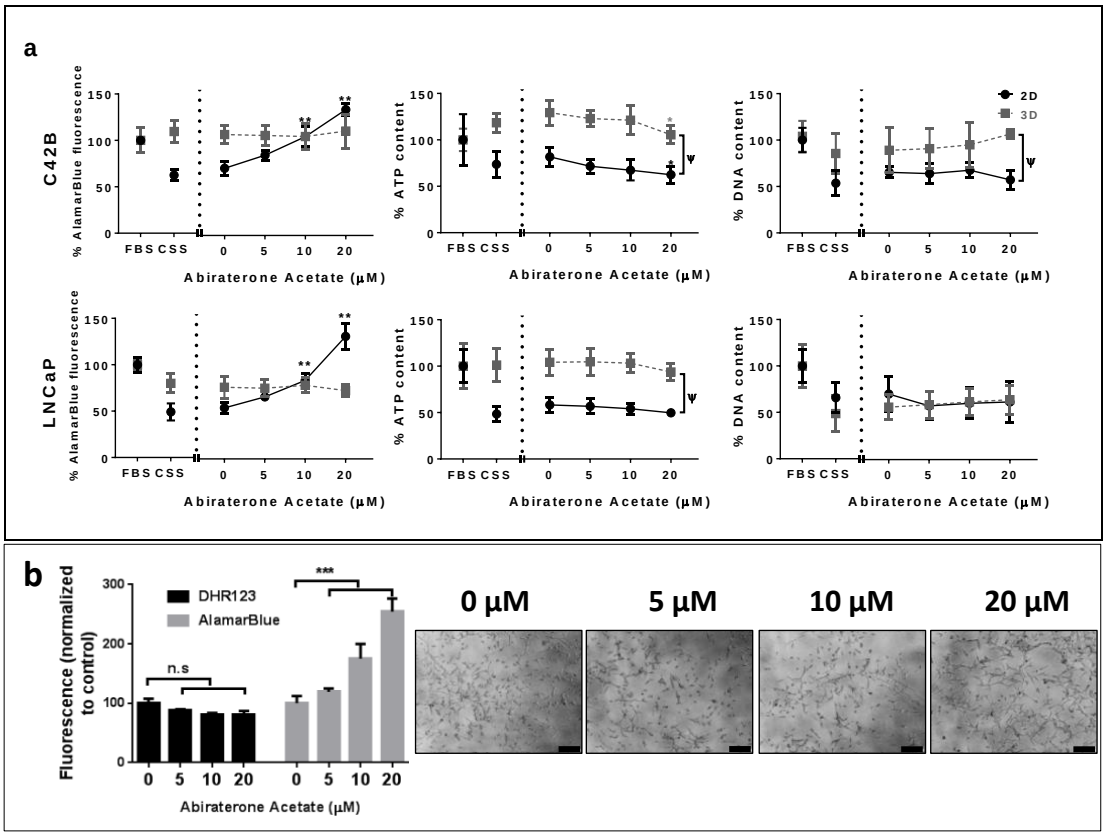

Figure 3.5. Monolayer and micro-tumour behaviour of C42B and LNCaP cell lines in androgen deprived conditions. (a) C42B (Top) and LNCaP (Bottom) cells were seeded in expansion culture medium for 24 hours followed by medium exchange to androgen-depleted medium (CSS) for a further 48 hours. Abiraterone Acetate was then added to the culture medium at the indicated concentrations for an additional 48 hours. AlamarBlue, Cell Titre-Glo 3D Cell Viability and PicoGreen assays were then performed to assess metabolic activity, ATP quantity, and DNA quantity, respectively. All results are represented as a percentage of the FBS-containing culture medium control values (Three independent experiments each has four technical replicate cultures). Statistical significance was calculated by two-way ANOVA compared to the corresponding zero value (** $P<0.0001$ and * $P<0.01$) or compare 2D and 3D values with the same drug treatment (Ψ $P<0.005$). **(b)** Metabolic activity (AlamarBlue assay) and DHR123 staining of LNCaP monolayers at specified Abiraterone Acetate concentrations. Results represented as the mean fluorescence values of four individual samples normalized to control culture values. Statistical significance was performed using one-way ANOVA (*** $P<0.001$). Side panel represents the cellular morphology of LNCaP cells at the indicated Abiraterone Acetate concentrations (μM). Scale bar = 200 μm.

2D and 3D PCa culture response to Docetaxel

Next, we evaluated the response of PCa cell lines in 2D and 3D cultures to a single dose of Docetaxel at varying concentrations in the range of 0 nM (Vehicle only) to 100 nM in expansion media (Figure 3.6). In 2D cultures, both C42B and LNCaP cells showed a significant drop in metabolic activity and DNA quantity at 1 nM Docetaxel, which was maximally reduced by 5 nM. While the metabolic activity of both cell lines slightly decreased in Docetaxel-treated 3D cultures, significant differences in metabolic activity and DNA content between 2D and 3D cultures were observed in cultures treated with ≥ 1nM Docetaxel. In this study, the IC50 values of Docetaxel in 3D cultures (>120 nM and 24 nM for C42B and LNCaP cells, respectively) were considerably elevated relative to IC50 values in 2D cultures (approximately 0.4 nM and 1 nM for C42B and LNCaP cells, respectively).

As the density of the cell culture is a critical factor in drug-screening platforms, we compared drug responses of short (1 day) and long (3 days) pre-treatment cultures. Interestingly, 2D and 3D cultures treated with Docetaxel after 1 day of establishing the cultures showed higher sensitivity towards Docetaxel treatment. However, micro-tumours cultured for prolonged periods (3 days) prior Docetaxel treatment showed lower sensitivity against the drug compared to corresponding 2D monolayer cultures (Supplementary Figure 3.6).

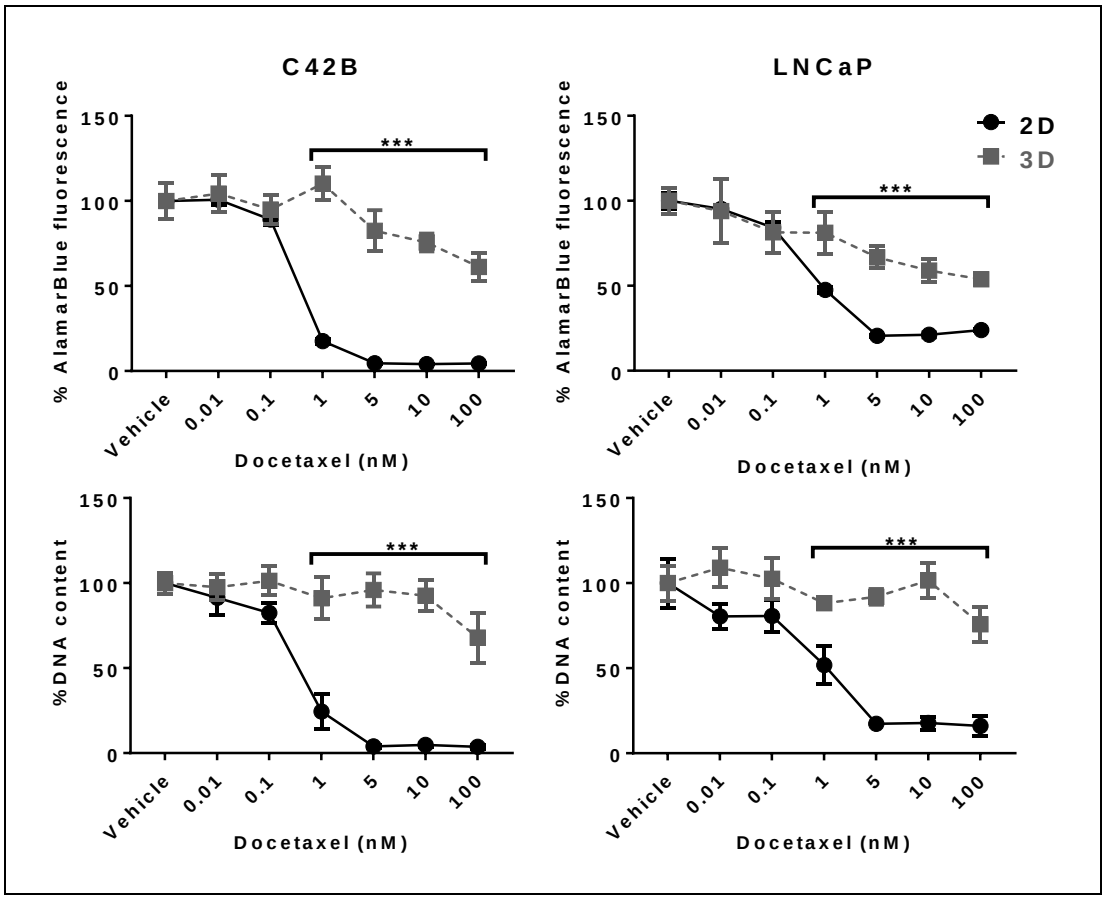

Figure 3.6. C42B, LNCaP Docetaxel drug response. C42B and LNCaP cells in 2D and 3D cultures were treated with Docetaxel in the indicated concentrations for 72 hours followed by metabolic activity and DNA content measurements. All results are represented as a percentage of the vehicle control values (Three independent experiments each had four replicate cultures n=4). Statistical significance was calculated by two-way ANOVA compared to the corresponding values in 2D cultures (*** P<0.0001).

Cellular recovery after sequential cytotoxic drug treatment is enhanced in 3D cultures

One of the many advantages of our 3D culture platform is that it permits several culture manipulations without displacement or loss of cellular spheroids from discrete microwells. This improvement enables testing metronomic or sequential treatments of one or several drugs for the preclinical studies.

We assessed the metabolic activity of PCa cells cultured in monolayers or 3D micro-tumours and treated with 5 nM Docetaxel in sequential doses (Figure 3.7a).

Despite the slight decline in metabolic activity of single dose-treated 3D micro-tumours after the first day of drug-free culture, the metabolic activity of 3D micro-tumours gradually restored by day 6 of culture. Following the second Docetaxel treatment at day 3, 3D micro-tumours showed a slight decrease in the metabolic activity compared to single dose-treated cultures. LNCaP microtissues showed higher sensitivity towards Docetaxel compared to C42B microtissues.

By contrast, PCa monolayers continued to suffer a decline in metabolic activity despite a transient increase in activity during the first day of culture following the first drug treatment. After 7 days of culture, both single and sequential Docetaxel-treated 2D monolayer cultures of C42B and LNCaP cells showed equal metabolic activities (<10% compared to vehicle treated cultures). In general, cells grown in 3D cultures were metabolically more active than that in 2D cultures either after single or sequential Docetaxel treatments.

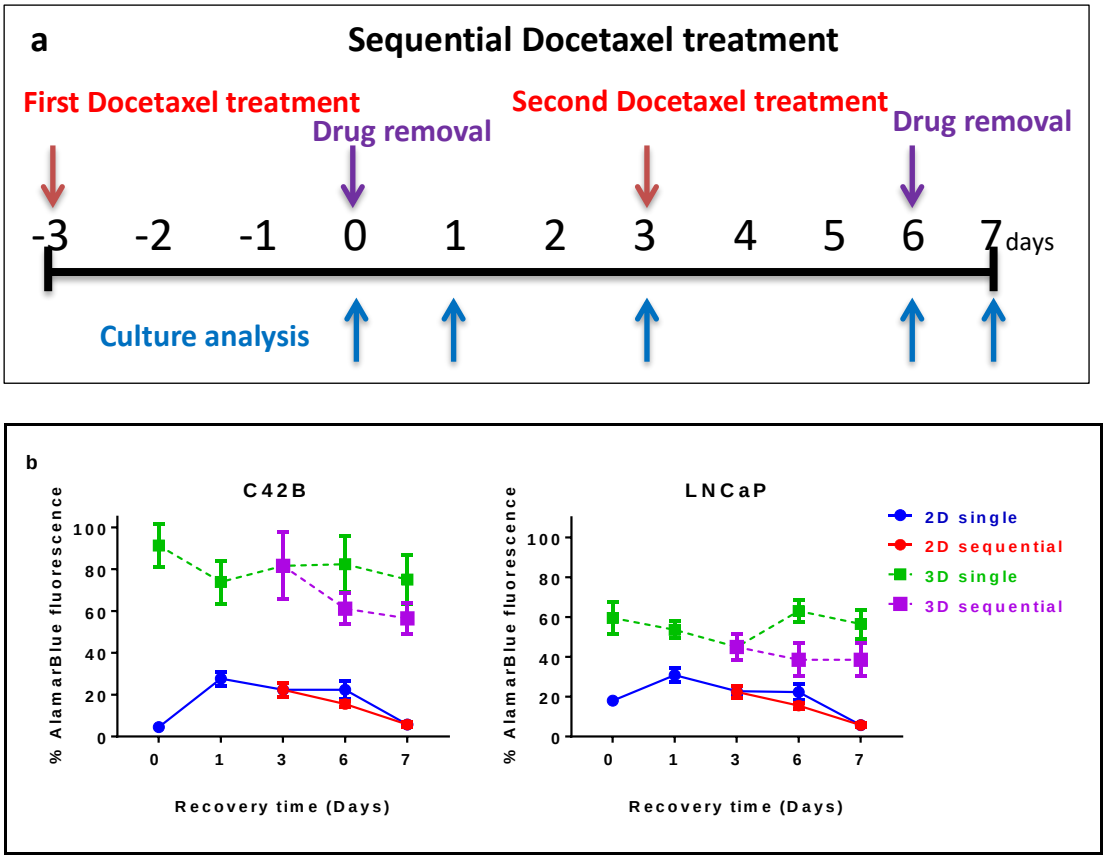

Figure 3.7. Sequential Docetaxel treatment and prostate cancer cell recovery. (a) Sequential treatment of Docetaxel was performed at the indicated time points (red arrows). Each treatment for 72 hours was followed by metabolic activity measurement (blue arrows) and drug removal (purple arrows) at day zero and 6. In addition, cell recovery assessment was also performed at days 1, 3, 6 and 7 for single treatments and at days 6 and 7 for sequential treatments. **(b)** 2D and 3D cultures of C42B and LNCaP cells were treated with 5 nM Docetaxel following the sequential treatment protocol and the metabolic activity of the survived cells were assessed at the indicated time points using AlamarBlue assay. All results are represented as a percentage of the vehicle control values (Two independent experiments each had four replicate cultures n=4).

3.5 DISCUSSION

Three dimensional tissue culture systems have gained popularity in recent years. However, widespread uptake of 3D models remains low. This is due to limitations associated with 3D culture systems including heterogeneity of cultured

spheroid sizes, or heterogeneity within single tissues when large macroscopic tissues are used [349], [350]. Additionally, the low throughput nature of some 3D tissue manufacturing approaches and the incompatibility of these 3D tissues with high-throughput imaging and other analytical tools has limited uptake. In seeking to engineer a powerful 3D culture system capable of enabling both high-throughput 3D micro-tumour formation and complex drug/medium manipulation, we aimed to improve on microwell platforms commonly used to generate 3D tissue models [290]. Our improvement was the inclusion of a nylon mesh bonded over the microwells (the Microwell-mesh) in such a way that would allow the retention of individual micro-tumours in discrete microwells over multiple culture medium manipulations, enabling complex sequential drug treatment and analysis (Figure 3.2). This platform retains the original significant advantage of other microwell systems, enabling the rapid manufacture of hundreds of replicate uniform sized micro-tumours, assembled in a way that allows precise control of the number of cells used to form each individual micro-tumour [258], [289], [319], [329].

Using the microwell platform, PCa micro-tumours grew in size over 14 days of culture (Figure 3.4a). The increase of cellular content and spheroid size was cell line-dependent. However, a decrease in proliferation over time was observed in all cell lines tested. Our group and others have reported similar observations previously [258], [351], [352]. Cells proliferation in 2D is often greater than in 3D spheroids because the increase in cell tension experienced by cells cultured on ultra-stiff 2D surfaces stimulates proliferation [353]. Cells in self-assembled spheroids do not experience similar tensile forces, and proliferation rates in spheroids are generally low [354]. Cells on the surface of the spheroids experience the greatest tension, where they can spread over the outside of the spheroid on a flat, albeit curved, surface [355]. Corresponding to this model, we observed that cell proliferation was largely localised to the surface of individual spheroids from days 1-7 for all cell types tested (Figure 3.4b).

As the cell spheroid grows, chemical and oxygen diffusion gradients develop across the radius of individual spheroids. These gradients can influence cellular proliferation and viability [267], [356], [357]. In cases where spheroids are very large, nutrient supply to the centre of the spheroid can be limiting, leading to the formation of a necrotic core [352], [358]. This is commonly reported in spheroids

with sizes >500 μm in diameter [350]. In our study, each spheroid was formed from 600 cells with size <300 μm after 14 days of culture, and we did not observe formation of a necrotic core suggesting that metabolite limitation was not a problem in our micro-tumour models. If a hypoxic or necrotic micro-tumour core was desired, this could easily be designed into the model simply by increasing the number of cells per spheroid. A benefit of the Microwell-mesh platform is that it would enable formation of multiple micro-tumours of similar sizes to facilitate such analysis. If very large micro-tumours are desired (up to ~1.5 mm diameter), then our previously reported larger microwell platform would be more suitable than the one described here [290].

A major focus of the PCa field is the identification of combination and sequential drug regimens that more effectively treat metastatic and/or castrate-resistant prostate cancer (CRPC) [71], [359]. Treatment with Abiraterone Acetate, a potent selective inhibitor of CYP17A, can enhance survival in metastatic CRPC patients [65]. Similarly, Docetaxel is commonly used to treat advanced PCa patients [205]. Resistance to one or both is common, and the capacity to predict the optimal sequence or combination of these drugs (including with other existing or novel drugs) using *in vitro* model systems is a major goal in the field. For the reasons described above, it is believed that 3D models are likely to be more effective tools enabling *in vitro* predication of drug efficacy.

In the study described here we characterised 3D micro-tumour response to two common PCa drugs, Abiraterone Acetate and Docetaxel. We considered both single and sequential treatment outcomes, and compared the results to 2D PCa cell culture controls. A primary goal of our study was to develop methods that would enable the high-throughput characterisation of PCa micro-tumours within the Microwell-mesh platform; we view the capacity for high throughput analysis to be a major obstacle in the widespread uptake of 3D culture as a preferred tool for *in vitro* drug-screening studies.

Our results demonstrated that AlamarBlue could be reliably used to indirectly predict viable cell number in the Microwell-mesh plate simply by adding reagent to the plate, incubating the culture with the AlamarBlue and reading the signal from the plate (Figure 3.3). The presence of the PDMS microwell insert and nylon mesh did not confound the reading, and data indicate that future high throughput

characterisation of culture drug response could be done directly within Microwell-mesh plates. We subsequently used this approach to characterise C42B and LNCaP micro-tumour sensitivity to Docetaxel. Over a number of experiments, we found that both C42B and LNCaP micro-tumours demonstrated less sensitivity to Docetaxel than control 2D monolayers (Figure 3.6). In addition, because the Microwell-mesh retains micro-tumours, we were able to explore cellular response to sequential Docetaxel treatment. Again, 3D micro-tumours displayed reduced hypersensitivity to Docetaxel relative to 2D monolayers. Future studies could use the Microwell-mesh platform to track the evolution of Docetaxel resistant cell populations, or the influence of combinations of drugs and/or different stromal cell populations on treatment outcomes. A critical observation was that the mesh did indeed retain micro-tumours over multiple medium exchanges and wash steps (no cell loss), something not possible when using conventional microwell platforms or 2D cultures.

While AlamarBlue could be used to indirectly estimate viable cell numbers in Docetaxel treated micro-tumour cultures, this was not the case for anti-androgen treated cultures. We were surprised to observe that AlamarBlue conversion (taken as a surrogate for metabolic activity) appeared to increase significantly in cultures treated with Abiraterone Acetate or Enzalutamide (Figure 3.5 and Supplementary Figure 3.4). This apparent increase in metabolic activity, as inferred by the AlamarBlue assay, was particularly evident in 2D control cultures. If taken on its own, the AlamarBlue data suggested that cell numbers were largely unchanged in 3D cultures in response to Abiraterone Acetate, while cell numbers significantly increased in 2D cultures in response to increasing doses of Abiraterone Acetate (Figure 3.5a). This would be an unexpected outcome. Reassuringly, microscopy images of 2D treated cultures (Figure 3.5b) suggested that there was increasing cell death in response to increasing dose of Abiraterone Acetate. To validate the microscopy observations, we measured ATP concentration and DNA content in 2D and 3D cultures treated with Abiraterone Acetate (Figure 3.5a). Both ATP and DNA quantification suggested that 3D cultures were not impacted by Abiraterone Acetate treatment, but that 2D cultures were indeed dying as the images suggested. Multiple replicate experiments demonstrated that there is a robust disconnect between ATP and DNA content relative to AlamarBlue signal evolving from 2D cultures treated with Abiraterone Acetate or Enzalutamide. It is well known that not only

mitochondrial enzymes can reduce AlamarBlue reagent to its fluorescent isoform (Resorufin), it can also be reduced by cytoplasmic reductases and the electron transport system of the cell [347]. We reasoned that mitochondria activity might be upregulated in response to the apoptotic signals generated by the Abiraterone Acetate treated cells [360], so we used DHR123 and flow cytometry to quantify mitochondria activity in these cells (Figure 3.5b). While AlamarBlue conversion was greater in the Abiraterone Acetate treated cells, there was a drop in DHR123 signal suggesting that mitochondria activity was not upregulated in the Abiraterone Acetate treated cells. Our results suggest the involvement of cytoplasmic reductases, rather than mitochondrial activity, which cause the drastic increase in AlamarBlue readings in 2D cultures. While it is common to characterise cellular response to anti-cancer drugs using AlamarBlue [347], we would caution against using AlamarBlue assay to study response to Abiraterone Acetate treatments. To our knowledge, the disconnect between the increase in AlamarBlue signal and Abiraterone Acetate and Enzalutamide mediated PCa cell death has not been previously reported.

Overall, our results indicate that 3D micro-tumour cultures are less sensitive, than 2D cultures, to changes in androgen signalling introduced either through depletion of androgen from the medium (CSS) or through pharmaceutical inhibition of CYP17A (Abiraterone). With Docetaxel treatment, the behaviour of the 3D micro-tumours was also markedly different from that seen in the 2D monolayers. The cytotoxic drug family of taxanes, including Docetaxel, target proliferating cells by stabilizing microtubules causing a cell cycle arrest and apoptosis [254]. Therefore, it was expected to observe a considerable difference in response in the slow proliferating 3D micro-tumours compared to more proliferative traditional 2D cultures.

In the present study, we demonstrated the utility of the Microwell-mesh as a viable high throughput platform for 3D cancer cell culture and drug-screening. A limitation with our proposal is that the Microwell-mesh must be manually fabricated. However, we do provide extensive details here and in our previous publications on the fabrication methods [289], [290]. Once a microwell mould has been fabricated, it is relatively easy and inexpensive to generate hundreds of microwell inserts. PDMS is inexpensive, and 500 grams of PDMS can be purchased for ~$100 USD. This is theoretically sufficient to generate 2500 inserts (~0.2 grams/insert), although casting

inefficiencies are likely to reduce actual yield to ~1000 inserts. With practice, mesh can be bonded to the microwells efficiently yielding many microwell-mesh well plates in a day. It is not currently possible to purchase the Microwell-mesh platform from a commercial vendor, but growth in the 3D cell culture field may motivate a vendor to consider manufacture of a similar product, which could facilitate quality control, and standardization across the field. Standardized products can have significant commercial value, and this value has motivated the establishment of companies such as QGel (Switzerland) that mass-produces hydrogels that can be used to culture cell spheroids, and multiwell plate products like InSphero GravityTRAP (InSphero, Switzerland) purpose built for spheroid culture. StemCell Technologies (Canada) already manufactures a microwell product (the AggrewellTM) that shares many common features with our Microwell-mesh, and the addition of a mesh to the Aggrewell platform might be a logical next step in StemCell Technologies' manufacturing process. In the absence of a commercial source, laboratories experienced with the fabrication of microdevices from PDMS will find fabrication of the Microwell-mesh to be a straightforward process that can be rapidly optimised.

Metabolic activity and many other characteristics of 3D micro-tumour cultures can be assessed directly within the Microwell-mesh, or simply removing the mesh allows direct access to hundreds of replicate micro-tumours for histology or other analysis methods such as flow cytometry. Spheroids produced in other platforms (gels or microfluidics) are not as readily accessible [361]. Relative to microfluidics devices, the Microwell-mesh is inexpensive to fabricate, and requires no complex pumps or other equipment to operate. Unlike many gel systems, it is unnecessary to expose cells to UV light to encapsulate them and to use enzyme to later recover/harvest cells from the gel [362], [363]. Future work might include the assembly of complex micro-tumours from combinations of PCa and stromal cells to better mimic the bone microenvironment commonly targeted by metastatic PCa [364], [365]. Micro-tumours assembled from PCa and bone cells are likely to provide an excellent model with which to screen drugs and to study cell-cell interactions that promote metastasis and/or contribute to drug resistance. In either application, multiple medium exchanges will likely be required. The retention of micro-tumours within discrete microwells in the Microwell-mesh by the nylon mesh

will represent a significant improvement over conventional microwell platforms, enabling microwell cultures to contribute to this logical scientific and platform evolution.

Acknowledgment

The authors would like to thank the National Health and Medical Research Council (NHMRC) of Australia for funding this research.

Author Contributions Statement

E.M. designed research, performed research, analysed data and wrote the paper.

K.C., K.F. and J.C. analysed data and wrote the paper.

M.D. designed research, analysed data and wrote the paper.

Competing financial interests

The authors declare no competing financial interests.

3.6 SUPPLEMENTARY DATA

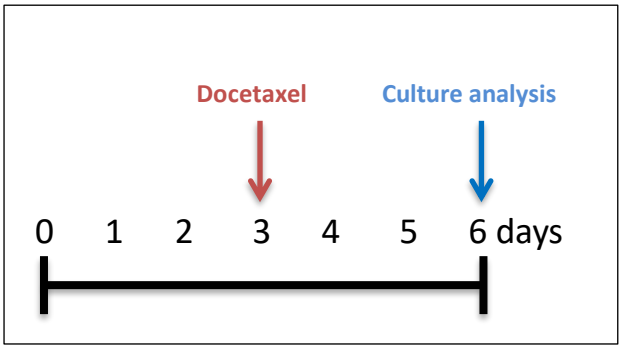

Supplementary Figure 3.1. Single Docetaxel treatment protocols of prolonged time cultures. A single treatment of Docetaxel was performed after 72 hours of seeding the cells. Drug response was then assessed following three days of exposure to Docetaxel (day 6).

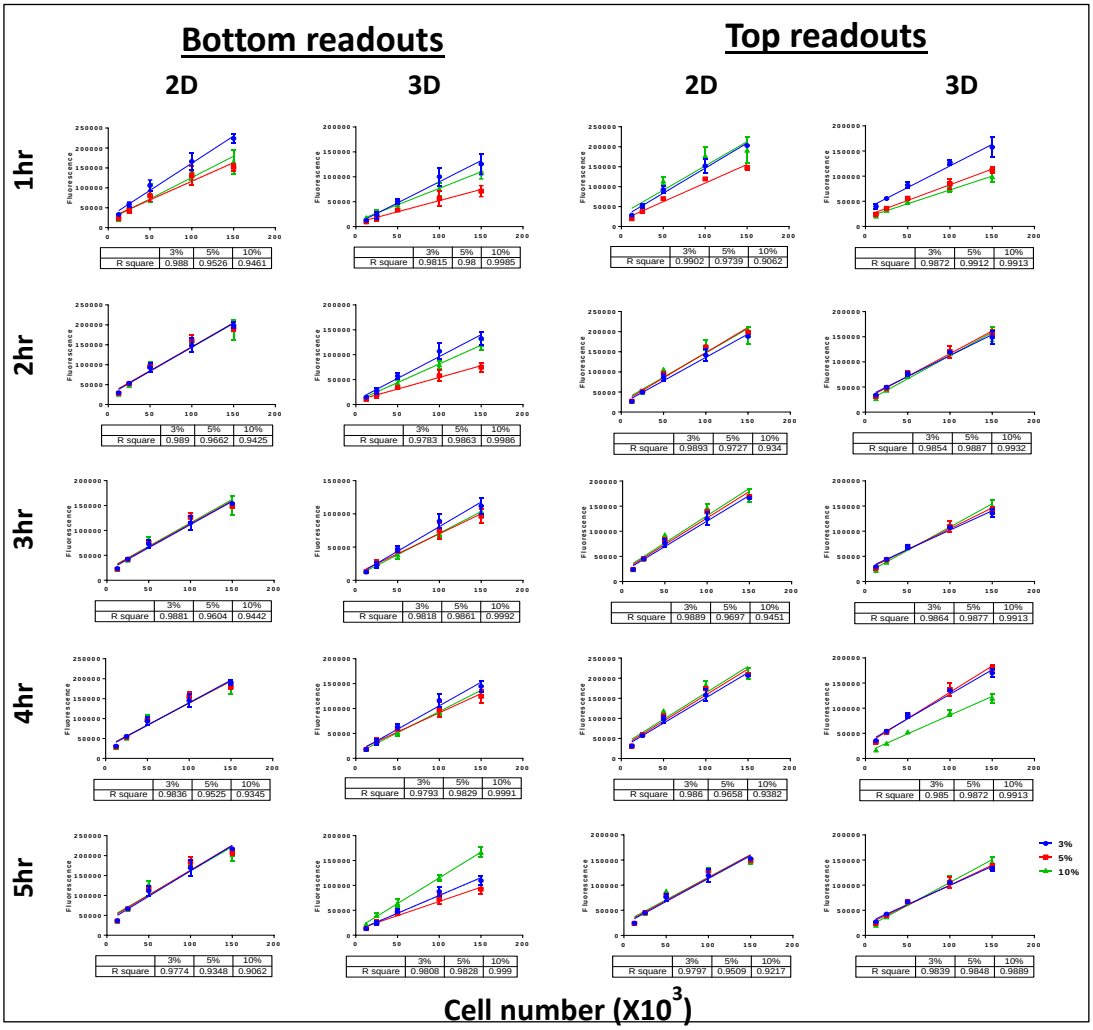

Supplementary Figure 3.2. AlamarBlue assay optimization in 48-well plate. Cells were seeded overnight in 2D and 3D cultures at the indicated cell densities (12.5, 25, 50, 100 and 150x10^3 cells/well). AlamarBlue reagent was added in three different concentrations (3, 5 and 10%). The fluorescence readouts (nm) were acquired after 1, 2, 3, 4 and 5 hours of incubation. At every time point, the fluorescence was measured from the top and the bottom of the plate. The fluorescence values were plotted against cell numbers to determine the linearity of the assay. R square values of the three tested AlamarBlue concentrations (3, 5 and 10%) are represented under each graph.

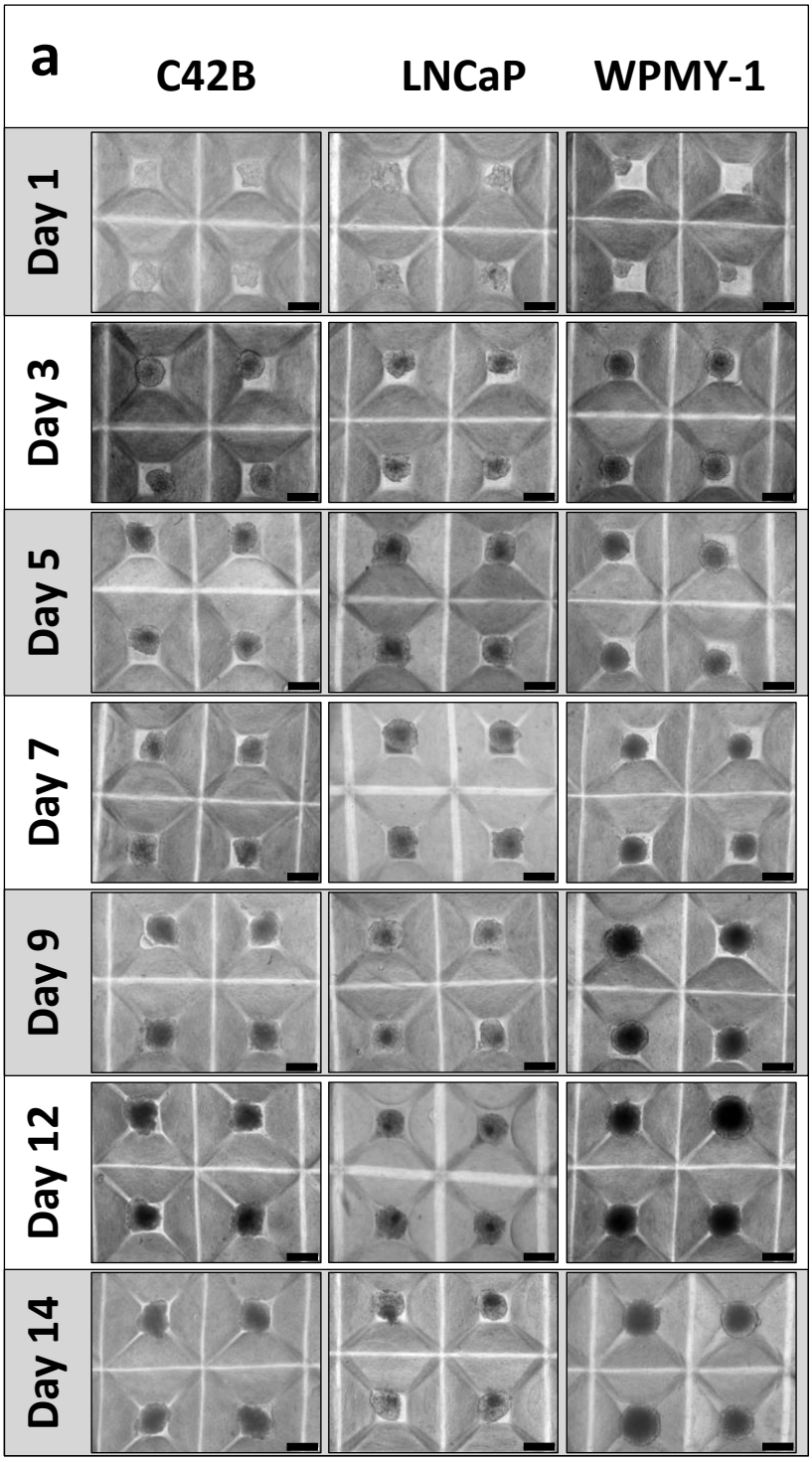
a
C42B
LNCaP
WPMY-1
Day 1
Day 3
Day 5
Day 7
Day 9
Day 12
Day 14

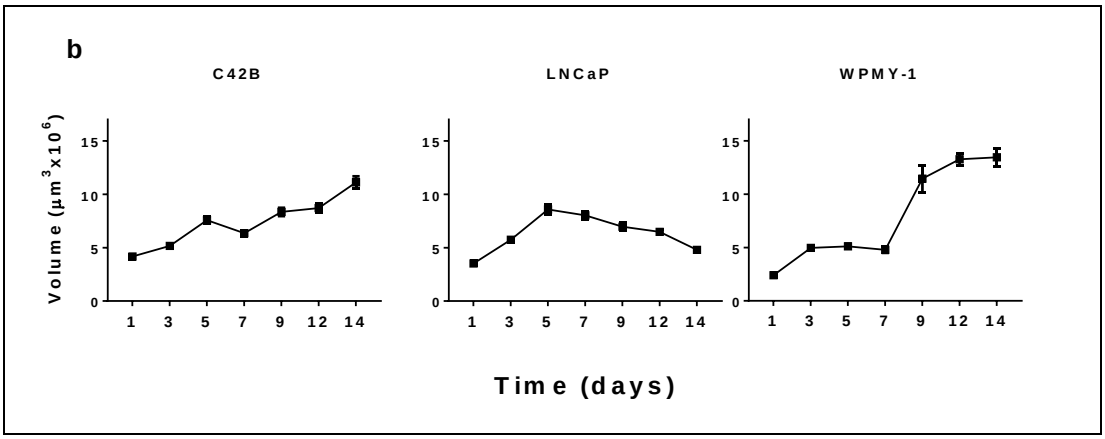

Supplementary Figure 3.3. Prostate cancer cell line in 3D micro-tumour culture. Prostate cancer (C42B and LNCaP) and prostate myofibroblasts (WPMY-1) cell lines were cultured in the 3D platform (600 cells/spheroid). **(a)** Bright field images were captured every two days. **(b)** Spheroids volume was calculated via diameter measurement of 50 spheroids every two days (mean ± SD). Scale bar = 200 µm.

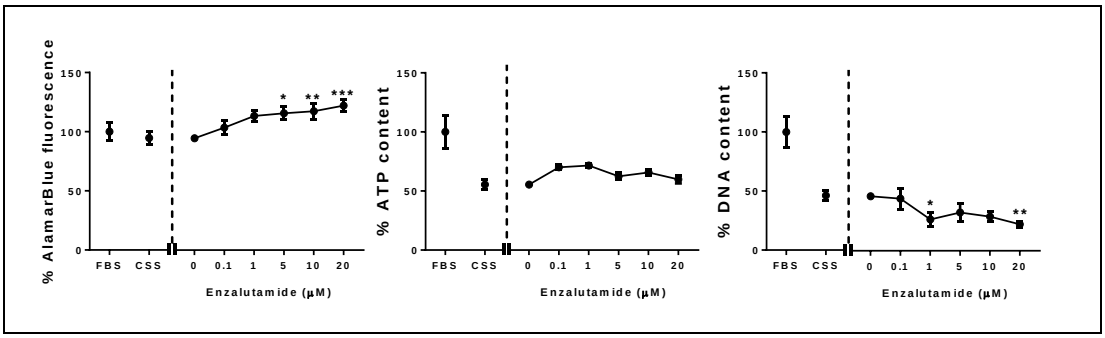

Supplementary Figure 3.4. Monolayer behaviour of LNCaP cells in androgen deprived conditions. LNCaP cells were seeded in expansion culture medium for 24 hours followed by medium exchange to androgen-depleted medium (CSS) for a further 48 hours. Enzalutamide was then added to the culture medium at the indicated concentrations for an additional 48 hours. AlamarBlue fluorescence, ATP quantity and DNA quantity were then assessed. All results are represented as a percentage of the FBS-containing culture medium control values (Three independent experiments each had four replicate cultures). Statistical significance was calculated by two-way ANOVA compared to the corresponding zero value (*** P<0.001, ** P<0.01 and * P<0.05).

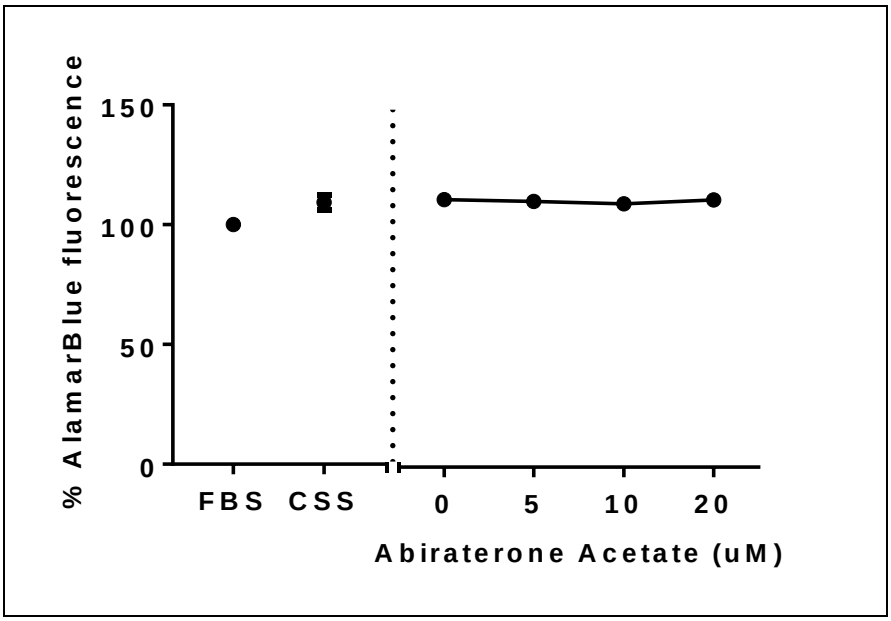

Supplementary Figure 3.5. AlamarBlue assay of cell-free cultures. In the absence of cancer cells, AlamarBlue signal unchanged with the serial concentrations of the antiandrogen drug, Abiraterone Acetate.

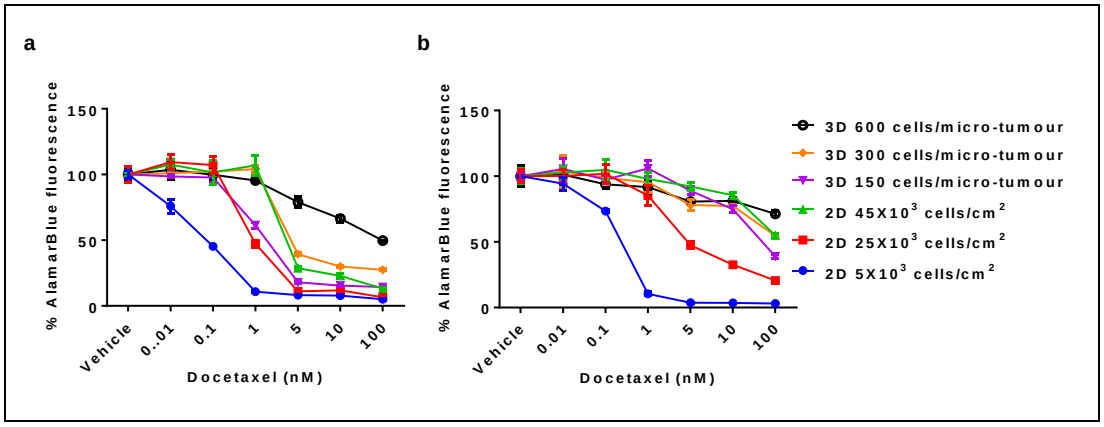

Supplementary Figure 3.6. Cell culture density impact on *in vitro* cytotoxic drug response. Cells were grown in 2D and 3D cultures in the indicated densities following the single Docetaxel treatment protocols in Figure 3.1b and Supplementary Figure 3.1. Compared to 1 day culture prior drug treatment **(a)**, the cultures with prolonged period (3 days) prior Docetaxel treatment **(b)** are less sensitive to the cytotoxic drug.

Chapter 4: Constraints to counting bioluminescence producing cells by a commonly used transgene promoter and its implications for experimental design

Chapter 4 preface:

As described in Chapter 2 and Chapter 3, microtissues formed from bone marrow stromal cells and PCa cells can be assembled in the Microwell-mesh platform to study the impact of the bone marrow microenvironment on PCa cell behaviour and drug response. However, PCa cell number cannot be quantified by conventional metabolic assays or total DNA quantification in the mixed cell population. In this Chapter, we characterised the stability and reliability of the luciferase reporter system, as a cell-specific assay, in prostate and breast cancer cell lines in mono- and co-cultures.

4.1 ABSTRACT

It is routine to genetically modify cells to express fluorescent or bioluminescent reporter proteins to enable tracking or quantification of cells *in vitro* and *in vivo*. Herein, we characterise the stability of luciferase reporter systems in C42B prostate cancer cells in mono-cultures and co-cultures with bone marrow-derived mesenchymal stromal cells (BMSC). An assumption made when employing the luciferase reporter is that the luciferase expressing cell number and bioluminescence signal are linearly proportional. We observed instances where luciferase expression was significantly upregulated in C42B cell populations when co-cultured with BMSC, resulting in a significant disconnect between bioluminescence signal and cell number. Whole-genome sequencing revealed that the stable C42B population had 84 luciferase genomic insertion sites, while the unstable population had only 4 insertion sites. We speculate that the reduced number of luciferase insertion sites made the unstable cells exquisitely sensitive to secretions from the BMSC. In this study, we show that it is possible to generate a range of stable and reliable luciferase reporter prostate and breast cancer cell populations, but advise not to assume stability in different culture conditions. Reporter stability should be validated, on a case-by-case basis, for each cell line and culture condition.

4.2 INTRODUCTION

Quantifying specific cell populations in complex co-cultures, or in animals, requires that cells of interest are distinguishable from neighbouring cells. To this end, it is increasingly common to genetically label cells such that they express a specific fluorescent or bioluminescent (e.g. luciferase) reporter protein, thereby enabling their tracking and quantification. Quantifying cancer cell number in complex co-cultures warrants strategies such as the use of luciferase-expressing cancer cell populations [366]–[368]. McMillin and colleagues described such an approach in their seminal 2010 publication in *Nature Medicine* [369]. They retrovirally transduced human multiple myeloma cells to express luciferase, and used this as a reporter to quantify myeloma cells in co-culture with bone marrow-derived mesenchymal stromal cells. As it is increasingly appreciated that non-cancerous cells in the tumour

microenvironment play a significant role in tumour establishment, growth and drug response [280], [281], [370], [371], this assay is likely to see great utility.

The underlying assumption when using bioluminescence to estimate the number of cells in a co-culture, or in an animal, is that there is a linear relationship between the bioluminescence signal and the number of viable cells expressing the reporter protein (typically luciferase). This requires that expression and production of the luciferase enzyme is stable in cell populations over time, and across different culture conditions. This is analogous to the properties desired by a housekeeping gene in qPCR [372]. It is common practice for research groups to calibrate their bioluminescence assays using a titration of luciferase-expressing cells in a monoculture. The derived data is next used to estimate the number of luciferase cells in a co-culture based on relative bioluminescence [373].

The luciferase reporter construct, which is inserted into the genome of the labelled cell population, is usually composed of at least two regions. The first region is a promoter designed to constitutively drive the expression of the reporter(s). The second region is the reporter, usually the gene sequence for bioluminescent luciferase, a fluorescent protein (for example red fluorescent protein, RFP; or green fluorescent protein, GFP), or both. The gene expression of the reporter is dependent on that of the promoter, and ideally the promoter activity should be uniform across all culture conditions [374].

In our own work, we observed instances where the luciferase bioluminescence signal generated by C42B cells, an LNCaP-derived cell line isolated from metastatic prostate cancer cells from the lumbar spine of castrated mice [224], [375], was significantly greater when these cells were co-cultured with bone marrow-derived mesenchymal stromal cells (BMSC), than when in mono-culture. These observations suggested that a luciferase reporter may not be a viable method to estimate relative cancer cell number under these culture conditions. Here, we wanted to better assess the utility and reliability of using the bioluminescence signal from luciferase transduced cells to estimate C42B cell numbers in BMSC co-culture. We compared bioluminescence signal, luciferase gene expression, and DNA content in C42B populations where the luciferase reporter appeared to be stable and in populations where the luciferase reporter appeared to be unstable. Next, we performed whole-genome sequencing to determine the genetic difference between these two cell

populations. Finally, we characterised the stability of six additional luciferase reporter cell populations, driven by distinct gene promoters, in mono-cultures and BMSC co-cultures.

4.3 MATERIALS AND METHODS

Bone marrow-derived mesenchymal stromal cell isolation and characterization

Human bone marrow aspirates were collected at the Mater Hospital (Brisbane, Australia) from fully informed and consenting healthy volunteer donors. Ethical approval was granted through the Mater Health Services Human Research Ethics Committee and the Queensland University of Technology Ethics Committee (number 1000000938); in accordance with the Australian National Health and Medical Research Council's Statement on Ethical Conduct in Research Involving Humans,

Monocyte isolation was achieved by density gradient centrifugation, using Ficoll-Paque Plus (GE Healthcare), as previously described [319]. Cells were maintained in DMEM-LG supplemented with 10% fetal bovine serum (FBS), 100 U/ml penicillin, and 100 μg/mL streptomycin (1% PS; Thermo Fisher) in a humidified incubator containing 5% CO_2 with 2% O_2 atmosphere at 37ºC. The isolated cells were characterized by flow cytometry for their expression of a bone marrow-derived mesenchymal stromal cells (BMSC) specific surface antigen panel (Supplementary Table 4.1). Mesodermal trilineage differentiation capacity was confirmed using the corresponding induction media for osteogenic, adipogenic, and chondrogenic differentiation; using methods described previously [289], [290] (Supplementary Figure 4.1).

Cancer cell line culture

Prostate cancer cell lines (C42B and PC3) were obtained from the American Type Culture Collection (American Type Culture Collection, ATCC). Breast cancer cell lines (MDA-MB-231 and MCF-7) were kindly provided by Dr Eloise Dray and Prof Lisa Chopin (Queensland University of Technology). Cell lines were authenticated at the Genomic Research Centre (GRC; Brisbane, Australia) using Short Tandem Repeat (STR) analysis. Briefly, STR profiles were compared to the ATCC STR Database to verify cell line identity. All cultures were performed in low

glucose Dulbecco's modified Eagle's medium (DMEM-LG; Thermo Fisher) supplemented with 10% FBS and 1% PS in a humidified incubator containing 5% CO_2 with a 20% O_2 atmosphere at 37°C.

Production of luciferase-tagged prostate cancer cell lines

All transduced cell lines are listed in Table 4.1, along with the terms used throughout this study to describe them. Luciferase expressing C42B cells were generated using the 3rd generation ViraPower lentiviral gene expression system (Thermo Fisher), as described previously [376]. In each cell line the CMV promoter drove luciferase expression. These two cell lines were a generous donation from Dr Patrick Ling (Queensland University of Technology), and are referred to as C42B-CMV1 in Table 4.1.

We generated a number of additional luciferase-expressing prostate cancer and breast cancer cell lines. MCF-7 breast cancer cells were transduced with commercial, pre-made 3rd generation lentiviral expression particles (AMSBIO, LVP020) as per the manufacturers' instructions. In these cells, luciferase and GFP were driven by the elongation factor 1 alpha (EF1a) promoter. Cultures were enriched for transduced cells by FACSorting (MoFlo Astrios; Beckman Coulter) for GFP^+ cells. Cultures were validated to be stably GFP^+ at subsequent culture time points via flow cytometer analysis.

Using Lentiviral particles manufactured in-house, we transduced C42B, MDA-MB-231, and PC3 with a plasmid expressing luciferase and a fluorescent reporter. These lentiviral particles contained constructs designed to express luciferase and red fluorescent protein (Luc-RFP) or luciferase and green fluorescent protein (Luc-GFP). Constructs were purchased from Bioluminescence Imaging Vectors (BLIV, System Biosciences). The promoter and colour combinations were cytomegalovirus (CMV), (CMV-Luc-RFP), murine stem cell virus (MSCV) (MSCV-Luc-GFP), or EF1a (EF1a-Luc-GFP). Please see Supplementary Figure 4.2 for construct details. Viral particles were manufactured, and cells transduced, as described below.

Plasmids were produced using Stbl3 Chemically Competent *E.coli* (Thermo Fisher) as per the manufacturers' instructions. Plasmids were purified using the NucleoBond Xtra EF plasmid purification kit (Midi EF, Macherey-Nagel). They were packaged in Lipofectamine 2000 (Thermo Fisher), and transfected into 293FT

cells (Thermo Fisher) to produce viral particles. Cancer cells were next exposed to the viral particles in the presence of 8 μg/mL polybrene to facilitate transduction. Transduced cells were FACs sorted to enrich for GFP^+ or RFP^+ cells, yielding cell lines stably expressing Luc-RFP or Luc-GFP with one of three regulatory promoters (MSCV, CMV, or EF1a).

Table 4.1. List of cancer cell lines used with respective transduced promoters

Parent cell line	Promoter-reporter	Referred to as	Construct source
C42B	CMV-Luc	C42B-CMV1	Plasmid (Dr. Patrick Ling [376])
C42B	CMV-Luc-RFP	C42B-CMV2	Plasmid (Supplementary Figure 4.2b)
C42B	MSCV-Luc-GFP	C42B-MSCV	Plasmid (Supplementary Figure 4.2a)
C42B	EF1a-luc-GFP	C42B-EF1a	Plasmid (Supplementary Figure 4.2c)
PC3	CMV-Luc-RFP	PC3-CMV2	Plasmid (Supplementary Figure 4.2b)
MCF-7	EF1a-Luc-GFP	MCF-7-EF1a	Viral particles (AMSBIO, LVP020)
MDA-MB-231	CMV-Luc-RFP	MDA-CMV2	Plasmid (Supplementary Figure 4.2b)
MDA-MB-231	MSCV-Luc-GFP	MDA-MSCV	Plasmid (Supplementary Figure 4.2a)

DNA quantitation

The Quant-iT PicoGreen dsDNA assay (Thermo Fisher) was performed as per the manufacturer's instructions to determine the quantity of the double stranded DNA in each culture condition.

Cell viability measurement

The AlamarBlue assay (Thermo Fisher) was used to measure the metabolic activity of cells. AlamarBlue reagent was added to the culture media at a final concentration of 3%. The plates were incubated for 1 hour at 37 ^oC, to permit reduction of the AlamarBlue reagent, and fluorescence read at 544 nm excitation and 590 nm emission (BMG Omega plate reader (BMG LABTECH).

Bioluminescence assay

For luciferase assays, D-luciferin (Promega) was added to the culture medium at a final concentration of 15 μg/mL, incubated at 37°C for 15 minutes, and bioluminescence measured using a PHERAstar FS plate reader (BMG LABTECH).

Data is presented as relative bioluminescence (RLU) compared to the control, unless stated otherwise.

Co-culture system

For direct co-cultures, BMSC (10×10^3) were seeded in 96-well plates for 24 hours to permit adherence to the tissue culture plate. The following day, a titration of cancer cells was seeded either on the top of adherent BMSC (co-cultures) or into empty wells (control mono-cultures). For Transwell assays, BMSC (10×10^3) were seeded into the top Transwell insert (Millicell culture inserts, Merck Millipore) and 90×10^3 cancer cells seeded in the bottom wells of 24-well plates. For C42B-MSCV cells, co-cultures were established using a reduced cell number (20×10^3 luciferase-tagged cells), because of their higher proliferation rate. Transwell insert pore sizes of 0.4 µm were employed to prevent passing of BMSC through the Transwell membrane, and to enable independent quantification of the cells on the top and bottom of the cultures at the endpoint. Co-cultures were incubated for 0, 5, 24 hours, bioluminescence measured, and cells harvested. At every time point, a parallel mono-culture was maintained as a control.

Quantitative real-time RT-PCR (qRT-PCR)

To assess the stability of luciferase gene expression in mono-cultures and co-cultures, RNA was extracted from cancer cells of mono-cultures and indirect co-cultures using the RNeasy Mini Kit (Qiagen). Luciferase gene primer pairs were designed using Primer3Plus [377] and were checked for specificity by querying the firefly (*Photinus pyralis*) luciferase gene (GenBank: M15077.1) and *Homo sapiens* genome using NCBI Primer-BLAST [378]. To optimize the housekeeping genes and luciferase gene primers for qRT-PCR, four primer concentrations were used with three different cDNA template amounts. The optimum primer concentrations were chosen according to the highest amplification efficiency.

All RNA samples were treated with *DNase I* (1 U/µl, final concentration) in solution, at 37 °C for 30 minutes followed by 10 minutes incubation at 65 °C to deactivate the enzyme. Next, cDNA was generated from 500 ng total RNA using the SuperScript III First-strand synthesis kit (Thermo Fisher). We measured relative gene expression using Power SYBR green PCR master mix (Applied Biosystems) on Viia7 Real Time PCR system (Applied Biosystems). Each sample was tested using 5

µL reactions in a 384-well plate with three technical replicates and a negative control, which did not contain SuperScript III Reverse Transcriptase. Each condition had four biological replicates. Amplification was performed with an initial cycle of 50 °C for 2 minutes and 60 °C for 1 minute, 40 quantification cycles (with one cycle consisting of 95 ° C for 15 seconds and 60 °C for 1 minute), followed by the thermal dissociation protocol for SYBR Green detection. Relative luciferase gene expression was normalized to the housekeeping gene ribosomal protein lateral stalk subunit P0 (*RPLP0*). Two housekeeping genes, glyceraldehyde-3-phosphate dehydrogenase (*GAPDH*) and *RPLP0*, were tested. RPLP0 was used in subsequent experimental analysis because it demonstrated the greatest expression stability across all culture conditions in transduced cell lines (see Supplementary Figure 4.3). The primers used are listed in Table 4.2 along with the annealing temperature and the primers' final concentrations in each reaction.

Table 4.2. Primers and annealing temperatures used for qRT-PCR

Gene	Sequence (5'- 3')	Annealing temperature (°C)	Final primers conc. (nM)	Amplicon size (bp)
GAPDH	F GGGAGGTAGAGGGGTGATGT R TTCAGCTCAGGGATGACCTT	60	200	204
RPLP0	F TGTGGGCTCCAAGCAGATGCA R GCAGCAGTTTCTCCAGAGCTGGG	60	200	137
Firefly luciferase	F GTGTTGGGCGCGTTATTTAT R TACGGTAGGCTGCGAAATGT	60.7	200	102

Whole-genome sequencing

Genomic DNA sequencing was performed at the Garvan Institute's Kinghorn Centre for Clinical Genomics (KCCG; Sydney, Australia). DNA was extracted from C42B-CMV1 and C42B-CMV2 cell populations using TRIzol reagent (Thermo Fisher). Whole-genome sequencing was performed on the HiSeqX Ten sequencing platform (TruSeq Nano) using HiSeq X Reagent Kit v2.5. Transgene insertion mapping was performed using STAR [379], and chimeric reads with at least 20 base

pair overhang between luciferase (GenBank: M15077.1) and human reference genome (hg38) retained. Discordant read-pair mappings from BWA-MEM [380] were used to independently verify the location of the transgene insertions. Insert locations were visualized using Circos [381]. Full sequence data is freely available upon request; please contact the authors.

Statistical analysis

Results are displayed as the mean values of three independent experiments, each with four technical replicates, unless mentioned otherwise. Error bars represent standard deviation. Statistical significance of data was evaluated using non-parametric one-way or two-way analysis of variance (ANOVA) in Prism v6.0 (GraphPad Software). *P*-values obtained in each comparison are represented by asterisks in graphs as detailed in the caption.

4.4 RESULTS

C42B-CMV1 characterisation in mono- and co-culture

BMSC were used in co-cultures. These cells were shown to manifest the expected BMSC characteristics, including marker profiles and tri-lineage differentiation capacity (See Supplementary Table 4.1 and Supplementary Figure 4.1). We characterised the bioluminescence signal and AlamarBlue conversion of cultures established from different numbers of C42B-CMV1 cells (Figure 4.1a). Both bioluminescence signal and AlamarBlue signal were linearly proportional to the number of C42B-CMV1 cells. When C42B-CMV1 cells were co-cultured with varying numbers of BMSC for 5 or 24 hours, the bioluminescence signal increased substantially in cultures where BMSC were present, relative to controls that contained no BMSC (Figure 4.1b). The bioluminescence signal did not appear to increase when greater than 10×10^3 BMSC were included in the co-cultures. When titrations of C42B-CMV1 cell numbers were made with fixed numbers of BMSC in co-culture, a bioluminescence signal proportional to C42B-CMV1 cell number was evident (Figure 4.1c). However, the linear relationship between bioluminescence signal and C42B-CMV1 cell number was different for mono- and co-cultures at 5 and 24 hours. The slope of the curves was always greater for co-cultures, relative to time-matched (5 or 24 hours) mono-culture controls. At 5 hours, the bioluminescence signal from C42B-CMV1 cells was significantly greater when these cells were

maintained either in direct co-culture (seeded on top of BMSC) or indirect co-culture (with BMSC in a Transwell assay), relative to mono-culture controls (Figure 4.1d). Direct and indirect co-culture resulted in ~7-fold or ~4-fold increase in bioluminescence signal after 5 hour of culture, respectively. As C42B cells double once every ~48 hours [382], the magnitude of bioluminescence signal increase after 5 hours could not be accounted for by cell proliferation.

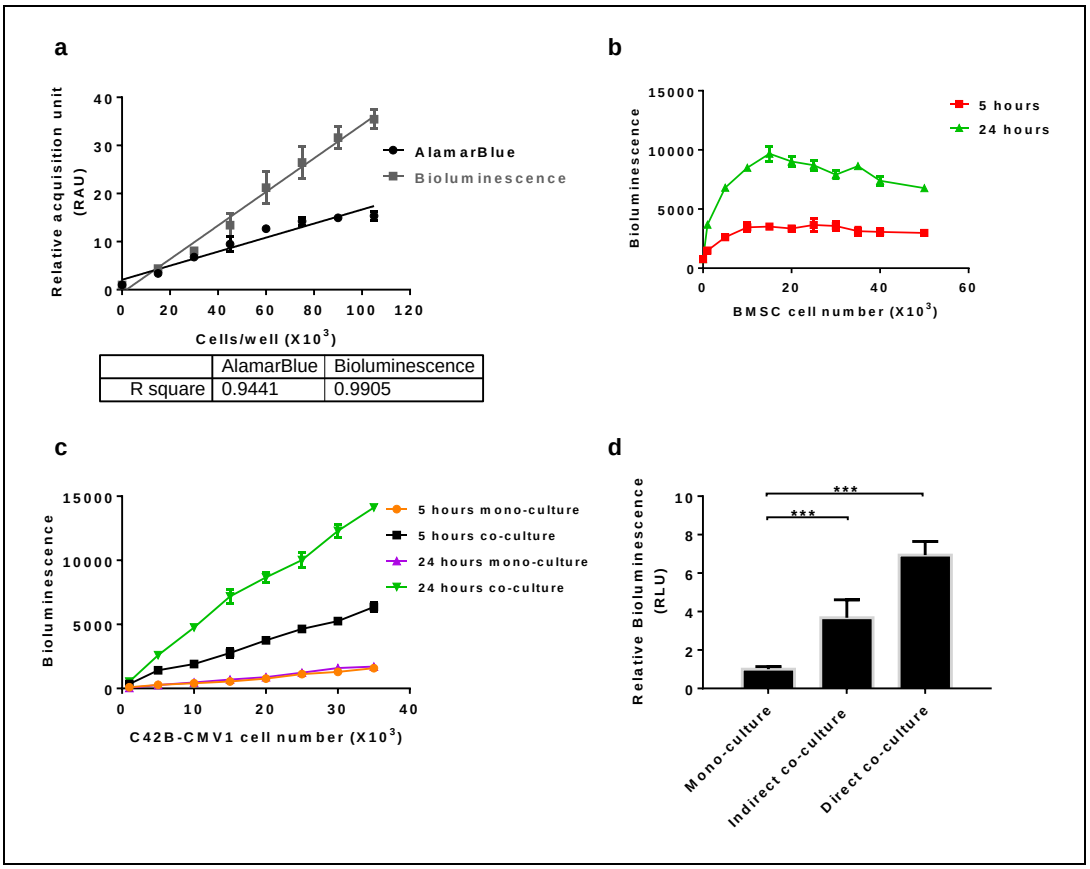

	AlamarBlue	Bioluminescence
R square	0.9441	0.9905

Figure 4.1. C42B-CMV1 behaviour in mono-cultures and co-cultures with bone marrow-derived mesenchymal stromal cells (BMSC). (a) Comparison of luciferase and AlamarBlue assay readouts in C42B-CMV1 mono-cultures. **(b)** Ten thousand C42B-CMV1 cells were directly cultured with increasing cell number of bone marrow-derived mesenchymal stromal cells (BMSC). Bioluminescence was measured at the indicated 3 time points. Data was normalized to the values of the lowest BMSC cell density at the corresponding time point (n=4). **(c)** Increasing numbers of C42B-CMV1 cells were directly cultured with 10×10^3 BMSC in 96-well plates. The graph represents the mean bioluminescence values of 2 independent experiments each with 3 technical replicates. **(d)** The relative bioluminescence values elevated after 24 hours of direct and indirect co-cultures of C42B-CMV1 and BMSC compared to mono-cultures. Three independent experiments each had four technical replicate cultures (*n*=4) were performed (A-D). Statistical significance was performed using nonparametric one-way ANOVA (*** P< 0.001).

C42B-CMV1 versus C42B-CMV2 culture characterisation

We compared the bioluminescence signal, DNA content, and luciferase gene expression in C42B-CMV1 versus C42B-CMV2 mono-cultures and co-cultures with BMSC in Transwell assay (Figure 4.2). At 5 and 24 hours there was a significant increase in the bioluminescence signal from C42B-CMV1 cell co-cultured with BMSC (Figure 4.2a). This was consistent with the data presented in Figure 4.1. This increase correlated with a significant upregulation in luciferase gene expression (Figure 4.2c). However, there was no corresponding increase in C42B-CMV1 cell culture DNA content in co-cultures, relative to mono-cultures. This suggested that the increase in luciferase expression and bioluminescence signal was not related to an increase in C42B-CMV1 cell number in co-cultures. Rather, luciferase expression and bioluminescence signal in C42B-CMV1 appeared to change independently of cell number in mono and co-cultures.

A small, but consistent increase in bioluminescence signal from C42B-CMV2 cells was detected after 24 hours of co-culture, relative to mono-culture controls. There was no measureable difference in luciferase gene expression or DNA content in C42B-CMV2 mono-cultures and BMSC co-cultures. C42B-CMV1 and C42B-CMV2 cell culture DNA content did increase over the 24 hours culture period, but the presence of BMSC did not measurably alter the rate of DNA content increase. Luciferase expression and bioluminescence signal was stable across mono- and co-culture conditions for C42B-CMV2 cells at 5 hours. By contrast, luciferase expression and bioluminescence signal was not stable across mono and co-culture conditions for C42B-CMV1 cells at 5 hours. We replicated these assays with different quantities of FBS or co-culture with parental C42B cells in place of BMSC (cells not modified to express luciferase) to determine if a change in any soluble signalling environment could cause this artefact shown in Figure 4.2. Neither changes in FBS concentration, nor co-culture with additional parental C42B cells, modified the bioluminescence signal (see Supplementary Figure 4.4). These data indicated that factors specifically secreted by BMSC, not contained in FBS or secreted by C42B cells, caused the increase in bioluminescence signal from the C42B-CMV1 cells.

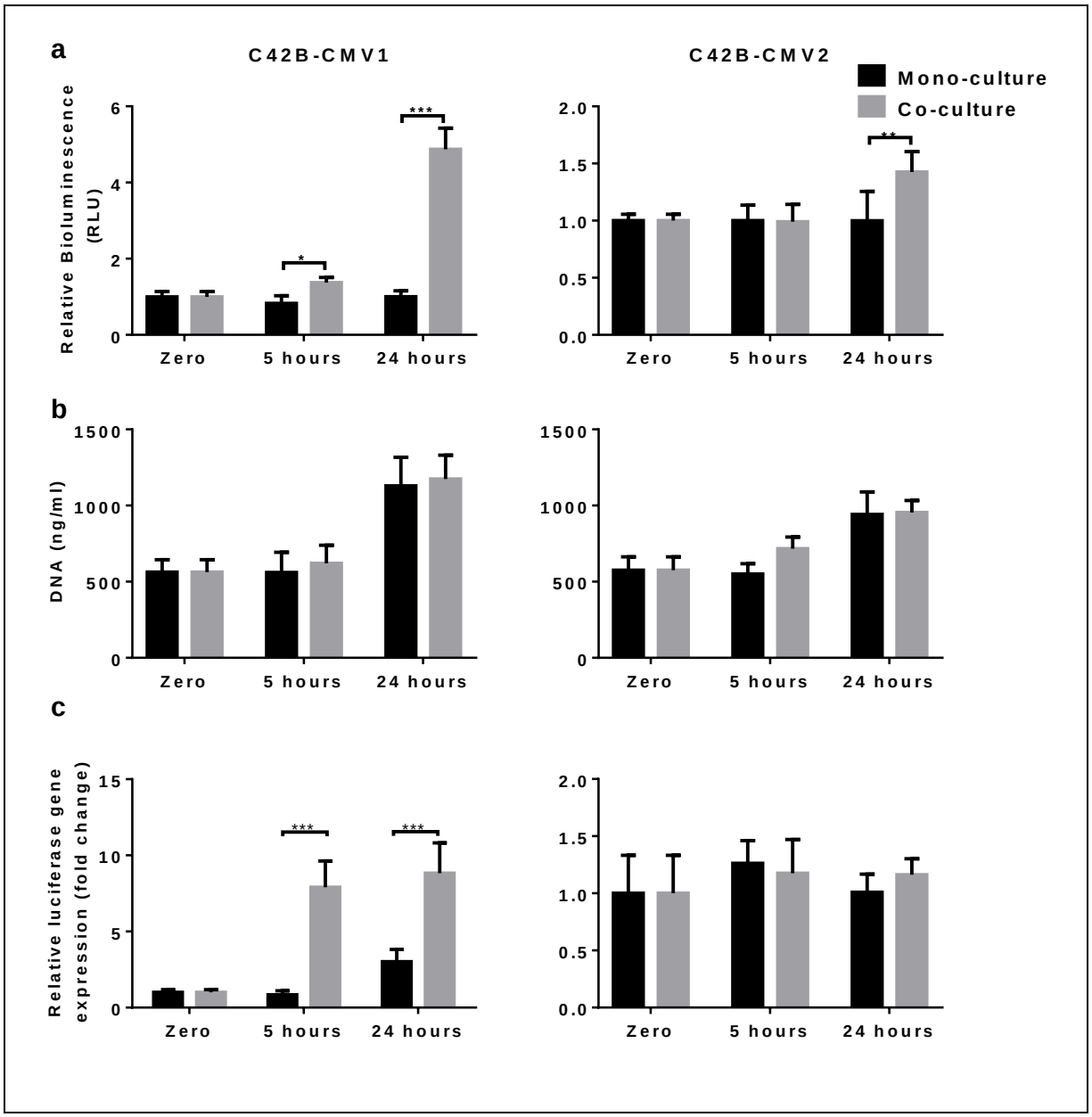

Figure 4.2. Luciferase gene expression is dependent on culture condition. C42B-CMV1 (left panel) and C42B-CMV2 cell lines (right panel) were either mono- or co-cultured with BMSC in a Transwell assay for the indicated time points. The relative bioluminescence **(a)**, DNA content **(b)** and relative luciferase gene expression **(c)** were assessed. Three independent experiments each had four technical replicate cultures (n=4) were performed. Statistical significance was determined using two-way ANOVA (* P< 0.05, ** P<0.001, *** P<0.00001).

C42B-CMV1 versus C42B-CMV2 genome characterisation

To gain insight into why the C42B-CMV1 and C42B-CMV2 cells behaved so differently, we conducted whole-genome sequencing of both populations (at 30× coverage). We firstly observed that firefly luciferase sequence was much more abundant in C42B-CMV2 genomes compared to C42B-CMV1 (Supplementary Figure 4.5). Using chimeric read mapping between the human genome and firefly luciferase, we mapped sites with evidence of CMV-luciferase insertion (Figure 4.3). This analysis mapped four CMV-luciferase insertion sites in the C42B-CMV1 cell population, while the C42B-CMV2 cell population had 84 insertion sites.

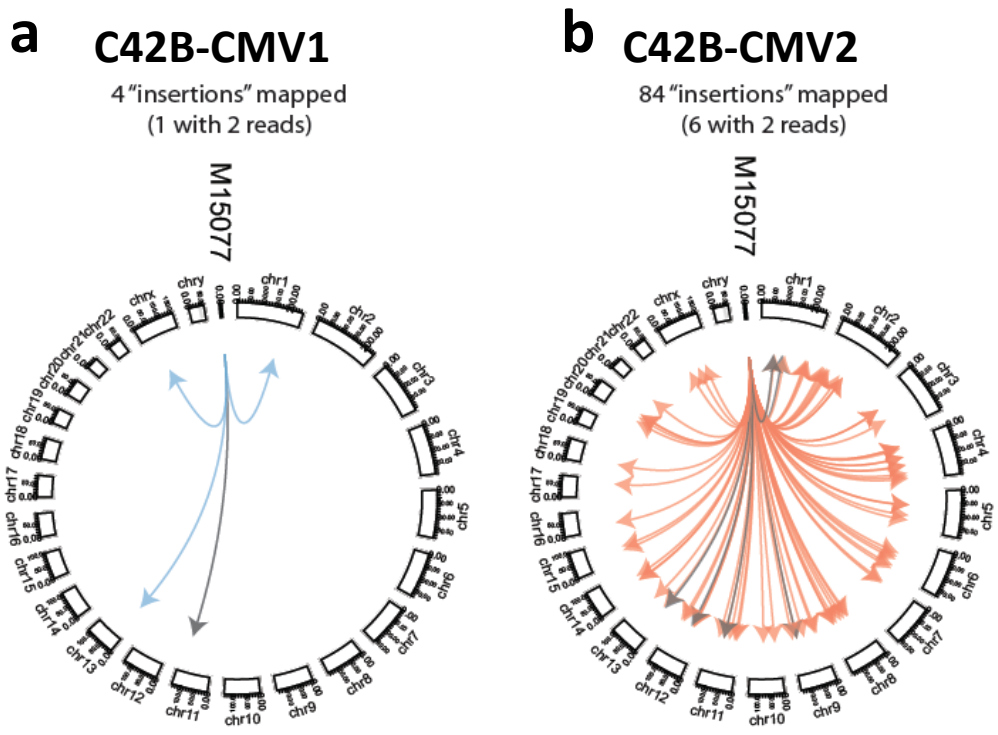

Figure 4.3. Luciferase gene insertion map. Whole-genome sequencing data analysis of **(a)** C42B-CMV1 and **(b)** C42B-CMV2 revealed the number of insertion sites is 4 and 84 insertions, respectively.

Stability of luciferase reporters in other breast and prostate cancer cell lines

To gain a general understanding of the stability of the luciferase reporter in BMSC co-cultures with prostate and breast cancer cell lines, we generated six additional reporter cell populations. We compared their bioluminescence signal in

mono-cultures and co-cultures with BMSC. We found that all six cell lines tested had stable luciferase reporter systems at both 5 and 24 hours (Figure 4.4). The cell lines and the different promoters used to drive luciferase expression are included in the cell population name, and described in the Figure caption. Prostate cancer reporter cell lines were generated from parental PC3 and C42B cells. Breast cancer reporter cell lines were generated from parental MDA-MB-231 and MCF-7 cells. Luciferase gene expression was driven by CMV2, MSCV, or EF1a promoters.

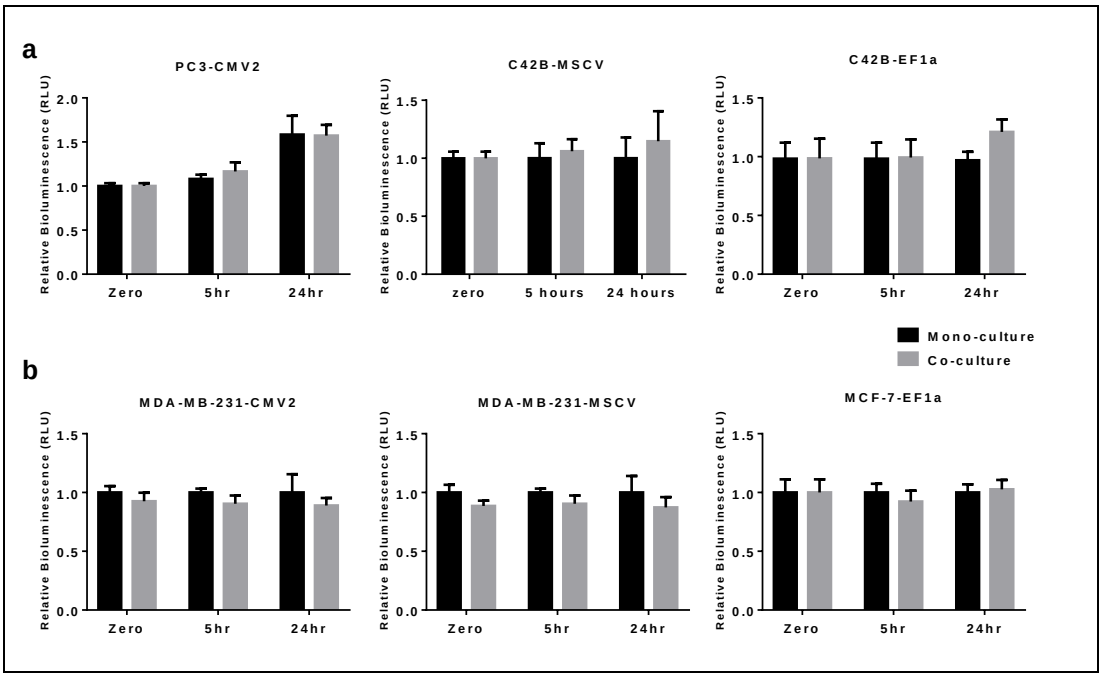

Figure 4.4. Luciferase reporter expression can be stable in prostate and breast cancer cells populations. (a) Prostate cancer cell lines (PC3 and C42B) and **(b)** breast cancer cell lines (MDA-MB-231 and MCF-7) cells were transduced by lentiviral particles to express luciferase driven by CMV2, MSCV or EF1a promoters. The bioluminescence was measured at the indicated time points of mono-cultures and co-cultures with bone marrow-derived mesenchymal stromal cells (BMSC) and normalized to the corresponding values at time point zero. Three independent experiments each had four technical replicate cultures (n=4) were performed.

4.5 DISCUSSION

Luciferase reporter systems are increasingly used to estimate luciferase-expressing cancer cell number in co-cultures [369], [371], [383] and in animal

models [384], [385]. This approach assumes that luciferase expression is stable in different culture conditions, and within the animal model. Most studies do not validate reporter stability in co-culture [369], [371], [383]. Our data (Figure 4.4) suggest that in most cases, reporter cell lines produce a bioluminescence signal that is proportional to the reporter cell number in mono-culture and co-culture with BMSC. However, in some cases (Figure 4.1 and 4.2) the bioluminescence signal generated by luciferase reporter cells can be significantly different. We made this observation with a population of C42B cells transduced to express luciferase driven by the CMV promoter (we described this population as C42B-CMV1).

Here, we report on the stability of luciferase reporters in a number of prostate and breast cancer cell lines maintained in mono-culture or co-culture with BMSC. In mono-culture, both cell lines (C42B-CMV1 and C42B-CMV2) generated strong bioluminescence signals that were proportional to the number of cells in culture. The bioluminescence signal from the C42B-CMV1 cell population increased 4 to 7-fold within 5 hours with indirect and direct co-culture with BMSC, respectively. This increase in bioluminescence signal was not associated with an increase in cell number, indicating that the C42B-CMV1 reporter population should not be used to estimate relative cell numbers in different culture conditions. This feature would not be detected unless standard curves were generated simultaneously in mono- and co-culture, likely explaining why investigations in the literature have not reported this anomaly.

When the genomes of C42B-CMV1 and C42B-CMV2 were sequenced and compared, we found that there were 4 versus 84 CMV-luciferase genome insertion sites, respectively (Figure 4.3). The low number of CMV-luciferase genome insertion sites in the C42B-CMV1 cell population appears to make these cells more sensitive to the modified BMSC co-culture environment. Our data could be interpreted as indicating that a higher number of luciferase insertion sites are required to yield a reporter cell population that can be used across a range of culture conditions. Indeed, it has been shown that the CMV promoter can be repressed or hyper-activated in various ways [386]–[388]. Thus, it is rational to assume that, if the reporter construct is only located at a few sites within the genome, the reporter may be hypersensitive to small changes in the culture microenvironment. Sequencing of reporter cell lines, and mapping of insertion sites is currently expensive (our cost was ~$2,000 AUS per

genome) and laborious. Because knowing the number of insertion sites will not definitively predict if a reporter is stable across multiple culture conditions, we recommend generating control cultures in each condition, and directly evaluating reporter stability. Indeed, we demonstrate that luciferase-expressing cell populations driven by a suitable promoter can function as excellent reporter systems in mono and co-cultures. In Figure 4.4 we show examples of three different breast and prostate cancer cell lines that express luciferase driven by different promoters. Bioluminescence signal was uniform between mono-cultures and BMSC co-cultures.

In summary, we show that a number of promoter-luciferase and cell combinations can be used to generate a reliable reporter cell line for use in mono- and co-cultures. We also show that, in some instances, reporter cell lines can be unreliable. Reliability is likely proportional to the number of reporter insertion sites. However, as it is expensive to sequence each reporter cell line and count the number of insertion sites, direct sequencing of reporter cell genomes is likely not a preferred way to predict reporter stability. Furthermore, greater-than-a-threshold-number of reporter insertion sites might not reliably equate to reporter stability. Instead, we recommend comparing reporter stability across a range of culture conditions before proceeding with the intended study. Luciferase reporter cells are powerful tools, but stability across culture conditions should never be assumed.

Acknowledgments

The authors would like to thank the National Health and Medical Research Council (NHMRC) of Australia for funding this research. I.S. is supported by a QUT Vice-Chancellor's Senior Research Fellowship.

Author Contributions Statement

E.M. designed research, performed research, analysed data and wrote the paper.

B.G. performed research, analysed data and wrote the paper.

I.S., K.C., and J.C. analysed data and wrote the paper.

M.D. designed research, analysed data and wrote the paper.

Competing financial interests

The authors declare no competing financial interests.

4.6 SUPPLEMENTARY DATA

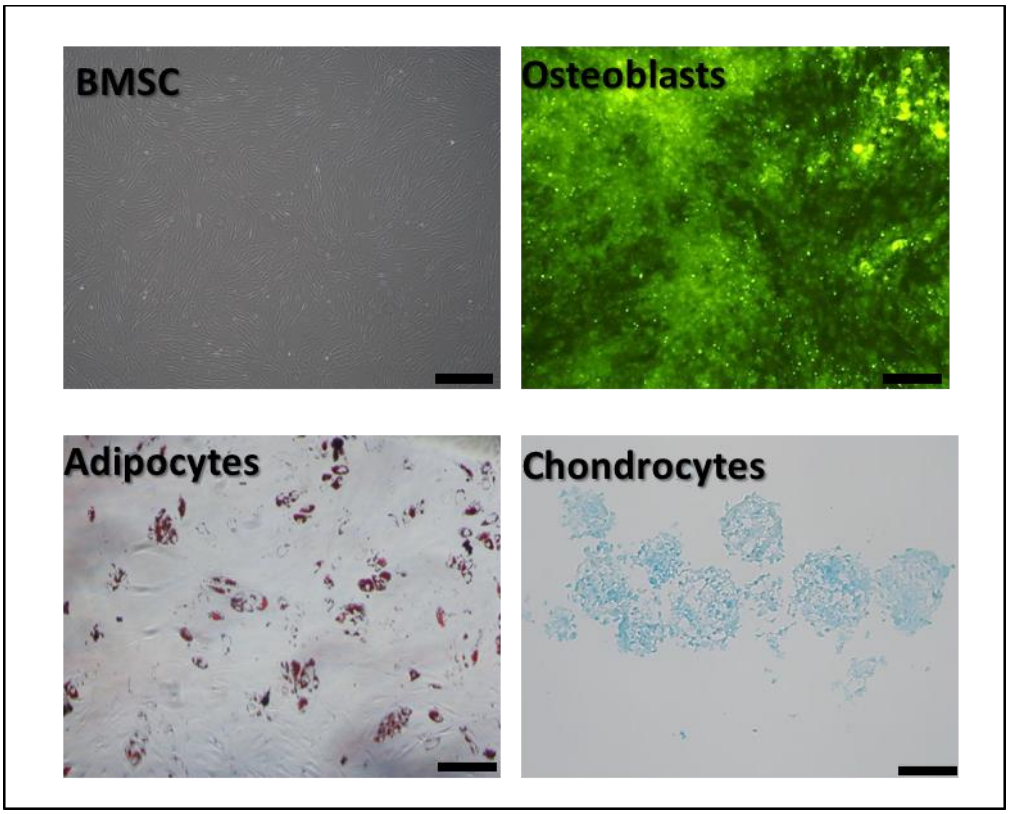

Supplementary Figure 4.1. Characterization of bone marrow-derived mesenchymal stromal cells (BMSC) trilineage differentiation. After isolation of BMSC, cells were seeded in monolayers for osteogenesis and adipogenesis induction; and in 3-dimensional cell aggregates for chondrogenesis induction. After 14 days, cells were fixed and stained with OsteoImage, Oil Red O staining or Alcian blue staining for osteo-, adipo-, and chondro-genesis, respectively. Positive staining indicated mesodermal differentiation potential. Scale bars = 100 µm.

Supplementary Table 4.1. List of bone marrow-derived mesenchymal stromal cell (BMSC) expression profile for cellular markers.

Marker	**Reactivity***
CD45, CD34, CD271, HLA-DR	-ve
CD90, CD73, CD105, CD44, CD146	+ve

* (+ve) means > 95% and (-ve) means < 5% of the cell population.

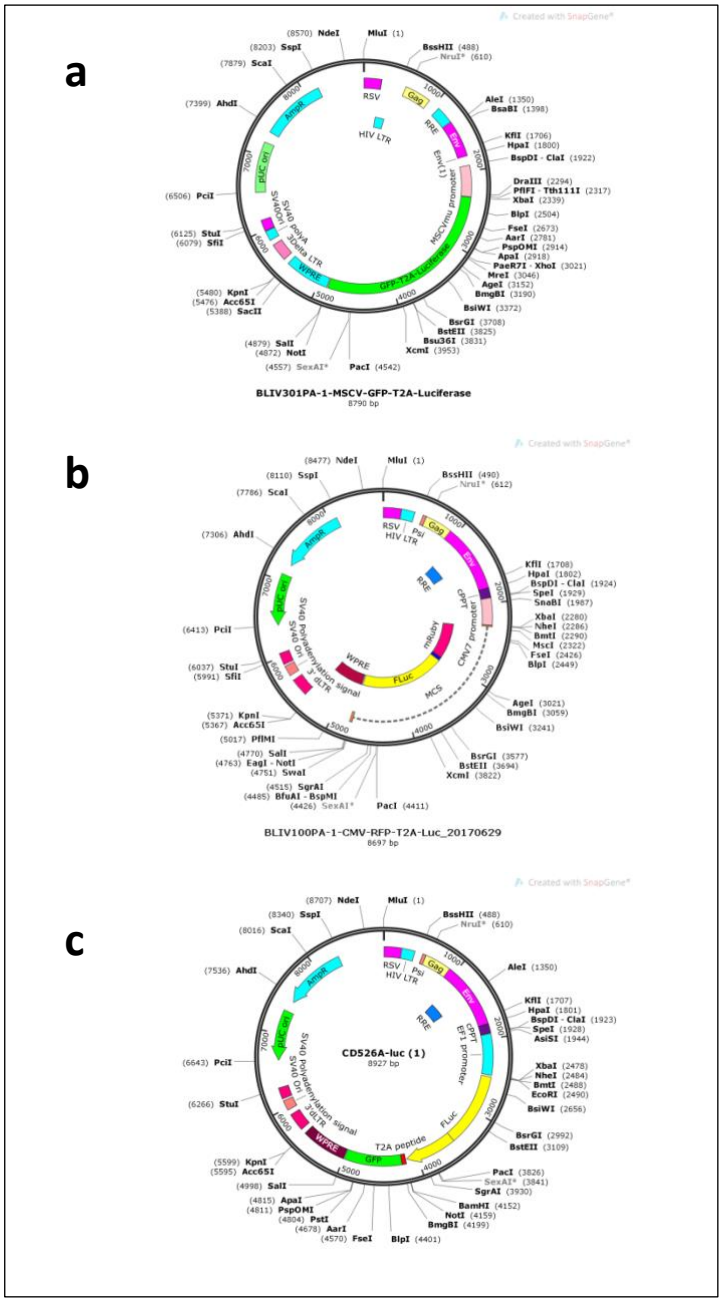

Supplementary Figure 4.2. Restriction maps of plasmids used in lentiviral particles production to transduce cells with luciferase gene with **(a)** MSCV, **(b)** CMV and **(c)** EF1a promoter regions. All plasmids were designed by System Biosciences (Bioluminescence Imaging Vectors, BLIV).

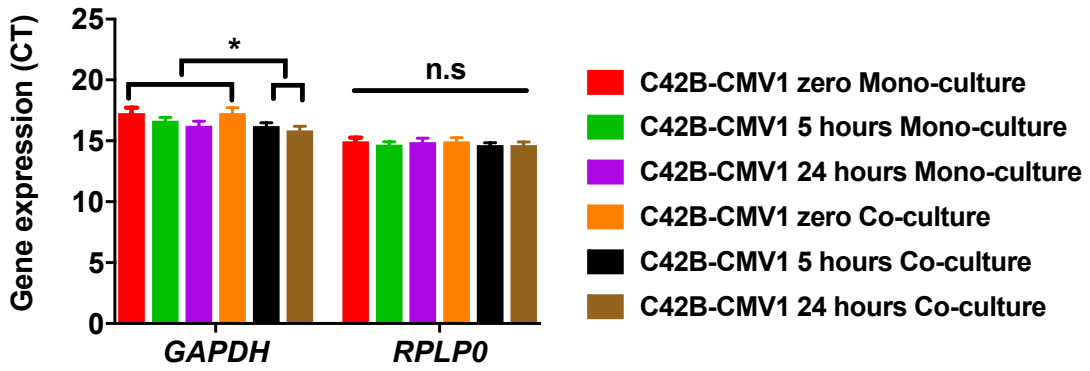

Supplementary Figure 4.3. Housekeeping genes expression in C42B-CMV1 cells. C42B-CMV1 cells were either mono- or co-cultured with BMSC in a Transwell assay for the indicated time points. The Housekeeping genes expression (CT values) were assessed. Three independent experiments each had four technical replicate cultures (n=4) were performed. Statistical significance was calculated using two-way ANOVA. * and n.s indicates $P<0.001$ and non-significant, respectively. No statistical difference was detected between RPLP0 expression in C42B-CMV1 cells in different culture conditions over zero, 5 and 24 hours.

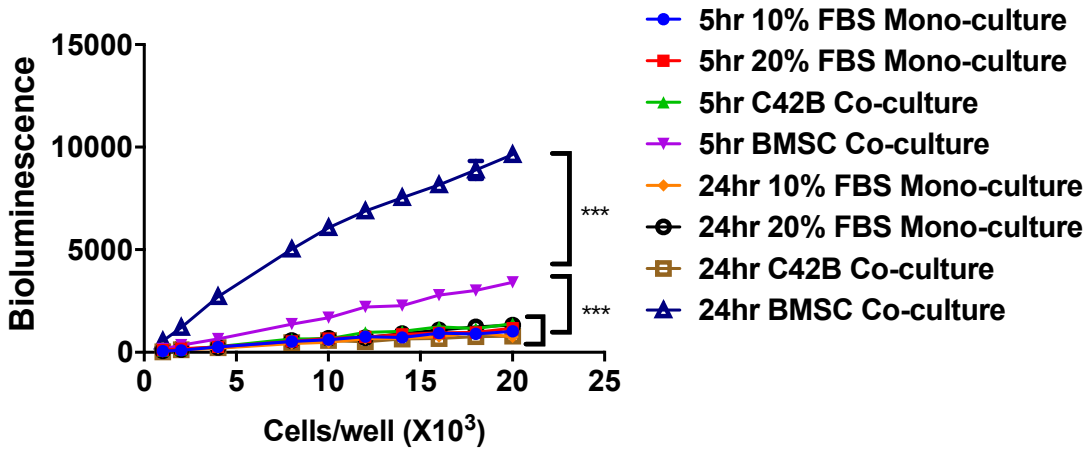

Supplementary Figure 4.4. The luciferase assay in mono- or co-culture with C42B-CMV1 cells or BMSC, or with different titrations of FBS. Increasing numbers of C42B-CMV1 cells were cultured in maintenance culture media (10% FBS Mono-culture), maintenance culture media supplemented with 20% FBS (20% FBS Mono-culture), directly cultured with 10×10^3 parental un-tagged C42B cells (C42B co-culture) or directly cultured with 10×10^3 BMSC (BMSC Co-culture) in 96-well plates. The bioluminescence was measured after 5 and 24 hours of culture establishment. Only co-culture with BMSC (open and closed purple triangles) resulted in an increase in bioluminescence signal. The graphed data represents the mean bioluminescence values of 6 replicate cultures at each time point and condition. Statistical significance was calculated using two-way ANOVA (*** $P< 0.001$).

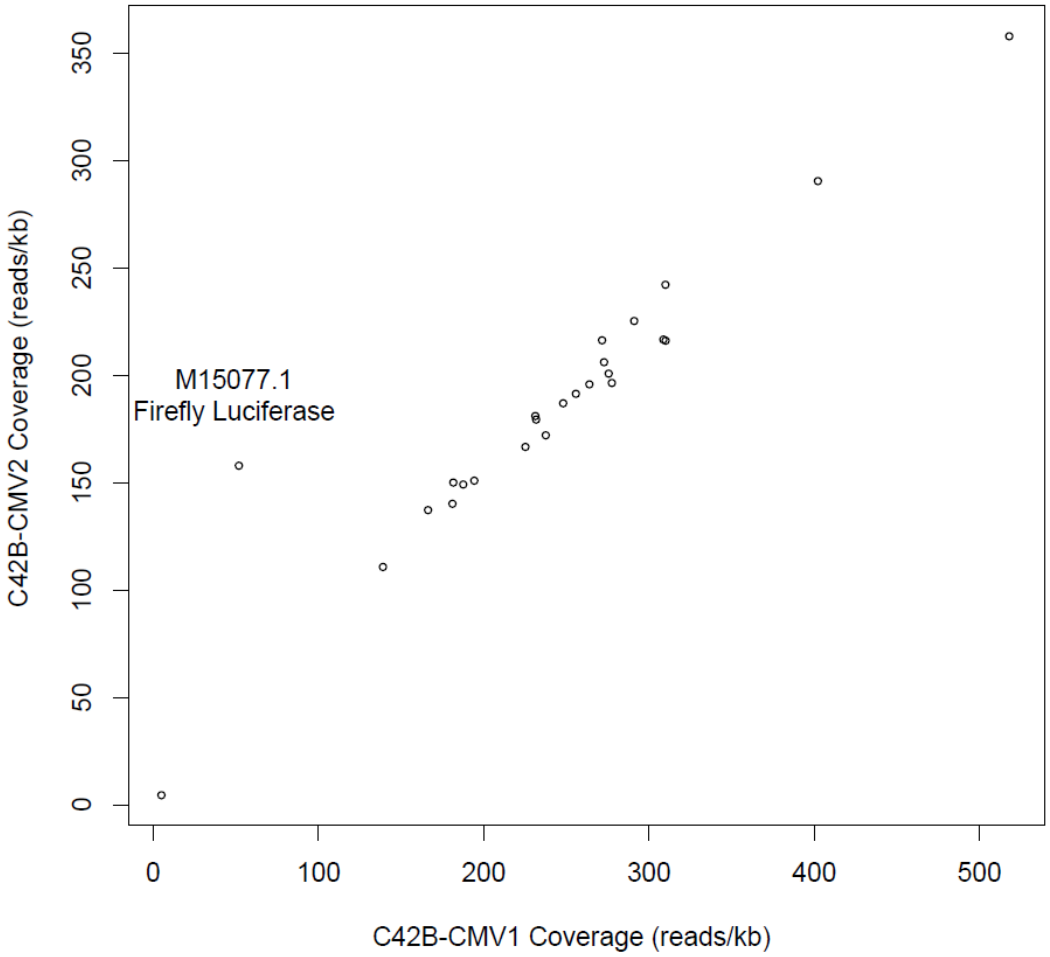

Supplementary Figure 4.5. Relative depth coverage of firefly luciferase gene in C42B-CMV1 and C42B-CMV2 genome. Numbers of reads mapping to each chromosome and firefly luciferase was normalized by target length and plotted for both samples.

Chapter 5: Using high throughput microtissue culture to study the difference in prostate cancer cell behaviour and drug response in 2D and 3D co-cultures

Chapter status: Manuscript submitted to BMC Cancer (28/11/2017)

Manuscript title: Using high throughput microtissue cultures to study the difference in prostate cancer cell behaviour and drug response in 2D and 3D co-cultures

Contributor	Statement of contribution
Eman Mosaad Signature: Date: 24/04/2018	Designed research (D) Performed research (P) Analysed data (A) Wrote Manuscript (M)
Judith Clements and Karen Chambers	Aided with A and M
Kathryn Futrega	Aided with M
Michael R. Doran	Aided with D, A and M

Principle Supervisor Confirmation

I have sighted email or other correspondence from all Co-authors confirming their certifying authorship.

Michael R. Doran

Signature: Date:

Chapter 5 preface:

As identified in Chapter 4, bioluminescence of C42B cells transduced with luciferase reporter system driven by MSCV promoter (C42B-MSCV-GFP-Luc) was proportional to cell number and luciferase gene expression was stable in mono- and co-cultures with BMSC. In Chapter 5, PCa cell behaviour in direct or indirect co-culture systems with bone marrow stromal cells were characterized. C42B-MSCV-GFP-Luc cells responses to Docetaxel and Abiraterone Acetate were quantified using the cell-specific bioluminescence assay verified in Chapter 4.

5.1 ABSTRACT

Background: There is increasing appreciation that non-cancer cells within the tumour microenvironment influence cancer progression and anti-cancer drug efficacy. For metastatic prostate cancer (PCa), the bone marrow microenvironment influences metastasis, drug response, and possibly drug resistance. **Methods:** Using a novel microwell platform, the *Microwell-mesh*, we manufactured hundreds of 3D co-culture microtissues formed from PCa cells and bone marrow stromal cells. We used luciferase-expressing C42B PCa cells to enable quantification of the number of PCa cells in complex microtissue co-cultures. This strategy enabled us to quantify specific PCa cell growth and death in response to drug treatment, in different co-culture conditions. In parallel, we used Transwell migration assays to characterize PCa cell migration towards different 2D and 3D stromal cell populations. **Results:** Our results reveal that PCa cell migration varied depending on the relative aggressiveness of the PCa cell lines, the stromal cell composition, and stromal cell 2D or 3D geometry. We found that C42B cell sensitivity to Docetaxel varied depending on culture geometry, and the presence or absence of different stromal cell populations. By contrast, the C42B cell response to Abiraterone Acetate was dependent on geometry, but not on the presence or absence of stromal cells. **Conclusion:** In summary, stromal cell composition and geometry influences PCa cell migration, growth and drug response. The Microwell-mesh and microtissues are powerful tools to study these complex 3D interactions.

5.2 INTRODUCTION

Despite significant improvements in the survival of prostate cancer (PCa) patients with localized disease, survival drops significantly if the cancer has metastasised to a distal site [115]. Approximately 90% of metastatic prostate cancer patients suffer from bone metastases [95], [101], making modeling of PCa cell behavior within the bone tissue microenvironment especially relevant.

Within the bone, there is evidence that the first site of metastasise is the haematopoietic stem cell (HSC) niche [115]. Key HSC niche microenvironmental cell populations include bone marrow mesenchymal stromal cells (BMSC), osteoblasts and adipocytes [389]–[391]. These cell populations are all thought to

influence PCa metastasis and disease progression [392]–[394]. Dissecting the influence played by each stromal cell population *in vivo* is challenging, and this is an area where *in vitro* model experimentation may offer an advantage over more complex animal models. An on-going challenge is the establishment of an *in vitro* model that mimics the *in vivo* microenvironment sufficiently to yield clinically relevant results or insights. The most common tissue culture models are 2D cell monolayers grown on tissue culture polystyrene. Monolayer cultures do not facilitate tissue-like cell-cell interactions [395], and cancer cells cultured in 2D monolayers tend to be hypersensitive to anti-cancer drugs [258]. This has motivated a surge in the development of 3D cancer models that are meant to better recapitulate 3D cellular organization and complex tissue microenvironments [279], [396].

Despite the potential advantages of 3D culture models, their use in PCa drug-screening remains limited. Traditional 2D tissue culture plates are inexpensive, the majority of imaging systems/protocols are designed to be compatible with 2D culture plates, and a range of automated fluidics systems are compatible with 2D culture systems. These features have not yet been efficiently integrated into 3D culture systems. For example, hydrogel matrix-based 3D cultures can be costly, they commonly suffer from significant 3D tissue size heterogeneity, and harvest from the gel is necessary for many forms of analysis [365]. Our team previously introduced the *Microwell-mesh* as a high throughput platform suitable for 3D tissue culture [290], [397]. This platform uses a microwell platform to facilitate the manufacture of hundreds of uniform multicellular 3D microtissues. It differs from previous microwell platforms in that it has a nylon mesh fixed over the microwells, and this enables retention of individual microtissues within discrete microwells even during repeat full medium exchanges. This design makes the Microwell-mesh platform ideal for use in the simultaneous manufacture, characterization and study of the drug response of hundreds of microtissues in high throughput manner.

An additional complexity associated with designing co-culture drug assays is that it is challenging, and potentially expensive, to specifically quantify the number of cancer cells without the co-culture population confounding this measurement. For example, simple Alamar blue metabolic readouts would include both metabolic contributions from the cancer and the stromal co-culture cell population(s), making specific cancer cell response challenging to delineate. To overcome this barrier, we

mimicked McMillin and colleagues who used a luciferase reporter system to enable the indirect estimation of cancer cell numbers in complex co-cultures via bioluminescence [369]. In our studies, the PCa cells were transduced to express a luciferase reporter, allowing us to indirectly quantify PCa cell number in complex co-cultures with stromal cell populations that did not express luciferase.

Herein, PCa cell migration and proliferation in response to bone marrow stromal cell populations cultured in 2D and 3D was contrasted. We used the Microwell-mesh system to form microtissues containing both PCa and bone marrow stromal cells, and used the luciferase reporter system to enable indirect quantification of PCa growth as well as death in response to anti-cancer drugs in complex co-cultures. The response to PCa cells to Docetaxel and Abiraterone Acetate in 2D or 3D, and in the presence or absence of stromal cells was characterized.

5.3 MATERIALS AND METHODS

PCa Cell lines culture

All PCa cell lines were obtained from the American Type Tissue Collection (ATCC) and included PC3, C42B and LNCaP cells. Cell lines were authenticated at the Genomic Research Centre (GRC; Brisbane, Australia) using Short Tandem Repeat (STR) analysis. STR profiles of the cell lines were compared to the ATCC STR Database to verify cell line identity; and all cell lines showed ≥80% match to the corresponding reference STR profile. Cells were cultured in low glucose Dulbecco's modified Eagle's medium (DMEM-LG) supplemented with 10% fetal bovine serum (FBS; Thermo Fisher) and 1% penicillin/streptomycin (Thermo Fisher). For some assays, FBS was replaced with 10% charcoal stripped fetal bovine serum (CSS; Thermo Fisher) to mimic androgen deprivation conditions. Cells were grown in a cell culture incubator at 37°C and 5% CO_2 and 2% O_2. All cells were passaged when monolayers reached ~80% confluency using 0.25% Trypsin/EDTA (Thermo Fisher).

Human bone marrow mesenchymal stromal cell (BMSC) isolation and differentiation

Human bone marrow aspirates were collected at the Mater Hospital from two fully informed and consenting healthy male volunteer donors. In accordance with the Australian National Health and Medical Research Council's Statement on Ethical

Conduct in Research Involving Humans, ethical approval was granted through the Mater Health Services Human Research Ethics Committee and Queensland University of Technology Ethics Committee (number: 1000000938). Aspirates were collected from the iliac crest of volunteers. Mononuclear cell isolation was achieved by density gradient centrifugation, using Ficoll-Paque Plus (GE Healthcare), as previously described [319]. Bone marrow samples were diluted 1:2 with PBS (Thermo Fisher) containing 2 mM EDTA. Then the diluted sample was carefully overlayed on the Ficoll-Paque plus layer and centrifuged for 30 minutes at 400x*g*. The mononuclear cells collected from the interface were then washed, resuspended in low glucose Dulbecco's modified Eagle's medium (DMEM-LG) supplemented with 10% fetal bovine serum (FBS, Thermo Fisher) and 1% penicillin/streptomycin (Thermo Fisher). Cells were then cultured overnight in a humidified incubator containing 5% CO_2 with 20% O_2 atmosphere at 37°C. Tissue culture plastic-adherent cells were enriched by removing the medium containing non-adherent cells, and fresh culture medium added to each flask. Subsequent BMSC expansion was performed in 2% O_2 and 5% CO_2 atmosphere at 37°C. Cells were passaged when the monolayer reached 80% confluency using 0.25% Trypsin/EDTA (Thermo Fisher). All experiments were performed using BMSC between passage 2 and 5.

The isolated cells were characterized for the expression of BMSC surface antigens; CD44, CD90, CD105, CD73, CD146, CD45, CD34 and HLADR; and mesodermal trilineage differentiation capacity and confirmed to be in accordance with the standard criteria of multipotent mesenchymal stromal cells reported previously by Dominici *et al.* [286].

Osteogenic and adipogenic differentiation were induced by culturing 60,000 and 40,000 cells/cm^2 in osteogenic and adipogenic induction medium for 14 days, respectively. The medium consisted of high glucose DMEM media (DMEM-HG; Thermo Fisher) containing 100 μM sodium pyruvate, 1X Gluta-Max (Thermo Fisher), 10% FBS, 100 U/mL penicillin, and 100 μg/mL streptomycin (1% P/S; Thermo Fisher), in addition to the supplements to induce differentiation which are listed as following: for osteogenesis, 100 nM dexamethasone (Sigma-Aldrich), 50 μM L-ascorbic acid 2-phosphate (Sigma-Aldrich) and 10 mM β-glycerol phosphate (Sigma-Aldrich); for adipogenesis, 10 μg/mL insulin (Sigma-Aldrich), 1 μM dexamethasone (Sigma-Aldrich), 200 μM indomethacin (Sigma-Aldrich) and 500

μM 3-isobutyl-1-methyl xanthine (Sigma-Aldrich). Culture medium was replaced with fresh media twice per week.

Generation of GFP-luciferase-tagged Prostate cancer cell lines

Firefly luciferase-expressing C42B cells were generated using fresh lentiviral expression particles manufactured inhouse. Luciferase-GFP (Luc-GFP) insertion constructs contained Bioluminescence Imaging Vectors (BLIV, System Biosciences) with MSCV (MSCV-Luc-GFP) promoters (Supplementary data, Supplementary Figure 5.1). Plasmid production was achieved by using Stbl3 Chemically competent *E.coli* (Thermo Fisher) as per the manufacturers' instructions. This was followed by a purification step using the NucleoBond Xtra EF plasmid purification kit (Midi EF, Macherey-Nagel) to obtain endotoxin-free plasmid DNA. Plasmid packaging was then performed using TGEN packaging plasmid mix with the transfection reagent, Lipofectamine 2000 (Thermo Fisher). The lentiviral particles were produced by 293FT cells (Thermo Fisher) following the manufacturers' instructions. Viral particle-containing media was then placed onto cancer cells, with the addition of 8 μg/mL polybrene to enhance transduction efficiency. Positive transduced cells were selected by double FACSorting using MoFlo Astrios (Beckman Coulter) for GFP^+ cells. This yielded a stable population of C42B cells that expressed Luc-GFP driven by a MSCV promoter. We validated the stability of the luciferase gene expression in mono and Transwell co-culture conditions using quantitative real time RT-PCR [290] (Supplementary Figure 5.2). The primers sets used are detailed in the supplementary data file (Supplementary Table 5.1).

3D culture system design and fabrication

An in-house fabricated microwell platform was fabricated from polydimethylsiloxane (PDMS, Slygard). PDMS microwell arrays were fabricated as described previously [258], [290]. Briefly, liquid PDMS (1:10 curing agent to polymer ratio) was permitted to cure over a patterned polystyrene mold having the negative of the microwell pattern for 1 hour at 80°C. A sheet of PDMS with the microwell array pattern cast into it (each microwell had dimensions of 800*x*800 μm square and a depth of 500 μm) was produced and peeled from the molds. PDMS discs of 1 cm^2 were punched from the PDMS sheets then glued into culture plates

with silicone glue (Selleys, Australia). For drug-testing experiments, Microwell-mesh inserts were made by fixing a nylon mesh (36 μm^2 pore openings, part number: CMN-0035, Amazon) to the top of the microwells using silicone glue. Once the glue had cured, excess mesh was trimmed from the disc inserts using scissors. Inserts were then anchored into individual wells in 24- or 48-well plates by placing a small amount of silicone glue at the bottom of the well, and the insert pressed into the well. Plates with microwell inserts were submerged in 70% ethanol for 1 hour for sterilisation, followed by rinsing of each culture well 4 times with Dulbecco's phosphate buffered saline (DPBS). To prevent cell adhesion to the PDMS during culture, the PDMS microwell inserts were soaked in a sterile solution of 5% Pluronic-F127 (Sigma-Aldrich) in DPBS for 10 minutes [346], and then rinsed 3 times with DPBS before cells were seeded.

Assembly of microtissues

In this study, we formed microtissues assembled from PCa, BMSC, osteoblasts or adipocytes alone or combination co-cultures of PCa and BMSC or BMSC differentiated into either osteoblasts or adipocytes. The Microwell-mesh platform was used to study PCa proliferation and drug response in direct co-cultures where multiple medium and drug exchanges were required. Figure 5.1 schematically illustrates how the Microwell-mesh differs from traditional open top microwell platforms, and how centrifugation can be used to evenly distribute the seeded cell suspension into the array of microwells. Each insert had approximately 150 microwells/cm^2, or ~150 microwells at the bottom of a 48-well plate. Seeding a different number of cells in suspension over the microwells could control the number of cells per microtissue. For example, if single a cell suspension containing 90,000 cells in 0.5 mL of medium was seeded, this yielded ~150 microtissues containing ~600 cells each. Following cell seeding as a cell suspension, plates were centrifuged at 400 x g for 5 minutes to aggregate the cells uniformly at the bottom of each microwell. The aggregation of cells into microwells was visually confirmed using an Olympus CKX14 microscope, and images captured using an Olympus DP26 digital camera (Japan) and Microscopy software (CKX14, CellSens Entry). Plates were then transferred to a cell culture incubator maintained at 37°C and 5% CO_2.

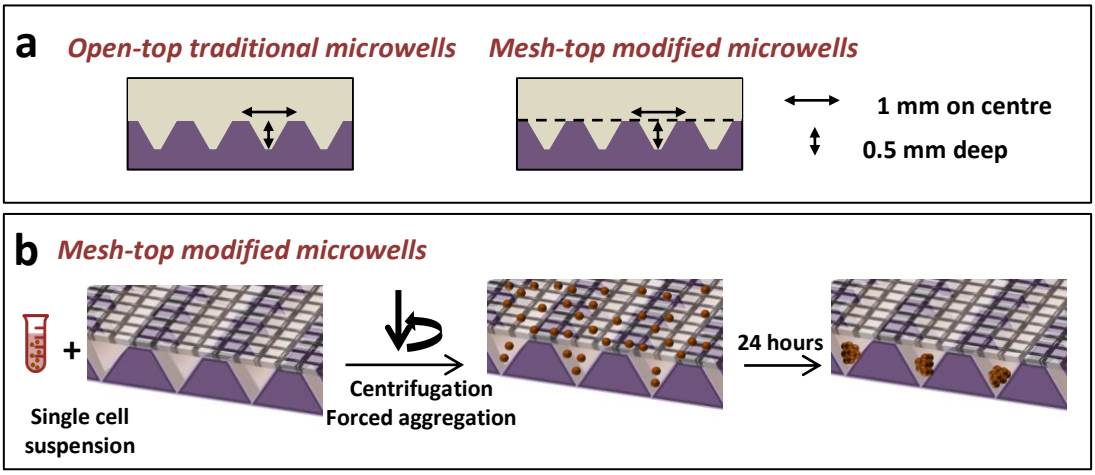

Figure 5.1. Microwell platforms and establishment of 3D microtissue culture. (a) Schematic illustrations show PDMS discs with and without the mesh which can be inserted in 48-well tissue culture plates. **(b)** Schematic illustration of cell seeding using Microwell-mesh being microwells modified with a 36 µm mesh-top large enough to allow single cells to pass through, but small enough to retain microtissues within discrete microwells aggregated after 24 hours of seeding the cells.

PCa cells migration (Transwell assay)

We were also interested in determining if PCa cell migration towards stromal cells differed depending on the geometry of the stromal cells. In 3D microtissue co-cultures, PCa cells localized to the outside of the microtissue, and this did not provide insight into how different stromal cells might influence cell migration. To overcome this obstacle, we developed a modified Transwell assay. Here we either cultured the stromal cells as 2D monolayers, or as 3D microtissues in open top microwell inserts. To quantify PCa cell migration, PCa cells were placed into Transwell inserts and positioned either on top of 2D stromal cell monolayers or on top of 3D stromal cell microtissues (see Figure 5.2). BMSC were seeded in 24-well tissue culture plates, and cells cultured in osteogenic, adipogenic or maintenance medium for 14 days. For 2D monolayers, 60,000, 10,000 and 20,000 cells/cm^2 were seeded and cultured in the corresponding culture media. For 3D microtissues, 600 cells/microtissue were seeded in the microwell inserts anchored in the 24-well tissue culture plate as described previously (see Cell seeding in 3D culture section). Transwell inserts seeded with 36,000 PC3, C42B or LNCaP cells (Transwell insert pore size of 8 µm, Millicell culture inserts, Merck Millipore) and permitted to

incubate for 24 hours. Inserts were then placed on top of either the 2D or 3D stromal cell populations, and incubated for 18 hours. At the end of the incubation period, Transwell inserts containing PCa cells were then washed and moved to a new tissue culture plate. Adherent cells attached to the top surface of the Transwell insert were removed using cotton buds, while cells that had migrated to the bottom surfaces of the Transwell inserts were fixed using ice cold methanol for 15 minutes. Fixed Transwell inserts were immersed in crystal violet stain (0.5 %, diluted in H_2O) for 15 minutes. Transwell inserts were washed in running tab water to remove excess stain. Stain contained within the cells was then extracted into 500 µl of acetic acid (10%) over a 10-minute incubation period. The optical density (OD) of the extract was measured at 595 nm using a Multiskan Go microplate spectrophotometer (ThermoFisher Scientific). Optical density of extracts from cell-free Transwell inserts functioned as controls for empty wells. For each cell line, parallel Transwell inserts containing PCa cells not exposed to the stromal co-culture conditions functioned as baseline migration controls.

Confocal imaging of 3D PCa-BMSC co-culture

PCa-BMSC microtissues were established using the microwell-mesh culture system. Single cell suspensions of C42B and BMSC were stained with green molecular probe (CellTrace green CFSE, Thermo Fisher) and red molecular probe (CellTracker Red CMTPX, Thermo Fisher), respectively. A cell suspension combining the two cell types in a 1:1 ratio was generated, and seeded into 48-well tissue culture plates with microwell-mesh inserts to obtain microtissues each containing 600 cells (300 C42B cells + 300 BMSC). Following 24 hours incubation at 37°C, 5% CO_2, microtissues were collected and imaged using a Zeiss 510 Meta confocal microscope to characterize 3D cellular organization.

Bioluminescence assay

In vitro bioluminescence of Luciferase-tagged PCa cells was used as an indirect method to estimate viable cancer cells in mono- and co-cultures. For the luciferase activity assay, D-luciferin (Promega) was added to the culture medium at a final concentration of 15 µg/mL, then incubated at 37ºC for 15 minutes and the bioluminescence acquired using a PHERAstar FS plate reader (BMG LABTECH).

Cell proliferation and drug-testing in direct co-culture system

PCa cell proliferation and responses to anti-cancer drugs were tested in both 2D and 3D co-cultures. In 48-well tissue culture plates, co-cultures were established in 2D monolayers or as 3D microtissue cultures. Two weeks prior to establishing co-cultures, BMSC were assembled into 3D microtissues of 300 cells/microtissue or as 2D monolayers of 60,000 and 100,000 cells/cm^2 to permit differentiation to osteogenic and adipogenic lineages, respectively. At day zero, C42B that expressed luciferase and GFP (Luc-GFP) were added as single cell suspension on top of stromal cell (BMSC, osteoblasts or adipocytes) monolayers or stromal cell microtissues in the microwell-mesh. C42B cells were seeded at either 10,000 cells/cm^2 on top of stromal cell monolayers, or 300 cells per microtissue on top of established stromal microtissues.

For cell proliferation experiments, PCa cells were permitted to grow for 24 and 48 hours in 2D and 3D co-cultures as mono- or co-cultures then the bioluminescence was measured as described above. Data is presented as relative bioluminescence (RLU) relative to luciferase-tagged PCa cells in mono-cultures.

Docetaxel and Abiraterone Acetate were used in the drug-testing studies. Docetaxel (Sigma-Aldrich, 01885) and Abiraterone Acetate (Sigma-Aldrich, SML 1527) were purchased as powders and dissolved in Dimethyl sulfoxide (DMSO; Sigma-Aldrich, 472301), then aliquoted and stored at -80^{o}C. On the day of treatment, an aliquot was thawed and diluted in culture medium to the desired concentrations.

PCa cells were permitted to adhere or aggregate into spheriods for 24 hours in co-cultures. For Docetaxel treatments, all cultures were treated with the indicated concentrations one day after the initiation of the co-cultures. For Abiraterone Acetate treatments, all cultures were first depleted of androgens for 48 hours by replacing the FBS-supplemented culture medium with medium supplemented with charcoal stripped serum (CSS). Cultures were then exposed to the described concentrations of Docetaxel or Abiraterone Acetate for 48 hours.

At the end of the drug treatment period, epifluorescence and phase contrast images were captured using an Olympus DP26 digital camera (Japan) and Microscopy software (CKX14, CellSens Entry). Bioluminescence signals from each

culture were measured as described above. Data is presented as a percentage of the relative bioluminescence units (RLU) compared to vehicle-treated cultures.

Statistical analysis

Results represent two independent experiments using two BMSC donors. Each of the replicate experiments included four biological replicate cultures (n=4), unless otherwise indicated. Error bars represent standard deviations. Statistical significance of data was evaluated using two-way analysis of variance (ANOVA), using Prism software, Version 6.0 (GraphPad). P-values for each comparison are represented by asterisks as indicated in figure captions.

5.4 RESULTS

Indirect Transwell co-culture of PCa cells with 2D and 3D bone marrow stromal cells

Using the Transwell assay, the migration of PCa cells towards BMSC, osteoblasts and adipocytes cultured in 2D monolayers or 3D microtissues was assessed following 18 hours of co-culture (Figure 5.2a). LNCaP, C42B and PC3 cells were used to represent or model different stages of PCa disease aggressiveness.

Of the 2D cultures, BMSC monolayers induced the greatest migration rates in all PCa cell lines tested. By contrast, the influence of osteoblasts and adipocytes on PCa migration was PCa cell line dependent. For the less aggressive cell lines, C42B and LNCaP, both osteoblasts and adipocytes had minimal influence on PCa cell migration rates. The highly aggressive bone metastatic PC3 cells demonstrated a significantly elevated migration rate towards osteoblasts and adipocytes cultured in 2D monolayers (Figure 5.2b).

Unlike 2D BMSC cultures, which upregulated the migration of all PCa cells tested, 3D BMSC microtissues only upregulated the migration of PC3 cells. Indirect co-culture with 3D adipocyte microtissues decreased PC3 cell migration, and had no measurable effect on C42B or LNCaP cell migration rates. Similarly, 3D osteoblasts microtissues did not increase the migration rate of any of the PCa cell lines tested (Figure 5.2b).

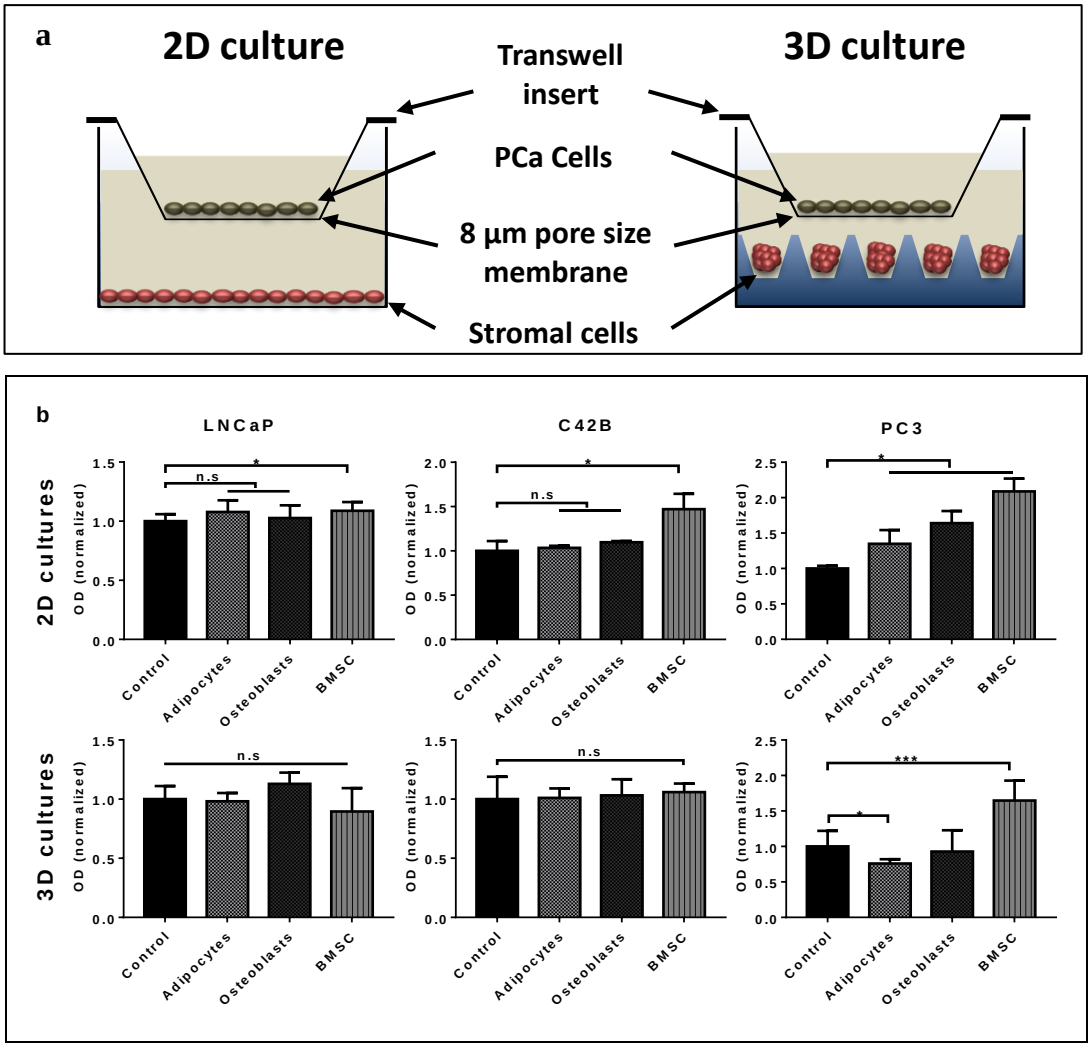

Figure 5.2. PCa migration potential in Transwell co-cultures with bone marrow stromal cells. (a) Schematic illustration of the Transwell assay. PCa cell suspensions were seeded in Transwell inserts with 8 µm pore size membrane. The co-cultures were performed over 18 hours to allow PCa cells migration towards 2D monolayers or 3D microtissues of stromal cells (BMSC, osteoblasts or adipocytes). Prior to co-culture establishment, the osteoblasts and adipocytes were differentiated for 14 days using osteogenic or adipogenic induction media; and BMSC controls were assembled 1 day prior to initiation of the Transwell co-culture. **(b)** PCa cells that had migrated to the bottom surface of the Transwell membrane were stained with 0.5% crystal violet, and this was extracted and quantified. Results are represented as the mean optical densities of crystal violet extracts normalized to the control mono-cultures. Similar results were obtained in three independent experiments with two different BMSC donors, each having four replicate cultures n=4. Statistical significance was performed using two-way ANOVA (* $P<0.05$, *** $P<0.001$ and n.s=non-significant).

Spatial organization of C42B cell-stromal cell 3D co-cultures

To characterize the spatial organization of 3D co-culture microtissues, we first labeled each cell type with different color fluorescent probes to enable the two cell types to be easily distinguished from each other. C42B cells were labeled with a green probe, while BMSC were labeled with a red probe. Figure 5.3a shows microtissue co-cultures formed from BMSC and C42B. Confocal images of 3D co-culture microtissues demonstrated a consistent and structured organization of the two cell types across the diameter of the microtissues. BMSC consistently localized within the core of the microtissue, whereas C42B cells were localized in the outer surface of the microtissue after 24 hours of co-culture (Figure 5.3b).

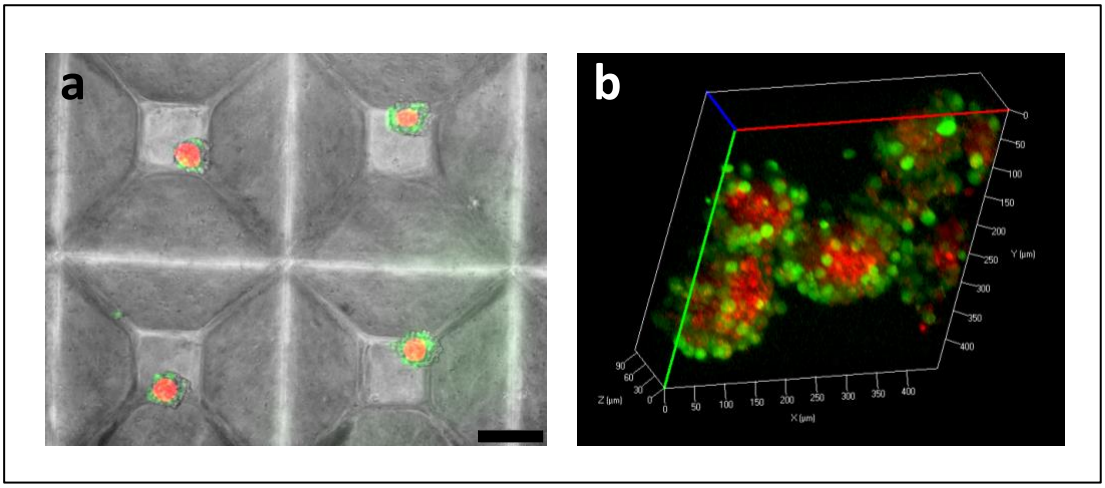

Figure 5.3. Co-culture microtissues of BMSC and C42B cells. Pre-stained BMSC (red molecular probe; CellTracker Red CMTPX, Thermo Fisher) and C42B cells (green molecular probe; CellTrace green CFSE, Thermo Fisher) were co-cultured in the 3D microwell platform **(a)** (scale bar = 200 µm) for 24 hours then collected and imaged using confocal Ziess microscopy **(b)**. BMSC consistently localise to microtissue cores, while C42B cells consistently formed a shell around the BMSC cores.

C42B cell proliferation in co-cultures with bone marrow stromal cells

Conventional methods of cell proliferation quantification, such as metabolic activity or cell viability assays, do not enable quantification of the cell growth of a single cell population within a mixed cell population co-culture. To study C42B cell proliferation in co-cultures, we labeled the PCa cell population with a luciferase reporter system. Relative bioluminescence signal from the PCa cell populations

functioned to provide an indirect estimate of the number of viable PCa cells in the different co-cultures.

To study PCa cell proliferation, we used C42B cells stably expressing Luciferase-GFP (Luc-GFP). Luciferase-Tagged cells were cultured in 2D monolayers or 3D microtissue cultures for 24 or 48 hours, as either mono-cultures of PCa cells (control) or co-cultures of PCa cells with stromal cells (BMSC, osteoblasts or adipocytes). The bioluminescence assay was then performed to estimate the number of C42B cells in each culture condition at each time point.

In 2D cultures, the bioluminescence values indicated a significant increase in C42B cell number in all co-culture conditions after 24 hours, relative to mono-culture controls. After 48 hours of culture, the effect of stromal cells on PCa cell proliferation was less pronounced. However, the overall bioluminescence after 48 hours was significantly greater than after 24 hours for all cultures (Figure 5.4a), indicating continual cell proliferation in all culture conditions.

In 3D cultures, co-culture with adipocytes enhanced C42B cell proliferation after 24 and 48 hours of culture, while co-culture with osteoblasts did not influence PCa cell proliferation rate. Despite the slight decrease in bioluminescence of C42B cells co-cultured with BMSC at 24 hours, the bioluminescence tended to increase (non-significant increase) after 48 hours of co-culture (Figure 5.4b). Similar to 2D cultures, an overall increase in the bioluminescence of C42B cells in 3D cultures was observed at 48 hours, relative to 24-hour cultures.

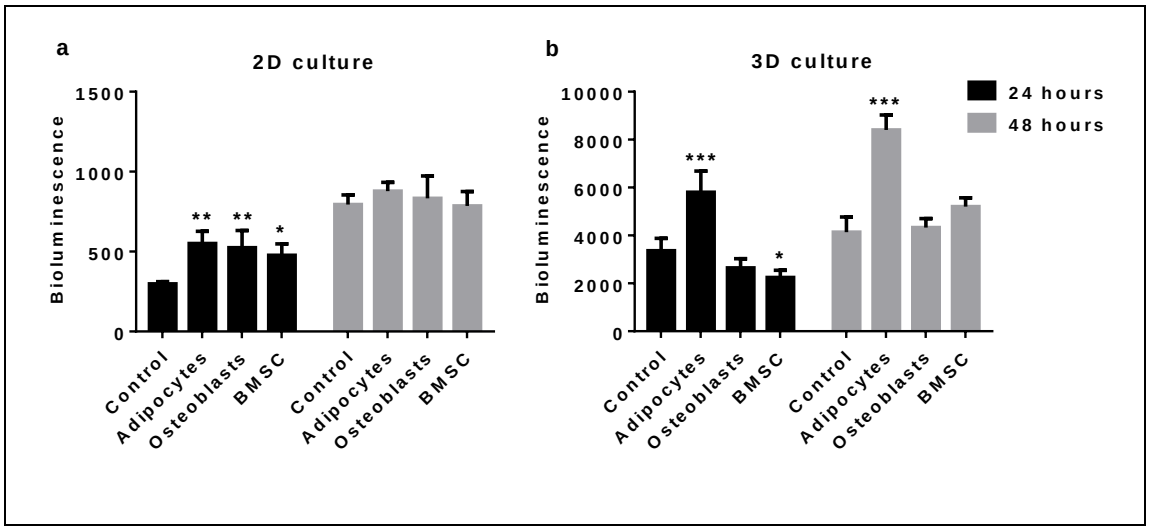

Figure 5.4. C42B cell proliferation in mono- and co-cultures with bone marrow stromal cells. C42B cells tagged with a luciferase reporter system were seeded in mono- or co-cultures with stromal cells (BMSC, osteoblasts or adipocytes) either in 2D monolayer cultures **(a)** or in 3D microtissue cultures **(b)**. Prior to co-culture establishment, the osteoblasts and adipocytes were differentiated for 14 days using osteogenic or adipogenic induction media; and the BMSC were seeded 1 day prior to co-culture. PCa cells were permitted to grow for 24 or 48 hours then the bioluminescence was measured after adding D-luciferin to the culture medium and incubating for 15 minutes. Results are represented as the mean bioluminescence values. Similar results were obtained in three independent experiments with two BMSC donors, each having four replicate cultures n=4. Statistical significance was performed using two-way ANOVA compared to the corresponding control mono-culture value (* $P<0.05$, ** $P<0.001$ and *** $P<0.0001$).

C42B cell drug response in co-cultures with bone marrow stromal cells

Next, we evaluated the response of PCa cells in 2D monolayers and 3D microtissues to Docetaxel and Abiraterone Acetate; two drugs used to treat advanced PCa. Luciferase-tagged C42B cells were used in these experiments, and the bioluminescence measurements provided an indirect estimate of the viable cell number in the cultures after 48-hours of drug treatments. Three replicate experiments were also performed using 2D and 3D co-culture of osteoblasts and Luciferase-expressing C42B cells. Over the total co-culture period, C42B cell viability fell

dramatically, even in control co-cultures with no drug. These data suggest that long-term stability of 2D and 3D co-culture is stromal cell type dependent. In the subsequent analysis below, we focused on results derived from 2D and 3D cultures of C42B cells alone, or in co-cultured with BMSC or adipocytes.

After 24 hours of establishing the mono- and co-cultures, Docetaxel treatment was performed for 48 hours. In 2D cultures, there was significantly greater bioluminescence signal from the PCa cells co-cultured with BMSC or adipocytes in all Docetaxel concentrations (0.01 – 10 nM) relative to the bioluminescence in mono-cultures at the same drug concentration (Figure 5.5a). Unexpectedly, 3D BMSC co-cultures showed a significant increase in bioluminescence. By contrast, adipocyte co-cultures behaved similarly to corresponding mono-cultures (Figure 5.5b). In general, 3D cultures demonstrated reduced sensitivity to Docetaxel in both mono- and co-cultures with BMSC or adipocytes (Figure 5.5).

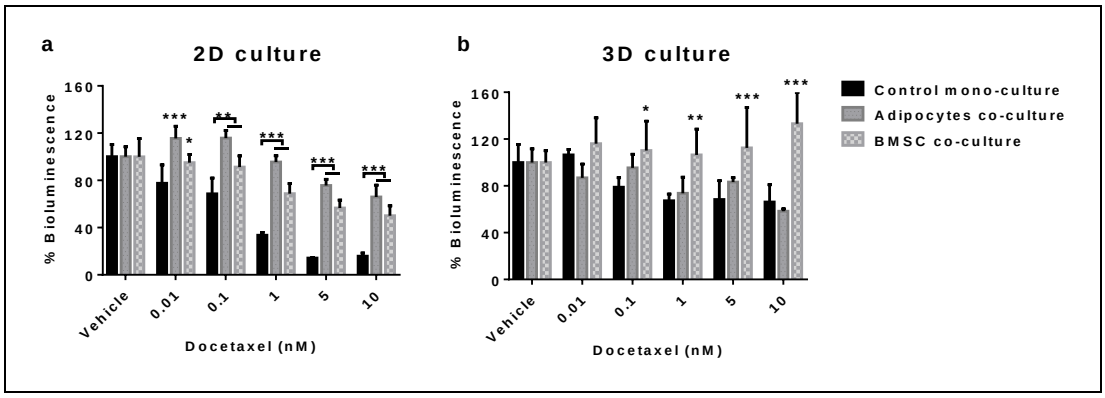

Figure 5.5. C42B cell Docetaxel drug response in mono- and co-cultures with bone marrow stromal cells. C42B cells tagged with luciferase reporter system were seeded in mono- or co-cultures with stromal cells (BMSC or adipocytes) either in 2D monolayer cultures **(a)** or in 3D microtissue cultures **(b)**. Prior to co-culture establishment, BMSC were induced to become adipocytes for 14 days; and BMSC control cultures were seeded 1 day prior to co-culture initiation. Cells were permitted to grow for 24 then treated with Docetaxel in the indicated concentrations for 48 hours. The bioluminescence was measured after adding D-luciferin to the culture medium and incubating for 15 minutes. Results are represented as a percentage of the vehicle control values. Similar results were obtained in three, including with two BMSC donors, independent experiment each having four replicate cultures n=4. Statistical significance was performed using two-way ANOVA compared to the corresponding control mono-culture value (* $P<0.05$, ** $P<0.01$ and *** $P<0.0001$).

For anti-androgen treatment, C42B cells were cultured in androgen deprived setting (CSS-supplemented culture media), and then treated with Abiraterone Acetate. Abiraterone Acetate is a first-in-class inhibitor of the CYP17A enzyme to prevent the biosynthesis of androgens intracellularly from their steroidal precursor [348]. The bioluminescence assay was used to assess PCa cell response in 2D and 3D mono- and co-cultures. Figure 5.6 shows the bioluminescence measurements as a percentage of the corresponding vehicle control culture.

In 2D cultures, co-cultures with BMSC and adipocytes demonstrated no significant change in the anti-androgen treatment response compared to the mono-cultures of C42B cells (Figure 5.6a). Similarly, 3D co-cultures did not result in change in the bioluminescence, except with BMSC co-cultures treated with 10 μM Abiraterone Acetate, which resulted in a decrease in bioluminescence (Figure 5.6b).

Generally, 3D mono- and co-cultures were less sensitive to increasing concentrations of Abiraterone Acetate relative to their corresponding 2D monolayer controls.

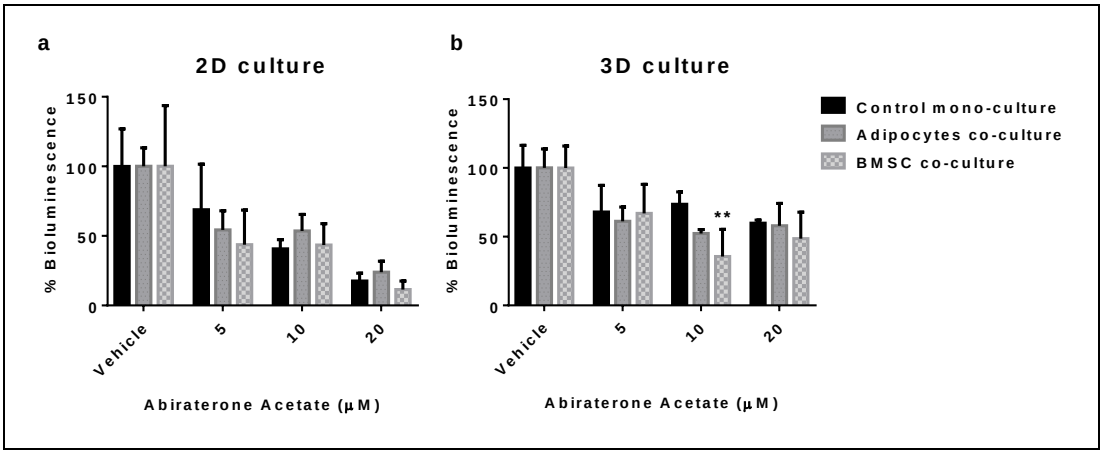

Figure 5.6. C42B cell Abiraterone Acetate drug response in mono- and co-cultures with bone marrow stromal cells. C42B cells tagged with luciferase reporter system were seeded in mono- or co-cultures with stromal cells (BMSC or adipocytes) either in 2D monolayer cultures **(a)** or in 3D microtissue cultures **(b)**. Prior to co-culture establishment, the osteoblasts and adipocytes were differentiated for 14 days using osteogenic and adipogenic induction media; and the BMSC were seeded 1 day prior to co-culture. Cells were permitted to grow for 24 followed by medium exchange to androgen-depleted medium for a further 48 hours. Abiraterone Acetate was then added to the culture medium at the indicated concentrations for an additional 48 hours. The bioluminescence was measured after adding D-luciferin to the culture medium for 15 minutes. Results are represented as a percentage of the vehicle control values. Similar results were obtained in three independent experiments, including with two different BMSC donors, with each experiment having four replicate cultures n=4. Statistical significance was performed using two-way ANOVA compared to the corresponding control mono-culture value (** $P<0.01$).

5.5 DISCUSSION

Metastatic, and particularly castrate-resistant prostate cancer (CRPC), remain challenging to treat [398]. It is thought that the bone marrow microenvironment

plays a pivotal role in promoting bone metastasis, possibly facilitating the transition to CRPC forms, and impacting on PCa cell drug response [399]–[402]. A barrier in understanding these interactions, in both drug development and testing, is the lack of *in vitro* models that adequately mimic aspects of the bone marrow microenvironment in a practical and high throughput manner.

Our team previously described the development of a high throughput 3D culture platform we termed the *Microwell-mesh* [290]. This platform uses a microwell insert to facilitate the manufacture of hundreds of uniform 3D multicellular microtissues. It differs from previous microwell platforms in that it has a nylon mesh fixed over the microwells, and this enables retention of individual microtissues within discrete microwells even during repeat full medium exchanges. This design is unique, and especially well suited to the assembly of 3D cultures which mimic aspects of the bone marrow microenvironment, and offers the opportunity to perform complex cultures that involve the differentiation of BMSC into different bone-like tissues, subsequent seeding of cultures with PCa cells, and the multiple medium exchanges required to study the interaction of cells and different drugs in these complex cultures. Using the Microwell-mesh to perform 3D cultures, and traditional 2D culture controls, we evaluated PCa cell migration and proliferation in response to bone marrow stromal cell populations, as well as PCa cell response to Docetaxel and Abiraterone Acetate. The goal of this study was to better understand the difference 2D and 3D stromal cell populations might have on PCa culture outcomes, and to describe models that could advance the field's capacity to study these differences.

To study the impact of bone marrow stromal cells on the migration potential of PCa cells, we used a modified Transwell assay to quantify the migration of three different PCa cell lines towards different populations of bone marrow stromal cells (see Figure 5.2). PCa cell migration rates varied depending on the aggressiveness of the PCa cell lines tested. In cell lines derived from less aggressive disease (LNCaP), relative to aggressive disease (C42B and PC3), there was a corresponding reduction in the rate of cell migration towards the bone marrow stromal cells cultured in 2D monolayers. PC3 cells (which model aggressive disease) demonstrated increased migration rates towards 2D monolayers of BMSC, osteoblasts and adipocytes. By contrast, PC3 cells demonstrated an increased rate of migration towards 3D

osteoblasts and a reduced rate of migration towards BMSC or adipocytes, relative to controls. This data highlights the difference in PCa cell response depending on the PCa cell phenotype, the bone marrow stromal cell phenotype, and depending on the 2D or 3D organization of the bone marrow stromal cells. Appreciating that there is a difference is important, as well as appreciating that there can be assay specific outcomes that may not translate to other *in vitro* assays, and finally it is necessary to appreciate that not all *in vitro* assay results will be reproducible *in vivo*. Transwell cultures enable quantification of the influence secreted factors have on PCa cell migration, but do not necessarily provide insight into how stromal cell-specific matrix or bound factors may directly influence PCa cell behavior. Thus, Transwell assay outcomes provide only part of the necessary insight.

Next, we investigated how 2D or 3D culture of different bone marrow stromal cell populations impacted on C42B cell proliferation. C42B cell proliferation was greater when these cells were seeded on 2D monolayers of BMSC, adipocytes or osteoblasts (see Figure 5.4a). This result is consistent with the general view that stromal cells can play a supportive role in co-cultures, and especially those that mimic aspects of the support environment found in the bone marrow niche [221], [222]. This result is also consistent with a previous report indicating that BMSC-conditioned media supports PCa cell proliferation [403]. In 3D co-cultures, only adipocytes were found to drive significant increases in C42B cell proliferation (see Figure 5.4b). This substantial difference in 2D and 3D culture outcomes is interesting, as it indicates that geometry can significantly impact co-culture outcomes. Future studies might compare the secretion profiles of BMSC, adipocytes or osteoblasts in 2D and 3D, with the hypothesis that culture geometry significantly influences what factors are produced by the stromal cell populations. There are already a number of papers that suggest the secretome of BMSC is more supportive when these cells are assembled into spheroids in the soluble culture environment [404], [405]. Characterizing precise changes in the gene expression or secretion profile of the mesenchymal and PCa cells assembled into spheroids would require digesting the co-culture microtissues into single cell suspensions, followed by FACSsorting and then gene or protein analysis. The considerable processing steps and time would likely confound the results. Thus, within this manuscript we focused on platform development and phenomenological characterization of PCa growth and

drug response as influenced by the presence or absence of different mesenchymal cell populations. Equally valuable would be to compare how 2D and 3D co-cultures influence the proliferation of primary PCa cells. Primary PCa cells are particularly challenging to culture *in vitro* [406], but their response to co-culture might be more meaningful than the response from any adapted cell line. We see these important investigations as beyond the scope of this manuscript, but obvious opportunities that could be explored next using the Microwell-mesh as tool to facilitate these important next steps.

In our studies, we found that the drug response of C42B cells drug response differed in 2D and 3D co-cultures, and that response varied depending on the stromal cell population used in the co-culture (see Figure 5.5 and Figure 5.6). Universally, the presence of BMSC or adipocytes in 2D or 3D co-culture reduced C42B cells sensitivity to Docetaxel, a drug commonly used to treat metastatic disease. Other groups have reported similar observations previously [369], [371], [407], suggesting that bone marrow stromal cells likely do influence PCa cell drug sensitivity. In contrast to tests conducted with Docetaxel, the drug response of C42B cells to Abiraterone Acetate did not appear to be influenced by the presence or absence of bone marrow stromal cells. However, the organization of C42B cells into 3D cultures did reduce these cells sensitivity to Abiraterone Acetate, relative to 2D cultures. This outcome suggests that relative proliferation rates, which are generally reduced in 3D cultures [353], [354], may play a greater role than the presence or absence of stromal cells in influencing the impact of anti-androgen treatment.

Overall, our results indicate that C42B cells behaviour can vary depending on the phenotype and geometry of bone marrow stromal cells included in co-culture. Through this work, we have described the development of a 3D co-culture platform, the microwell-mesh, that enables the assembly of 3D bone stromal cell microtissues, the subsequent introduction of PCa cells, and then evaluation of PCa cell proliferation or drug response. Using this novel 3D culture platform, we show that PCa cell response to drugs varies considerably in 2D and in 3D, and culture outcomes are also stromal cell-type dependent. This culture tool, and the corresponding 2D culture tools will enable more complex *in vitro* analysis, and hopefully lead to the more efficient identification of improved PCa treatment strategies.

Acknowledgment

The authors would like to thank the National Health and Medical Research Council (NHMRC) of Australia and the Prostate Cancer Foundation of Australia (PCFA) for supporting this research. E.M is supported by the Ministry of Higher Education of Egypt.

Author Contributions

E.Mosaad designed research, performed research, analysed data and wrote the paper.

K.C. and J.C. analysed data and wrote the paper.

K.F. wrote the paper.

M.D. designed research, analysed data and wrote the paper.

Conflict of interest

The authors declare that they have no conflict of interest.

5.6 SUPPLEMENTARY DATA

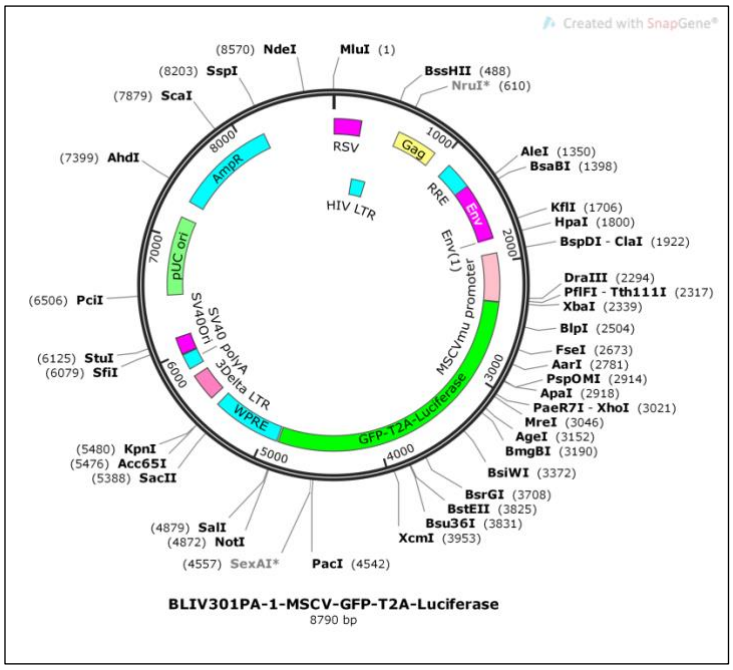

Supplementary Figure 5.1. Restriction map of plasmid used in lentiviral particles production to transduce C42B cells with luciferase gene with MSCV promoter region. Plasmid was designed by System Biosciences (Bioluminescence Imaging Vectors, BLIV).

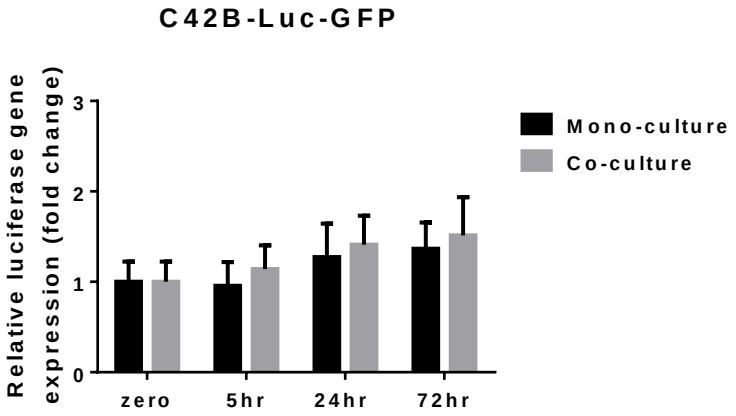

Supplementary Figure 5.2. Luciferase gene expression in C42B-MSCV cell lines. Cells were either mono- or co-cultured with BMSC in a Transwell assay for the indicated time points. The relative luciferase gene expression was assessed and normalized to *RPLPO* housekeeping gene. Three independent experiments were performed, each had four replicate cultures (n=4).

Supplementary Table 5.1. Primers and annealing temperatures used for qRT-PCR

Gene	Sequence (5'- 3')	Annealing temperature (°C)	Final primers conc. (nM)	Amplicon size (bp)
RPLP0	F TGTGGGCTCCAAGCAGATGCA	60	200	137
	R GCAGCAGTTTCTCCAGAGCTGGG			
Firefly	F GTGTTGGGCGCGTTATTTAT	60.7	200	102
luciferase	R TACGGTAGGCTGCGAAATGT			

Chapter 6: Conclusions and future directions

In this Chapter I aim to summarise my observations, and suggest future work that could be undertaken to advance this project.

6.1 CONCLUSIONS

6.1.1 Studies into 3D BMSC microtissues

3D spheroid cultures are increasingly recognized as promising tools for studying cell-cell interactions and for use in tissue regeneration [408]. Because 3D spheroids often provide superior tissue mimics, these multicellular aggregates are often referred to as "microtissues". Previous studies using scaffold-free microtissue culture techniques reported enhancement in the differentiation capacity of BMSC, relative to 2D monolayer cultures [328]. Additionally, 3D microtissue cultures of BMSC showed modified transcriptional and paracrine secretion profiles [334], [409].

The aim of Chapter 2 was to use a microwell platform to manufacture hundreds of microtissues from BMSC, and study their differentiation into osteoblasts, adipocytes or chondrocytes. Supplementation of the medium with exogenous cytokine (BMP-2) improved osteogenesis in 2D and in 3D microtissue cultures. To our knowledge, this is the first time that this has been reported in 3D microtissue cultures. A critically important observation is that supplementation of 3D cultures with BMP-2 also induced adipogenesis (Figure 2.9 and 2.10). This highlights the risk that BMP-2 may lead to poor quality bone formation.

The work in Chapter 2 described a major limitation of the microwell platform, which is the displacement of microtissues from discrete microwells when exchanging culture media. The displaced microtissues can be lost through medium exchange or fall into adjacent microwells where they can amalgamate with other microtissues, resulting in a culture of heterogeneous microtissue sizes and numbers. Therefore, caution was taken in all the culture manipulations to minimise any media disturbance. This additional effort made the culture process more laborious.

6.1.2 Studies into 3D PCa micro-tumours in the Microwell-mesh platform

Further improvements on the microwell platform enabled culture media exchange without displacing the microtissues from discrete microwells (using the Microwell-mesh [290]). The Microwell-mesh functions by having a mesh fixed over the microwells. The pore size in the mesh was large enough to allow single cells pass through the mesh, and aggregate in the bottom of the microwells. When the aggregated cells self-assembled into microtissues, they were too large to pass back through the mesh. This design feature retained microtissues in discrete microwells over repeated medium exchanges. This modification enhanced the potential of this device to be used as a drug-testing platform. In Chapter 3, the aim was to characterise PCa micro-tumours and utilise the Microwell-mesh platform as a robust drug-screening platform. As a proof of concept, PCa micro-tumours response to two therapeutic drugs, Docetaxel and Abiraterone Acetate, were tested. In addition, the Microwell-mesh enabled testing sequential drug doses.

6.1.3 Studies into cell-specific quantification in co-culture system

Quantifying viability or cell number of specific cell type in a mixture of more than one cell type is a challenging goal and conventional viability assays are unable to achieve this. Recently, the luciferase reporter system was utilised to solve this research problem where the bioluminescence emitted from a single cell population tagged with luciferase could be a surrogate to estimate the viable luciferase-tagged cell number in co-culture [369]. This assay was termed as cell-specific bioluminescence (CS-BLI) assay. The results reported in Chapter 4 have proved that this assay is not necessarily reliable in all transduced cell populations. The method of transducing the cells with the reporter system, the promoter and the cell type to be tested are all crucial factors affecting the CS-BLI assay accuracy.

Despite the possible limitations of bioluminescence assay, a stable reporter system was used to produce PCa and breast cancer cell lines that stably express the luciferase gene driven by CMV, MSCV and EF1a promoters in both mono- and co-cultures over 24 hours of cultures. Whole genome sequencing of the cells transduced with CMV-controlled reporter systems could give insights into the genomic regions/genes that can affect the promoter stability. The CMV promoter expression

was found to fluctuate between various conditions of culture [386]–[388]. The number of insertions of the CMV-derived reporter was very high (84 insertions) in the stable cell line, while it was only 4 sites in the unstable cell line which indicated that the stability of the reporter expression can also be affected by the number of insertions.

6.1.4 Studies into 3D PCa-stromal cell co-culture

PCa is the second most common cancer in men worldwide [1] and approximately 80% of PCa metastasis is to the bone. Once bone metastasis occurs, treatments become more elusive and survival rates are low [29]. In Chapter 5, the outcomes of the previous chapters have served in modelling a 3D bone metastatic PCa model and its use as a drug-testing platform. The Microwell-mesh was used to manufacture microtissues formed from PCa and BMSC. To achieve this, 1) we first established BMSC, bone or fat microtissues for the required period of time (24 hours for BMSC and 14 days for bone and fat microtissues); 2) this was followed by establishing PCa mono-culture control microtissues or adding PCa cells to stromal microtissues to establish co-cultures; thus, PCa cells in all conditions had been in culture for the same length of time; 3) then after 24 hours, all cultures were treated with anti-tumour drug. This model system was used to test the responsiveness of the PCa cells in the co-culture system to Docetaxel or Abiraterone Acetate, two drugs commonly used in the clinic with advanced PCa patients. The verified CS-BLI assay was used to quantify PCa cell viability in co-culture system.

According to our findings in Chapter 2, Chapter 3 and what is widely acknowledged in the field, the cell proliferation in 3D cultures is much lower than that in 2D cultures [397], [258], [333], [334]. This can explain the lower drug sensitivity in 3D co-cultures, especially in cultures treated with Docetaxel which targets highly proliferative cells [254]. However, in 3D cultures cells behave similar to its native tumour environment where tumour proliferation rate is relatively low and shows differential proliferation rates between different regions of the tumour [410]–[412]. In low vascularised areas in *in vivo* tumours, low oxygen and nutrient supplies can lead to necrosis and low proliferating cells [257]. Presumably, 2D cultures cannot replicate these critical *in vivo* tumour features because 2D cultures

has unrealistic high proliferation rates where the cell number can be doubled in a very short time.

Our results showed a significant change in growth rate and chemotherapeutic sensitivity of PCa cells in the presence of stromal cells. In our study, several results suggested a higher chemotherapeutic drug sensitivity of PCa in co-cultures; because 1) PCa cell proliferation in co-culture was greater than in mono-cultures; 2) co-cultures were treated with Docetaxel after only 24 hours of establishing the co-cultures while the tumour cells were presumably in log phase growth after reasonable time in 2D culture for cell expansion; 3) the tumour cells were organized in the outer surface of the co-culture microtissues where cells are more proliferative than in inner layers (as shown in Chapter 3). Despite these observations, which provide evidence of high growth rates of PCa cells in co-cultures, PCa cells showed less drug sensitivity in co-cultures, and thus stromal cells provided a protective effect to the tumour cells against Docetaxel treatment. Therefore, the supportive role of stromal cells minimises the influence of the proliferation state of the tumour cells on the drug sensitivity in co-cultures in the tested time point. It is worth noting that longer time in 3D culture may decrease PCa cell proliferation and consequently reduce response to drugs that target dividing cells.

Since PCa cells were cultured for the same length of time in all conditions, the difference in culture duration was not a confounding variable. However, the timing of the drug treatment may have influenced our results. In this study, we treated the cultures with the drug after 24 hours of establishing the co-cultures. Prolonged co-culture periods in 3D may cause a decrease in cell proliferation rates and may subsequently decrease the PCa cell sensitivity against chemotherapeutic drugs.

6.2 FUTURE DIRECTIONS

6.2.1 3D BMSC microtissues and bone regeneration

Bone defects can be caused by many reasons, including osteoporosis, bone cancer, and bone fractures. These debilitating conditions are commonly treated with the “gold standard” treatment, autografts [413]. However, there are several complications associated with autografts which means that the outcomes are still limited [414]. Additionally, growth factors, such as BMP-2 and BMP-7, are

commonly used in the clinics to enhance bone regeneration [415]. The emerging tissue engineering field offers therapies to improve the outcomes of the bone defects treatment. Nonetheless, a limited number of clinical trials have been executed to prove the feasibility of treatment strategies proposed by findings in *in vitro* and *in vivo* studies.

Future studies might aim to utilise the microwell system in bone regeneration studies. In Chapter 2, the microwell platform was introduced as a tool to manufacture microtissues in a high throughput capacity. Manufacturing hundreds of microtissues with uniform size is an important feature to facilitate applications in the clinic and in mass production. The microtissues formed in the microwell platform are easily accessible which make further cellular mechanism studies more possible. The impact of other growth factor such as BMP-7 can be studied using this platform. The transcriptional profiles of the growth factor-treated BMSC can give a deeper insight into the alterations in BMSC 3D cultures. This can help guide the alterations toward enhanced *in vivo* or clinical outcomes by sequential/combination treatments with several growth factors to activate/inhibit specific cellular mechanisms to finally obtain a functional bone construct. We propose that this platform can be used to enhance further studies in this aspect of bone tissue engineering research.

6.2.2 Improvements in 3D cultures of PCa micro-tumours

A small yet growing number of studies are now acknowledging the likely role of 3D cultures in *in vitro* cancer research [257], [251], [279], [416]. One of the main advantages of 3D cultures is the accumulation of cell-secreted extracellular matrix. The extracellular matrix governs tissue homeostasis by regulating cell growth, motility and survival in 3D supramolecular structures with specific biochemical and biomechanical properties [417]. Indeed, the cancer-associated extracellular matrix has an important role in cell behaviour and response to drug treatments [418]. In the Microwell-mesh platform, the impact of extracellular matrix of the tumour microenvironment is partially considered where the extracellular matrix is mainly formed by the cells organised in 3D cultures. The influence of the matrix secreted by other cell types or the microenvironment milieu is absent in our system. However, our 3D Microwell-mesh system can enable formation of 3D cultures formed from a combination of different cell types for further studies on cellular interactions.

Although the Microwell-mesh model is unable to mimic all aspects of the metastasis process including migration and invasion of the tumour cells to the bone marrow, the use of this model system can enhance our understanding of the cellular interactions between PCa cells and bone marrow stromal cells. Additionally, using primary tumour cells or circulating tumour cells in these co-culture studies could provide a more robust mimic of actual disease processes, compared to studies that use cancer cell lines. This can also enable future studies in *in vitro* prediction of drug efficacy.

A major challenge in cancer research is the use of cell lines. Some cell lines are poorly characterized and inadequately mimic human disease [247]. Therefore, patient-derived explants that are implanted in an animal model, also called patient-derived xenografts (PDX), have demonstrated better surrogates of human cancer in terms of histology, gene expression and drug response [218], [419]–[421]. PDX can be derived by serial propagation of primary tumour cells in animal hosts due to their poor adaptation in *in vitro* cultures. However, a fundamental advantage of using *in vitro* methods over *in vivo* models to propagate primary tumour cells is that the absence of any animal components that may impact human cell behaviour. Therefore, several studies on organoid cultures are now widely acknowledged [406], [422]. Organoid cultures aim to recapitulate the cellular organisation of the tissue of origin by culturing stem cells in 3D cultures to model organ development or disease [423], [424]. Recently, human prostate organoids have been developed from single luminal cells in Matrigel using organoid culture medium containing EGF, Noggin and R-spondin 1 [422], or containing EGF and Dihydrotestosterone [425]. In future studies, fusing the benefits of the current methods of human PCa organoid cultures with the Microwell-mesh system may evolve into more feasible model system. For example, using the Microwell-mesh system may replace the use of Matrigel, which is murine-derived ECM, to minimize the interference with human cell behaviour and enhance 3D cell organization. An alternative way is to replace Matrigel with synthetic or natural hydrogel with defined chemical composition and mechanical properties that resemble physiological conditions. These approaches may facilitate studies on drug penetration and responses to current and novel drugs.

The major drawback of both the microwell and the Microwell-mesh platforms is that these platforms were manually manufactured. However, the platform concept could be readily manufactured commercially, which would save a lot of time and effort and improve consistancy. One of the advantages of the Microwell-mesh platform is that it can provide a universal 3D platform for high throughput techniques that is compatible with automation to be used with different solid tumour tissue modelling.

6.2.3 PCa modelling and drug-testing platforms

A major limitation in the cancer research field is the prediction of drug efficacy. Billions of dollars are spent every year in pharmaceutical research and development with much less valuable outcomes than expected [426]. Many researchers in the field reasoned the poor outcomes of drug-screening strategy to the fact that most of the *in vitro* drug-testing platforms are based on using conventional 2D monolayer cultures regardless of the ability of the 2D culture to mimic *in vivo* settings [427]. On the other hand, 3D cultures can provide a more physiological mimic of tissues, resulting in a more reliable responsiveness to toxic drugs. Using the Microwell-mesh platform, further studies on PCa and other solid tumours can be performed to test efficacy of treatment protocols of novel drugs. The effect of current drugs with similar mechanisms to Docetaxel, such as Paclitaxel and Cabazitaxel could be tested in the Microwell-mesh platform.

Several studies revealed the association between obesity and the aggressiveness of PCa [428]–[431]. Adipocyte-secreted chemokines were found to enhance the ability of PCa stem-like cells to self-renew [432]. In another study, bone marrow adipocytes promoted tumour growth *in vivo* [433]. In our study, a significant observation was the impact of adipocyte co-cultures on PCa cell growth and responses to drug treatments that have not been studied previously in 3D direct *in vitro* co-cultures. Further studies might aim to explain the interplay between adipocytes and PCa response to different drug treatments; and if the mechanisms controlling this cellular interaction can be influenced by drug treatment.

In our study, we co-cultured PCa cells with stromal cells in a 1:1 ratio for 48 hours. In future studies, different cell ratios and longer culture periods could be

tested to replicate the different stages of the disease. The number of PCa cells could initially be small mimicking early bone metastasis and permitted to increase with time to mimic disease progression. The Microwell-mesh enables control over cell numbers in microtissue co-cultures, and so variations on the described experiments are possible. Equally valuable, would be to test various timing of drug treatment in 3D co-cultures and study how this may impact the drug sensitivity.

To date, no *in vitro* model has replicated the complex bone marrow HSC niche. Our simple model can provide the building blocks of the HSC niche by culturing different cell types in 3D cultures then combine them together in a complex model. The parental BMSC and adipocytes can be cultured as cell spheroids then introduced to a mineralized monolayer culture of osteoblasts, combining these cell types with suspended immune cells such as macrophages to model the HSC osteoblastic niche. Replacing the osteoblasts with endothelial cells could mimic the HSC vascular niche. Such models could be used also to study breast cancer or leukaemia. Considering other cell types, such as macrophages or cancer-associated fibroblasts, can also enrich the model system to mimic physiological cancer microenvironment. These suggested complex models could be used as a robust high throughput drug-testing platform.

6.2.4 Cell-specific quantification assays in a co-culture system

Although multicellular environments are now widely appreciated in cancer research, a limited number of high throughput cell-specific techniques have been introduced to the field. Beside the cell-specific bioluminescence assay for cell number quantification, other cell-specific techniques have been developed. For example, Gauthier *et. al.*, have introduced a technique to selectively label the proteomes of specific cell type in co-cultures using amino acid precursors [434]. Likewise, another study has introduced an automated fluorescence microscope platform to distinguish between BMSC and myeloma cells according to a nuclear staining intensity and nuclear shape [435].

Generally, the concept of the cell-specific bioluminescence assay was certainly a leading innovation. However, caution should be taken in reporter system selection according to the culture conditions. The stability of the reporter system expression,

or in other words the promoter stability, in specific culture conditions requires validation before utilization as an indirect quantification of cell number or cell viability.

For future studies, the identification of the gene(s) flanking the reporter system may explain the differential behaviour between different cell lines/promoters. In our study, co-cultures were established using BMSC. BMSC are known to secrete a vast number of growth factors, such as FGF, TGF-β1 and VEGF [436], [437]. If the expression of the flanking gene of the promoter is influenced by BMSC-secreted growth factors, this may influence the expression of the reporter.

By regular methods of transduction of cells, such as using viral particles, researchers cannot control the site of insertion. Various technologies can achieve selective insertions of the reporter system such as using guided genome editing technique or the CRISPR-cas system to minimize perturbation possibility of reporter system stability.

Cumulatively, through this Thesis, the merits of using a high throughput microwell platform to efficiently manufacture hundreds of multicellular spheroids was evaluated which was used for further evaluation of the Microwell-mesh platform as a drug-screening platform. A critical factor was the discovery of instability of the CS-BLI assay, which was promoter and/or cell line dependent and which would need to be verified with each cell line before use. Finally, the first multicellular co-culture micro-tumour system as a potential drug-screening platform for bone metastatic PCa was developed. The outcome of this Thesis may help in developing personalised therapy by using the Microwell-mesh system to culture patient-derived tumour samples and study drug response prediction for better outcomes of patient treatment.

Bibliography

[1] A. Jemal, F. Bray, M. M. Center, J. Ferlay, E. Ward, and D. Forman, "Global cancer statistics," *CA. Cancer J. Clin.*, vol. 61, no. 2, pp. 69–90, 2011.

[2] J. Ferlay, I. Soerjomataram, R. Dikshit, S. Eser, C. Mathers, M. Rebelo, D. M. Parkin, D. Forman, and F. Bray, "Cancer incidence and mortality worldwide: sources, methods and major patterns in GLOBOCAN 2012.," *Int. J. cancer*, vol. 136, no. 5, pp. E359-86, Mar. 2015.

[3] J. Ferlay, H. R. Shin, F. Bray, D. Forman, C. Mathers, and D. M. Parkin, "GLOBOCAN 2008, cancer incidence and mortality worldwide: IARC CancerBase No. 10," *Lyon, Fr. Int. Agency Res. Cancer*, vol. 2010, p. 29, 2010.

[4] U. S. C. S. W. Group, "US Cancer Statistics: 1999–2007 incidence and mortality web-based report," *Atlanta GA DHHS. CDC Natl. Cancer Inst. www. cdc. gov/uscs*, 2010.

[5] Y. Ben-Shlomo, S. Evans, F. Ibrahim, B. Patel, K. Anson, F. Chinegwundoh, C. Corbishley, D. Dorling, B. Thomas, and D. Gillatt, "The risk of prostate cancer amongst black men in the United Kingdom: the PROCESS cohort study," *Eur. Urol.*, vol. 53, no. 1, pp. 99–105, 2008.

[6] A. Heidenreich, J. Bellmunt, M. Bolla, S. Joniau, M. Mason, V. Matveev, N. Mottet, H.-P. Schmid, T. van der Kwast, and T. Wiegel, "EAU guidelines on prostate cancer. Part 1: screening, diagnosis, and treatment of clinically localised disease," *Eur. Urol.*, vol. 59, no. 1, pp. 61–71, 2011.

[7] C. H. Bangma, S. Roemeling, and F. H. Schr?der, "Overdiagnosis and overtreatment of early detected prostate cancer," *World J. Urol.*, vol. 25, no. 1, pp. 3–9, Mar. 2007.

[8] D. Thorek, M. Evans, and S. Carlsson, "Prostate-specific kallikrein-related peptidases and their relation to prostate cancer biology and detection," *Thromb. Haemost.*, vol. 110, pp. 484–492, 2013.

[9] J. Shoag, J. A. Halpern, D. J. Lee, S. Mittal, K. V. Ballman, C. E. Barbieri, and J. C. Hu, "Decline in Prostate Cancer Screening by Primary Care Physicians: An Analysis of Trends in the Use of Digital Rectal Examination and Prostate Specific Antigen Testing," *J. Urol.*, vol. 196, no. 4, pp. 1047–1052, Oct. 2016.

[10] M. D. Eckhardt, G. E. van Venrooij, H. H. van Melick, and T. A. Boon, "Prevalence and bothersomeness of lower urinary tract symptoms in benign prostatic hyperplasia and their impact on well-being.," *J. Urol.*, vol. 166, no. 2, pp. 563–8, Aug. 2001.

[11] A. Jedinak, A. Curatolo, D. Zurakowski, S. Dillon, M. K. Bhasin, T. A. Libermann, R. Roy, M. Sachdev, K. R. Loughlin, and M. A. Moses, "Novel non-invasive biomarkers that distinguish between benign prostate hyperplasia and prostate cancer," *BMC Cancer*, vol. 15, no. 1, p. 259, Dec. 2015.

[12] C. G. Roehrborn, J. D. McConnell, M. Lieber, S. Kaplan, J. Geller, G. H. Malek, R. Castellanos, S. Coffield, B. Saltzman, M. Resnick, T. J. Cook, and J. Waldstreicher, "Serum prostate-specific antigen concentration is a powerful predictor of acute urinary retention and need for surgery in men with clinical benign prostatic hyperplasia," *Urology*, vol. 53, no. 3, pp. 473–480, Mar. 1999.

[13] I. A. Thangasamy, V. Chalasani, A. Bachmann, and H. H. Woo, "Photoselective Vaporisation of the Prostate Using 80-W and 120-W Laser Versus Transurethral Resection of the Prostate for Benign Prostatic Hyperplasia: A Systematic Review with Meta-Analysis from 2002 to 2012," *Eur. Urol.*, vol. 62, no. 2, pp. 315–323, Aug. 2012.

[14] E. Anastasiadis, J. van der Meulen, and M. Emberton, "Incidental prostate cancer diagnosed following a transurethral resection of the prostate: A national database analysis in England," *J. Clin. Urol.*, vol. 9, no. 3, pp. 170–176, May 2016.

[15] S. Dason, C. B. Allard, I. Wright, and B. Shayegan, "Transurethral Resection of the Prostate Biopsy of Suspected Anterior Prostate Cancers Identified by Multiparametric Magnetic Resonance Imaging: A Pilot Study of a Novel Technique," *Urology*, vol. 91, pp. 129–135, May 2016.

[16] P. Leidinger, M. Hart, C. Backes, S. Rheinheimer, B. Keck, B. Wullich, A. Keller, and E. Meese, "Differential blood-based diagnosis between benign prostatic hyperplasia and prostate cancer: miRNA as source for biomarkers independent of PSA level, Gleason score, or TNM status," *Tumor Biol.*, vol. 37, no. 8, pp. 10177–10185, Aug. 2016.

[17] N. Mottet, J. A. Schalken, A. Heidenreich, P. J. Bastian, J. Irani, L. Salomon, and M. Soulié, "Highlights on prostate cancer from urological and oncological congresses in 2007," *Eur. Urol. Suppl.*, vol. 7, no. 6, pp. 460–476, 2008.

[18] D. F. Gleason, G. T. Mellinger, L. J. Arduino, J. C. Bailar, L. E. Becker, H. I. Berman, A. J. Bischoff, D. P. Byar, C. E. Blackard, R. P. Doe, J. S. Elliot, E. Haltiwanger, R. B. Higgins, J. Jorgens, H. C. Kramer, L. E. Lee, M. Malament, F. K. Mostofi, W. L. Parry, L. S. Rogers, A. H. Ulm, and V. R. Quiambao, "Prediction of Prognosis for Prostatic Adenocarcinoma by Combined Histological Grading and Clinical Staging," *J. Urol.*, vol. 111, no. 1, pp. 58–64, Jan. 1974.

[19] J. I. Epstein, L. Egevad, M. B. Amin, B. Delahunt, J. R. Srigley, P. A. Humphrey, and Grading Committee, "The 2014 International Society of Urological Pathology (ISUP) Consensus Conference on Gleason Grading of Prostatic Carcinoma," *Am. J. Surg. Pathol.*, vol. 40, no. 2, p. 1, Oct. 2015.

[20] J. Gordetsky and J. Epstein, "Grading of prostatic adenocarcinoma: current state and prognostic implications.," *Diagn. Pathol.*, vol. 11, p. 25, Mar. 2016.

[21] G. L. Andriole, L. R. Kavoussi, R. J. Torrence, H. Lepor, and W. J. Catalona, "Transrectal ultrasonography in the diagnosis and staging of carcinoma of the prostate.," *J. Urol.*, vol. 140, no. 4, pp. 758–60, Oct. 1988.

[22] J. Platt, R. Bree, and R. Schwab, "The accuracy of CT in the staging of carcinoma of the prostate," *Am. J. Roentgenol.*, vol. 149, no. 2, pp. 315–318, Aug. 1987.

[23] S. T. Houston, L. W. Jones, and V. Waluch, “Nuclear magnetic resonance imaging in detecting and staging prostatic cancer,” *Urology*, vol. 31, no. 2, pp. 171–175, Feb. 1988.

[24] L. H. Klotz, “Active surveillance for good risk prostate cancer: rationale, method, and results.,” *Can. J. Urol.*, vol. 12 Suppl 2, pp. 21–4, Jun. 2005.

[25] M. Shipitsin, C. Small, S. Choudhury, E. Giladi, S. Friedlander, J. Nardone, S. Hussain, A. D. Hurley, C. Ernst, Y. E. Huang, H. Chang, T. P. Nifong, D. L. Rimm, J. Dunyak, M. Loda, D. M. Berman, and P. Blume-Jensen, “Identification of proteomic biomarkers predicting prostate cancer aggressiveness and lethality despite biopsy-sampling error,” *Br. J. Cancer*, vol. 111, no. 6, pp. 1201–1212, Sep. 2014.

[26] A. Briganti, N. Suardi, A. Gallina, F. Abdollah, G. Novara, V. Ficarra, and F. Montorsi, “Predicting the risk of bone metastasis in prostate cancer,” *Cancer Treat. Rev.*, vol. 40, no. 1, pp. 3–11, Feb. 2014.

[27] S. R. Denmeade and J. T. Isaacs, “A history of prostate cancer treatment,” *Nat. Rev. Cancer*, vol. 2, no. 5, pp. 389–396, May 2002.

[28] J.-P. Droz, M. Aapro, L. Balducci, H. Boyle, T. Van den Broeck, P. Cathcart, L. Dickinson, E. Efstathiou, M. Emberton, J. M. Fitzpatrick, A. Heidenreich, S. Hughes, S. Joniau, M. Kattan, N. Mottet, S. Oudard, H. Payne, F. Saad, and T. Sugihara, “Management of prostate cancer in older patients: updated recommendations of a working group of the International Society of Geriatric Oncology,” *Lancet Oncol.*, vol. 15, no. 9, pp. e404–e414, Aug. 2014.

[29] N. Mottet, J. Bellmunt, M. Bolla, E. Briers, M. G. Cumberbatch, M. De Santis, N. Fossati, T. Gross, A. M. Henry, S. Joniau, T. B. Lam, M. D. Mason, V. B. Matveev, P. C. Moldovan, R. C. N. van den Bergh, T. Van den Broeck, H. G. van der Poel, T. H. van der Kwast, O. Rouvière, I. G. Schoots, T. Wiegel, and P. Cornford, “EAU-ESTRO-SIOG Guidelines on Prostate Cancer. Part 1: Screening, Diagnosis, and Local Treatment with Curative Intent,” 2017.

[30] P. Cornford, J. Bellmunt, M. Bolla, E. Briers, M. De Santis, T. Gross, A. M. Henry, S. Joniau, T. B. Lam, M. D. Mason, H. G. van der Poel, T. H. van der Kwast, O. Rouvière, T. Wiegel, and N. Mottet, “EAU-ESTRO-SIOG Guidelines on Prostate Cancer. Part II: Treatment of Relapsing, Metastatic, and Castration-Resistant Prostate Cancer,” 2017.

[31] C. A. Salinas, A. Tsodikov, M. Ishak-Howard, and K. A. Cooney, “Prostate cancer in young men: an important clinical entity,” *Nat. Rev. Urol.*, 2014.

[32] T. J. Wilt, R. MacDonald, I. Rutks, T. A. Shamliyan, B. C. Taylor, and R. L. Kane, “Systematic Review: Comparative Effectiveness and Harms of Treatments for Clinically Localized Prostate Cancer,” *Ann. Intern. Med.*, vol. 148, no. 6, pp. 435–448, 2008.

[33] A. A. Aizer, J. J. Paly, M. D. Michaelson, S. K. Rao, P. L. Nguyen, I. D. Kaplan, A. Niemierko, A. F. Olumi, and J. A. Efstathiou, “Medical Oncology Consultation and Minimization of Overtreatment in Men With Low-Risk Prostate Cancer,” *J. Oncol. Pract.*, vol. 10, no. 2, pp. 107–112, 2014.

[34] A. Sidana, D. J. Hernandez, Z. Feng, A. W. Partin, B. J. Trock, S. Saha, and J.

I. Epstein, “Treatment decision-making for localized prostate cancer: What younger men choose and why,” *Prostate*, vol. 72, no. 1, pp. 58–64, 2012.

[35] S. B. Zeliadt, S. D. Ramsey, D. F. Penson, I. J. Hall, D. U. Ekwueme, L. Stroud, and J. W. Lee, “Why do men choose one treatment over another?,” *Cancer*, vol. 106, no. 9, pp. 1865–1874, 2006.

[36] A. Bill-Axelson, L. Holmberg, H. Garmo, J. R. Rider, K. Taari, C. Busch, S. Nordling, M. H?ggman, S.-O. Andersson, A. Sp?ngberg, O. Andr?n, J. Palmgren, G. Steineck, H.-O. Adami, and J.-E. Johansson, “Radical Prostatectomy or Watchful Waiting in Early Prostate Cancer,” *N. Engl. J. Med.*, vol. 370, no. 10, pp. 932–942, Mar. 2014.

[37] J. W. Jang, M. R. Drumm, J. A. Efstathiou, J. J. Paly, A. Niemierko, M. Ancukiewicz, J. A. Talcott, J. A. Clark, and A. L. Zietman, “Long-term quality of life after definitive treatment for prostate cancer: patient-reported outcomes in the second posttreatment decade,” *Cancer Med.*, May 2017.

[38] M. Avila, V. Becerra, F. Guedea, J. F. Suarez, P. Fernandez, V. Macias, A. Marino, A. Hervas, I. Herruzo, M. J. Ortiz, J. Ponce de Leon, G. Sancho, O. Cunillera, Y. Pardo, F. Cots, and M. Ferrer, “Estimating Preferences for Treatments in Patients With Localized Prostate Cancer,” *Int. J. Radiat. Oncol.*, vol. 91, no. 2, pp. 277–287, Feb. 2015.

[39] D. Palma, E. Vollans, K. James, S. Nakano, V. Moiseenko, R. Shaffer, M. McKenzie, J. Morris, and K. Otto, “Volumetric Modulated Arc Therapy for Delivery of Prostate Radiotherapy: Comparison With Intensity-Modulated Radiotherapy and Three-Dimensional Conformal Radiotherapy,” *Int. J. Radiat. Oncol.*, vol. 72, no. 4, pp. 996–1001, Nov. 2008.

[40] C. A. Perez, G. E. Hanks, S. A. Leibel, A. L. Zietman, Z. Fuks, and W. R. Lee, “Localized carcinoma of the prostate (Stages T1B, T1C, T2, and T3). Review of management with external beam radiation therapy,” *Cancer*, vol. 72, no. 11, pp. 3156–3173, Dec. 1993.

[41] L. J. Verhey, “Comparison of three-dimensional conformal radiation therapy and intensity-modulated radiation therapy systems,” *Semin. Radiat. Oncol.*, vol. 9, no. 1, pp. 78–98, Jan. 1999.

[42] R. C. Wortel, L. Incrocci, F. J. Pos, U. A. van der Heide, J. V. Lebesque, S. Aluwini, M. G. Witte, and W. D. Heemsbergen, “Late Side Effects After Image Guided Intensity Modulated Radiation Therapy Compared to 3D-Conformal Radiation Therapy for Prostate Cancer: Results From 2 Prospective Cohorts,” *Int. J. Radiat. Oncol.*, vol. 95, no. 2, pp. 680–689, Jun. 2016.

[43] G. S. Merrick, W. M. Butler, R. W. Galbreath, and J. H. Lief, “Five-year biochemical outcome following permanent interstitial brachytherapy for clinical T1-T3 prostate cancer,” *Int. J. Radiat. Oncol.*, vol. 51, no. 1, pp. 41–48, Sep. 2001.

[44] A. J. Stephenson, P. T. Scardino, M. W. Kattan, T. M. Pisansky, K. M. Slawin, E. A. Klein, M. S. Anscher, J. M. Michalski, H. M. Sandler, D. W. Lin, J. D. Forman, M. J. Zelefsky, L. L. Kestin, C. G. Roehrborn, C. N. Catton, T. L. DeWeese, S. L. Liauw, R. K. Valicenti, D. A. Kuban, and A. Pollack, “Predicting the outcome of salvage radiation therapy for recurrent prostate cancer after radical prostatectomy.,” *J. Clin. Oncol.*, vol. 25, no. 15,

pp. 2035–41, May 2007.

[45] C. Huggins, R. E. Stevens, and C. V Hodges, “Studies on prostatic cancer: II. The effects of castration on advanced carcinoma of the prostate gland,” *Arch. Surg.*, vol. 43, no. 2, pp. 209–223, 1941.

[46] F. Labrie, A. B?langer, V. Luu-The, C. Labrie, J. Simard, L. Cusan, J. Gomez, and B. Candas, “Gonadotropin-Releasing Hormone Agonists in the Treatment of Prostate Cancer,” *Endocr. Rev.*, vol. 26, no. 3, pp. 361–379, May 2005.

[47] X. Yuan, C. Cai, S. Chen, S. Chen, Z. Yu, and S. P. Balk, “Androgen receptor functions in castration-resistant prostate cancer and mechanisms of resistance to new agents targeting the androgen axis.,” *Oncogene*, vol. 33, no. 22, pp. 2815–25, May 2014.

[48] H. I. Scher and C. L. Sawyers, “Biology of progressive, castration-resistant prostate cancer: directed therapies targeting the androgen-receptor signaling axis,” *J Clin Oncol*, vol. 23, no. 32, pp. 8253–8261, 2005.

[49] N. Mitsiades, C. C. Sung, N. Schultz, D. C. Danila, B. He, V. K. Eedunuri, M. Fleisher, C. Sander, C. L. Sawyers, and H. I. Scher, “Distinct patterns of dysregulated expression of enzymes involved in androgen synthesis and metabolism in metastatic prostate cancer tumors.,” *Cancer Res.*, vol. 72, no. 23, pp. 6142–52, Dec. 2012.

[50] C. D. Chen, D. S. Welsbie, C. Tran, S. H. Baek, R. Chen, R. Vessella, M. G. Rosenfeld, and C. L. Sawyers, “Molecular determinants of resistance to antiandrogen therapy,” *Nat. Med.*, vol. 10, no. 1, pp. 33–39, Jan. 2004.

[51] T. Karantanos, P. G. Corn, and T. C. Thompson, “Prostate cancer progression after androgen deprivation therapy: mechanisms of castrate resistance and novel therapeutic approaches.,” *Oncogene*, vol. 32, no. 49, pp. 5501–11, Dec. 2013.

[52] K. Haapala, E.-R. Hyytinen, M. Roiha, M. Laurila, I. Rantala, H. J. Helin, and P. A. Koivisto, “Androgen Receptor Alterations in Prostate Cancer Relapsed during a Combined Androgen Blockade by Orchiectomy and Bicalutamide,” *Lab. Investig.*, vol. 81, no. 12, pp. 1647–1651, Dec. 2001.

[53] J. Thompson, E.-R. Hyytinen, K. Haapala, I. Rantala, H. J. Helin, O. A. Jänne, J. J. Palvimo, and P. A. Koivisto, “Androgen Receptor Mutations in High-Grade Prostate Cancer before Hormonal Therapy,” *Lab. Investig.*, vol. 83, no. 12, pp. 1709–1713, Dec. 2003.

[54] W. D. Tilley, C. M. Wilson, M. Marcelli, and M. J. McPhaul, “Androgen receptor gene expression in human prostate carcinoma cell lines.,” *Cancer Res.*, vol. 50, no. 17, pp. 5382–6, Sep. 1990.

[55] Z. Culig, A. Hobisch, M. V Cronauer, A. C. Cato, A. Hittmair, C. Radmayr, J. Eberle, G. Bartsch, and H. Klocker, “Mutant androgen receptor detected in an advanced-stage prostatic carcinoma is activated by adrenal androgens and progesterone.,” *Mol. Endocrinol.*, vol. 7, no. 12, pp. 1541–1550, Dec. 1993.

[56] X.-Y. Zhao, P. J. Malloy, A. V. Krishnan, S. Swami, N. M. Navone, D. M. Peehl, and D. Feldman, “Glucocorticoids can promote androgen-independent growth of prostate cancer cells through a mutated androgen receptor,” *Nat. Med.*, vol. 6, no. 6, pp. 703–706, Jun. 2000.

[57] Y. Li, T. H. Hwang, L. A. Oseth, A. Hauge, R. L. Vessella, S. C. Schmechel, B. Hirsch, K. B. Beckman, K. A. Silverstein, and S. M. Dehm, "AR intragenic deletions linked to androgen receptor splice variant expression and activity in models of prostate cancer progression," *Oncogene*, vol. 31, no. 45, pp. 4759–4767, Nov. 2012.

[58] S. M. Dehm and D. J. Tindall, "Alternatively spliced androgen receptor variants.," *Endocr. Relat. Cancer*, vol. 18, no. 5, pp. R183-96, Oct. 2011.

[59] J. A. Locke, E. S. Guns, A. A. Lubik, H. H. Adomat, S. C. Hendy, C. A. Wood, S. L. Ettinger, M. E. Gleave, and C. C. Nelson, "Androgen levels increase by intratumoral de novo steroidogenesis during progression of castration-resistant prostate cancer," *Cancer Res.*, vol. 68, no. 15, pp. 6407–6415, 2008.

[60] J. Mohler, C. Gregory, O. Ford, D. Kim, C. Weaver, P. Petrsz, E. Wilson, and F. French, "The androgen axis in recurrent prostate cancer," *AACR*, vol. 10, no. 2, pp. 440–448, 2004.

[61] R. B. Montgomery, E. A. Mostaghel, R. Vessella, D. L. Hess, T. F. Kalhorn, C. S. Higano, L. D. True, and P. S. Nelson, "Maintenance of intratumoral androgens in metastatic prostate cancer: a mechanism for castration-resistant tumor growth," *Cancer Res.*, vol. 68, no. 11, pp. 4447–4454, 2008.

[62] S. Sun, C. C. T. Sprenger, R. L. Vessella, K. Haugk, K. Soriano, E. A. Mostaghel, S. T. Page, I. M. Coleman, H. M. Nguyen, H. Sun, P. S. Nelson, and S. R. Plymate, "Castration resistance in human prostate cancer is conferred by a frequently occurring androgen receptor splice variant.," *J. Clin. Invest.*, vol. 120, no. 8, pp. 2715–30, Aug. 2010.

[63] R. Hu, C. Lu, E. A. Mostaghel, S. Yegnasubramanian, M. Gurel, C. Tannahill, J. Edwards, W. B. Isaacs, P. S. Nelson, E. Bluemn, S. R. Plymate, and J. Luo, "Distinct transcriptional programs mediated by the ligand-dependent full-length androgen receptor and its splice variants in castration-resistant prostate cancer.," *Cancer Res.*, vol. 72, no. 14, pp. 3457–62, Jul. 2012.

[64] T. M. Beer, A. J. Armstrong, D. E. Rathkopf, Y. Loriot, C. N. Sternberg, C. S. Higano, P. Iversen, S. Bhattacharya, J. Carles, S. Chowdhury, I. D. Davis, J. S. de Bono, C. P. Evans, K. Fizazi, A. M. Joshua, C.-S. Kim, G. Kimura, P. Mainwaring, H. Mansbach, K. Miller, S. B. Noonberg, F. Perabo, D. Phung, F. Saad, H. I. Scher, M.-E. Taplin, P. M. Venner, and B. Tombal, "Enzalutamide in Metastatic Prostate Cancer before Chemotherapy," *N. Engl. J. Med.*, vol. 371, no. 5, pp. 424–433, Jul. 2014.

[65] J. S. de Bono, C. J. Logothetis, A. Molina, K. Fizazi, S. North, L. Chu, K. N. Chi, R. J. Jones, O. B. Goodman, F. Saad, J. N. Staffurth, P. Mainwaring, S. Harland, T. W. Flaig, T. E. Hutson, T. Cheng, H. Patterson, J. D. Hainsworth, C. J. Ryan, C. N. Sternberg, S. L. Ellard, A. Fl?chon, M. Saleh, M. Scholz, E. Efstathiou, A. Zivi, D. Bianchini, Y. Loriot, N. Chieffo, T. Kheoh, C. M. Haqq, H. I. Scher, A. Fléchon, M. Saleh, M. Scholz, E. Efstathiou, A. Zivi, D. Bianchini, Y. Loriot, N. Chieffo, T. Kheoh, C. M. Haqq, H. I. Scher, and COU-AA-301 Investigators, "Abiraterone and Increased Survival in Metastatic Prostate Cancer," *N. Engl. J. Med.*, vol. 364, no. 21, pp. 1995–2005, May 2011.

[66] D. G. Mcleod, “Hormonal therapy: historical perspective to future directions,” *Urology*, vol. 61, no. 2, pp. 3–7, Feb. 2003.

[67] M. E. Jung, S. Ouk, D. Yoo, C. L. Sawyers, C. Chen, C. Tran, and J. Wongvipat, “Structure− activity relationship for thiohydantoin androgen receptor antagonists for castration-resistant prostate cancer (CRPC),” *J. Med. Chem.*, vol. 53, no. 7, pp. 2779–2796, 2010.

[68] H. I. Scher, T. M. Beer, C. S. Higano, A. Anand, M.-E. Taplin, E. Efstathiou, D. Rathkopf, J. Shelkey, E. Y. Yu, and J. Alumkal, “Antitumour activity of MDV3100 in castration-resistant prostate cancer: a phase 1–2 study,” *Lancet*, vol. 375, no. 9724, pp. 1437–1446, 2010.

[69] G. Attard, A. S. Belldegrun, and J. S. De Bono, “Selective blockade of androgenic steroid synthesis by novel lyase inhibitors as a therapeutic strategy for treating metastatic prostate cancer,” *BJU Int.*, vol. 96, no. 9, pp. 1241–1246, 2005.

[70] C. J. Ryan, M. R. Smith, K. Fizazi, F. Saad, P. F. A. Mulders, C. N. Sternberg, K. Miller, C. J. Logothetis, N. D. Shore, E. J. Small, J. Carles, T. W. Flaig, M.-E. Taplin, C. S. Higano, P. de Souza, J. S. de Bono, T. W. Griffin, P. De Porre, M. K. Yu, Y. C. Park, J. Li, T. Kheoh, V. Naini, A. Molina, and D. E. Rathkopf, “Abiraterone acetate plus prednisone versus placebo plus prednisone in chemotherapy-naive men with metastatic castration-resistant prostate cancer (COU-AA-302): final overall survival analysis of a randomised, double-blind, placebo-controlled phase 3 study,” *Lancet Oncol.*, vol. 16, no. 2, pp. 152–160, Feb. 2015.

[71] I. F. Tannock, R. de Wit, W. R. Berry, J. Horti, A. Pluzanska, K. N. Chi, S. Oudard, C. Th?odore, N. D. James, I. Turesson, M. A. Rosenthal, and M. A. Eisenberger, “Docetaxel plus Prednisone or Mitoxantrone plus Prednisone for Advanced Prostate Cancer,” *N. Engl. J. Med.*, vol. 351, no. 15, pp. 1502–1512, Oct. 2004.

[72] J. S. de Bono, S. Oudard, M. Ozguroglu, S. Hansen, J.-P. Machiels, I. Kocak, G. Gravis, I. Bodrogi, M. J. Mackenzie, L. Shen, M. Roessner, S. Gupta, and A. O. Sartor, “Prednisone plus cabazitaxel or mitoxantrone for metastatic castration-resistant prostate cancer progressing after docetaxel treatment: a randomised open-label trial.,” *Lancet (London, England)*, vol. 376, no. 9747, pp. 1147–54, Oct. 2010.

[73] F. Boccardo, A. Rubagotti, L. Tacchini, A. Lapini, G. Cruciani, G. De Rubertis, M. Battaglia, and G. Conti, “Gefitinib (G) plus prednisone (P) versus placebo (pl) plus prednisone in the treatment of hormone-refractory prostate cancer (HRPC): A randomized phase II trial,” in *J Clin Oncol (Meeting Abstracts)*, 2007, vol. 25, no. 18_suppl, p. 5070.

[74] K. E. Ware, T. K. Hinz, E. Kleczko, K. R. Singleton, L. A. Marek, B. A. Helfrich, C. T. Cummings, D. K. Graham, D. Astling, A.-C. Tan, and L. E. Heasley, “A mechanism of resistance to gefitinib mediated by cellular reprogramming and the acquisition of an FGF2-FGFR1 autocrine growth loop,” *Oncogenesis*, vol. 2, no. 3, p. e39, Mar. 2013.

[75] M. E. Pickup, “Clinical Pharmacokinetics of Prednisone and Prednisolone,” *Clin. Pharmacokinet.*, vol. 4, no. 2, pp. 111–128, 1979.

[76] R. W. Ross, W. Xie, M. M. Regan, M. Pomerantz, M. Nakabayashi, T. J. Daskivich, O. Sartor, M. Taplin, P. W. Kantoff, and W. K. Oh, "Efficacy of androgen deprivation therapy (ADT) in patients with advanced prostate cancer," *Cancer*, vol. 112, no. 6, pp. 1247–1253, 2008.

[77] R. S. Herbst and F. R. Khuri, "Mode of action of docetaxel–a basis for combination with novel anticancer agents," *Cancer Treat. Rev.*, vol. 29, no. 5, pp. 407–415, 2003.

[78] S. Osanto and S. A. C. Luelmo, "Chemotherapy and Androgen Receptor-Directed Treatment of Castration Resistant Metastatic Prostate Cancer," in *Management of Prostate Cancer*, Cham: Springer International Publishing, 2017, pp. 327–342.

[79] C. Parker, S. Nilsson, D. Heinrich, S. I. Helle, J. M. O'Sullivan, S. D. Foss?, A. Chodacki, P. Wiechno, J. Logue, M. Seke, A. Widmark, D. C. Johannessen, P. Hoskin, D. Bottomley, N. D. James, A. Solberg, I. Syndikus, J. Kliment, S. Wedel, S. Boehmer, M. Dall'Oglio, L. Franz?n, R. Coleman, N. J. Vogelzang, C. G. O'Bryan-Tear, K. Staudacher, J. Garcia-Vargas, M. Shan, ?.S. Bruland, and O. Sartor, "Alpha Emitter Radium-223 and Survival in Metastatic Prostate Cancer," *N. Engl. J. Med.*, vol. 369, no. 3, pp. 213–223, Jul. 2013.

[80] Ø. S. Bruland, S. Nilsson, D. R. Fisher, and R. H. Larsen, "High-Linear Energy Transfer Irradiation Targeted to Skeletal Metastases by the α-Emitter 223Ra: Adjuvant or Alternative to Conventional Modalities?," *Clin. Cancer Res.*, vol. 12, no. 20, 2006.

[81] M. S. Litwin, J. L. Gore, L. Kwan, J. M. Brandeis, S. P. Lee, H. R. Withers, and R. E. Reiter, "Quality of life after surgery, external beam irradiation, or brachytherapy for early-stage prostate cancer," *Cancer*, vol. 109, no. 11, pp. 2239–2247, Jun. 2007.

[82] F. Dayyani, G. E. Gallick, C. J. Logothetis, and P. G. Corn, "Novel therapies for metastatic castrate-resistant prostate cancer," *J. Natl. Cancer Inst.*, vol. 103, no. 22, pp. 1665–1675, 2011.

[83] R. McDonald, E. Chow, L. Rowbottom, G. Bedard, H. Lam, E. Wong, M. Popovic, N. Pulenzas, and M. Tsao, "Quality of life after palliative radiotherapy in bone metastases: A literature review," *J. Bone Oncol.*, vol. 4, no. 1, pp. 24–31, Mar. 2015.

[84] J. Pinski and T. B. Dorff, "Prostate cancer metastases to bone: Pathophysiology, pain management, and the promise of targeted therapy," *Eur. J. Cancer*, vol. 41, no. 6, pp. 932–940, 2005.

[85] M. Rogers, "New Insights Into the Molecular Mechanisms of Action of Bisphosphonates," *Curr. Pharm. Des.*, vol. 9, no. 32, pp. 2643–2658, Dec. 2003.

[86] M. J. Rogers, D. J. Watts, and R. G. G. Russell, "Overview of bisphosphonates," *Cancer*, vol. 80, no. S8, pp. 1652–1660, 1997.

[87] G. R. Mundy, "Bisphosphonates as anticancer drugs," *Expert Opin. Investig. Drugs*, vol. 8, no. 12, pp. 2009–2015, 1999.

[88] M. R. McClung, E. M. Lewiecki, S. B. Cohen, M. A. Bolognese, G. C.

Woodson, A. H. Moffett, M. Peacock, P. D. Miller, S. N. Lederman, and C. H. Chesnut, “Denosumab in postmenopausal women with low bone mineral density,” *N. Engl. J. Med.*, vol. 354, no. 8, pp. 821–831, 2006.

[89] U. E. Studer, P. Whelan, W. Albrecht, J. Casselman, T. de Reijke, D. Hauri, W. Loidl, S. Isorna, S. K. Sundaram, and M. Debois, “Immediate or deferred androgen deprivation for patients with prostate cancer not suitable for local treatment with curative intent: European Organisation for Research and Treatment of Cancer (EORTC) Trial 30891,” *J. Clin. Oncol.*, vol. 24, no. 12, pp. 1868–1876, 2006.

[90] U. E. Studer, L. Collette, P. Whelan, W. Albrecht, J. Casselman, T. De Reijke, H. Knönagel, W. Loidl, S. Isorna, and S. K. Sundaram, “Using PSA to guide timing of androgen deprivation in patients with T0–4 N0–2 M0 prostate cancer not suitable for local curative treatment (EORTC 30891),” *Eur. Urol.*, vol. 53, no. 5, pp. 941–949, 2008.

[91] J. M. Fitzpatrick and R. de Wit, “Taxane Mechanisms of Action: Potential Implications for Treatment Sequencing in Metastatic Castration-resistant Prostate Cancer,” *Eur. Urol.*, vol. 65, no. 6, pp. 1198–1204, Jun. 2014.

[92] E. D. Crawford, C. S. Higano, N. D. Shore, M. Hussain, and D. P. Petrylak, “Treating Patients with Metastatic Castration Resistant Prostate Cancer: A Comprehensive Review of Available Therapies,” *J. Urol.*, vol. 194, no. 6, pp. 1537–1547, Dec. 2015.

[93] A. Heidenreich, P. J. Bastian, J. Bellmunt, M. Bolla, S. Joniau, T. van der Kwast, M. Mason, V. Matveev, T. Wiegel, F. Zattoni, and N. Mottet, “EAU Guidelines on Prostate Cancer. Part II: Treatment of Advanced, Relapsing, and Castration-Resistant Prostate Cancer,” *Eur. Urol.*, vol. 65, no. 2, pp. 467–479, Feb. 2014.

[94] D. Lorente, J. Mateo, R. Perez-Lopez, J. S. de Bono, and G. Attard, “Sequencing of agents in castration-resistant prostate cancer,” *Lancet Oncol.*, vol. 16, no. 6, pp. e279–e292, Jun. 2015.

[95] L. Bubendorf, A. Schöpfer, U. Wagner, G. Sauter, H. Moch, N. Willi, T. C. Gasser, and M. J. Mihatsch, “Metastatic patterns of prostate cancer: an autopsy study of 1,589 patients,” *Hum. Pathol.*, vol. 31, no. 5, pp. 578–583, 2000.

[96] W. A. Sakr, D. J. Grignon, J. D. Crissman, L. K. Heilbrun, B. J. Cassin, J. J. Pontes, and G. P. Haas, “High grade prostatic intraepithelial neoplasia (HGPIN) and prostatic adenocarcinoma between the ages of 20-69: an autopsy study of 249 cases.,” *In Vivo*, vol. 8, no. 3, pp. 439–43, 1994.

[97] B. Hølund, “Latent Prostatic Cancer in a Consecutive Autopsy Series,” *Scand. J. Urol. Nephrol.*, vol. 14, no. 1, pp. 29–35, Jan. 1980.

[98] K. Weingartner, A. Ramaswamy, A. Bittinger, E. W. Gerharz, D. Voge, and H. Riedmiller, “Anatomical Basis for Pelvic Lymphadenectomy in Prostate Cancer: Results of an Autopsy Study and Implications for the Clinic,” *J. Urol.*, vol. 156, no. 6, pp. 1969–1971, Dec. 1996.

[99] S. Lundberg and T. Berge, “Prostatic Carcinoma: *An Autopsy Study*,” *Scand. J. Urol. Nephrol.*, vol. 4, no. 2, pp. 93–97, Jan. 1970.

[100] J. McNeal, R. Kindrachuk, F. Freiha, D. Bostwick, E. Redwine, and T. Stamey, “PATTERNS OF PROGRESSION IN PROSTATE CANCER,” *Lancet*, vol. 327, no. 8472, pp. 60–63, 1986.

[101] S. C. Jacobs, “Spread of prostatic cancer to bone,” *Urology*, vol. 21, no. 4, pp. 337–344, 1983.

[102] S. Ziaee, G. C.-Y. Chu, J.-M. Huang, S. Sieh, and L. W. K. Chung, “Prostate cancer metastasis: roles of recruitment and reprogramming, cell signal network and three-dimensional growth characteristics.,” *Transl. Androl. Urol.*, vol. 4, no. 4, pp. 438–54, Aug. 2015.

[103] E. I. Deryugina and J. P. Quigley, “Matrix metalloproteinases and tumor metastasis,” *Cancer Metastasis Rev.*, vol. 25, no. 1, pp. 9–34, Mar. 2006.

[104] L. J. McCawley and L. M. Matrisian, “Matrix metalloproteinases: multifunctional contributors to tumor progression,” *Mol. Med. Today*, vol. 6, no. 4, pp. 149–156, 2000.

[105] L. M. Coussens, B. Fingleton, and L. M. Matrisian, “Matrix metalloproteinase inhibitors and cancer—trials and tribulations,” *Science (80-.).*, vol. 295, no. 5564, pp. 2387–2392, 2002.

[106] J. S. Ross, P. Kaur, C. E. Sheehan, H. A. G. Fisher, R. A. Kaufman, and B. V. S. Kallakury, “Prognostic Significance of Matrix Metalloproteinase 2 and Tissue Inhibitor of Metalloproteinase 2 Expression in Prostate Cancer,” *Mod. Pathol.*, vol. 16, no. 3, pp. 198–205, Mar. 2003.

[107] R. A. Ghossein, H. I. Scher, W. L. Gerald, W. K. Kelly, T. Curley, A. Amsterdam, Z.-F. Zhang, and J. Rosai, “Detection of circulating tumor cells in patients with localized and metastatic prostatic carcinoma: clinical implications,” *J. Clin. Oncol.*, vol. 13, no. 5, pp. 1195–1200, 1995.

[108] M. Antfolk, S. H. Kim, S. Koizumi, T. Fujii, and T. Laurell, “Label-free single-cell separation and imaging of cancer cells using an integrated microfluidic system.,” *Sci. Rep.*, vol. 7, p. 46507, Apr. 2017.

[109] J. Massagué and A. Obenauf, “Metastatic colonization by circulating tumour cells,” *Nature*, vol. 529, pp. 298–306, 2016.

[110] B. Beck and C. Blanpain, “Unravelling cancer stem cell potential,” *Nat. Rev. Cancer*, vol. 13, pp. 727–738, 2013.

[111] A. Kreso and J. E. Dick, “Evolution of the Cancer Stem Cell Model,” *Cell Stem Cell*, vol. 14, no. 3, pp. 275–291, 2014.

[112] C. Liu, K. Kelnar, B. Liu, X. Chen, T. Calhoun-Davis, H. Li, L. Patrawala, H. Yan, C. Jeter, and S. Honorio, “The microRNA miR-34a inhibits prostate cancer stem cells and metastasis by directly repressing CD44,” *Nat. Med.*, vol. 17, no. 2, pp. 211–215, 2011.

[113] I. Tinhofer, M. Saki, F. Niehr, U. Keilholz, and V. Budach, “Cancer stem cell characteristics of circulating tumor cells,” *Int. J. Radiat. Biol.*, vol. 90, no. 8, pp. 622–627, Aug. 2014.

[114] R. E. Coleman, “Skeletal complications of malignancy,” *Cancer*, vol. 80, no. S8, pp. 1588–1594, 1997.

[115] Y. Shiozawa, E. A. Pedersen, A. M. Havens, Y. Jung, A. Mishra, J. Joseph, J.

K. Kim, L. R. Patel, C. Ying, A. M. Ziegler, M. J. Pienta, J. Song, J. Wang, R. D. Loberg, P. H. Krebsbach, K. J. Pienta, and R. S. Taichman, “Human prostate cancer metastases target the hematopoietic stem cell niche to establish footholds in mouse bone marrow.,” *J. Clin. Invest.*, vol. 121, no. 4, pp. 1298–312, Apr. 2011.

[116] Y. Shiozawa, A. M. Havens, K. J. Pienta, and R. S. Taichman, “The bone marrow niche: habitat to hematopoietic and mesenchymal stem cells, and unwitting host to molecular parasites,” *Leukemia*, vol. 22, no. 5, pp. 941–950, 2008.

[117] D. T. Scadden, “Nice neighborhood: Emerging concepts of the stem cell niche,” *Cell*, vol. 157, no. 1, pp. 41–50, 2014.

[118] F. Arai and T. Suda, “Maintenance of quiescent hematopoietic stem cells in the osteoblastic niche,” *Ann. N. Y. Acad. Sci.*, vol. 1106, no. 1, pp. 41–53, 2007.

[119] D. Dingli, A. Traulsen, and J. M. Pacheco, “Compartmental architecture and dynamics of hematopoiesis,” *PLoS One*, vol. 2, no. 4, p. e345, 2007.

[120] M. Tavian and B. Péault, “Embryonic development of the human hematopoietic system,” *Int J Dev Biol*, vol. 49, no. 2–3, pp. 243–250, 2005.

[121] T. Sugiyama, H. Kohara, M. Noda, and T. Nagasawa, “Maintenance of the Hematopoietic Stem Cell Pool by CXCL12-CXCR4 Chemokine Signaling in Bone Marrow Stromal Cell Niches,” *Immunity*, vol. 25, no. 6, pp. 977–988, 2006.

[122] P. Bianco, B. Sacchetti, and M. Riminucci, “Osteoprogenitors and the hematopoietic microenvironment,” *Best Pract. Res. Clin. Haematol.*, vol. 24, no. 1, pp. 37–47, 2011.

[123] Y. Shiozawa and R. S. Taichman, “Getting blood from bone: An emerging understanding of the role that osteoblasts play in regulating hematopoietic stem cells within their niche,” *Exp. Hematol.*, vol. 40, no. 9, pp. 685–694, 2012.

[124] M. J. Kiel and S. J. Morrison, “Uncertainty in the niches that maintain haematopoietic stem cells,” *Nat. Rev. Immunol.*, vol. 8, no. 4, pp. 290–301, 2008.

[125] I. Petit, M. Szyper-Kravitz, A. Nagler, M. Lahav, A. Peled, L. Habler, T. Ponomaryov, R. S. Taichman, F. Arenzana-Seisdedos, N. Fujii, J. Sandbank, D. Zipori, and T. Lapidot, “G-CSF induces stem cell mobilization by decreasing bone marrow SDF-1 and up-regulating CXCR4,” *Nat. Immunol.*, vol. 3, no. 7, pp. 687–694, 2002.

[126] C. L. Semerad, M. J. Christopher, F. Liu, B. Short, P. J. Simmons, I. Winkler, J.-P. Levesque, J. Chappel, F. P. Ross, and D. C. Link, “G-CSF potently inhibits osteoblast activity and CXCL12 mRNA expression in the bone marrow,” *Blood*, vol. 106, no. 9, pp. 3020–3027, 2005.

[127] K. Baumann, “Stem cells: A metabolic switch,” *Nat. Rev. Mol. Cell Biol.*, vol. 14, no. 2, pp. 64–65, 2013.

[128] D. A. Sipkins, X. Wei, J. W. Wu, J. M. Runnels, D. Côté, T. K. Means, A. D. Luster, D. T. Scadden, and C. P. Lin, “In vivo imaging of specialized bone

marrow endothelial microdomains for tumour engraftment," *Nature*, vol. 435, no. 7044, pp. 969–973, 2005.

[129] A. Dar, P. Goichberg, V. Shinder, A. Kalinkovich, O. Kollet, N. Netzer, R. Margalit, M. Zsak, A. Nagler, and I. Hardan, "Chemokine receptor CXCR4–dependent internalization and resecretion of functional chemokine SDF-1 by bone marrow endothelial and stromal cells," *Nat. Immunol.*, vol. 6, no. 10, pp. 1038–1046, 2005.

[130] T. Ponomaryov, A. Peled, I. Petit, R. S. Taichman, L. Habler, J. Sandbank, F. Arenzana-Seisdedos, A. Magerus, A. Caruz, and N. Fujii, "Induction of the chemokine stromal-derived factor-1 following DNA damage improves human stem cell function," *J. Clin. Invest.*, vol. 106, no. 11, pp. 1331–1339, 2000.

[131] R. S. Taichman, C. Cooper, E. T. Keller, K. J. Pienta, N. S. Taichman, and L. K. McCauley, "Use of the stromal cell-derived factor-1/CXCR4 pathway in prostate cancer metastasis to bone," *Cancer Res.*, vol. 62, no. 6, pp. 1832–1837, 2002.

[132] F. Arai, A. Hirao, M. Ohmura, H. Sato, S. Matsuoka, K. Takubo, K. Ito, G. Y. Koh, and T. Suda, "Tie2/angiopoietin-1 signaling regulates hematopoietic stem cell quiescence in the bone marrow niche," *Cell*, vol. 118, no. 2, pp. 149–161, 2004.

[133] G. V Priestley, L. M. Scott, T. Ulyanova, and T. Papayannopoulou, "Lack of α4 integrin expression in stem cells restricts competitive function and self-renewal activity," *Blood*, vol. 107, no. 7, pp. 2959–2967, 2006.

[134] Y. Jung, Y. Shiozawa, J. Wang, L. R. Patel, A. M. Havens, J. Song, P. H. Krebsbach, G. D. Roodman, and R. S. Taichman, "Annexin-2 is a regulator of stromal cell-derived factor–1/CXCL12 function in the hematopoietic stem cell endosteal niche," *Exp. Hematol.*, vol. 39, no. 2, p. 151–166. e1, 2011.

[135] H. M. Kronenberg, "Gs signaling in osteoblasts and hematopoietic stem cells," *Ann. N. Y. Acad. Sci.*, vol. 1192, no. 1, pp. 327–329, 2010.

[136] G. B. Adams, K. T. Chabner, I. R. Alley, D. P. Olson, Z. M. Szczepiorkowski, M. C. Poznansky, C. H. Kos, M. R. Pollak, E. M. Brown, and D. T. Scadden, "Stem cell engraftment at the endosteal niche is specified by the calcium-sensing receptor," *Nature*, vol. 439, no. 7076, pp. 599–603, 2005.

[137] N. Urao and M. Ushio-Fukai, "Redox regulation of stem/progenitor cells and bone marrow niche," *Free Radic. Biol. Med.*, vol. 54, no. 0, pp. 26–39, 2013.

[138] K. Parmar, P. Mauch, J.-A. Vergilio, R. Sackstein, and J. D. Down, "Distribution of hematopoietic stem cells in the bone marrow according to regional hypoxia," *Proc. Natl. Acad. Sci.*, vol. 104, no. 13, pp. 5431–5436, 2007.

[139] P. Eliasson and J.-I. J?nsson, "The hematopoietic stem cell niche: Low in oxygen but a nice place to be," *J. Cell. Physiol.*, vol. 222, no. 1, pp. 17–22, Jan. 2010.

[140] M. C. Simon, "Coming up for air: HIF-1 and mitochondrial oxygen consumption," *Cell Metab.*, vol. 3, no. 3, pp. 150–151, Mar. 2006.

[141] K. Takubo, G. Nagamatsu, C. I. Kobayashi, A. Nakamura-Ishizu, H. Kobayashi, E. Ikeda, N. Goda, Y. Rahimi, R. S. Johnson, and T. Soga,

"Regulation of glycolysis by Pdk functions as a metabolic checkpoint for cell cycle quiescence in hematopoietic stem cells," *Cell Stem Cell*, vol. 12, no. 1, pp. 49–61, 2013.

[142] E. Pedemonte, F. Benvenuto, S. Casazza, G. Mancardi, J. Oksenberg, A. Uccelli, and S. Baranzini, "The molecular signature of therapeutic mesenchymal stem cells exposes the architecture of the hematopoietic stem cell niche synapse," *BMC Genomics*, vol. 8, no. 1, p. 65, 2007.

[143] L. M. Calvi, G. B. Adams, K. W. Weibrecht, J. M. Weber, D. P. Olson, M. C. Knight, R. P. Martin, E. Schipani, P. Divieti, and F. R. Bringhurst, "Osteoblastic cells regulate the haematopoietic stem cell niche," *Nature*, vol. 425, no. 6960, pp. 841–846, 2003.

[144] H. Yoshihara, F. Arai, K. Hosokawa, T. Hagiwara, K. Takubo, Y. Nakamura, Y. Gomei, H. Iwasaki, S. Matsuoka, and K. Miyamoto, "Thrombopoietin/MPL signaling regulates hematopoietic stem cell quiescence and interaction with the osteoblastic niche," *Cell Stem Cell*, vol. 1, no. 6, pp. 685–697, 2007.

[145] W. Tong and H. F. Lodish, "Lnk inhibits Tpo–mpl signaling and Tpo-mediated megakaryocytopoiesis," *J. Exp. Med.*, vol. 200, no. 5, pp. 569–580, 2004.

[146] A. Bersenev, C. Wu, J. Balcerek, and W. Tong, "Lnk controls mouse hematopoietic stem cell self-renewal and quiescence through direct interactions with JAK2," *J. Clin. Invest.*, vol. 118, no. 8, p. 2832, 2008.

[147] S. Stier, Y. Ko, R. Forkert, C. Lutz, T. Neuhaus, E. Grünewald, T. Cheng, D. Dombkowski, L. M. Calvi, and S. R. Rittling, "Osteopontin is a hematopoietic stem cell niche component that negatively regulates stem cell pool size," *J. Exp. Med.*, vol. 201, no. 11, pp. 1781–1791, 2005.

[148] Y. Jung, J. Wang, A. Havens, Y. Sun, J. Wang, T. Jin, and R. S. Taichman, "Cell-to-cell contact is critical for the survival of hematopoietic progenitor cells on osteoblasts," *Cytokine*, vol. 32, no. 3, pp. 155–162, 2005.

[149] J. P. Chute, G. G. Muramoto, H. K. Dressman, G. Wolfe, N. J. Chao, and S. Lin, "Molecular Profile and Partial Functional Analysis of Novel Endothelial Cell-Derived Growth Factors that Regulate Hematopoiesis," *Stem Cells*, vol. 24, no. 5, pp. 1315–1327, 2006.

[150] X. Wu, G. Yu, H. Parks, T. Hebert, B. C. Goh, M. A. Dietrich, G. Pelled, R. Izadpanah, D. Gazit, and B. A. Bunnell, "Circadian mechanisms in murine and human bone marrow mesenchymal stem cells following dexamethasone exposure," *Bone*, vol. 42, no. 5, pp. 861–870, 2008.

[151] J. Fujisaki, J. Wu, A. L. Carlson, L. Silberstein, P. Putheti, R. Larocca, W. Gao, T. I. Saito, C. Lo Celso, H. Tsuyuzaki, T. Sato, D. Côté, M. Sykes, T. B. Strom, D. T. Scadden, and C. P. Lin, "In vivo imaging of Treg cells providing immune privilege to the haematopoietic stem-cell niche," *Nature*, vol. 474, no. 7350, pp. 216–219, 2011.

[152] C. Yu, Y. Shiozawa, R. S. Taichman, L. K. McCauley, K. J. Pienta, and E. Keller, "Prostate Cancer and Parasitism of the Bone Hematopoietic Stem Cell Niche," *Crit. Rev. Eukaryot. Gene Expr.*, vol. 22, no. 2, pp. 131–148, 2012.

[153] H.-G. Kopp, S. T. Avecilla, A. T. Hooper, and S. Rafii, “The Bone Marrow Vascular Niche: Home of HSC Differentiation and Mobilization,” *Physiology*, vol. 20, no. 5, 2005.

[154] M. J. Domingues, H. Cao, S. Y. Heazlewood, B. Cao, and S. K. Nilsson, “Niche Extracellular Matrix Components and their Influence on HSC,” *J. Cell. Biochem.*, no. January, 2017.

[155] C. R. Cooper, C. H. Chay, J. D. Gendernalik, H. Lee, J. Bhatia, R. S. Taichman, L. K. McCauley, E. T. Keller, and K. J. Pienta, “Stromal factors involved in prostate carcinoma metastasis to bone,” *Cancer*, vol. 97, no. S3, pp. 739–747, 2003.

[156] Y. Sun, A. Schneider, Y. Jung, J. Wang, J. Dai, J. Wang, K. Cook, N. I. Osman, A. J. Koh-Paige, and H. Shim, “Skeletal Localization and Neutralization of the SDF-1 (CXCL12)/CXCR4 Axis Blocks Prostate Cancer Metastasis and Growth in Osseous Sites In Vivo,” *J. Bone Miner. Res.*, vol. 20, no. 2, pp. 318–329, 2005.

[157] K. N. Weilbaecher, T. A. Guise, and L. K. McCauley, “Cancer to bone: a fatal attraction,” *Nat. Rev. Cancer*, vol. 11, no. 6, pp. 411–425, 2011.

[158] R. Silva, G. D’Amico, K. M. Hodivala-Dilke, and L. E. Reynolds, “Integrins The Keys to Unlocking Angiogenesis,” *Arterioscler. Thromb. Vasc. Biol.*, vol. 28, no. 10, pp. 1703–1713, 2008.

[159] K. J. Luzzi, I. C. MacDonald, E. E. Schmidt, N. Kerkvliet, V. L. Morris, A. F. Chambers, and A. C. Groom, “Multistep nature of metastatic inefficiency: dormancy of solitary cells after successful extravasation and limited survival of early micrometastases,” *Am. J. Pathol.*, vol. 153, no. 3, pp. 865–873, 1998.

[160] K. Miller, A. Stenzl, and B. Tombal, “Advances in the Therapy of Prostate Cancer–Induced Bone Disease: Current Insights and Future Perspectives on the RANK/RANKL Pathways,” *Eur. Urol. Suppl.*, vol. 8, no. 9, pp. 747–752, Sep. 2009.

[161] M. P. Roudier, H. Vesselle, L. D. True, C. S. Higano, S. M. Ott, S. H. King, and R. L. Vessella, “Bone histology at autopsy and matched bone scintigraphy findings in patients with hormone refractory prostate cancer: The effect of bisphosphonate therapy on bone scintigraphy results,” *Clin. Exp. Metastasis*, vol. 20, no. 2, pp. 171–180, 2003.

[162] F. Saad, R. Markus, and C. Goessl, “Targeting the receptor activator of nuclear factor-?B (RANK) ligand in prostate cancer bone metastases,” *BJU Int.*, vol. 101, no. 9, pp. 1071–1075, May 2008.

[163] J. Dai, Y. Kitagawa, J. Zhang, Z. Yao, A. Mizokami, S. Cheng, J. Nör, L. K. McCauley, R. S. Taichman, and E. T. Keller, “Vascular endothelial growth factor contributes to the prostate cancer-induced osteoblast differentiation mediated by bone morphogenetic protein,” *Cancer Res.*, vol. 64, no. 3, pp. 994–999, 2004.

[164] T. A. Guise, J. J. Yin, and K. S. Mohammad, “Role of endothelin-1 in osteoblastic bone metastases,” *Cancer*, vol. 97, no. S3, pp. 779–784, 2003.

[165] N. Kurihara, D. Bertolini, T. Suda, Y. Akiyama, and G. D. Roodman, “IL-6 stimulates osteoclast-like multinucleated cell formation in long term human

marrow cultures by inducing IL-1 release," *J. Immunol.*, vol. 144, no. 11, pp. 4226–4230, 1990.

[166] S. F. Shariat, B. Andrews, M. W. Kattan, J. Kim, T. M. Wheeler, and K. M. Slawin, "Plasma levels of interleukin-6 and its soluble receptor are associated with prostate cancer progression and metastasis," *Urology*, vol. 58, no. 6, pp. 1008–1015, 2001.

[167] P. I. Croucher, M. M. McDonald, and T. J. Martin, "Bone metastasis: the importance of the neighbourhood.," *Nat. Rev. Cancer*, vol. 16, no. 6, pp. 373–86, 2016.

[168] M. R. Junttila and F. J. de Sauvage, "Influence of tumour micro-environment heterogeneity on therapeutic response," *Nature*, vol. 501, no. 7467, pp. 346–354, 2013.

[169] D. Hanahan, G. Bergers, R. Brekken, G. McMahon, T. H. Vu, T. Itoh, K. Tamaki, K. Tanzawa, P. Thorpe, S. Itohara, and Z. Werb, "Matrix metalloproteinase-9 triggers the angiogenic switch during carcinogenesis," *Nat. Cell Biol.*, vol. 2, no. 10, pp. 737–744, Oct. 2000.

[170] E. Švastová, A. Hulíková, M. Rafajová, M. Zat'ovičová, A. Gibadulinová, A. Casini, A. Cecchi, A. Scozzafava, C. T. Supuran, J. Pastorek, and S. Pastoreková, "Hypoxia activates the capacity of tumor-associated carbonic anhydrase IX to acidify extracellular pH," *FEBS Lett.*, vol. 577, no. 3, pp. 439–445, Nov. 2004.

[171] A. B. Ariffin, P. F. Forde, S. Jahangeer, D. M. Soden, and J. Hinchion, "Releasing Pressure in Tumors: What Do We Know So Far and Where Do We Go from Here? A Review," *Cancer Res.*, vol. 74, no. 10, 2014.

[172] S. S. W. Hayward and G. G. R. Cunha, "The prostate development and physiology," *Radiol. Clin. North Am.*, vol. 38, no. 1, pp. 1–14, 2000.

[173] P. C. Marker, A. A. Donjacour, R. Dahiya, and G. R. Cunha, "Hormonal, cellular, and molecular control of prostatic development," *Dev. Biol.*, vol. 253, no. 2, pp. 165–174, 2003.

[174] P. Gandellini, F. Andriani, G. Merlino, F. D'Aiuto, L. Roz, and M. Callari, "Complexity in the tumour microenvironment: Cancer associated fibroblast gene expression patterns identify both common and unique features of tumour-stroma crosstalk across cancer types," *Semin. Cancer Biol.*, vol. 35, pp. 96–106, 2015.

[175] R. Kalluri and M. Zeisberg, "Fibroblasts in cancer," *Nat. Rev. Cancer*, vol. 6, no. 5, pp. 392–401, May 2006.

[176] R. A. Taylor, R. Toivanen, M. Frydenberg, J. Pedersen, L. Harewood, A. T. Australian Prostate Cancer Bioresou, A. T. Collins, N. J. Maitland, and G. P. Risbridger, "Human Epithelial Basal Cells Are Cells of Origin of Prostate Cancer, Independent of CD133 Status," *Stem Cells*, vol. 30, no. 6, pp. 1087–1096, Jun. 2012.

[177] A. K. Clark, A. V. Taubenberger, R. A. Taylor, B. Niranjan, Z. Y. Chea, E. Zotenko, S. Sieh, J. S. Pedersen, S. Norden, M. Frydenberg, J. P. Grummet, D. W. Pook, C. Stirzaker, S. J. Clark, M. G. Lawrence, S. J. Ellem, D. W. Hutmacher, and G. P. Risbridger, "A bioengineered microenvironment to

quantitatively measure the tumorigenic properties of cancer-associated fibroblasts in human prostate cancer," *Biomaterials*, vol. 34, no. 20, pp. 4777–4785, 2013.

[178] A. F. Olumi, G. D. Grossfeld, S. W. Hayward, P. R. Carroll, T. D. Tlsty, and G. R. Cunha, "Carcinoma-associated fibroblasts direct tumor progression of initiated human prostatic epithelium.," *Cancer Res.*, vol. 59, no. 19, pp. 5002–11, Oct. 1999.

[179] N. A. Bhowmick, E. G. Neilson, and H. L. Moses, "Stromal fibroblasts in cancer initiation and progression," *Nature*, vol. 432, no. 7015, pp. 332–337, Nov. 2004.

[180] N. McCabe, S. De, A. Vasanji, J. Brainard, and T. Byzova, "Prostate cancer specific integrin αvβ3 modulates bone metastatic growth and tissue remodeling," *Oncogene*, vol. 26, no. 42, p. 6238, 2007.

[181] J. Zhang, J. Dai, Y. Qi, D. L. Lin, P. Smith, C. Strayhorn, A. Mizokami, Z. Fu, J. Westman, and E. T. Keller, "Osteoprotegerin inhibits prostate cancer-induced osteoclastogenesis and prevents prostate tumor growth in the bone.," *J. Clin. Invest.*, vol. 107, no. 10, pp. 1235–44, May 2001.

[182] G. R. Mundy, "Metastasis to bone: causes, consequences and therapeutic opportunities.," *Nat. Rev. Cancer*, vol. 2, no. 8, pp. 584–93, 2002.

[183] H. Wang, C. Yu, X. Gao, T. Welte, A. M. Muscarella, L. Tian, H. Zhao, Z. Zhao, S. Du, J. Tao, B. Lee, T. F. Westbrook, S. T. C. Wong, X. Jin, J. M. Rosen, C. K. Osborne, and X. H.-F. Zhang, "The Osteogenic Niche Promotes Early-Stage Bone Colonization of Disseminated Breast Cancer Cells," *Cancer Cell*, vol. 27, no. 2, pp. 193–210, Feb. 2015.

[184] P. I. Croucher, M. M. McDonald, and T. J. Martin, "Bone metastasis: the importance of the neighbourhood.," *Nat. Rev. Cancer*, vol. 16, no. 6, pp. 373–86, 2016.

[185] Y. Shiozawa, A. M. Havens, Y. Jung, A. M. Ziegler, E. A. Pedersen, J. Wang, J. Wang, G. Lu, G. D. Roodman, R. D. Loberg, K. J. Pienta, and R. S. Taichman, "Annexin II/Annexin II receptor axis regulates adhesion, migration, homing, and growth of prostate cancer," *J. Cell. Biochem.*, vol. 105, no. 2, pp. 370–380, Oct. 2008.

[186] E. T. Keller and J. Brown, "Prostate cancer bone metastases promote both osteolytic and osteoblastic activity," *J. Cell. Biochem.*, vol. 91, no. 4, pp. 718–729, Mar. 2004.

[187] S. L. Shiao, G. C.-Y. Chu, and L. W. K. Chung, "Regulation of prostate cancer progression by the tumor microenvironment.," *Cancer Lett.*, Jan. 2016.

[188] Z.-Y. Zhang, S.-H. Teoh, J. H. P. Hui, N. M. Fisk, M. Choolani, and J. K. Y. Chan, "The potential of human fetal mesenchymal stem cells for off-the-shelf bone tissue engineering application," *Biomaterials*, vol. 33, no. 9, pp. 2656–2672, 2012.

[189] P. Bianco, P. G. Robey, and P. J. Simmons, "Mesenchymal stem cells: revisiting history, concepts, and assays.," *Cell Stem Cell*, vol. 2, no. 4, pp. 313–9, Apr. 2008.

[190] L. Prantl, F. Muehlberg, N. M. Navone, Y. Song, J. Vykoukal, C. J.

Logothetis, and E. U. Alt, “Adipose tissue-derived stem cells promote prostate tumor growth,” *Prostate*, vol. 70, no. 15, pp. 1709–1715, 2010.

[191] N. A. Bhowmick, E. G. Neilson, and H. L. Moses, “Bhowmick 2004_Stromal fibroblasts in cancer initiation,” vol. 432, no. November, 2004.

[192] R. Tucker, G. Shipley, H. Moses, and R. Holley, “Growth inhibitor from BSC-1 cells closely related to platelet type beta transforming growth factor,” *Science (80-.).*, 1984.

[193] C. Amendt, P. Schirmacher, H. Weber, and M. Blessing, “Expression of a dominant negative type II TGF-β receptor in mouse skin results in an increase in carcinoma incidence and an acceleration of carcinoma development.,” *Oncogene*, 1998.

[194] A. E. Gorska, R. A. Jensen, Y. Shyr, M. E. Aakre, N. A. Bhowmick, and H. L. Moses, “Transgenic Mice Expressing a Dominant-Negative Mutant Type II Transforming Growth Factor-β Receptor Exhibit Impaired Mammary Development and Enhanced Mammary Tumor Formation,” *Am. J. Pathol.*, vol. 163, no. 4, pp. 1539–1549, 2003.

[195] A. Mantovani, “Cancer: Inflaming metastasis.,” *Nature*, vol. 457, no. 7225, pp. 36–37, 2009.

[196] P. Allavena, A. Sica, G. Solinas, C. Porta, and A. Mantovani, “The inflammatory micro-environment in tumor progression: The role of tumor-associated macrophages,” *Crit. Rev. Oncol. Hematol.*, vol. 66, no. 1, pp. 1–9, 2008.

[197] G. Comito, E. Giannoni, C. P. Segura, P. Barcellos-de-Souza, M. R. Raspollini, G. Baroni, M. Lanciotti, S. Serni, and P. Chiarugi, “Cancer-associated fibroblasts and M2-polarized macrophages synergize during prostate carcinoma progression,” *Oncogene*, vol. 33, no. 19, pp. 2423–2431, May 2014.

[198] F. O. Martinez, L. Helming, and S. Gordon, “Alternative Activation of Macrophages: An Immunologic Functional Perspective,” *Annu. Rev. Immunol.*, vol. 27, no. 1, pp. 451–483, Apr. 2009.

[199] D. J. Prockop, “Concise Review: Two negative feedback loops place mesenchymal stem/stromal cells at the center of early regulators of inflammation,” *Stem Cells*, vol. 31, no. 10, pp. 2042–2046, Oct. 2013.

[200] J. B. Wyckoff, Y. Wang, E. Y. Lin, J. Li, S. Goswami, E. R. Stanley, J. E. Segall, J. W. Pollard, and J. Condeelis, “Direct visualization of macrophage-assisted tumor cell intravasation in mammary tumors.,” *Cancer Res.*, vol. 67, no. 6, pp. 2649–56, Mar. 2007.

[201] A. Mantovani and A. Sica, “Macrophages, innate immunity and cancer: balance, tolerance, and diversity,” *Curr. Opin. Immunol.*, vol. 22, no. 2, pp. 231–237, 2010.

[202] K. Gollapudi, C. Galet, T. Grogan, H. Zhang, J. W. Said, J. Huang, D. Elashoff, S. J. Freedland, M. Rettig, and W. J. Aronson, “Association between tumor-associated macrophage infiltration, high grade prostate cancer, and biochemical recurrence after radical prostatectomy.,” *Am. J. Cancer Res.*, vol. 3, no. 5, pp. 523–9, 2013.

[203] P. Chiarugi, “Cancer-associated fibroblasts and macrophages,” *Oncoimmunology*, vol. 2, no. 9, p. e25563, Sep. 2013.

[204] G. Taverna, E. Pedretti, G. Di Caro, E. M. Borroni, F. Marchesi, and F. Grizzi, “Inflammation and prostate cancer: friends or foe?,” *Inflamm. Res.*, vol. 64, no. 5, pp. 275–286, May 2015.

[205] C. M. Armstrong and A. C. Gao, “Drug resistance in castration resistant prostate cancer: resistance mechanisms and emerging treatment strategies.,” *Am. J. Clin. Exp. Urol.*, vol. 3, no. 2, pp. 64–76, Jan. 2015.

[206] M. Parisotto and D. Metzger, “Genetically engineered mouse models of prostate cancer,” *Mol. Oncol.*, vol. 7, no. 2, pp. 190–205, 2013.

[207] S. Kasper, “Survey of genetically engineered mouse models for prostate cancer: Analyzing the molecular basis of prostate cancer development, progression, and metastasis,” *J. Cell. Biochem.*, vol. 94, no. 2, pp. 279–297, Feb. 2005.

[208] C. Abate-Shen and M. M. Shen, “Molecular genetics of prostate cancer.,” *Genes Dev.*, vol. 14, no. 19, pp. 2410–34, Oct. 2000.

[209] C. Marks, “Mouse Models of Human Cancers Consortium (MMHCC) from the NCI.,” *Dis. Model. Mech.*, vol. 2, no. 3–4, p. 111, 2009.

[210] M. S. Song, L. Salmena, and P. P. Pandolfi, “The functions and regulation of the PTEN tumour suppressor,” *Nat. Rev. Mol. Cell Biol.*, vol. 13, no. 5, pp. 283–296, May 2012.

[211] T. Iwata, D. Schultz, J. Hicks, G. K. Hubbard, L. N. Mutton, T. L. Lotan, C. Bethel, M. T. Lotz, S. Yegnasubramanian, W. G. Nelson, C. V. Dang, M. Xu, U. Anele, C. M. Koh, C. J. Bieberich, and A. M. De Marzo, “MYC Overexpression Induces Prostatic Intraepithelial Neoplasia and Loss of Nkx3.1 in Mouse Luminal Epithelial Cells,” *PLoS One*, vol. 5, no. 2, p. e9427, Feb. 2010.

[212] K. C. Valkenburg and B. O. Williams, “Mouse models of prostate cancer.,” *Prostate Cancer*, vol. 2011, p. 895238, Feb. 2011.

[213] H. Beltran, J. M. Mosquera, and M. A. Rubin, “Neuroendocrine Prostate Cancer,” in *Prostate Cancer: A Comprehensive Perspective*, London: Springer London, 2013, pp. 277–282.

[214] M. M. Grabowska, D. J. DeGraff, X. Yu, R. J. Jin, Z. Chen, A. D. Borowsky, and R. J. Matusik, “Mouse models of prostate cancer: picking the best model for the question.,” *Cancer Metastasis Rev.*, vol. 33, no. 2–3, pp. 377–97, Sep. 2014.

[215] J. R. Gingrich, R. J. Barrios, M. W. Kattan, H. S. Nahm, M. J. Finegold, and N. M. Greenberg, “Androgen-independent Prostate Cancer Progression in the TRAMP Model,” *Cancer Res.*, vol. 57, no. 21, 1997.

[216] J. Tuomela and P. H?rk?nen, “Tumor models for prostate cancer exemplified by fibroblast growth factor 8-induced tumorigenesis and tumor progression,” *Reprod. Biol.*, vol. 14, no. 1, pp. 16–24, Mar. 2014.

[217] S. Yasmin-Karim, M. R. King, E. M. Messing, and Y.-F. Lee, “E-selectin ligand-1 controls circulating prostate cancer cell rolling/adhesion and

metastasis.," *Oncotarget*, vol. 5, no. 23, pp. 12097–110, Dec. 2014.

[218] E. L. S. Fong, X. Wan, J. Yang, M. Morgado, A. G. Mikos, D. A. Harrington, N. M. Navone, and M. C. Farach-Carson, "A 3D in vitro model of patient-derived prostate cancer xenograft for controlled interrogation of in vivo tumor-stromal interactions," *Biomaterials*, Nov. 2015.

[219] W. M. van Weerden and J. C. Romijn, "Use of nude mouse xenograft models in prostate cancer research," *Prostate*, vol. 43, no. 4, pp. 263–271, Jun. 2000.

[220] N. J. M. & G. P. R. Mitchell G Lawrence, Renea A Taylor, Roxanne Toivanen, John Pedersen, Sam Norden, David W Pook, Mark Frydenberg, Australian Prostate Cancer BioResource, Melissa M Papargiris, Birunthi Niranjan, Michelle G Richards, Hong Wang, Anne T Collins, "A preclinical xenograft model of prostate cancer using human tumors," *Nat. Protoc.*, 2013.

[221] J. A. Tuxhorn, S. J. McAlhany, T. D. Dang, G. E. Ayala, and D. R. Rowley, "Stromal Cells Promote Angiogenesis and Growth of Human Prostate Tumors in a Differential Reactive Stroma (DRS) Xenograft Model," *Cancer Res.*, vol. 62, no. 11, 2002.

[222] W. N. Brennen, S. R. Denmeade, and J. T. Isaacs, "Mesenchymal stem cells as a vector for the inflammatory prostate microenvironment," *Endocr. Relat. Cancer*, vol. 20, no. 5, pp. 269–290, 2013.

[223] T. J. Rosol, S. H. Tannehill-Gregg, B. E. LeRoy, S. Mandl, and C. H. Contag, "Animal models of bone metastasis," *Cancer*, vol. 97, no. S3, pp. 748–757, 2003.

[224] G. N. Thalmann, P. E. Anezinis, S. M. Chang, H. E. Zhau, E. E. Kim, V. L. Hopwood, S. Pathak, A. C. von Eschenbach, and L. W. Chung, "Androgen-independent cancer progression and bone metastasis in the LNCaP model of human prostate cancer," *Cancer Res*, vol. 54, no. 10, pp. 2577–2581, 1994.

[225] T. T. Wu, R. A. Sikes, and Q. Cui, "Establishing human prostate cancer cell xenografts in bone : induction of osteoblastic reaction by PSA producing tumors in athymic and SCID mice using LNCaP and lineage related," *Int. J. Cancer*, vol. 894, no. November, pp. 887–894, 1998.

[226] P. Lin, D. Correa, T. J. Kean, A. Awadallah, J. E. Dennis, and A. I. Caplan, "Serial Transplantation and Long-term Engraftment of Intra-arterially Delivered Clonally Derived Mesenchymal Stem Cells to Injured Bone Marrow," *Mol. Ther.*, vol. 22, no. 1, pp. 160–168, Jan. 2014.

[227] C. Kyriakou, N. Rabin, A. Pizzey, A. Nathwani, and K. Yong, "Factors that influence short-term homing of human bone marrow-derived mesenchymal stem cells in a xenogeneic animal model.," *Haematologica*, vol. 93, no. 10, pp. 1457–65, Oct. 2008.

[228] O. Raheem, A. A. Kulidjian, C. Wu, Y. B. Jeong, T. Yamaguchi, K. M. Smith, D. Goff, H. Leu, S. R. Morris, N. A. Cacalano, K. Masuda, C. H. M. Jamieson, C. J. Kane, and C. A. M. Jamieson, "A novel patient-derived intra-femoral xenograft model of bone metastatic prostate cancer that recapitulates mixed osteolytic and osteoblastic lesions.," *J. Transl. Med.*, vol. 9, p. 185, Oct. 2011.

[229] E. Corey, J. E. Quinn, F. Bladou, L. G. Brown, M. P. Roudier, J. M. Brown,

K. R. Buhler, and R. L. Vessella, “Establishment and characterization of osseous prostate cancer models: Intra-tibial injection of human prostate cancer cells,” *Prostate*, vol. 52, no. 1, pp. 20–33, Jun. 2002.

[230] N. Wang, F. E. Docherty, H. K. Brown, K. J. Reeves, A. Fowles, P. D. Ottewell, T. N. Dear, I. Holen, P. I. Croucher, and C. L. Eaton, “Prostate Cancer Cells Preferentially Home to Osteoblast-Rich Areas in the Early Stages of Bone Metastasis–Evidence from In Vivo Models,” *J. Bone Miner. Res.*, 2014.

[231] E. M. Hurt, B. T. Kawasaki, G. J. Klarmann, S. B. Thomas, and W. L. Farrar, “CD44+, CD24− prostate cells are early cancer progenitor/stem cells that provide a model for patients with poor prognosis,” *Br. J. Cancer*, vol. 98, no. 4, pp. 756–765, 2008.

[232] H. Yonou, T. Yokose, T. Kamijo, N. Kanomata, T. Hasebe, K. Nagai, T. Hatano, Y. Ogawa, and A. Ochiai, “Establishment of a Novel Species- and Tissue-specific Metastasis Model of Human Prostate Cancer in Humanized Non-Obese Diabetic/Severe Combined Immunodeficient Mice Engrafted with Human Adult Lung and Bone,” *Cancer Res.*, vol. 61, no. 5, 2001.

[233] C. Wiesner, S. M. Nabha, R. D. Bonfil, E. B. Dos Santos, H. Yamamoto, H. Meng, S. W. Melchior, F. Bittinger, J. W. Th?roff, R. L. Vessella, and M. L. Cher, “C-Kit and Its Ligand Stem Cell Factor: Potential Contribution to Prostate Cancer Bone Metastasis,” *Neoplasia*, vol. 10, no. 9, pp. 996–1003, Sep. 2008.

[234] L. E. Mainetti, X. Zhe, J. Diedrich, A. D. Saliganan, W. J. Cho, M. L. Cher, E. Heath, R. Fridman, H.-R. C. Kim, and R. D. Bonfil, “Bone-induced c-kit expression in prostate cancer: A driver of intraosseous tumor growth,” *Int. J. Cancer*, vol. 136, no. 1, pp. 11–20, Jan. 2015.

[235] J. A. Nemeth, J. F. Harb, U. Barroso, Z. He, D. J. Grignon, and M. L. Cher, “Severe Combined Immunodeficient-hu Model of Human Prostate Cancer Metastasis to Human Bone,” *Cancer Res.*, vol. 59, no. 8, 1999.

[236] J. K. Simmons, B. E. Hildreth, W. Supsavhad, S. M. Elshafae, B. B. Hassan, W. P. Dirksen, R. E. Toribio, and T. J. Rosol, “Animal Models of Bone Metastasis,” *Vet. Pathol.*, vol. 52, no. 5, pp. 827–841, Sep. 2015.

[237] P. Hesami, B. M. Holzapfel, A. Taubenberger, M. Roudier, L. Fazli, S. Sieh, L. Thibaudeau, L. S. Gregory, D. W. Hutmacher, and J. A. Clements, “A humanized tissue-engineered in vivo model to dissect interactions between human prostate cancer cells and human bone,” *Clin. Exp. Metastasis*, vol. 31, no. 4, pp. 435–446, Apr. 2014.

[238] L. C. Martine, B. M. Holzapfel, J. A. McGovern, F. Wagner, V. M. Quent, P. Hesami, F. M. Wunner, C. Vaquette, E. M. De-Juan-Pardo, T. D. Brown, B. Nowlan, D. J. Wu, C. O. Hutmacher, D. Moi, T. Oussenko, E. Piccinini, P. W. Zandstra, R. Mazzieri, J.-P. Lévesque, P. D. Dalton, A. V Taubenberger, and D. W. Hutmacher, “Engineering a humanized bone organ model in mice to study bone metastases,” *Nat. Protoc.*, vol. 12, no. 4, pp. 639–663, Mar. 2017.

[239] S. Bersini, J. S. Jeon, G. Dubini, C. Arrigoni, S. Chung, J. L. Charest, M. Moretti, and R. D. Kamm, “A microfluidic 3D in vitro model for specificity of breast cancer metastasis to bone,” *Biomaterials*, vol. 35, no. 8, pp. 2454–2461,

2014.

[240] S.-Y. Sung, C.-L. Hsieh, A. Law, H. E. Zhau, S. Pathak, A. S. Multani, S. Lim, I. M. Coleman, L.-C. Wu, W. D. Figg, W. L. Dahut, P. Nelson, J. K. Lee, M. B. Amin, R. Lyles, P. A. J. Johnstone, F. F. Marshall, and L. W. K. Chung, "Coevolution of prostate cancer and bone stroma in three-dimensional coculture: implications for cancer growth and metastasis.," *Cancer Res.*, vol. 68, no. 23, pp. 9996–10003, Dec. 2008.

[241] B. Mognetti, G. La Montagna, M. G. Perrelli, P. Pagliaro, and C. Penna, "Bone marrow mesenchymal stem cells increase motility of prostate cancer cells *via* production of stromal cell-derived factor-1 *α*," *J. Cell. Mol. Med.*, vol. 17, no. 2, pp. 287–292, Feb. 2013.

[242] D. W. Hutmacher, "Biomaterials offer cancer research the third dimension.," *Nat. Mater.*, vol. 9, no. 2, pp. 90–93, 2010.

[243] C. Arrigoni, P. De Luca, M. Gilardi, S. Previdi, M. Broggini, and M. Moretti, "Direct but not indirect co-culture with osteogenically differentiated human bone marrow stromal cells increases RANKL / OPG ratio in human breast cancer cells generating bone metastases," *Mol. Cancer*, vol. 13, no. 238, pp. 1–6, 2014.

[244] S. Sieh, A. V. Taubenberger, M. L. Lehman, J. A. Clements, C. C. Nelson, and D. W. Hutmacher, "Paracrine interactions between LNCaP prostate cancer cells and bioengineered bone in 3D in vitro culture reflect molecular changes during bone metastasis," *Bone*, vol. 63, pp. 121–131, 2014.

[245] F. Hofstaedter and R. Ebner, "The Use of 3-D Cultures for High-Throughput Screening : The Multicellular Spheroid Model," *J. Biomol. Screen.*, vol. 9, no. 4, pp. 273–285, 2004.

[246] L. Hutchinson and R. Kirk, "High drug attrition rates—where are we going wrong?," *Nat. Rev. Clin. Oncol.*, vol. 8, no. 4, pp. 189–190, Apr. 2011.

[247] C. Begley and L. Ellis, "Drug development: Raise standards for preclinical cancer research," *nature.com*, vol. 483, pp. 531–533, 2012.

[248] S. Li, M. Kennedy, S. Payne, K. Kennedy, V. L. Seewaldt, S. V Pizzo, and R. E. Bachelder, "Model of Tumor Dormancy/Recurrence after Short-Term Chemotherapy," *PLoS One*, vol. 9, no. 5, p. e98021, 2014.

[249] R. G. Harrison, M. J. Greenman, F. P. Mall, and C. M. Jackson, "Observations of the living developing nerve fiber," *Anat. Rec.*, vol. 1, no. 5, pp. 116–128, Jun. 1907.

[250] C. G. Begley and L. M. Ellis, "Raise standards for preclinical cancer research," *Nature*, vol. 483, no. 7391, pp. 531–533, Mar. 2012.

[251] T. Jacks and R. A. Weinberg, "Taking the Study of Cancer Cell Survival to a New Dimension," *Cell*, vol. 111, no. 7, pp. 923–925, Dec. 2002.

[252] J. Bin Kim, "Three-dimensional tissue culture models in cancer biology," in *Seminars in cancer biology*, 2005, vol. 15, no. 5, pp. 365–377.

[253] K. Bhadriraju, M. Yang, S. Alom Ruiz, D. Pirone, J. Tan, and C. S. Chen, "Activation of ROCK by RhoA is regulated by cell adhesion, shape, and cytoskeletal tension," *Exp. Cell Res.*, vol. 313, no. 16, pp. 3616–3623, 2007.

[254] J. Cassinello, J. Carballido Rodríguez, and L. Antón Aparicio, “Role of taxanes in advanced prostate cancer,” *Clin. Transl. Oncol.*, 2016.

[255] D. Bello-DeOcampo, H. K. Kleinman, and M. M. Webber, “The role of α6β1 integrin and EGF in normal and malignant acinar morphogenesis of human prostatic epithelial cells,” *Mutat. Res. Mol. Mech. Mutagen.*, vol. 480, pp. 209–217, 2001.

[256] S. Breslin and L. O’Driscoll, “Three-dimensional cell culture: the missing link in drug discovery,” *Drug Discov. Today*, vol. 18, no. 5, pp. 240–249, 2013.

[257] D. W. Hutmacher, D. Loessner, S. Rizzi, D. L. Kaplan, D. J. Mooney, and J. A. Clements, “Can tissue engineering concepts advance tumor biology research?,” *Trends Biotechnol.*, vol. 28, no. 3, pp. 125–33, Mar. 2010.

[258] K. F. Chambers, E. M. O. Mosaad, P. J. Russell, J. A. Clements, and M. R. Doran, “3D Cultures of prostate cancer cells cultured in a novel high-throughput culture platform are more resistant to chemotherapeutics compared to cells cultured in monolayer.,” *PLoS One*, vol. 9, no. 11, p. e111029, Jan. 2014.

[259] N. C. Rivron, C. C. Raiss, J. Liu, A. Nandakumar, C. Sticht, N. Gretz, R. Truckenmüller, J. Rouwkema, and C. A. van Blitterswijk, “Sonic Hedgehog-activated engineered blood vessels enhance bone tissue formation.,” *Proc. Natl. Acad. Sci. U. S. A.*, vol. 109, no. 12, pp. 4413–8, Mar. 2012.

[260] K. V. Greco, A. J. Iqbal, L. Rattazzi, G. Nalesso, N. Moradi-Bidhendi, A. R. Moore, M. B. Goldring, F. Dell’Accio, and M. Perretti, “High density micromass cultures of a human chondrocyte cell line: A reliable assay system to reveal the modulatory functions of pharmacological agents,” *Biochem. Pharmacol.*, vol. 82, no. 12, pp. 1919–1929, Dec. 2011.

[261] J. M. Kelm, N. E. Timmins, C. J. Brown, M. Fussenegger, and L. K. Nielsen, “Method for generation of homogeneous multicellular tumor spheroids applicable to a wide variety of cell types,” *Biotechnol. Bioeng.*, vol. 83, no. 2, pp. 173–180, Jul. 2003.

[262] Y.-C. Tung, A. Y. Hsiao, S. G. Allen, Y. Torisawa, M. Ho, and S. Takayama, “High-throughput 3D spheroid culture and drug testing using a 384 hanging drop array,” *Analyst*, vol. 136, no. 3, pp. 473–478, Jan. 2011.

[263] H. Kurosawa, “Methods for inducing embryoid body formation: in vitro differentiation system of embryonic stem cells,” *J. Biosci. Bioeng.*, vol. 103, no. 5, pp. 389–398, May 2007.

[264] T. J. Goodwin, T. L. Prewett, D. A. Wolf, and G. F. Spaulding, “Reduced shear stress: A major component in the ability of mammalian tissues to form three-dimensional assemblies in simulated microgravity,” *J. Cell. Biochem.*, vol. 51, no. 3, pp. 301–311, Mar. 1993.

[265] H. Song, O. David, S. Clejan, C. L. Giordano, H. Pappas-Lebeau, L. Xu, and K. C. O’connor, “Spatial Composition of Prostate Cancer Spheroids in Mixed and Static Cultures,” *Tissue Eng.*, vol. 10, no. 7–8, pp. 1266–1276, Jul. 2004.

[266] S. L. Nyberg, J. Hardin, B. Amiot, U. A. Argikar, R. P. Remmel, and P. Rinaldo, “Rapid, large-scale formation of porcine hepatocyte spheroids in a novel spheroid reservoir bioartificial liver,” *Liver Transplant.*, vol. 11, no. 8,

pp. 901–910, Aug. 2005.

[267] R. Z. Lin and H. Y. Chang, “Recent advances in three-dimensional multicellular spheroid culture for biomedical research,” *Biotechnol. J.*, vol. 3, no. 9–10, pp. 1172–1184, 2008.

[268] E. Fennema, N. Rivron, J. Rouwkema, C. van Blitterswijk, and J. de Boer, “Spheroid culture as a tool for creating 3D complex tissues.,” *Trends Biotechnol.*, vol. 31, no. 2, pp. 108–15, Feb. 2013.

[269] F. Sabeh, R. Shimizu-Hirota, and S. J. Weiss, “Protease-dependent versus -independent cancer cell invasion programs: three-dimensional amoeboid movement revisited.,” *J. Cell Biol.*, vol. 185, no. 1, pp. 11–9, Apr. 2009.

[270] M. M. Stevens and J. H. George, “Exploring and Engineering the Cell Surface Interface,” *Science (80-.).*, vol. 310, no. 5751, 2005.

[271] M. J. Paszek, N. Zahir, K. R. Johnson, J. N. Lakins, G. I. Rozenberg, A. Gefen, C. A. Reinhart-King, S. S. Margulies, M. Dembo, D. Boettiger, D. A. Hammer, and V. M. Weaver, “Tensional homeostasis and the malignant phenotype,” *Cancer Cell*, vol. 8, no. 3, pp. 241–254, Sep. 2005.

[272] D. Falconnet, G. Csucs, H. Michelle Grandin, and M. Textor, “Surface engineering approaches to micropattern surfaces for cell-based assays,” *Biomaterials*, vol. 27, no. 16, pp. 3044–3063, Jun. 2006.

[273] D. Wlodkowic and J. M. Cooper, “Tumors on chips: oncology meets microfluidics,” *Curr. Opin. Chem. Biol.*, vol. 14, no. 5, pp. 556–567, Oct. 2010.

[274] I. Zervantonakis, S. Chung, R. Sudo, M. Zhang, J. Charest, and R. Kamm, “Concentration gradients in microfluidic 3D matrix cell culture systems,” *Int. J. Micro-Nano Scale Transp.*, vol. 1, no. 1, pp. 27–36, 2010.

[275] Y. Gao, D. Majumdar, B. Jovanovic, C. Shaifer, P. C. Lin, A. Zijlstra, D. J. Webb, and D. Li, “A versatile valve-enabled microfluidic cell co-culture platform and demonstration of its applications to neurobiology and cancer biology,” *Biomed. Microdevices*, vol. 13, no. 3, pp. 539–548, Jun. 2011.

[276] A. M. Ghaemmaghami, M. J. Hancock, H. Harrington, H. Kaji, and A. Khademhosseini, “Biomimetic tissues on a chip for drug discovery,” *Drug Discov. Today*, vol. 17, no. 3–4, pp. 173–181, Feb. 2012.

[277] A. Ivascu and M. Kubbies, “Rapid Generation of Single-Tumor Spheroids for High-Throughput Cell Function and Toxicity Analysis,” *J. Biomol. Screen.*, vol. 11, no. 8, pp. 922–932, Dec. 2006.

[278] B. Kul, P. Ghanavi, P. Levett, W. B. Lott, T. Klein, J. J. Cooper-White, R. Crawford, M. R. Doran, B. K. Babur, P. Ghanavi, P. Levett, W. B. Lott, T. Klein, J. J. Cooper-White, R. Crawford, and M. R. Doran, “The interplay between chondrocyte redifferentiation pellet size and oxygen concentration,” *PLoS One*, vol. 8, no. 3, p. e58865, Jan. 2013.

[279] X. Xu, M. C. Farach-Carson, and X. Jia, “Three-dimensional in vitro tumor models for cancer research and drug evaluation.,” *Biotechnol. Adv.*, vol. 32, no. 7, pp. 1256–68, Nov. 2014.

[280] D. F. Quail and J. A. Joyce, “Microenvironmental regulation of tumor

progression and metastasis," *Nat. Med.*, vol. 19, no. 11, pp. 1423–1437, Nov. 2013.

[281] D. Hanahan and R. A. Weinberg, "Hallmarks of cancer: The next generation," *Cell*, vol. 144, no. 5, pp. 646–674, 2011.

[282] B. Sacchetti, A. Funari, C. Remoli, G. Giannicola, G. Kogler, S. Liedtke, G. Cossu, M. Serafini, M. Sampaolesi, E. Tagliafico, E. Tenedini, I. Saggio, P. G. Robey, M. Riminucci, and P. Bianco, "No Identical 'Mesenchymal Stem Cells' at Different Times and Sites: Human Committed Progenitors of Distinct Origin and Differentiation Potential Are Incorporated as Adventitial Cells in Microvessels," *Stem Cell Reports*, vol. 6, no. 6, pp. 897–913, 2016.

[283] J. J. Bara, R. G. Richards, M. Alini, and M. J. Stoddart, "Concise Review: Bone Marrow-Derived Mesenchymal Stem Cells Change Phenotype Following In Vitro Culture: Implications for Basic Research and the Clinic," *Stem Cells*, vol. 32, no. 7, pp. 1713–1723, Jul. 2014.

[284] Y. Fukuchi, H. Nakajima, D. Sugiyama, I. Hirose, T. Kitamura, and K. Tsuji, "Human Placenta-Derived Cells Have Mesenchymal Stem/Progenitor Cell Potential," *Stem Cells*, vol. 22, no. 5, pp. 649–658, Sep. 2004.

[285] P. A. Zuk, M. Zhu, H. Mizuno, J. Huang, J. W. Futrell, A. J. Katz, P. Benhaim, H. P. Lorenz, and M. H. Hedrick, "Multilineage Cells from Human Adipose Tissue: Implications for Cell-Based Therapies," *Tissue Eng.*, vol. 7, no. 2, pp. 211–228, Apr. 2001.

[286] M. Dominici, K. Le Blanc, I. Mueller, I. Slaper-Cortenbach, F. Marini, D. Krause, R. Deans, a Keating, D. Prockop, and E. Horwitz, "Minimal criteria for defining multipotent mesenchymal stromal cells. The International Society for Cellular Therapy position statement.," *Cytotherapy*, vol. 8, no. 4, pp. 315–7, 2006.

[287] M. Stadler, S. Walter, A. Walzl, N. Kramer, C. Unger, M. Scherzer, D. Unterleuthner, M. Hengstschläger, G. Krupitza, and H. Dolznig, "Increased complexity in carcinomas: Analyzing and modeling the interaction of human cancer cells with their microenvironment," *Semin. Cancer Biol.*, vol. 35, pp. 107–124, 2015.

[288] A. H. Undale, J. J. Westendorf, M. J. Yaszemski, and S. Khosla, "Mesenchymal Stem Cells for Bone Repair and Metabolic Bone Diseases," *Mayo Clin. Proc.*, vol. 84, no. 10, pp. 893–902, 2009.

[289] B. K. Babur, K. Futrega, W. B. Lott, T. J. Klein, J. Cooper-White, and M. R. Doran, "High-throughput bone and cartilage micropellet manufacture, followed by assembly of micropellets into biphasic osteochondral tissue," *Cell Tissue Res.*, vol. 361, no. 3, pp. 755–768, Sep. 2015.

[290] K. Futrega, J. S. Palmer, M. Kinney, W. B. Lott, M. D. Ungrin, P. W. Zandstra, and M. R. Doran, "The microwell-mesh: A novel device and protocol for the high throughput manufacturing of cartilage microtissues.," *Biomaterials*, vol. 62, pp. 1–12, Sep. 2015.

[291] C. A. Tannoury and H. S. An, "Complications with the use of bone morphogenetic protein 2 (BMP-2) in spine surgery," *Spine J.*, vol. 14, no. 3, pp. 552–559, Mar. 2014.

[292] S. Bhumiratana and G. Vunjak-Novakovic, “Concise Review: Personalized Human Bone Grafts for Reconstructing Head and Face,” *Stem Cells Transl. Med.*, vol. 1, no. 1, pp. 64–69, Jan. 2012.

[293] H. L. Holtorf, J. A. Jansen, and A. G. Mikos, “Modulation of Cell Differentiation in Bone Tissue Engineering Constructs Cultured in a Bioreactor,” in *Tissue Engineering*, Boston, MA: Springer US, 2006, pp. 225–241.

[294] S. Kadiyala, N. Jaiswal, and S. P. Bruder, “Culture-Expanded, Bone Marrow-Derived Mesenchymal Stem Cells Can Regenerate a Critical-Sized Segmental Bone Defect,” *Tissue Eng.*, vol. 3, no. 2, pp. 173–185, Jun. 1997.

[295] C. Di Bella, P. Farlie, and A. J. Penington, “Bone Regeneration in a Rabbit Critical-Sized Skull Defect Using Autologous Adipose-Derived Cells,” *Tissue Eng. Part A*, vol. 14, no. 4, pp. 483–490, Apr. 2008.

[296] A. S. Mistry and A. G. Mikos, “Tissue Engineering Strategies for Bone Regeneration,” 2005, pp. 1–22.

[297] E. Hesse, T. E. Hefferan, J. E. Tarara, C. Haasper, R. Meller, C. Krettek, L. Lu, and M. J. Yaszemski, “Collagen type I hydrogel allows migration, proliferation, and osteogenic differentiation of rat bone marrow stromal cells,” *J. Biomed. Mater. Res. Part A*, vol. 9999A, no. 2, p. NA-NA, 2010.

[298] J. I. Dawson, J. Kanczler, R. Tare, M. Kassem, and R. O. C. Oreffo, “Concise Review: Bridging the Gap: Bone Regeneration Using Skeletal Stem Cell-Based Strategies-Where Are We Now?,” *Stem Cells*, vol. 32, no. 1, pp. 35–44, Jan. 2014.

[299] A. Arthur, A. Zannettino, and S. Gronthos, “The therapeutic applications of multipotential mesenchymal/stromal stem cells in skeletal tissue repair,” *J. Cell. Physiol.*, vol. 218, no. 2, pp. 237–245, Feb. 2009.

[300] P. Giannoni, M. Mastrogiacomo, M. Alini, S. G. Pearce, A. Corsi, F. Santolini, A. Muraglia, P. Bianco, and R. Cancedda, “Regeneration of large bone defects in sheep using bone marrow stromal cells,” *J. Tissue Eng. Regen. Med.*, vol. 2, no. 5, pp. 253–262, Jul. 2008.

[301] B. M. Abdallah and M. Kassem, “New factors controlling the balance between osteoblastogenesis and adipogenesis.,” *Bone*, vol. 50, no. 2, pp. 540–5, Mar. 2012.

[302] J. M. Gimble, S. Zvonic, Z. E. Floyd, M. Kassem, and M. E. Nuttall, “Playing with bone and fat,” *J. Cell. Biochem.*, vol. 98, no. 2, pp. 251–266, May 2006.

[303] R. McBeath, D. M. Pirone, C. M. Nelson, K. Bhadriraju, and C. S. Chen, “Cell Shape, Cytoskeletal Tension, and RhoA Regulate Stem Cell Lineage Commitment,” *Dev. Cell*, vol. 6, no. 4, pp. 483–495, 2004.

[304] B. Cosgrove, K. Mui, T. Driscoll, and S. Caliari, “N-cadherin adhesive interactions modulate matrix mechanosensing and fate commitment of mesenchymal stem cells,” *Nat. Mater.*, 2016.

[305] Z. Liu, X. Yuan, G. Fernandes, R. Dziak, C. N. Ionita, C. Li, C. Wang, and S. Yang, “The combination of nano-calcium sulfate/platelet rich plasma gel scaffold with BMP2 gene-modified mesenchymal stem cells promotes bone regeneration in rat critical-sized calvarial defects,” *Stem Cell Res. Ther.*, vol.

8, no. 1, p. 122, Dec. 2017.

[306] E. Carlisle and J. S. Fischgrund, “Bone morphogenetic proteins for spinal fusion,” *Spine J.*, vol. 5, no. 6, pp. S240–S249, 2005.

[307] D. K. Hamilton, S. M. Jones-Quaidoo, C. Sansur, C. I. Shaffrey, R. Oskouian, and J. A. Jane, “Outcomes of bone morphogenetic protein-2 in mature adults: posterolateral non–instrument-assisted lumbar decompression and fusion,” *Surg. Neurol.*, vol. 69, no. 5, pp. 457–461, 2008.

[308] B. McKay and H. S. Sandhu, “Use of Recombinant Human Bone Morphogenetic Protein-2 in Spinal Fusion Applications,” *Spine (Phila. Pa. 1976).*, vol. 27, no. 16, pp. 66–85, 2002.

[309] S. K. Lam, C. Sayama, D. A. Harris, V. Briceño, T. G. Luerssen, and A. Jea, “Nationwide practice patterns in the use of recombinant human bone morphogenetic protein–2 in pediatric spine surgery as a function of patient-, hospital-, and procedure-related factors,” *J. Neurosurg. Pediatr.*, vol. 14, no. 5, pp. 476–485, 2014.

[310] Medtronic and A, “InFuse Bone Graft/LT-Cage: Summary of Safety and Effectiveness,” *Saf. Eff. Data*, vol. P000058, pp. 1–40, 2002.

[311] J. N. Zara, R. K. Siu, X. Zhang, J. Shen, R. Ngo, M. Lee, W. Li, M. Chiang, J. Chung, J. Kwak, B. M. Wu, K. Ting, and C. Soo, “High Doses of Bone Morphogenetic Protein 2 Induce Structurally Abnormal Bone and Inflammation In Vivo,” *Tissue Eng. Part A*, vol. 17, no. 9–10, pp. 1389–1399, 2011.

[312] C. for D. and R. Health, “Public Health Notifications (Medical Devices) - FDA Public Health Notification: Life-threatening Complications Associated with Recombinant Human Bone Morphogenetic Protein in Cervical Spine Fusion.” [Online]. Available: https://wayback.archive-it.org/7993/20161022130910/http://www.fda.gov/MedicalDevices/Safety/AlertsandNotices/PublicHealthNotifications/ucm062000.htm. [Accessed: 05-Jun-2017].

[313] K. T. Sampath and A. H. Reddi, “Historical Perspective of Bone Morphogenetic Proteins,” in *Bone Morphogenetic Proteins: Systems Biology Regulators*, Cham: Springer International Publishing, 2017, pp. 1–13.

[314] G. S. Krishnakumar, A. Roffi, D. Reale, E. Kon, and G. Filardo, “Clinical application of bone morphogenetic proteins for bone healing: a systematic review,” *Int. Orthop.*, vol. 41, no. 6, pp. 1073–1083, Jun. 2017.

[315] S. A. Zadegan, A. Abedi, S. B. Jazayeri, H. Nasiri Bonaki, S. B. Jazayeri, A. R. Vaccaro, and V. Rahimi-Movaghar, “Bone morphogenetic proteins in anterior cervical fusion: a systematic review and meta-analysis,” *World Neurosurg.*, 2017.

[316] W. Wagner, P. Horn, M. Castoldi, A. Diehlmann, S. Bork, R. Saffrich, V. Benes, J. Blake, S. Pfister, V. Eckstein, and A. D. Ho, “Replicative Senescence of Mesenchymal Stem Cells: A Continuous and Organized Process,” *PLoS One*, vol. 3, no. 5, p. e2213, May 2008.

[317] S. Bork, S. Pfister, H. Witt, P. Horn, B. Korn, A. D. Ho, and W. Wagner, “DNA methylation pattern changes upon long-term culture and aging of

human mesenchymal stromal cells," *Aging Cell*, vol. 9, no. 1, pp. 54–63, Feb. 2010.

[318] K. Futrega, K. Atkinson, W. B. Lott, and M. R. Doran, "Spheroid Coculture of Hematopoietic Stem/Progenitor Cells and Monolayer Expanded Mesenchymal Stem/Stromal Cells in Polydimethylsiloxane Microwells Modestly Improves In Vitro Hematopoietic Stem/Progenitor Cell Expansion," *Tissue Eng. Part C Methods*, vol. 23, no. 4, pp. 200–218, Feb. 2017.

[319] B. D. Markway, G.-K. Tan, G. Brooke, J. E. Hudson, J. J. Cooper-White, and M. R. Doran, "Enhanced chondrogenic differentiation of human bone marrow-derived mesenchymal stem cells in low oxygen environment micropellet cultures," *Cell Transplant.*, vol. 19, no. 1, pp. 29–42, 2010.

[320] J. van den Dolder, G. N. Bancroft, V. I. Sikavitsas, P. H. M. Spauwen, A. G. Mikos, and J. A. Jansen, "Effect of Fibronectin- and Collagen I-Coated Titanium Fiber Mesh on Proliferation and Differentiation of Osteogenic Cells," *Tissue Eng.*, vol. 9, no. 3, pp. 505–515, Jun. 2003.

[321] F. Langenbach, K. Berr, C. Naujoks, and A. Hassel, "Generation and differentiation of microtissues from multipotent precursor cells for use in tissue engineering," *Nat. Protoc.*, 2011.

[322] E. V. Badiavas, F. V, A. DG, S. ML, M. JO, P. HY, and M. F, "Treatment of Chronic Wounds With Bone Marrow–Derived Cells," *Arch. Dermatol.*, vol. 139, no. 4, p. 510, Apr. 2003.

[323] E. Tateishi-Yuyama, H. Matsubara, T. Murohara, U. Ikeda, S. Shintani, H. Masaki, K. Amano, Y. Kishimoto, K. Yoshimoto, H. Akashi, K. Shimada, T. Iwasaka, and T. Imaizumi, "Therapeutic angiogenesis for patients with limb ischaemia by autologous transplantation of bone-marrow cells: a pilot study and a randomised controlled trial," *Lancet*, vol. 360, no. 9331, pp. 427–435, Aug. 2002.

[324] P. A. Kenny, G. Y. Lee, C. A. Myers, R. M. Neve, J. R. Semeiks, P. T. Spellman, K. Lorenz, E. H. Lee, M. H. Barcellos-Hoff, O. W. Petersen, J. W. Gray, and M. J. Bissell, "The morphologies of breast cancer cell lines in three-dimensional assays correlate with their profiles of gene expression.," *Mol. Oncol.*, vol. 1, no. 1, pp. 84–96, Jun. 2007.

[325] L. Guo, Y. Zhou, S. Wang, and Y. Wu, "Epigenetic changes of mesenchymal stem cells in three-dimensional (3D) spheroids," *J. Cell. Mol. Med.*, vol. 18, no. 10, pp. 2009–2019, Oct. 2014.

[326] J. Han, P. Mistriotis, P. Lei, D. Wang, S. Liu, and S. T. Andreadis, "Nanog reverses the effects of organismal aging on mesenchymal stem cell proliferation and myogenic differentiation potential.," *Stem Cells*, vol. 30, no. 12, pp. 2746–59, Dec. 2012.

[327] Y. Zhou, H. Chen, H. Li, and Y. Wu, "3D culture increases pluripotent gene expression in mesenchymal stem cells through relaxation of cytoskeleton tension," *J. Cell. Mol. Med.*, vol. XX, no. X, pp. 1–12, 2016.

[328] P. R. Baraniak and T. C. McDevitt, "Scaffold-free culture of mesenchymal stem cell spheroids in suspension preserves multilineage potential," *Cell Tissue Res.*, vol. 347, no. 3, pp. 701–711, Mar. 2012.

[329] M. Kabiri, B. Kul, W. B. Lott, K. Futrega, P. Ghanavi, Z. Upton, and M. R. Doran, “3D mesenchymal stem/stromal cell osteogenesis and autocrine signalling,” *Biochem. Biophys. Res. Commun.*, vol. 419, no. 2, pp. 142–147, 2012.

[330] J. M. Belmonte, S. G. Clendenon, G. M. Oliveira, M. H. Swat, E. V Greene, S. Jeyaraman, J. A. Glazier, and R. L. Bacallao, “Virtual-tissue computer simulations define the roles of cell adhesion and proliferation in the onset of kidney cystic disease.,” *Mol. Biol. Cell*, vol. 27, no. 22, pp. 3673–3685, Nov. 2016.

[331] S. C. Ramaiahgari, M. W. den Braver, B. Herpers, V. Terpstra, J. N. M. Commandeur, B. van de Water, and L. S. Price, “A 3D in vitro model of differentiated HepG2 cell spheroids with improved liver-like properties for repeated dose high-throughput toxicity studies,” *Arch. Toxicol.*, vol. 88, no. 5, pp. 1083–1095, Mar. 2014.

[332] A. C. Lloyd, “The Regulation of Cell Size,” *Cell*, vol. 154, no. 6, pp. 1194–1205, 2013.

[333] M. Singh, S. Mukundan, M. Jaramillo, S. Oesterreich, and S. Sant, “Three-dimensional breast cancer models mimic hallmarks of size-induced tumor progression,” *Cancer Res.*, vol. 76, no. 13, pp. 3732–43, Jul. 2016.

[334] T. J. Bartosh, J. H. Ylöstalo, A. Mohammadipoor, N. Bazhanov, K. Coble, K. Claypool, R. H. Lee, H. Choi, and D. J. Prockop, “Aggregation of human mesenchymal stromal cells (MSCs) into 3D spheroids enhances their antiinflammatory properties.,” *Proc. Natl. Acad. Sci. U. S. A.*, vol. 107, no. 31, pp. 13724–9, Aug. 2010.

[335] J. M. Kelm and M. Fussenegger, “Scaffold-free cell delivery for use in regenerative medicine,” *Adv. Drug Deliv. Rev.*, vol. 62, no. 7, pp. 753–764, 2010.

[336] J. M. Kelm, V. Lorber, J. G. Snedeker, D. Schmidt, A. Broggini-Tenzer, M. Weisstanner, B. Odermatt, A. Mol, G. Zünd, and S. P. Hoerstrup, “A novel concept for scaffold-free vessel tissue engineering: Self-assembly of microtissue building blocks,” *J. Biotechnol.*, vol. 148, no. 1, pp. 46–55, 2010.

[337] F. Langenbach, C. Naujoks, R. Smeets, K. Berr, R. Depprich, N. Kübler, and J. Handschel, “Scaffold-free microtissues: Differences from monolayer cultures and their potential in bone tissue engineering,” *Clin. Oral Investig.*, vol. 17, no. 1, pp. 9–17, 2013.

[338] F. Langenbach, C. Naujoks, A. Laser, M. Kelz, P. Kersten-Thiele, K. Berr, R. Depprich, N. Kübler, G. Kögler, and J. Handschel, “Improvement of the Cell-loading Efficiency of Biomaterials by Inoculation with Stem Cell-based Microspheres, in Osteogenesis,” *J. Biomater. Appl.*, vol. 26, no. 5, pp. 549–564, Jan. 2012.

[339] M. Kim and S. Choe, “BMPs and their clinical potentials.,” *BMB Rep.*, vol. 44, no. 10, pp. 619–34, Oct. 2011.

[340] H. Senta, H. Park, E. Bergeron, O. Drevelle, D. Fong, E. Leblanc, F. Cabana, S. Roux, G. Grenier, and N. Faucheux, “Cell responses to bone morphogenetic proteins and peptides derived from them: biomedical applications and

limitations.," *Cytokine Growth Factor Rev.*, vol. 20, no. 3, pp. 213–22, Jun. 2009.

[341] S. Vanhatupa, M. Ojansivu, R. Autio, M. Juntunen, and S. Miettinen, "Bone Morphogenetic Protein-2 Induces Donor-Dependent Osteogenic and Adipogenic Differentiation in Human Adipose Stem Cells.," *Stem Cells Transl. Med.*, p. sctm.2015-0042, Oct. 2015.

[342] X. Ji, D. Chen, C. Xu, S. E. Harris, G. R. Mundy, and T. Yoneda, "Patterns of gene expression associated with BMP-2-induced osteoblast and adipocyte differentiation of mesenchymal progenitor cell 3T3-F442A," *J. Bone Miner. Metab.*, vol. 18, no. 3, pp. 132–139, Apr. 2000.

[343] H. Page, P. Flood, and E. G. Reynaud, "Three-dimensional tissue cultures: current trends and beyond," *Cell Tissue Res.*, vol. 352, no. 1, pp. 123–131, Apr. 2013.

[344] Y. Chen, D. Gao, H. Liu, S. Lin, and Y. Jiang, "Drug cytotoxicity and signaling pathway analysis with three-dimensional tumor spheroids in a microwell-based microfluidic chip for drug screening.," *Anal. Chim. Acta*, vol. 898, pp. 85–92, Oct. 2015.

[345] Y. Miyamoto, M. Ikeuchi, H. Noguchi, T. Yagi, and S. Hayashi, "Spheroid Formation and Evaluation of Hepatic Cells in a Three-Dimensional Culture Device.," *Cell Med.*, vol. 8, no. 1–2, pp. 47–56, Dec. 2015.

[346] M. D. Ungrin, C. Joshi, A. Nica, C. Bauwens, and P. W. Zandstra, "Reproducible, Ultra High-Throughput Formation of Multicellular Organization from Single Cell Suspension-Derived Human Embryonic Stem Cell Aggregates," *PLoS One*, vol. 3, no. 2, p. e1565, Feb. 2008.

[347] S. N. Rampersad, "Multiple applications of alamar blue as an indicator of metabolic function and cellular health in cell viability bioassays," *Sensors (Switzerland)*, vol. 12, no. 9, pp. 12347–12360, 2012.

[348] Z. Li, M. Alyamani, J. Li, K. Rogacki, M. Abazeed, S. K. Upadhyay, S. P. Balk, M.-E. Taplin, R. J. Auchus, and N. Sharifi, "Redirecting abiraterone metabolism to fine-tune prostate cancer anti-androgen therapy," *Nature*, vol. 533, no. 7604, pp. 547–551, 2016.

[349] A. Asthana and W. S. Kisaalita, "Microtissue size and hypoxia in HTS with 3D cultures.," *Drug Discov. Today*, vol. 17, no. 15–16, pp. 810–7, Aug. 2012.

[350] F. Hirschhaeuser, H. Menne, C. Dittfeld, J. West, W. Mueller-Klieser, and L. A. Kunz-Schughart, "Multicellular tumor spheroids: An underestimated tool is catching up again," *J. Biotechnol.*, vol. 148, no. 1, pp. 3–15, Jul. 2010.

[351] V. Härmä, J. Virtanen, R. Mäkelä, A. Happonen, J.-P. Mpindi, M. Knuuttila, P. Kohonen, J. Lötjönen, O. Kallioniemi, and M. Nees, "A comprehensive panel of three-dimensional models for studies of prostate cancer growth, invasion and drug responses.," *PLoS One*, vol. 5, no. 5, p. e10431, Jan. 2010.

[352] K. M. Charoen, B. Fallica, Y. L. Colson, M. H. Zaman, and M. W. Grinstaff, "Embedded multicellular spheroids as a biomimetic 3D cancer model for evaluating drug and drug-device combinations," *Biomaterials*, vol. 35, no. 7, pp. 2264–2271, 2014.

[353] S. Rhee and F. Grinnell, "Fibroblast mechanics in 3D collagen matrices," *Adv.*

Drug Deliv. Rev., vol. 59, no. 13, pp. 1299–1305, 2007.

[354] D. Ambrosi and F. Mollica, "The role of stress in the growth of a multicell spheroid," *J. Math. Biol.*, vol. 48, no. 5, pp. 477–499, May 2004.

[355] F. Montel, M. Delarue, J. Elgeti, D. Vignjevic, G. Cappello, and J. Prost, "Isotropic stress reduces cell proliferation in tumor spheroids," *New J. Phys.*, vol. 14, no. 5, p. 55008, May 2012.

[356] M. Alemany-Ribes and C. E. Semino, "Bioengineering 3D environments for cancer models.," *Adv. Drug Deliv. Rev.*, vol. 79–80, pp. 40–9, Dec. 2014.

[357] J. El-Ali, P. K. Sorger, and K. F. Jensen, "Cells on chips," *Nature*, vol. 442, no. 7101, pp. 403–411, Jul. 2006.

[358] D. Khaitan and B. S. Dwarakanath, "Multicellular spheroids as an in vitro model in experimental oncology: applications in translational medicine," *Expert Opin. Drug Discov.*, vol. 1, no. 7, pp. 663–675, Dec. 2006.

[359] D. L. Berry, C. M. Moinpour, C. S. Jiang, D. P. Ankerst, D. P. Petrylak, L. V Vinson, P. N. Lara, S. Jones, M. E. Taplin, P. A. Burch, M. H. A. Hussain, and E. D. Crawford, "Quality of life and pain in advanced stage prostate cancer: results of a Southwest Oncology Group randomized trial comparing docetaxel and estramustine to mitoxantrone and prednisone.," *J. Clin. Oncol.*, vol. 24, no. 18, pp. 2828–35, Jun. 2006.

[360] N. N. C. Tam, Y. Gao, and Y. Leung, "Androgenic Regulation of Oxidative Stress in the Rat Prostate," *Ambio*, vol. 163, no. 6, pp. 2513–2522, 2003.

[361] Y. Torisawa, B. Chueh, D. Huh, P. Ramamurthy, T. M. Roth, K. F. Barald, S. Takayama, S.-Y. Hwang, K. S. Lee, and B. Oh, "Efficient formation of uniform-sized embryoid bodies using a compartmentalized microchannel device," *Lab Chip*, vol. 7, no. 6, p. 770, 2007.

[362] S. Khetan and J. Burdick, "Cellular encapsulation in 3D hydrogels for tissue engineering.," *J. Vis. Exp.*, no. 32, Oct. 2009.

[363] C.-C. Lin, A. Raza, and H. Shih, "PEG hydrogels formed by thiol-ene photo-click chemistry and their effect on the formation and recovery of insulin-secreting cell spheroids," *Biomaterials*, vol. 32, no. 36, pp. 9685–9695, 2011.

[364] X. Fang, S. Sittadjody, K. Gyabaah, E. C. Opara, and K. C. Balaji, "Novel 3D Co-Culture Model for Epithelial-Stromal Cells Interaction in Prostate Cancer," *PLoS One*, vol. 8, no. 9, p. e75187, Sep. 2013.

[365] C. R. Thoma, M. Zimmermann, I. Agarkova, J. M. Kelm, and W. Krek, "3D cell culture systems modeling tumor growth determinants in cancer target discovery," *Adv. Drug Deliv. Rev.*, vol. 69, pp. 29–41, 2014.

[366] J.-B. Kim, K. Urban, E. Cochran, S. Lee, A. Ang, B. Rice, A. Bata, K. Campbell, R. Coffee, A. Gorodinsky, Z. Lu, H. Zhou, T. K. Kishimoto, and P. Lassota, "Non-Invasive Detection of a Small Number of Bioluminescent Cancer Cells In Vivo," *PLoS One*, vol. 5, no. 2, p. e9364, Feb. 2010.

[367] D. M. Close, R. E. Hahn, S. S. Patterson, S. J. Baek, S. A. Ripp, and G. S. Sayler, "Comparison of human optimized bacterial luciferase, firefly luciferase, and green fluorescent protein for continuous imaging of cell culture and animal models," *J. Biomed. Opt.*, vol. 16, no. 4, p. 47003, 2011.

[368] G. Choy, S. O'Connor, F. E. Diehn, N. Costouros, H. R. Alexander, P. Choyke, and S. K. Libutti, "Comparison of noninvasive fluorescent and bioluminescent small animal optical imaging.," *Biotechniques*, vol. 35, no. 5, pp. 1022–6, 1028–30, Nov. 2003.

[369] D. W. McMillin, J. Delmore, E. Weisberg, J. M. Negri, D. C. Geer, S. Klippel, N. Mitsiades, R. L. Schlossman, N. C. Munshi, A. L. Kung, J. D. Griffin, P. G. Richardson, K. C. Anderson, and C. S. Mitsiades, "Tumor cell-specific bioluminescence platform to identify stroma-induced changes to anticancer drug activity," *Nat. Med.*, vol. 16, no. 4, pp. 483–489, 2010.

[370] R. Bam, S. Khan, W. Ling, S. S. Randal, X. Li, B. Barlogie, R. Edmondson, and S. Yaccoby, "Primary myeloma interaction and growth in coculture with healthy donor hematopoietic bone marrow.," *BMC Cancer*, vol. 15, no. 1, p. 864, Jan. 2015.

[371] N. Yang, T. Yan, H. Zhu, X. Liang, L. Leiss, P. Sakariassen, K. Skaftnesmo, B. Huang, D. Costea, P. Enger, X. Li, and J. Wang, "A co-culture model with brain tumor-specific bioluminescence demonstrates astrocytes-induced drug resistance in glioblastoma.," *J. Transl. Med.*, vol. 12, no. 1, p. 278, 2014.

[372] V. P. Mane, M. A. Heuer, P. Hillyer, M. B. Navarro, and R. L. Rabin, "Systematic method for determining an ideal housekeeping gene for real-time PCR analysis.," *J. Biomol. Tech.*, vol. 19, no. 5, pp. 342–7, Dec. 2008.

[373] S. Christoph, J. Schlegel, F. Alvarez-Calderon, Y.-M. Kim, L. N. Brandao, D. DeRyckere, and D. K. Graham, "Bioluminescence imaging of leukemia cell lines in vitro and in mouse xenografts: effects of monoclonal and polyclonal cell populations on intensity and kinetics of photon emission," *J. Hematol. Oncol.*, vol. 6, no. 1, p. 10, 2013.

[374] Z.-L. Xu, H. Mizuguchi, A. Ishii-Watabe, E. Uchida, T. Mayumi, and T. Hayakawa, "Optimization of transcriptional regulatory elements for constructing plasmid vectors," *Gene*, vol. 272, no. 1–2, pp. 149–156, Jul. 2001.

[375] H.-C. Wu, J.-T. Hsieh, M. E. Gleave, N. M. Brown, S. Pathak, and L. W. K. Chung, "Derivation of androgen-independent human LNCaP prostatic cancer cell sublines: Role of bone stromal cells," *Int. J. Cancer*, vol. 57, no. 3, pp. 406–412, May 1994.

[376] S. U. Luk, W. N. Yap, Y. T. Chiu, D. T. W. Lee, S. Ma, T. K. W. Lee, R. S. Vasireddy, Y. C. Wong, Y. P. Ching, C. Nelson, Y. L. Yap, and M. T. Ling, "Gamma-tocotrienol as an effective agent in targeting prostate cancer stem cell-like population," *Int. J. Cancer*, vol. 128, no. 9, pp. 2182–2191, 2011.

[377] A. Untergasser, H. Nijveen, X. Rao, T. Bisseling, R. Geurts, and J. A. M. Leunissen, "Primer3Plus, an enhanced web interface to Primer3," *Nucleic Acids Res.*, vol. 35, no. Web Server, pp. W71–W74, May 2007.

[378] J. Ye, G. Coulouris, I. Zaretskaya, I. Cutcutache, S. Rozen, and T. L. Madden, "Primer-BLAST: a tool to design target-specific primers for polymerase chain reaction.," *BMC Bioinformatics*, vol. 13, no. suppl_1, p. 134, Jan. 2012.

[379] A. Dobin, C. A. Davis, F. Schlesinger, J. Drenkow, C. Zaleski, S. Jha, P. Batut, M. Chaisson, and T. R. Gingeras, "STAR: ultrafast universal RNA-seq

aligner.," *Bioinformatics*, vol. 29, no. 1, pp. 15–21, Jan. 2013.

[380] H. Li and R. Durbin, "Fast and accurate short read alignment with Burrows-Wheeler transform," *Bioinformatics*, vol. 25, no. 14, pp. 1754–1760, Jul. 2009.

[381] M. Krzywinski, J. Schein, I. Birol, J. Connors, R. Gascoyne, D. Horsman, S. J. Jones, and M. A. Marra, "Circos: An information aesthetic for comparative genomics," *Genome Res.*, vol. 19, no. 9, pp. 1639–1645, Sep. 2009.

[382] D. Cunningham and Z. You, "In vitro and in vivo model systems used in prostate cancer research," *Journal of Biological Methods*, vol. 2, no. 1. p. e17, 04-Jun-2015.

[383] D. W. McMillin, J. Delmore, J. M. Negri, M. Vanneman, S. Koyama, R. L. Schlossman, N. C. Munshi, J. Laubach, P. G. Richardson, G. Dranoff, K. C. Anderson, and C. S. Mitsiades, "Compartment-Specific Bioluminescence Imaging platform for the high-throughput evaluation of antitumor immune function.," *Blood*, vol. 119, no. 15, pp. e131-8, 2012.

[384] M. F. Kircher, S. S. Gambhir, and J. Grimm, "Noninvasive cell-tracking methods," *Nat. Rev. Clin. Oncol.*, vol. 8, no. 11, pp. 677–688, Sep. 2011.

[385] B. A. Rabinovich, Y. Ye, T. Etto, J. Q. Chen, H. I. Levitsky, W. W. Overwijk, L. J. N. Cooper, J. Gelovani, and P. Hwu, "Visualizing fewer than 10 mouse T cells with an enhanced firefly luciferase in immunocompetent mouse models of cancer.," *Proc. Natl. Acad. Sci. U. S. A.*, vol. 105, no. 38, pp. 14342–6, Sep. 2008.

[386] U. Kamensek, G. Sersa, S. Vidic, G. Tevz, S. Kranjc, and M. Cemazar, "Irradiation, Cisplatin, and 5-Azacytidine Upregulate Cytomegalovirus Promoter in Tumors and Muscles: Implementation of Non-invasive Fluorescence Imaging," *Mol. Imaging Biol.*, vol. 13, no. 1, pp. 43–52, Feb. 2011.

[387] C.-C. Hsu, H.-P. Li, Y.-H. Hung, Y.-W. Leu, W.-H. Wu, F.-S. Wang, K.-D. Lee, P.-J. Chang, C.-S. Wu, Y.-J. Lu, T. H.-M. Huang, Y.-S. Chang, and S.-H. Hsiao, "Targeted methylation of CMV and E1A viral promoters," *Biochem. Biophys. Res. Commun.*, vol. 402, no. 2, pp. 228–234, Nov. 2010.

[388] C. Teschendorf, K. H. Warrington, D. W. Siemann, and N. Muzyczka, "Comparison of the EF-1 alpha and the CMV promoter for engineering stable tumor cell lines using recombinant adeno-associated virus.," *Anticancer Res.*, vol. 22, no. 6A, pp. 3325–30.

[389] Y. Sakaguchi, I. Sekiya, K. Yagishita, S. Ichinose, K. Shinomiya, and T. Muneta, "Suspended cells from trabecular bone by collagenase digestion become virtually identical to mesenchymal stem cells obtained from marrow aspirates," *Blood*, vol. 104, no. 9, 2004.

[390] P. Bianco, M. Riminucci, S. Gronthos, and P. G. Robey, "Bone Marrow Stromal Stem Cells: Nature, Biology, and Potential Applications," *Stem Cells*, vol. 19, no. 3, pp. 180–192, May 2001.

[391] M. Corselli, C. J. Chin, C. Parekh, A. Sahaghian, W. Wang, S. Ge, D. Evseenko, X. Wang, E. Montelatici, L. Lazzari, G. M. Crooks, and B. Péault, "Perivascular support of human hematopoietic stem/progenitor cells," *Blood*,

vol. 121, no. 15, 2013.

[392] S. A. Bliss, G. Sinha, O. Sandiford, L. Williams, D. J. Engelberth, K. Guiro, L. L. Isenalumhe, S. J. Greco, S. Ayer, M. Bryan, R. Kumar, N. Ponzio, and P. Rameshwar, "Mesenchymal stem cell-derived exosomes stimulates cycling quiescence and early breast cancer dormancy in bone marrow.," *Cancer Res.*, p. canres.1092.2016, Aug. 2016.

[393] S. Sieh, A. A. Lubik, J. A. Clements, C. C. Nelson, and D. W. Hutmacher, "Interactions between human osteoblasts and prostate cancer cells in a novel 3D in vitro model," *Organogenesis*, vol. 6, no. 3, p. 181, 2010.

[394] Y. Tokuda, Y. Satoh, C. Fujiyama, S. Toda, H. Sugihara, and Z. Masaki, "Prostate cancer cell growth is modulated by adipocyte-cancer cell interaction," *BJU Int.*, vol. 91, no. 7, pp. 716–720, Apr. 2003.

[395] A. P. D. N. de Barros, C. M. Takiya, L. R. Garzoni, M. L. Leal-Ferreira, H. S. Dutra, L. B. Chiarini, M. N. Meirelles, R. Borojevic, and M. I. D. Rossi, "Osteoblasts and Bone Marrow Mesenchymal Stromal Cells Control Hematopoietic Stem Cell Migration and Proliferation in 3D In Vitro Model," *PLoS One*, vol. 5, no. 2, p. e9093, Feb. 2010.

[396] L. C. Kimlin, G. Casagrande, and V. M. Virador, "In vitro three-dimensional (3D) models in cancer research: an update.," *Mol. Carcinog.*, vol. 52, no. 3, pp. 167–82, Mar. 2013.

[397] E. O. Mosaad, K. F. Chambers, K. Futrega, J. A. Clements, and M. R. Doran, "The Microwell-mesh: A high-throughput 3D prostate cancer spheroid and drug-testing platform," *Sci. Rep.*, vol. 8, no. 1, p. 253, Dec. 2018.

[398] S. Arcangeli, T. Zilli, B. De Bari, and F. Alongi, "'Hit the primary': A paradigm shift in the treatment of metastatic prostate cancer?," *Crit. Rev. Oncol. Hematol.*, vol. 97, pp. 231–7, Jan. 2016.

[399] A. M. Decker, Y. Jung, F. Cackowski, and R. S. Taichman, "The role of hematopoietic stem cell niche in prostate cancer bone metastasis," *J. Bone Oncol.*, vol. 5, no. 3, pp. 117–120, Sep. 2016.

[400] M. Mimeault and S. K. Batra, "New Concepts on the Critical Functions of Cancer- and Metastasis-Initiating Cells in Treatment Resistance and Disease Relapse: Molecular Mechanisms, Signaling Transduction Elements and Novel Targeting Therapies," Springer, Dordrecht, 2010, pp. 175–207.

[401] G. Ren, M. Esposito, and Y. Kang, "Bone metastasis and the metastatic niche," *J. Mol. Med.*, vol. 93, no. 11, pp. 1203–1212, Nov. 2015.

[402] M. Mimeault, R. Hauke, and S. Batra, "Recent Advances on the Molecular Mechanisms Involved in the Drug Resistance of Cancer Cells and Novel Targeting Therapies," *Clin. Pharmacol. Ther.*, vol. 83, no. 5, pp. 673–691, May 2008.

[403] J. Luo, S. Ok Lee, L. Liang, C.-K. Huang, L. Li, S. Wen, and C. Chang, "Infiltrating bone marrow mesenchymal stem cells increase prostate cancer stem cell population and metastatic ability via secreting cytokines to suppress androgen receptor signaling.," *Oncogene*, vol. 33, no. 21, pp. 2768–78, 2014.

[404] J. H. YlÖstalo, T. J. Bartosh, K. Coble, and D. J. Prockop, "Human Mesenchymal Stem/Stromal Cells Cultured as Spheroids are Self-activated to

Produce Prostaglandin E2 that Directs Stimulated Macrophages into an Anti-inflammatory Phenotype," *Stem Cells*, vol. 30, no. 10, pp. 2283–2296, Oct. 2012.

[405] S. Pinho, J. Lacombe, M. Hanoun, T. Mizoguchi, I. Bruns, Y. Kunisaki, and P. S. Frenette, "PDGFRα and CD51 mark human Nestin+ sphere-forming mesenchymal stem cells capable of hematopoietic progenitor cell expansion," *J. Exp. Med.*, vol. 210, no. 7, 2013.

[406] D. Gao, I. Vela, A. Sboner, P. J. Iaquinta, W. R. Karthaus, A. Gopalan, C. Dowling, J. N. Wanjala, E. A. Undvall, V. K. Arora, J. Wongvipat, M. Kossai, S. Ramazanoglu, L. P. Barboza, W. Di, Z. Cao, Q. F. Zhang, I. Sirota, L. Ran, T. Y. MacDonald, H. Beltran, J.-M. Mosquera, K. A. Touijer, P. T. Scardino, V. P. Laudone, K. R. Curtis, D. E. Rathkopf, M. J. Morris, D. C. Danila, S. F. Slovin, S. B. Solomon, J. A. Eastham, P. Chi, B. Carver, M. A. Rubin, H. I. Scher, H. Clevers, C. L. Sawyers, and Y. Chen, "Organoid Cultures Derived from Patients with Advanced Prostate Cancer," *Cell*, vol. 159, no. 1, pp. 176–187, 2014.

[407] R. Straussman, T. Morikawa, K. Shee, M. Barzily-Rokni, Z. R. Qian, J. Du, A. Davis, M. M. Mongare, J. Gould, D. T. Frederick, Z. A. Cooper, P. B. Chapman, D. B. Solit, A. Ribas, R. S. Lo, K. T. Flaherty, S. Ogino, J. A. Wargo, and T. R. Golub, "Tumour micro-environment elicits innate resistance to RAF inhibitors through HGF secretion.," *Nature*, vol. 487, no. 7408, pp. 500–4, 2012.

[408] P. Bajaj, R. M. Schweller, A. Khademhosseini, J. L. West, and R. Bashir, "3D Biofabrication Strategies for Tissue Engineering and Regenerative Medicine," *Annu. Rev. Biomed. Eng.*, vol. 16, no. 1, pp. 247–276, Jul. 2014.

[409] I. A. Potapova, G. R. Gaudette, P. R. Brink, R. B. Robinson, M. R. Rosen, I. S. Cohen, and S. V. Doronin, "Mesenchymal Stem Cells Support Migration, Extracellular Matrix Invasion, Proliferation, and Survival of Endothelial Cells In Vitro," *Stem Cells*, vol. 25, no. 7, pp. 1761–1768, Jul. 2007.

[410] M. E. Harper, E. Glynne-Jones, L. Goddard, D. W. Wilson, S. S. Matenhelia, I. G. Conn, W. B. Peeling, and K. Griffiths, "Relationship of proliferating cell nuclear antigen (PCNA) in prostatic carcinomas to various clinical parameters.," *Prostate*, vol. 20, no. 3, pp. 243–53, 1992.

[411] X. Z. Wang, B. Wang, Z. Q. Gao, J. G. Liu, Z. Q. Liu, Q. L. Niu, Z. K. Sun, and Y. X. Yuan, "Diffusion-weighted imaging of prostate cancer: Correlation between apparent diffusion coefficient values and tumor proliferation," *J. Magn. Reson. Imaging*, vol. 29, no. 6, pp. 1360–1366, Jun. 2009.

[412] C. Fischbach, R. Chen, T. Matsumoto, T. Schmelzle, J. S. Brugge, P. J. Polverini, and D. J. Mooney, "Engineering tumors with 3D scaffolds," *Nat. Methods*, vol. 4, no. 10, pp. 855–860, Oct. 2007.

[413] E. Gómez-Barrena, P. Rosset, D. Lozano, J. Stanovici, C. Ermthaller, and F. Gerbhard, "Bone fracture healing: Cell therapy in delayed unions and nonunions," *Bone*, vol. 70, pp. 93–101, Jan. 2015.

[414] M. K. Sen and T. Miclau, "Autologous iliac crest bone graft: Should it still be the gold standard for treating nonunions?," *Injury*, vol. 38, no. 1, pp. S75–S80, Mar. 2007.

[415] T. J. Blokhuis, G. M. Calori, and G. Schmidmaier, “Autograft versus BMPs for the treatment of non-unions: What is the evidence?,” *Injury*, vol. 44, pp. S40–S42, Jan. 2013.

[416] R. Edmondson, J. J. Broglie, A. F. Adcock, and L. Yang, “Three-dimensional cell culture systems and their applications in drug discovery and cell-based biosensors.,” *Assay Drug Dev. Technol.*, vol. 12, no. 4, pp. 207–18, May 2014.

[417] R. O. Hynes, “The Extracellular Matrix: Not Just Pretty Fibrils,” *Science (80-.).*, vol. 326, no. 5957, 2009.

[418] L. Seguin, J. S. Desgrosellier, S. M. Weis, and D. A. Cheresh, “Integrins and cancer: regulators of cancer stemness, metastasis, and drug resistance,” *Trends Cell Biol.*, vol. 25, no. 4, pp. 234–240, Apr. 2015.

[419] Y. S. DeRose, G. Wang, Y.-C. Lin, P. S. Bernard, S. S. Buys, M. T. W. Ebbert, R. Factor, C. Matsen, B. A. Milash, E. Nelson, L. Neumayer, R. L. Randall, I. J. Stijleman, B. E. Welm, and A. L. Welm, “Tumor grafts derived from women with breast cancer authentically reflect tumor pathology, growth, metastasis and disease outcomes,” *Nat. Med.*, vol. 17, no. 11, pp. 1514–1520, Nov. 2011.

[420] P. Loukopoulos, K. Kanetaka, M. Takamura, T. Shibata, M. Sakamoto, and S. Hirohashi, “Orthotopic transplantation models of pancreatic adenocarcinoma derived from cell lines and primary tumors and displaying varying metastatic activity,” *Pancreas*, vol. 29, no. 3, pp. 193–203, 2004.

[421] X. Zhao, Z. Liu, L. Yu, Y. Zhang, P. Baxter, H. Voicu, S. Gurusiddappa, J. Luan, J. M. Su, H. E. Leung, and X.-N. Li, “Global gene expression profiling confirms the molecular fidelity of primary tumor-based orthotopic xenograft mouse models of medulloblastoma.,” *Neuro. Oncol.*, vol. 14, no. 5, pp. 574–83, May 2012.

[422] W. R. Karthaus, P. J. Iaquinta, J. Drost, A. Gracanin, R. van Boxtel, J. Wongvipat, C. M. Dowling, D. Gao, H. Begthel, N. Sachs, R. G. J. Vries, E. Cuppen, Y. Chen, C. L. Sawyers, and H. C. Clevers, “Identification of Multipotent Luminal Progenitor Cells in Human Prostate Organoid Cultures,” *Cell*, vol. 159, no. 1, pp. 163–175, Sep. 2014.

[423] H. Clevers, “Modeling Development and Disease with Organoids,” *Cell*, vol. 165, no. 7, pp. 1586–1597, Jun. 2016.

[424] X. Yin, B. E. Mead, H. Safaee, R. Langer, J. M. Karp, and O. Levy, “Engineering Stem Cell Organoids,” *Cell Stem Cell*, vol. 18, no. 1, pp. 25–38, Jan. 2016.

[425] C. W. Chua, M. Shibata, M. Lei, R. Toivanen, L. J. Barlow, S. K. Bergren, K. K. Badani, J. M. McKiernan, M. C. Benson, H. Hibshoosh, and M. M. Shen, “Single luminal epithelial progenitors can generate prostate organoids in culture,” *Nat. Cell Biol.*, vol. 16, no. 10, pp. 951–961, Oct. 2014.

[426] B. Munos, “Lessons from 60 years of pharmaceutical innovation,” *Nat. Rev. Drug Discov.*, vol. 8, no. 12, pp. 959–968, Dec. 2009.

[427] J. Friedrich, C. Seidel, R. Ebner, and L. A. Kunz-Schughart, “Spheroid-based drug screen: considerations and practical approach,” *Nat. Protoc.*, vol. 4, no. 3, pp. 309–324, 2009.

[428] E. Scosyrev, E. M. Messing, S. Mohile, D. Golijanin, and G. Wu, “Prostate cancer in the elderly,” *Cancer*, vol. 118, no. 12, pp. 3062–3070, Jun. 2012.

[429] C. J. Keto, W. J. Aronson, M. K. Terris, J. C. Presti, C. J. Kane, C. L. Amling, and S. J. Freedland, “Obesity is associated with castration-resistant disease and metastasis in men treated with androgen deprivation therapy after radical prostatectomy: results from the SEARCH database.,” *BJU Int.*, vol. 110, no. 4, pp. 492–8, Aug. 2012.

[430] S. J. Freedland, L. L. Bañez, L. L. Sun, N. J. Fitzsimons, and J. W. Moul, “Obese men have higher-grade and larger tumors: an analysis of the duke prostate center database,” *Prostate Cancer Prostatic Dis.*, vol. 12, no. 3, pp. 259–263, Sep. 2009.

[431] Â. Moreira, S. S. Pereira, M. Costa, T. Morais, A. Pinto, R. Fernandes, and M. P. Monteiro, “Adipocyte secreted factors enhance aggressiveness of prostate carcinoma cells.,” *PLoS One*, vol. 10, no. 4, p. e0123217, 2015.

[432] K.-D. Tang, J. Liu, L. Jovanovic, J. An, M. M. Hill, I. Vela, T. K.-W. Lee, S. Ma, C. Nelson, P. J. Russell, J. A. Clements, and M.-T. Ling, “Adipocytes promote prostate cancer stem cell self-renewal through amplification of the cholecystokinin autocrine loop.,” *Oncotarget*, vol. 7, no. 4, pp. 4939–48, Jan. 2016.

[433] M. K. Herroon, E. Rajagurubandara, A. L. Hardaway, K. Powell, A. Turchick, D. Feldmann, and I. Podgorski, “Bone marrow adipocytes promote tumor growth in bone via FABP4-dependent mechanisms.,” *Oncotarget*, vol. 4, no. 11, pp. 2108–23, Nov. 2013.

[434] N. P. Gauthier, B. Soufi, W. E. Walkowicz, V. A. Pedicord, K. J. Mavrakis, B. MacEk, D. Y. Gin, C. Sander, and M. L. Miller, “Cell-selective labeling using amino acid precursors for proteomic studies of multicellular environments,” *Nat. Methods*, vol. 10, no. 8, pp. 768–773, 2013.

[435] K. Misund, K. A. Baranowska, T. Holien, C. Rampa, D. C. G. Klein, M. Børset, A. Waage, and A. Sundan, “A Method for Measurement of Drug Sensitivity of Myeloma Cells Co-Cultured with Bone Marrow Stromal Cells,” *J. Biomol. Screen.*, vol. 18, no. 6, pp. 637–646, Jul. 2013.

[436] C. P. Hodgkinson, J. A. Gomez, M. Mirotsou, and V. J. Dzau, “Genetic engineering of mesenchymal stem cells and its application in human disease therapy.,” *Hum. Gene Ther.*, vol. 21, no. 11, pp. 1513–26, Nov. 2010.

[437] F. A. Fierro, S. Kalomoiris, C. S. Sondergaard, and J. A. Nolta, “Effects on Proliferation and Differentiation of Multipotent Bone Marrow Stromal Cells Engineered to Express Growth Factors for Combined Cell and Gene Therapy,” *Stem Cells*, vol. 29, no. 11, pp. 1727–1737, Nov. 2011.